Promoting the Conversion of Ruthenium Aqua to Ruthenium Oxo Complexes with Specially Designed Ancillary Ligands

A Thesis

forwarded to

Department of Applied Biology & Chemical Technology

in

Partial Fulfilment of the Requirements

for

the Degree of Doctor of Philosophy

at

The Hong Kong Polytechnic University

by

CHEUNG Kwong Chak

December, 2003

Declaration

I hereby declare that the thesis summaries my own work carried out since my registration for the Degree of Doctor of Philosophy in April, 1998, and that it has not been previously included in a thesis, dissertation or report submitted to this or any other institution for a degree, diploma or other qualification.

CHEUNG Kwong Chak

December, 2003.

Acknowledgments

I wish to express my deepest gratitude to my supervisor, Prof. K. Y. Wong, for his valuable suggestions, encouragement and discussion throughout the course of my work, and for his valuable comments on the draft of this thesis. Working with him is a rewarding experience for me.

Prof. Z. Y. Zhou and Prof. W. T. Wong are sincerely thanked for solving the X-ray structure of the ruthenium complexes.

I wish to thank a number of friends and postgraduate colleagues for their kind support throughout my study: Dr. P. Guo, Dr. K. W. Yeung, Dr. W. H. Fung, Mr. Y. F. Lam, Mr. H. L. Pang, Miss N. Y. Kwok, Dr. M. L. Man, Dr. K. W. Ma, Mr. T. C. Chan, Mr. K. H. Tong, Mr. K. P. Ho, Mr. S. C. Choy, Mr. M. K. Chan and Mr. H. Y. Chan. I must also acknowledge my family for their encouragement and support. Special thanks are due to Dr. P. Guo for his invaluable discussion and assistance in organic and inorganic synthesis.

I am also greatly indebted to Miss Sandy Choi for her consistent support and concern.

Last, but not least, I would like to thank the Research Committee of The Hong Kong Polytechnic University for the award of a studentship throughout my study and for a traveling grant supporting my conference presentation in the 34th International Conference on Coordination Chemistry held in Edinburgh in July, 2000.

Abstract of thesis entitled "Promoting the Conversion of Ruthenium Aqua to Ruthenium Oxo Complexes with Specially Designed Ancillary Ligands"

Submitted by CHEUNG Kwong Chak

for the Degree of Doctor of Philosophy

at The Hong Kong Polytechnic University in December,2003

Abstract

Ruthenium oxo complexes are important intermediates in ruthenium-catalyzed oxidation reactions such as epoxidation of alkenes, oxidation of hydrocarbons and the oxidation of water to dioxygen. The electrochemical interconversion of ruthenium aqua and ruthenium oxo species has been a subject of extensive interest in the past two decades. By generating the ruthenium oxo complexes electrochemically, oxidation reactions can be achieved under electrocatalytic conditions with catalysts recycled *in-situ* on the electrode surface. However, the electrochemical oxidation of ruthenium aqua to oxo species is kinetically slow on electrode surface. The objective of this project is to promote the electrochemical conversion of Ru-OH_2 to Ru=O through specially designed ancillary ligands of the metal complexes.

In the first part of this study, a new electropolymerizable pyrrole-containing ruthenium complex $[Ru(tpy)(PPP)(H_2O)](ClO_4)_2$ (PPP = N-(3-N,N'-bis(2-pyridyl)propylamino) pyrrole) was prepared. The structure of the ruthenium complex $[Ru(tpy)(PPP)(Cl)](ClO_4)$ has been confirmed by X-ray crystallography. The ruthenium monomer can be electropolymerized onto glassy carbon electrode surface via anodic oxidation of the pyrrole function group in aqueous medium. This is the first example of a pyrrole-containing ruthenium aqua complex that can be electropolymerized in aqueous medium. It is believed that by placing the ruthenium centres close to each other in the polymer film on the electrode surface, interaction between the Ru^{III}-OH moieties (which are eletrogenerated from Ru^{II}-OH_2) is facilitated. This interaction should assist the deprotonation of the hydroxo ligand in the further oxidation of Ru^{III}-OH to Ru^{IV}=O. The generation of Ru^{IV}=O species can be

easily observed in the cyclic voltammograms.

In the second part of the thesis, the X-ray structure of two ruthenium aqua complexes containing 6,6'-dichloro-2,2'-bipyridine (dcbpy), *cis*-$[Ru(dcbpy)_2(H_2O)_2](CF_3SO_3)_2$ and $[Ru(tpy)(bpy)(H_2O)](CF_3SO_3)_2$ were reported. The cyclic voltammograms of these two complexes show that the oxidation of Ru-OH to Ru=O is much more facile than the analogues without the chloro-substituents. On comparing the structure of these complexes with analogues without the chloro-substituents, it is anticipated that intramolecular hydrogen bonding exists between the chloro-substituent at the ortho-position of the bipyridine ligand and the hydrogen of the aqua ligand on the ruthenium centre. It is suggested that the intramolecular hydrogen bonding facilitates the deprotonation of the hydroxo ligand during the oxidation of Ru-OH to Ru=O.

In the third part of the thesis, the synthesis of two novel binuclear ligands N,N,N'N'-tetra(2-pyridyl) ethylenediamine (ETHPY) and 1,8-bis(2,2'-dipyridylamino)anthracene (BDPAA) and their ruthenium aqua complexes were reported. The structure of the ruthenium binuclear complex $[Ru_2(tpy)_2(ETHPY)(CH_3CN)_2]^{4+}$ has been confirmed by X-ray crystallography. The $O=Ru^{IV}$-$Ru^{IV}=OH$/ $HO-Ru^{III}$-$Ru^{III}-OH$ couple is only observed in the cyclic voltammogram of $[Ru_2(tpy)_2(ETHPY)(H_2O)_2]^{4+}$ but not $[Ru_2(tpy)_2(BDPAA)(H_2O)_2]^{4+}$. It is proposed that the flexibility of the ethylene bridge in $[Ru_2(tpy)_2(ETHPY)(H_2O)_2]^{4+}$ facilitates the interaction of Ru-OH moieties and hence promotes the conversion of $Ru-OH_2$ to Ru=O.

Table of Contents

DECLARATION II

ACKNOWLEDGMENTS III

ABSTRACT V

TABLE OF CONTENTS VII

CHAPTER 1 1

INTRODUCTION 1

1.1 Background 2

1.1.1 Heterogeneous electrocatalysts 2

1.1.2 Homogeneous electrocatalysts 4

1.1.3 Electrode reactions involving electrocatalysts 5

1.2 Review on the Electrogeneration of Metal Oxo Complexes and Their Applications in Electrocatalysis 12

1.2.1 Chromium oxo complexes 12

1.2.2 Manganese oxo complexes 13

1.2.3 Rhenium oxo complexes 13

1.2.4 Osmium oxo complexes 14

1.2.5 Ruthenium oxo complexes 16

1.3 Aims and Objectives of this Project 25

CHAPTER 2 27

SYNTHESIS, CHARACTERIZATION AND ELECTROCHEMICAL STUDIES OF A ELECTROPOLYMERIZABLE RUTHENIUM AQUA COMPLEX WITH PYRROLE - FUNCTIONALIZED 2,2'-DIPYRIDYLAMINE 27

2.1 Introduction 28

2.2 Experimental Section 30

2.2.1 Synthesis 30

2.2.2 Physical Measurements 35

2.3 Results and Discussion 38

2.3.1 Synthesis and characterization 38

2.3.2 X-ray structural determination of $[Ru^{II}(tpy)(PPP)Cl]ClO_4$ 42

2.3.3 Electrochemical behaviour of the ruthenium complexes 47

2.3.4 *In-situ* reflectance FT-IR spectroelectrochemistry 74

2.3.5 Scanning electron microscopy 76

2.4 Conclusion 79

CHAPTER 3 80

X-RAY STRUCTURE OF RUTHENIUM AQUA COMPLEXES WITH 6,6'-DICHLORO-2,2'-BIPYRIDINE LIGAND – CORRELATION BETWEEN STRUCTURE AND ELECTROCHEMISTRY 80

3.1. Introduction 81

3.2. Experimental Section 83

3.2.1. Synthesis 83

3.2.2. Physical measurements 90

3.3. Results and Discussion 95

3.3.1. X-ray structure of the ruthenium complexes 95

3.3.2. Correlation between structure and electrochemistry 112

3.4. Conclusion 129

CHAPTER 4 130

SYNTHESIS AND REDOX PROPERTIES OF SOME NEW BINUCLEAR RUTHENIUM COMPLEXES WITH SPECIALLY DESIGNED LIGANDS 130

4.1 Introduction 131

4.2 Experimental Section **133**

4.2.1 Synthesis 133

4.2.2 Physical measurements 144

4.3 Results and Discussion **145**

4.3.1 X-ray structural determination of BDPAA and ruthenium complexes 145

4.3.2 Electrochemical properties of the ruthenium binuclear complexes in non-aqueous solution 166

4.3.3 Electrochemical properties of the binuclear ruthenium complexes in aqueous medium 170

4.4 Conclusion **189**

CHAPTER 5 **190**

CONCLUSIONS **190**

REFERENCES **194**

APPENDIX **230**

Chapter 1

Introduction

1.1 Background

Similar to chemical reactions, many electrode reactions occur only at high overpotentials because of unfavourable kinetics. For such electrochemical reactions to be useful, it is necessary to find a electrocatalyst that will lower the overpotential and speed up the rate of reaction. The objective of electrocatalysis is therefore to seek alternative, lower energy of activation pathways which allow such electrode reactions to occur at high current density and at a low overpotential. Electrocatalysis is important to many applications in electrochemistry since the energy efficiency of any electrochemical cell is determined in part, by the potential of the anode and cathode. There are two basic different types of electrocatalysis: heterogeneous, and homogeneous. Each of these types of electrocatalysis are shown in Figures 1.1 and 1.2 respectively [1]:

1.1.1 Heterogeneous electrocatalysts

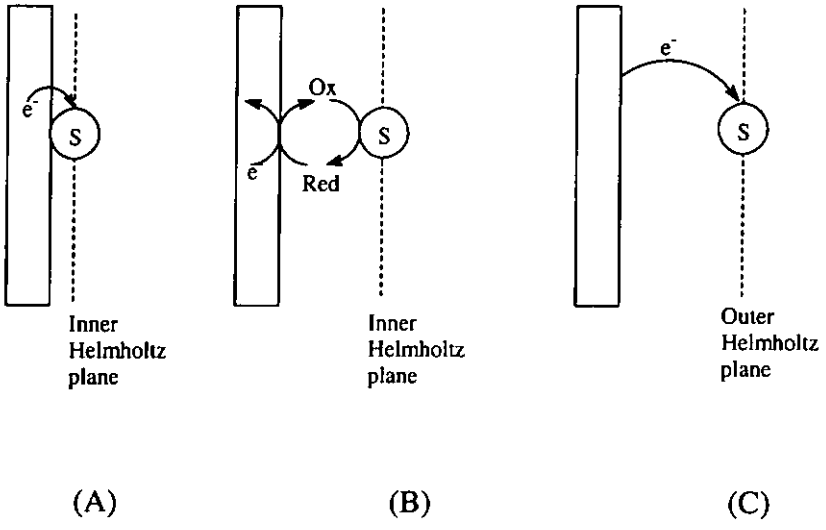

Figure 1.1 Schematic diagrams of different heterogeneous electrocatalysts.

It is the presence of the above-mentioned electric fields, which differentiates

heterogeneous electrochemical catalysis from thermal or chemical reactions. The process involves three different steps:

1. Transfer of electroactive species from bulk solution to the electrode surface or within the double layer ;
2. Exchange of electrons between the electrode and the electroactive species;
3. Removal of the products from the electrode, which may involve desorption. In heterogeneous electrocatalysis, direct charge transfer from electrode to substrate gives the product.

Three examples are shown in Figure 1.1. In the first (Fig. 1.1(A)), the substrate adsorbs onto the electrode surface and undergoes an electron transfer reaction. In the second (Fig. 1.1(B)), a mediator coating the surface acts as "electron shuttle" to transport electrons from/to the adsorbed intermediate. In the last example (Fig. 1.1(C), the substrate is not strongly bound, and instead electron tunnelling from the electrode allows the reaction to occur.

1.1.2 Homogeneous electrocatalysts

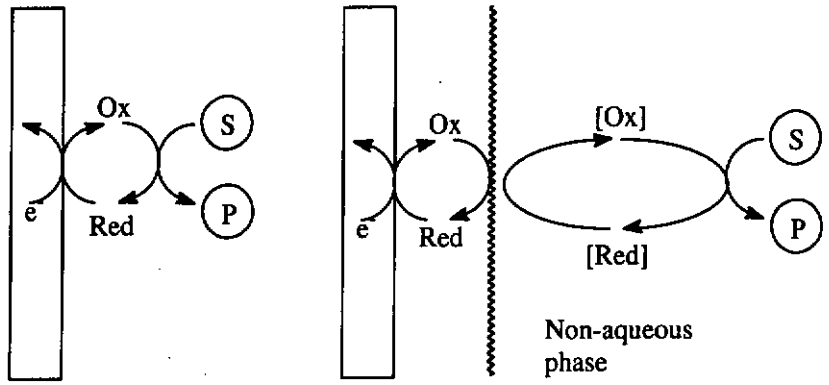

(A) (B)

Figure 1.2 Schematic diagrams of homogeneous electrocatalysis.

In homogeneous electrocatalysis the substrate does not exchange electrons with the electrode directly, but with some intermediates. Electron transfers and chemical reactions can then take place in the bulk. This process usually occurs for redox systems. The principle difference between the heterogeneous and homogeneous case is that in the former the redox couple is physically attached to the electrode surface whereas in the later case it is free to diffuse through the solution. In Fig 1.2(A) the mediator and reactant are both present in the same solution. In the second example (Fig. 1.2(B)) the substrate is present in a secondary phase, and it is necessary to introduce a transfer catalyst into the system.

1.1.3 Electrode reactions involving electrocatalysts

Many industrially important electrochemical reactions, such as hydrogen evolution [2-8], oxygen reduction [9-16], chlorine formation [17-20] and oxidation of CO [21-38], require the presence of electrocatalysts. The most well-known example of electrocatalysts is perhaps the Dimensionally Stable Anode (DSA) for chlorine production. The DSA consists of a ruthenium dioxide electocatalyst coated on a titanium support. The electrode can maintain a very high current density, 0.1-1.0 Acm^{-2}, at an overpotential of only 30-70 mV. This is in contrast with the 500 mV overpotential with the graphite anode. [39]

Besides ruthenium dioxide, nickel oxide / hydroxide is another example of commonly used electrocatalyst in oxidation reactions. Nickel hydroxide modified electrodes have been applied in the amperometric detection of carbohydrates, amino acids and amines [40-45] and oxidation of alcohols [40, 46-48].

Although transition metals and their oxides are commonly used as heterogeneous electrocatalysts, transition metal complexes are often selected as homogeneous catalysts in electrochemical reactions. Compared to the solid state electrocatalysts, transition metal complexes are more selective in catalytic reactions and their reactivites can be tuned through the spectator ligands. In electrochemical oxidations, metal oxo complexes are the most important class of electrocatalysts and they have been

extensively studied. Metal oxo complexes are molecules that contain a M=O moiety. As shown in Figure 1.3, the metal oxygen bond can be viewed as a ligand O^{2-} bound to the metal centre.

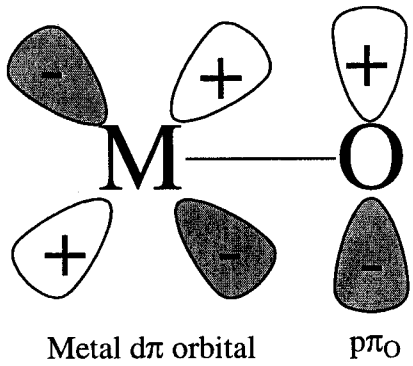

Figure 1.3 Bonding in metal oxo complex.

Metal oxo complexes are important catalysts and intermediates for various oxidation reactions, including chloride oxidation, oxidation of alcohols and hydrocarbons as well as epoxidation of olefins. Perhaps the most well known example in the literature are the iron(IV) oxo porphyrin cation radical intermediate in the enzymatic cycle of cytochrome P450 [49-62] and the manganese(V) oxo Schiff base in Jacobsen's catalyst for the asymmetric epoxidation of olefins [63-69].

Electrochemically, metal oxo species can be generated by oxidation of metal aqua or hydroxo species on the electrode surface:

$$M{-}OH_2 \xrightarrow{-e^-,\,-H^+} M{-}OH \xrightarrow{-e^-,\,-H^+} M{=}O$$

The loss of electron from the M-OH_2 or M-OH species is accompanied by the loss

of a proton. The formation of the oxo species stabilizes the higher oxidation state of the metal. These electron transfer reactions is accompanied by proton transfer and called 'proton-coupled electron transfers'. The stabilization of the metal in high oxidation states is revealed in Scheme 1.1 in which a ruthenium polypyridyl oxo complex is used as an example:

Scheme 1.1

$$\underset{d\pi^4}{cis\text{-}[Ru^{IV}(bpy)_2(Cl)_2]^{2-}} \xrightarrow{1.7\ V} \underset{d\pi^5}{cis\text{-}[Ru^{III}(bpy)_2(Cl)_2]^{-}} \xrightarrow{0.0\ V} \underset{d\pi^6}{cis\text{-}[Ru^{II}(bpy)_2(Cl)_2]^{0}}$$

(V verus NHE in 0.1 M $[N(n\text{-}Bu_4)]PF_6/CH_3CN$) (1.1)[70]

$$\underset{d\pi^4}{cis\text{-}[Ru^{IV}(bpy)_2(py)(O)]^{2+}} \xrightarrow{0.78\ V} \underset{d\pi^5}{cis\text{-}[Ru^{III}(bpy)_2(py)(OH)]^{2+}} \xrightarrow{0.67\ V} \underset{d\pi^6}{cis\text{-}[Ru^{II}(bpy)_2(py)(H_2O)]^{2+}}$$

(V verus NHE, μ = 0.1 M at pH 7)

Where bpy = 2,2'-bipyridine and py = pyridine (1.2)[71]

The example shown in eq 1.1 is typical for Ru polypyridyl couples with oxidation of Ru(II) to Ru(III) occurring at easily accessible potentials. The 1.7 V increase in potential for the Ru^{IV}/Ru^{III} couple is due to the increase in charge and oxidation state compared to the Ru^{III}/Ru^{II} couple [70].

In the couples shown in eq. 1.2, the anionic Cl^- ligands are replaced by the neutral pyridine (py) and H_2O ligands. The increase in charge and changes in bonding increase the potential for oxidation of *cis*-$[Ru^{II}(bpy)_2(py)(H_2O)]^{2+}$ (Ru^{II}-OH_2^{2+}) to *cis*-

$[Ru^{III}(bpy)_2(py)(OH)]^{2+}$ (Ru^{II}-OH^{2+}) by over 0.6 V [71-73]. The potential for oxidation to the aqua complex Ru^{III}-OH_2^{3+} based on the Ru^{III}-OH_2^{3+}/Ru^{II}-OH_2^{2+} couple is even higher, 1.06 V. However, at pH 7 the relevant couple is Ru^{III}-OH^{2+}/Ru^{II}-OH_2^{2+}. The acidity of the Ru^{III}-OH_2^{3+} form is greatly enhanced compared to Ru^{II}-OH_2^{2+}, pKa = 0.85, and the hydroxo complex Ru^{III}-OH^{2+} is the dominant form at pH 7. [72]

The big surprise in eq 1.2 is the much smaller difference between the Ru^{IV} / Ru^{III} and Ru^{III} / Ru^{II} couples, 0.11 V compared to 1.7 V. These data point to a dramatic stabilization of Ru(IV) in the aqua-containing coordination environment. This is caused by proton loss and electronic stabilization of the higher oxidation state by oxo formation. pK_a values are 10.6 for Ru^{II}-H_2O^{2+}, and 0.8 and > 13 for the first and second protons in *cis*-$[Ru^{III}(bpy)_2(py)(H_2O)]^{3+}$ [74]. The Ru(IV) form exists as the oxo complex, *cis*-$[Ru^{IV}(bpy)_2(py)(O)]^{2+}$ (Ru^{IV}=O^{2+}). There is no sign of protonation at the oxo group even in strong acids.

Stabilization of Ru(IV) as the oxo complex causes the near overlap of Ru^{IV}/Ru^{III} and Ru^{III}/Ru^{II} potentials. There is an important implication for reactivity in this near overlap. Thermodynamically, Ru(IV) is nearly as good a two-electron oxidant as a one-electron oxidant at pH 7.

In proton-coupled electron transfers, there is an initial association between reactants, probably with hydrogen bonding between the O-H proton of the H_2O or OH

ligand in Ru^{II}-OH_2^{2+} or Ru^{III}-OH^{2+} and the oxidant. Association is followed by proton-coupled electron transfer which is a synchronous process with simultaneous transfer of both an electron and a proton from Ru^{II}-OH_2 or Ru^{III}-OH to the oxidant.

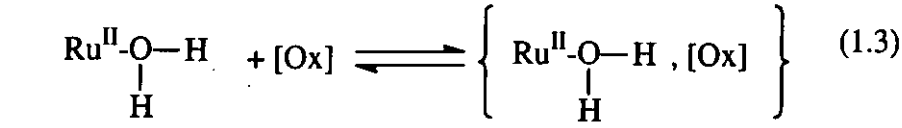

(1.3)

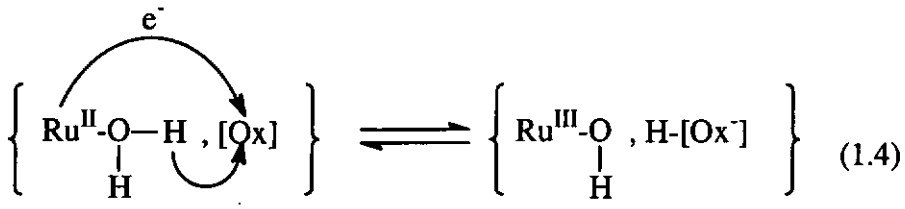

(1.4)

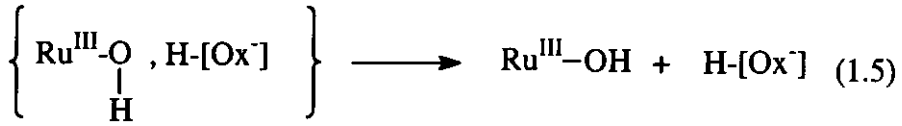

(1.5)

Proton-coupled electron transfer is different from H-atom transfer [75]. In H-atom transfer, both the electron and proton come from the same O-H bond. If H-atom transfer occurred in eq. 1.4, it would give the intermediate $Ru^{II}(\bullet OH)^{2+}$ rather than $Ru^{III}(OH^-)^{2+}$. From spectroscopic measurements, a $OH^- \rightarrow Ru^{III}$ charge-transfer band is observed at 312 nm [75], which suggests that $Ru^{II}(\bullet OH)^{2+}$ is higher in energy by >2eV, ruling it out as an intermediate in the reaction.

It is interesting to note why a proton-coupled electron transfer should occur, but not electron transfer followed by proton transfer or vice versa. The answer can be illustrated by the energetic of the possible pathways as shown in Scheme 1.2, in which the oxidant for Ru^{II}-OH_2 is a Ru^{IV}=O species. This comproportionation reaction has

been reported by Meyer and his co-workers [72, 74].

Scheme 1.2

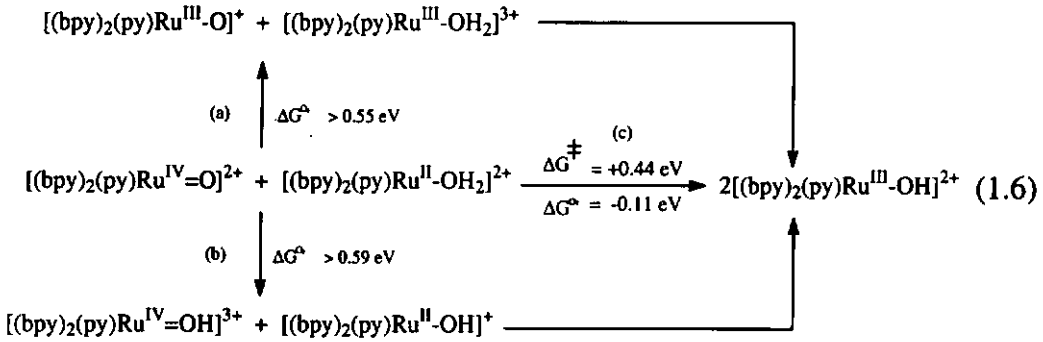

(1.6)

The net reaction in Scheme 1.2 requires that both an electron and a proton are transferred from Ru^{II}-OH_2^{2+} to Ru^{IV}=O^{2+}. Three possible mechanisms can do this. In reaction (a), electron transfer is followed by proton transfer. This is an accessible pathway. However, because Ru^{III}-O^{+} is formed without a proton and the estimated pKa for Ru^{III}-OH^{2+} is >13, this pathway is uphill by at least 0.55 eV. This is the minimum free energy of activation. Its magnitude rules out a major role for this pathway since the experimental value for $\Delta G^{\ddagger}$ is 0.44 eV. In reaction (b), proton transfer is followed by electron transfer. The driving force is even less favorable (> +0.59 eV) due to the initial formation of protonated Ru^{IV}=OH^{3+} and deprotonated Ru^{II}-OH^{+}.

Because of the special orbital characteristics of Ru^{IV}=O^{2+}, which allow it to accept both an electron and a proton, and of Ru^{II}-OH_2^{2+}, which allow it to donate both an electron an a proton, proton-coupled electron transfer in reaction (c) is orbitally accessible. It is by far the low-energy pathway, being favoured by -0.11 eV, and

dominates reactivity in this case. Simple electron transfer is disfavoured because of the thermodynamic instability of the deprotonated Ru^{III}-O^{+} intermediate. Proton transfer is disfavoured largely because of the low affinity of the oxo group for a proton. The above explanation also implies that in order for an oxidant to promote proton-coupled electron transfer in metal aqua or hydroxo complexes, it should contain certain special features which can facilitate this complicated mechanism. A summary on the literature reported electrochemical generation of metal oxo species is given in section 1.2.

1.2 Review on the Electrogeneration of Metal Oxo Complexes and Their Applications in Electrocatalysis

A number of metal oxo complexes, including those of chromium, manganese, rhenium, osmium and ruthenium, have been generated electrochemically from their corresponding aqua or hydroxo complexes. In the following sections we will review briefly these processes in order to have a better understanding on the interconversion between metal aqua, metal hydroxo and metal oxo species.

1.2.1 Chromium oxo complexes

Murray and co-workers have reported the electrochemical generation of a stable formed Cr(V)-oxo porphyrin species from the corresponding Cr(IV)-oxo porphyrin in dichloromethane [76]. This Cr(V)-oxo species is active towards the epoxidation of olefins. Anson and co-workers have reported the electrochemical generation of a Cr^{V}=O species from Cr^{III}-OH_2 in chromium-substituted heteropolytungstate anions [77]. The Cr^{V}=O species reacted with alcohols, but the rate of the oxidation were too slow to make the Cr(V) derivatives attractive as electrocatalysts. Bruce and co-workers [78, 79] have studied the electrochemical behaviour and pK_a values of various oxidation states of chromium tetraphenylporphyrin in aqueous solution. As complexes of Cr^{V} and Cr^{IV} are considered to be carcinogens and mutagens [80, 81], this limits their use and applications in oxidation reactions.

1.2.2 Manganese oxo complexes

Electrocatalytic epoxidation of olefins with manganese porphyrin and Schiff-base complexes was first studied by Murray and co-workers [82-84]. The electrocatalytic epoxidation of cyclooctene with dioxygen using different manganese Schiff-base complexes has recently been reported by Moutet and co-workers [85]. Devynck and co-workers [86, 87] have reported the electrocatalytic oxidation of hydrocarbons by immobilized manganese porphyrin complexes via conducting polymers onto glassy carbon electrodes. Wong and co-workers [88] and Tanaka and co-workers [89] have also reported the enantioselective electrocatalytic epoxidation of olefins by chiral manganese Schiff-base catalysts. The immobilization of the manganese catalysts onto electrode surface can inhibit the formation of inactive manganese dimer, and moderate *ee* values of 65 to 77% were obtained in the asymmetric epoxidation of stilbene and styrene. Most interestingly, a number of polynuclear manganese oxo complexes are active catalysts for the electrochemical oxidation of water to dioxygen [90-92]. A major drawback of these manganese oxo catalysts is that the catalyst life is relatively short, some can only survive a few catalytic cycles.

1.2.3 Rhenium oxo complexes

Rhenium aqua complexes with pyridine or bipyridine as ancillary ligand can be

oxidized to Re^{V}=O species with the loss of two protons and two electrons. An extensive study of Re^{V}-oxo and Re^{V}-dioxo complexes, including $[(PPh_3)(Cl_3)Re^{V}=O]$, $[(CN)_4Re^{V}(O)_2]^{3-}$, $[(en)_2Re^{V}(O)_2]^{+}$, *trans*-$[(py)_4Re^{V}(O)_2]^{+}$ and $[(sal_2phen)_2Re^{V}(O)_3]$ (sal_2phen = N,N'-*o*-phenylenebis(salicylideneaminate) anion, en = ethyleneaiamine and py = pyridine) [93-96] shows rhenium (V) oxo species are stable in both solid state and solution state. However, the rhenium oxo complexes are poor oxidants with low oxidation potentials and the stability of the these species makes them inviable candidates in catalytic oxidation reactions. Nevertheless, the stability of the rhenium oxo complexes makes them attractive for fundamental studies to understand the kinetics and mechanisms of metal oxo complexes.

1.2.4 Osmium oxo complexes

The aqueous electrochemistry of osmium polypyridyl complexes $[Os(tpy)(O)_2(OH)]^{+}$ and $[Os(tpy)(O)_2(OH)_2]$ has been extensively studies by Meyer and co-workers [97]. The electrochemistry of osmium di-oxo complexes *trans*-$[OsL(O)_2]^{2+}$ and *cis*-$[OsL(O)_2]^{2+}$ with macrocyclic tertiary amine ligands (L = 1,4,8,11-tetramethyl-1,4,8,11-tetra-azacyclotetradecane,1,4,8,12-tetramethyl-1,4,8,12-tetra-azacyclopentadecane, 1,5,9,13-tetramethyl-1,5,9,13-tetra-azacyclohexadecane, and meso-2,3,7,11,12-pentamethyl-3,7,11,17-tetra-azabicyclo[11.3.1]heptadeca-1(17),13,15-triene) [98] have been reported by Che and co-workers. The osmium oxo complexes, similar to the rhenium oxo complexes, are poor oxidants with low oxidation potentials.

No reaction with norbon-2-ene, styrene, and *cis*- and *trans*-stilbenes was found to occur. Nevertheless, osmium oxo complexes are very stable and can be isolated easily. It serves as an analogue for the more reactive ruthenium and even iron complexes for a better understanding of the reaction mechanisms and kinetics in the formation of metal oxo complexes.

1.2.5 Ruthenium oxo complexes

Among the various transition metal oxo complexes, ruthenium oxo complexes are of particular interest and have received extensive attention in the past two decades. Ruthenium (VIII) oxide [99] is a powerful oxidizing agent for organic substances such as alkenes, aromatic hydrocarbons and alkanes. However, these oxidation reactions often result in poor selectivity. Ruthenium (VI), ruthenium (V) and ruthenium (IV) oxo complexes with different ancillary ligands have all been synthesized, isolated and characterized. These ruthenium oxo complexes can be prepared either by chemical or electrochemical oxidations.

All the reported Ru^{IV}-oxo complexes are mono-oxo species, most are paramagnetic and contain at least one N-donor ligand. The Ru^{IV}=O complex can be prepared by cerium(IV) or electrochemical oxidation of Ru^{II}-OH_2. The complex $[Ru^{II}(tpy)(bpy)(H_2O)]^{2+}$ has been extensively studied by Meyer and co-workers [100-102], and it was shown to effectively oxidize a variety of organic substrates including alcohols, aromatic hydrocarbons, alkenes, phenols, hydroquinone and even DNA [103-109]. Other Ru^{IV}=O complexes containing multi-dentate N-donor ligands have also been reported. These include $[Ru^{IV}(tpm)(bpy)(O)]^{2+}$, $[Ru^{IV}(tpy)(dcbpy)(O)]^{2+}$, $[Ru^{IV}(Me_3tacn)(bpy)(O)]^{2+}$, $[Ru(tpm)(phen)(O)]^{2+}$, $[Ru(bpy)(damp)(O)]^{2+}$,$[Ru(biq)(bpy)(PEt_3)(O)]^{2+}$ and $[Ru^{IV}(tpy)((S)\text{-}bpop)(O)]^{2+}$ [105, 110-114] (tpm = tris(1-pyrazolyl)methane, tpy = 2,2':6,'2"-terpyridine, dcbpy =

6,6'-dichloro-2,2'-bipyridine, Me_3tacn = 1,4,7-trimethyl-1,4,7-triazacyclononane, phen = 1,10-phenanthroline, biq = 2,2'-biquinoline, (S)-bpop = 2,2-bis(2-(4-(S)-phenyl-1,3-oxazolinyl))propane, damp = 2,6-bis-((dimethylamino)methyl)pyridine).

Ruthenium(IV) oxo complexes can be electrochemically generated *in-situ* on electrode surface which then act as electrocatalyst for the oxidation of various organic and inorganic substrates.

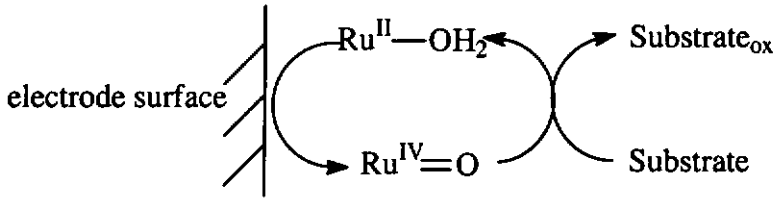

Figure 1.5 Electrocatalytic oxidation by $Ru^{IV}=O$.

Early work in the 1980's by Meyer and co-workers on ruthenium polypyridyl complexes [72, 115, 116] showed that the aqua ligand can be electrochemically oxidized to the corresponding oxo complexes. Studies on the use of these complexes for the electro-oxidation of organic substrates have been reported [117-119]. In general, the electrochemical oxidation of the ruthenium (II) aqua complexes to ruthenium (IV) oxo complexes proceeds in two one-electron one-proton steps as shown in equations (1.7) and (1.8):

$$Ru^{II}\text{-}OH_2 \rightleftharpoons Ru^{III}\text{-}OH + H^+ + e^- \qquad E_1^o \quad (1.7)$$

$$Ru^{III}\text{-}OH \rightleftharpoons Ru^{IV}=O + H^+ + e^- \qquad E_2^o \quad (1.8)$$

The E° values of the Ru^{IV}=O/Ru^{III}-OH and Ru^{III}-OH/Ru^{II}-OH_2 couples shift cathodically with increase in pH in a manner predicted by the Nernst equation. The two couples observed which are found to shift cathodically by –60 mV per pH unit as the pH range 1 < pH < 9, which is consistent with one-electron, one-proton transfers [116].

Many research groups have attempted to tune the reactivity of the ruthenium complexes by changing the spectator ligands. For $[Ru^{IV}(tpy)(diamine)(O)]^{2+}$ [110, 116, 120, 121], the $E_{1/2}$ values for the Ru^{IV} / Ru^{III} and Ru^{III} / Ru^{II} couples fall in the order of diamine: tmea < bpy < dcbpy (tmea = N,N,N',N'-tetramethyl-1,2-ethylenediamine), which follows the order of their relative σ-donor strength. A comparison of the electrochemical data for some $[Ru^{IV}(L)(bpy)(O)]^{2+}$ complexes also reveals that replacement of the pyridyl ligands by Me_3tacn leads to a substantial decrease in $E_{1/2}$ values for the of the Ru^{IV}/Ru^{III} and Ru^{III}/Ru^{II} couples (in Table 1.1). At pH 7, $[Ru^{IV}(tpy)(bpy)(O)]^{2+}$ and $[Ru^{IV}(tpm)(bpy)(O)]^{2+}$ are more oxidizing than $[Ru^{IV}(Me_3tacn)(bpy)(O)]^{2+}$ by ca. 80 and 170 mV, respectively.

In the voltammograms recorded for the ruthenium aqua complexes in aqueous medium, it is noted that the Ru^{III}-OH / Ru^{II}-OH_2 couple is usually reversible with $E_{1/2}$ shifting cathodically by –60 mV per pH units. The size of the Ru^{IV}=O / Ru^{III}-OH, however, is usually much smaller than the Ru^{III}-OH / Ru^{II}-OH_2 couple and its reversibility is strongly affected by electrode surface conditions. The use of different

electrodes e.g. gold, platinum and glassy carbon electrodes will give different voltammograms for the Ru^{IV}=O/Ru^{III}-OH couple. This indicated that the electrochemical formation of Ru^{IV}=O from Ru^{III}-OH is kinetically slow. The slow kinetics of the formation of Ru^{IV}=O limits the applications of ruthenium oxo complexes as electrocatalysts.

Table 1.1 Summary of Formal Potentials for Selected Ru Complexes in Aqueous medium

Complex	$E_{1/2}$ (V vs. Ag/AgCl)			
	$E_{1/2}$ (III/II)	$E_{1/2}$ (IV/III)	pH	Ref.
$[Ru(tpy)(bpy)(H_2O)]^{2+}$	0.49	0.62	7.0	[116]
$[Ru(tpy)(tmea)(H_2O)]^{2+}$	0.35	0.54	7.0	[120]
$[Ru(tpy)(dcbpy)(H_2O)]^{2+}$	0.55	0.74	7.0	[110]
$[Ru(tpm)(bpy)(H_2O)]^{2+}$	0.40	0.71	7.0	[112]
$[Ru(tpm)(phen)(H_2O)]^{2+}$	0.41	0.71	7.0	[112]
$[Ru(Me_3tacn)(bpy)(H_2O)]^{2+}$	0.28	0.53	7.0	[111]
$[Ru(biq)(bpy)(PEt_3)(H_2O)]^{2+}$	0.48	0.69	6.8	[113]
$[Ru(bpy)_2(PMe_3)(H_2O)]^{2+}$	0.49	0.80	7.0	[122]
$[Ru(bpy)_2(PPh_3)(H_2O)]^{2+}$	0.50	0.76	7.0	[122]
$[Ru(tpy)((S)\text{-}bpop)(H_2O)]^{2+}$	0.41	0.54	6.86	[114]
$[Ru(bpy)(damp)(H_2O)]^{2+}$	0.61	0.75	7.0	[105]

tmea = N,N,N',N'-tetramethyl-1,2-ethylenediamine, tpm = tris(1-pyrazolyl)methane, tpy = 2,2':6,'2''-terpyridine, dcbpy = 6,6'-dichloro-2,2'-bipyridine, phen = 1,10-phenanthroline, Me_3tacn = 1,4,7-trimethyl-1,4,7-triazacyclononane, biq = 2,2'-biquinoline, (S)-bpop = 2,2-bis(2-(4-(S)-phenyl-1,3-oxazolinyl))propane, damp = 2,6-bis-((dimethylamino)methyl)pyridine)

Meyer and co-workers [123] have investigated the use of activated glassy carbon to promote the oxidation of Ru^{III}-OH to Ru^{IV}=O. Oxidative activation of glassy carbon electrodes leads to the catalysis of heterogeneous charge transfer for couples involving $[Ru^{III}(bpy)_2(H_2O)(OH)]^{2+}$ and $[Ru^{III}(NH_3)_5(OH)]^{2+}$ where there are changes in proton content upon oxidation. By comparing the spectral and electrochemical results, they suggested the basis for electrode activation may be the appearance of phenolic-like group on the glassy carbon surface and their subsequent involvement in proton-coupled electron transfer. Based on these results, Anson and co-workers [124, 125] have investigated the electrogeneration of Ru^{IV}=O species on edge-plane pyrolytic graphite electrode (EPG) and glassy carbon electrodes with adsorbed quinones, and rate enhancement was observed in some, but not all, cases. It is believed that the phenolic group on EPG facilitates the proton-coupled electro-oxidation reactions.

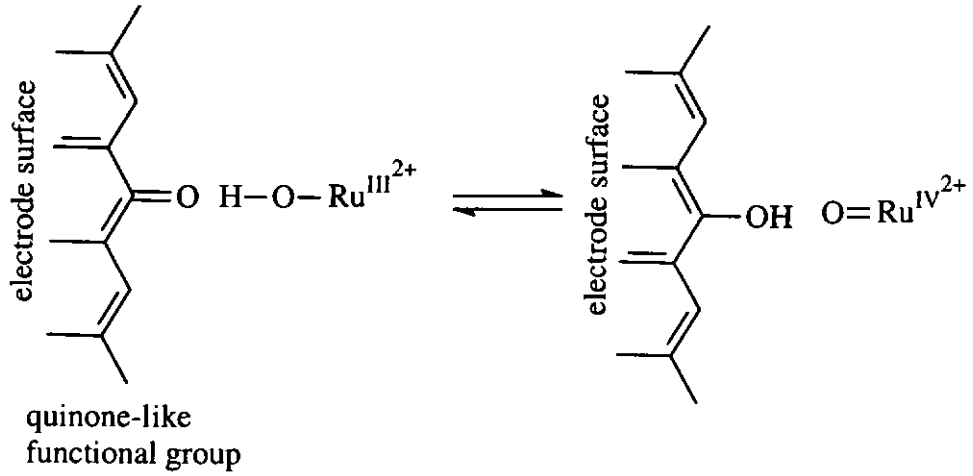

quinone-like
functional group

Meyer and co-workers then investigated the comproportionation reaction between $[Ru(bpy)_2(py)(O)]^{2+}$ and $[Ru(bpy)_2(py)(H_2O)]^{2+}$ to give $[Ru(bpy)_2(py)(OH)]^{2+}$. The reaction was found to occur at a rate constant of 2.1 x 10^5 $M^{-1}s^{-1}$ and a kinetic

isotope effect of $k(H_2O)/k(D_2O) = 16.1$ at 25°C. [73] The importance of proton transfer in the comproportionation reaction has thus been demonstrated. Recently, they have re-investigated the electrochemical oxidation of Ru^{II}-OH_2 to Ru^{IV}=O by using ruthenium complexes with a modified bipyridine ligand 4,4'-$(PO_3H_2)_2$bpy (4,4'-$(PO_3H_2)_2$bpy = 2,2'-bipyridyl-4,4'-diphosphonic acid) which allows the ruthenium complex to be covalently linked onto indium tin-oxide electrode surface.

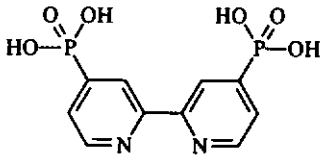

(4,4'-$(PO_3H_2)_2$bpy)

They found that the appearance of the Ru^{IV}/Ru^{III} couple depends on the loading of ruthenium complex on indium tin-oxide electrode. The Ru^{IV}/Ru^{III} couple only appears at high complex coverage of the electrode surface. Based on this observation, they purposed that the oxidation of Ru^{III}-OH to Ru^{IV}=O occurs via a disproportionation mechanism as follows

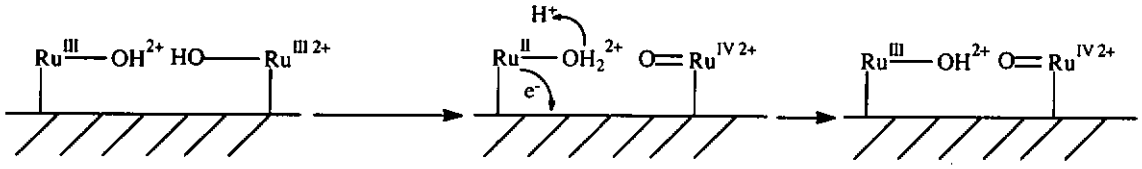

According to their proposal, the second couple assigned previously as Ru^{IV}/Ru^{III} arrives from the further oxidation of the Ru^{II}-OH_2 generated from the disproportionation reaction.

Besides ruthenium polypyridyl complexes, high valent *trans*-dioxo and *cis*-dioxo

Ru(VI) and Ru(V) complexes of macrocyclic tetramine ligands such as 2,3,2-tet, cyclam, [15]aneN$_4$ and [16]aneN$_4$ (2,3,2-tet = 3,7-diazanonane-1,9-diamine, cyclam = 1,4,8,11-tetraazacyclotetradecane, [15]aneN$_4$ = 1,4,8,12-tetraazacyclopentadecane, [16]aneN$_4$ = 1,4,8,11-tetraazacyclohexadecane) [126-128] have also been extensively investigated by Che and his co-workers. Similar to the polypyridyl complexes, the electrogeneration of Ru=O species from the ruthenium aqua macrocyclic complexes is also kinetically slow.

Whereas mono ruthenium complexes are active oxidants for various organic substrates, binuclear ruthenium oxo complexes are active catalysts for multi-electron processes such as the electrochemical generation of O_2 from H_2O. The most well known example is the μ-oxo ruthenium dimer $[(H_2O)(bpy)_2Ru^{III}\text{-}O\text{-}Ru^{III}(bpy)_2(OH_2)]^{4+}$ reported by Meyer and co-workers [129-131]. Recently, Tanaka and co-workers have also reported a binuclear complex $[Ru^{II}(3,6\text{-}^tBu_2q)(OH)(btpyan)(HO)(3,6\text{-}^tBu_2q)Ru^{II}]^{2+}$ (btpyan = 1,8-bis(2,2':6',2"-terpyridyl)anthracene, $^tBu_2q$ = 3,6-di-tert-butyl-1,2'-benzoquinone) [132, 133] that is active towards the electrocatalytic oxidation of water to dioxygen.

Several research groups have tried to immobilize the ruthenium complexes onto the electrode surface to fabricate chemically modified electrodes for electrocatalysis. Deronzier and co-workers [134-140] have designed several bipyridine-based ligands with pendant pyrrolyic groups. The ruthenium complexes of these ligands have been

prepared and they can be electropolymerized onto electrode surface by anodic oxidation of the pyrrole group. The immobilized ruthenium complexes have been used to catalyze alcohol oxidations [135, 141]. However, these ruthenium complexes can only be electropolymerized in non-aqueous medium such as dichloromethane or acetonitrile, and the resulting polymer films are electroinactive in aqueous medium. Thus the electrochemical formation of Ru^{IV}=O species, which requires the presence of water in the electrolyte, is prohibited.

1.3 Aims and Objectives of this Project

Ruthenium oxo complexes are potentially useful in electrocatalytic oxidation reactions. However, the slow kinetic in the electrogeneration of the ruthenium oxo species limits their applications. Based on the literature results and previous study in our laboratory, it appears that the kinetics for the electrochemical formation of Ru=O can be promoted by the presence of nearby functional groups such as quinones, which can facilitate the deprotonation of the Ru-OH species, and by the interaction of nearby Ru-OH species during the oxidation process. In this project, we aim at designing ruthenium catalysts with fast kinetics in oxo formation. Several approaches were adapted in our investigation.

(1) We have designed an electropolymerizable ligand containing both a dipyridylamine and a pyrrolyic unit, N-(3-N,N'-bis(2-pyridyl)propylamino) pyrrole (PPP). The synthetic procedures allow the preparation of the ligand in gram quantity method. The ruthenium aqua complex of this PPP ligand has been prepared. This ruthenium aqua complex can be electropolymerized in aqueous medium which is the first example in the literature. It is shown that the placement of a high concentration of ruthenium moieties in the polymer film would facilitate the formation of Ru=O species through interaction of nearby Ru-OH moieties. The results will be discussed in chapter 2 of this thesis.

(2) Previous studies have shown that ruthenium aqua complexes with 6,6'-dichloro-2,2'-bipyridine (dcbpy) have relatively fast kinetics on oxo formation [110]. We have obtained the X-ray crystal structure of $[Ru(tpy)(dcbpy)(H_2O)]^{2+}$ and *cis*-$[Ru(dcbpy)_2(H_2O)_2]^{2+}$. The correlation between structure and electrochemistry will be discussed in chapter 3 of the thesis.

(3) We have designed and synthesized two new binuclear ligands that contain two dipyridylamine units N,N,N',N'-tetra(2-pyridyl) ethylenediamine (ETHPY) and 1,8-bis(2,2-dipyridylamino) anthracene (BDPAA). The binuclear ruthenium aqua complexes of these two ligand have been prepared with the aim to promote the formation of Ru=O through the close interaction of two ruthenium moieties. The results will be discussed in chapter 4 of this thesis.

Chapter 2

Synthesis, Characterization and Electrochemical Studies of a Electropolymerizable Ruthenium Aqua Complex with Pyrrole - Functionalized 2,2'-Dipyridylamine

2.1 Introduction

Polypyridines are one of the most versatile classes of ligands in coordination chemistry. Various attempts have been made to prepare chemically modified electrodes for electrocatalysis by immobilizing these ligands and their metal complexes onto the electrode surface. Murrary, Meyer, Abruña, Pickup and Moutet have pioneered the area of the electrode surface modification with polypyridyl based transition metal complexes [142-148]. Their strategy is to add a vinyl substituent on the polypyridine ligand which can then be electropolymerized. Deronzier and co-workers has synthesized a number of polypyridine ligands with a pyrrole pendant group [140, 149-151]. They have also conducted extensive studies on the electropolymerization of the Ru [152-154], Re [149-151] and Mn [155, 156] complexes of these ligands. However, these pyrrole-containing polypyridine ligands are difficult to synthesize and the yields are often extremely low (only a few percent).

2,2'-Dipyridylamine (dpa) is a ligand closely related to 2,2'-bipyridine. It contains a –NH group bridging two pyridines in the ortho positions. There has been much interest in the coordination chemistry of 2,2'-dipyridylamine [157]. We reasoned that the amine nitrogen in this ligand can be easily functionalized to incorporate an electropolymerizable moiety such as a pendant pyrrolic unit. This has led us to design the synthesis of a novel ligand, N-(3-N,N'-bis(2-pyridyl)propylamino)pyrrole (PPP). We will report the synthesis of the PPP ligand and its ruthenium complexes in this

chapter. The electropolymerization process was probed by cyclic voltammetry in both aqueous and non-aqueous media.

2.2 Experimental Section

2.2.1 Synthesis

Materials

Ruthenium trichloride trihydrate, N-(2-cyanoethyl)pyrrole(97%), 2,2'-dipyridylamine (99%), $LiAlH_4$ (95%), 2,2':6',2"-terpyridine (tpy, 98%), 2,2'-bipyridine (bpy, 98%), lithium perchlorate (99%), tetrabutylammonium perchlorate (TBAP, 98%), silver *p*-toluene sulfonate (99%) and *t*-BuONa (97%) were purchased from Aldrich Co. BINAP (98%, racemic) was purchased from Strem Co. $[Ru(tpy)Cl_3]$ [116], [Ru(tpy)(bpy)Cl] [116], $Pd_2(dba)_3$ (dba = dibenzylideneacetone) [158] N-(3-aminopropyl)pyrrole [159, 160] were synthesized by literature reported methods.

Synthesis of ligands

N-(3-aminopropyl) pyrrole [159, 160]

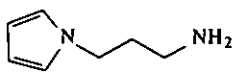

A solution of 5.0 g N-(2-cyanoethyl)pyrrole in 50ml dry diethyl ether was added very slowly to a slurry of $LiAlH_4$ (1.2 eq.) in 50 ml of dry diethyl ether. The mixture was gently heated at reflux under argon in darkness for 24 h. After cooling to room

temperature and chilled in an ice bath, 50 ml of double distilled water was added very slowly and cautiously (*Caution:* $LiAlH_4$ *reacts with water vigorously*). The aqueous layer was extracted with diethyl ether (3 × 50 ml). The combined organic layers were dried over anhydrous Na_2SO_4 and diethyl ether was then removed by rotary evaporation to yield pale brown oil. The crude product was distilled under vacuum to give a clear colourless oil. Yield: 3.1 g (62%). IR (cm^{-1}): 3369 (s), 3097 (s) 2931 (s), 1552 (m), 1501 (s), 1352 (s), 1280 (s), 1090 (s), 1060 (s), 727 (s) 653 (m), 618 (s). ^{1}H-NMR (C_6D_6, δ ppm): 6.45 (t, 2H), 6.31 (t, 2H), 3.39 (t, Pyr-CH_2CH_2-), 2.16(t, -CH_2NH_2), 1.28 (qnt, -$CH_2CH_2CH_2$-), 0.27 (br s, -CH_2NH_2). UV-vis(CH_2Cl_2/ λ_{max}, nm / ε, $M^{-1}cm^{-1}$): 295 (13500). ESI-MS *m/z*: 124 $(M+H)^+$.

N-(3-N,N'-bis(2-pyridyl)propylamino) pyrrole (PPP)

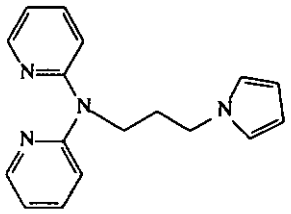

A mixture of 2-bromopyridine (5 mmol, 0.5 ml), N-(3-aminopropyl)pyrrole (6 mmol, 0.75 g), $Pd_2(dba)_3$ (0.2 mmol, 8 mmol% Pd, 90 mg), BINAP (0.2 mmol, 0.125 g) and *t*-BuONa (10 mmol, 0.67 g) was stirred at room temperature under argon for 5 minutes. A solution of 2-bromopyridine in toluene (0.5 ml of 2-bromopyridine in 45 ml toluene, 0.11 M) was added to the above mixture at room temperature. The resulting mixture was heated at 70 °C under argon for 16 h, and stirred at room temperature for another 4 h. After this period, 50 ml of diethyl ether was added, and the mixture was washed with saturated brine (3 × 50 ml). The organic layer was dried over anhydrous

sodium sulfate, and the solvents were removed under vacuum to give dark brown oil. The crude product was purified on a silica column using ethyl acetate/*n*-hexane (1:2) containing 0.5~1% triethylamine as eluent to give a yellow-brown oil. Yield: 0.75 g (45%) ^{1}H-NMR ($CDCl_3$, δ ppm): 8.34 (d, 2H), 7.48 (qnt, 2H), 7.03 (d, 2H), 6.84 (t, 2H), 6.61 (d, 2H), 6.13 (d, 2H), 4.22 (t, 2H), 3.95 (t, 2H), 2.18 (qnt, 2H). IR: 3369 (s), 3298 (m), 3121 (s), 3097 (s), 2931 (s), 2867 (s), 1599 (s), 1552 (s), 1501 (s), 1499 (m), 1280 (s), 1090 (s), 727 (s), 618 (s). ESI-MS: *m/z* 279 $(M+H)^+$, UV-Vis(CH_2Cl_2/ λ_{max}, nm / ε, $M^{-1}\,cm^{-1}$): 292 (18300).

Synthesis of ruthenium complexes

[Ru(tpy)(PPP)Cl]ClO_4

A mixture of 330 mg of [Ru (tpy)Cl_3] (0.75 mmol), 0.5 g of LiCl, 200 mg of N-(3-N,N'-bis(2-pyridyl)propylamino) pyrrole (PPP) (0.75 mmol) and 1.0 ml of triethylamine was gently refluxed under argon for 2.5 h in about 40 ml of absolute ethanol. After the mixture had been cooled to room temperature, the solution was filtered to remove any insoluble material. The filtrate was concentrated to about 5 ml and 20 ml of saturated $NaClO_4$ aqueous solution was added. Pale brown microcrystalline solid separated out upon standing which was collected by filtration, washed thoroughly with water and ether and dried in a vacuum oven. Yield: 0.52 g (93%) ^{1}H-NMR (CD_3CN, δ ppm): 9.54 (d, 1H), 836 (d, 2H), 8.30 (d, 2H), 8.16 (d,

2H), 8.05 (t, 1H), 7.87 (dt, 3H), 7.36 (dt, 5H), 6.75 (d, 1H), 6.67 (d, 1H), 6.57 (s, 2H), 6.40 (t, 1H), 6.00 (s, 2H), 3.85 (t, 2H), 3.36 (t, 2H), 1.05 (t, 2H). ESI-MS: *m/z* 747. IR (KBr pellet, cm^{-1}): 1599 (m, ν C=N), 1462 (s), 1486 (w), 1090 (s), 768 (m), 733 (m), 623 (m). UV-Vis (CH_3CN/ λ_{max}, nm / ε, $M^{-1}cm^{-1}$): 275 (27600), 318 (24300), 368 (sh), 503 (br) (5300). Elemental analysis for $C_{32}H_{29}N_7Cl_2O_4Ru$. Calcd : C, 51.4; H, 3.9; N, 13.1. Found: C, 51.8; H, 4.1; N, 13.3. ESI-MS *m/z*: 649 $(M+H)^+$ .Crystals suitable for X-ray diffraction study were obtained by diffusing diethyl ether to an acetonitrile solution of [Ru(tpy)(PPP)Cl](ClO_4).

[Ru(tpy)(PPP)(H_2O)](ClO_4)$_2$

A mixture of 0.24 g of [Ru(tpy)(PPP)Cl]ClO_4 and 0.13 g of silver *p*-toluenesulfonate was gently refluxed for 1 h in 40 ml of 1:3 acetone-water in the dark. After being cooled to room temperature, the mixture was filtered to remove the precipitated AgCl. 15 ml of $LiClO_4$ saturated solution was then added to the filtrate and the resulting mixture was chilled overnight in a refrigerator. The microcrystalline dark-red precipitate of $[Ru^{II}(tpy)(L)(H_2O)](ClO_4)_2$ was collected by filtration, washed with minimum amount of cold water and diethyl ether and air dried. Yield: 0.18 g (68.9%) IR (cm^{-1}, KBr pellet): 3440 (m), 3093 (w), 2972 (w), 2925 (w), 1633 (w), 1600 (w), 1463 (w), 1445 (s), 1093 (s), 769 (s), 624 (m). UV-Vis (H_2O/ λ_{max}, nm / ε, $M^{-1}cm^{-1}$): 273 (28420), 310 (27000), 350 (sh), 464 (br) (5000). Elemental analysis for $C_{32}H_{31}N_7Cl_2O_4Ru$. Calcd: C, 46.3; H, 3.7; N, 11.8. Found: C, 46.8; H, 3.5; N, 12.0.

ESI-MS *m/z*: 306 $(M\text{-}H_2O)^{2+}$

$[Ru(tpy)(PPP)(CH_3CN)](ClO_4)_2$

0.5 g of $[Ru(tpy)(PPP)(H_2O)](ClO_4)_2$ was dissolved in 30 ml of dry CH_3CN. The mixture was gently refluxed for 30 minutes in the dark. After being cooled to room temperature, the solvents were removed under vacuum. The microcrystalline dark-red precipitate of $[Ru(tpy)(PPP)(CH_3CN)][ClO_4]_2$ was collected by filtration. Yield: 0.46 g (90%). UV-Vis (CH_3CN/ λ_{max}, nm / ε, $M^{-1}cm^{-1}$): 271 (28820), 308 (27350), 354 (sh), 472 (br) (5000). Elemental analysis for $C_{35}H_{35}Cl_2N_8O_8Ru$. Calcd: C,48.5; H, 4.07; N, 12.91. Found: C, 49.2; H, 4.10; N, 12.85. ESI-MS *m/z*: 327 $(M)^{2+}$

$[Ru(tpy)(dpa)Cl]ClO_4$

The complex can be prepared by procedures similar to those of $[Ru(tpy)(PPP)Cl]ClO_4$. A mixture of 220 mg of $[Ru(tpy)Cl_3]$ (0.5 mmol), 0.5 g of LiCl, 85.5 mg of 2,2'-dipyridylamine (dpa) (0.5 mmol) and 1.0 ml of triethylamine was gently refluxed under argon for 1.5 h in about 40 ml of absolute ethanol. After the mixture had been cooled to room temperature, the solution was filtered to remove any insoluble material. The filtrate was concentrated to about 3 ml, and 20 ml of saturated $NaClO_4$ aqueous solution was added to the concentrated residue. Pale brown microcrystalline solid separated out upon standing which was collected by filtration, washed thoroughly with water and ether and dried in a vacuum oven. Yield: 0.32 g

(87%). IR (cm^{-1}, KBr pellet): 3430 (m), 2955 (w), 2923 (m), 2825 (w), 3093 (w), 1628 (m), 1601 (m), 1447 (s), 1420 (w), 1109 (s), 769 (s), 624 (w).). UV-Vis (CH_3CN/ λ_{max}, nm / ε, $M^{-1}cm^{-1}$): 239 (17700), 280 (18800), 310(sh) (15700), 492 (2200). Elemental analysis for $C_{25}H_{20}Cl_2N_6O_4Ru$. Calcd: C, 46.89; H, 3.15; N, 13.12. Found: C, 47.0; H, 3.2; N, 13.0. ESI-MS *m/z*: 542 $(M+H)^+$

2.2.2 Physical Measurements

Cyclic voltammetry was performed in a conventional two-compartment cell at room temperature. A glassy carbon of area 0.07 cm^2 (BAS M2070) was used as the working electrode. The counter electrode was a platinum wire loop and a Ag/AgCl (3.0 M NaCl) electrode (BAS M2074) was used as reference electrode. Cyclic voltammetry and chronocoulometry were performed with a BAS 100 B/W potentiostat controlled by a 586 microcomputer.

Non-aqueous electrochemistry was carried out in acetonitrile which was distilled over CaH_2 under vacuum. The $E_{1/2}$ of the ferrocenium / ferrocene couple ($Cp_2Fe^{+/0}$) measured in the solution was used as an internal reference.

UV-visible spectra were recorded on a Milton-Roy Spectronic 3000 diode array spectrophotometer. ^1H NMR spectra were obtained on a Brucker DPX-400 FT-NMR spectrometer. Chemical shifts (δ ppm) were reported relative to tetramethylsilane

(TMS). Electrospray-ionization mass spectra were recorded on a Finnigan mass spectrometer (MAT 95). SEM spectra were obtained on a Leica Stereoscan 440 scanning electron microscope. The samples for scanning electron microscopy were prepared by polymerizing ruthenium complex onto a demountable glassy carbon disk electrode, and the resulting polymer films were dried under an air blower and sputter coated with gold. Elemental analyses were performed by M-H-W Laboratories, Phoenix, AZ, USA.

X-ray Crystallography

A suitable crystal of each of the complexes was mounted on a Bruker CCD area detector using MoKα radiation (λ =0.71073 Å) from generator operating at 50KV, 30 mA condition. The intensity data of [Ru(tpy)(PPP)Cl](ClO_4) was collected in the range 0 to 180 degree. Frames of 1321 were taken in 4 shells. An empirical absorption correction of SADABS (Sheldrick, 1996) program based on Fourier coefficient fitting was applied. The crystal structures were determined by the direct method, yielding the positions of part of the non-hydrogen atoms, and subsequent difference Fourier syntheses were employed to locate all of the remaining non-hydrogen atoms which did not show up in the initial structure. Hydrogen atoms were located based on Difference Fourier Syntheses connecting geometrical analysis. All non-hydrogen atoms were refined anisotropically with weight function $W= 1/[\sigma^2(Fo^2)+0.1000p]^2+0.0000p$, where $p=(Fo^2+2Fc^2)/3$. Hydrogen atoms were refined with fixed individual displacement

parameters. All experiments and computations were performed on a Bruker CCD Area Detector Diffractometer and PC computer with the program of the Bruker Smart and Bruker Shelxtl packages. Further crystallographic details and selected bond distances and angles for [Ru(tpy)(PPP)Cl](ClO_4) can be found in the Results and Discussion section.

2.3 Results and Discussion

2.3.1 Synthesis and characterization

The synthesis of $[Ru(tpy)(L)Cl]^+$ (L = PPP, dpa) can be accomplished with high yield from the reaction between $[Ru(tpy)Cl_3]$ and L [116]:

$$[Ru^{III}(tpy)Cl_3] + L + e^- \xrightarrow{Et_3N} [Ru^{II}(tpy)(L)Cl]^+ + 2Cl^- \quad (2.1)$$

In this reaction, triethylamine acts as a base as well as a reducing agent to assist the dissociation of Cl^- from $[Ru^{III}(tpy)Cl_3]$. The ruthenium complex was isolated as perchlorate salt and fully characterized by ^{1}H-NMR, IR, UV-Vis, mass spectrometry and elemental analysis.

The monomeric ruthenium complex has similar electronic spectroscopic properties to the bpy or dpa analogues. A summary of the electronic absorption spectral data is given in Table 2.1. The spectra of the different complexes are shown in Fig. 2.1. The incorporation of PPP in place of bpy or dpa in the ruthenium complexes does not result in any significant changes in the electronic spectrum. The Ru ($d\pi$)→tpy (π^*) transition appears to overlap with the Ru ($d\pi$)→L (π^*) charge transfer bands resulting in a very broad absorption band centered at round 500 nm. The similarity in the electronic spectrum of $[Ru(tpy)(PPP)Cl]^+$ and $[Ru(tpy)(dpa)Cl]^+$ suggests that the grafted pyrrolic

group with saturated carbon chain on the N atom of the dpa ligand introduces only minor perturbation to the dpa unit.

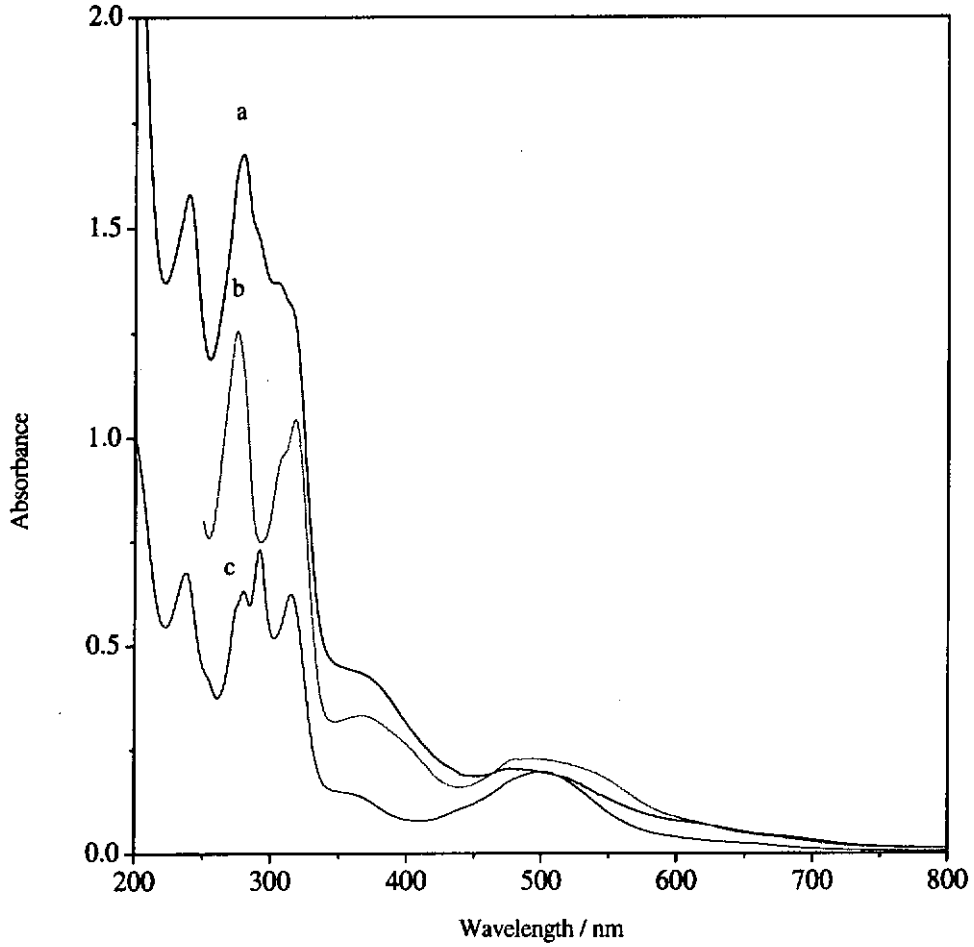

Fig 2.1 Electronic absorption spectra for $[Ru(tpy)(PPP)(Cl)]^+$, $[Ru(tpy)(dpa)(Cl)]^+$ and $[Ru(tpy)(bpy)(Cl)]^+$ in CH_3CN at room temperature.

a: [Ru(tpy)(PPP)(Cl)], b: $[Ru(tpy)(dpa)(Cl)]^+$ c: $[Ru(tpy)(bpy)(Cl)]^+$

Table 2.1 Electronic absorption spectroscopic data for the $[Ru(tpy)(L)Cl]^+$ [a]

Complex	Wavelength (nm)	ε ($M^{-1}cm^{-1}$)	Assignment
$[Ru(tpy)(PPP)Cl]^+$	238	2.76×10^4	L: π-π^*
	279	2.93×10^4	tpy: π-π^*
	318	2.43×10^4	tpy: π-π^*
	503	0.53×10^4	MLCT
$[Ru(tpy)(bpy)Cl]^+$	237	2.44×10^4	π-π^*
	280	2.27×10^4	π-π^*
	291	2.64×10^4	π-π^*
	315	2.25×10^4	tpy: π-π^*
	501	0.71×10^4	MLCT
$[Ru(tpy)(dpa)Cl]^+$	239	1.77×10^4	π-π^*
	280	1.88×10^4	π-π^*
	310 (sh)	1.57×10^4	tpy: π-π^*
	492	0.22×10^4	MLCT

[a] Recorded at room temperature in acetonitrile solution.

PPP = N-(3-N,N'-bis(2-pyridyl)propylamino)pyrrole, bpy = 2,2'-bipyridine,

tpy = 2,2':6',2"-terpyridine, dpa = 2,2'-dipyridylamine

2.3.2 X-ray structural determination of $[Ru^{II}(tpy)(PPP)Cl]ClO_4$

The ORTEP plot of ruthenium complex $[Ru^{II}(tpy)(PPP)Cl]^+$ is depicted in Figure 2.2. Crystallographic data are summarized in Table 2.2. Selected bond distances and angles are tabulated in Tables 2.3 and 2.4 respectively.

The ruthenium coordination environment is a distorted octahedron with the tpy ligand coordinated, as expected, in meridional fashion, the L ligand in *cis* fashion, and the chloride atom *trans* to one of the PPP nitrogen atoms. The angle of N(1)-Ru(1)-N(3) is approximately 159° and shortening of the Ru(1)-N(2) distance to the central pyridyl of approximately 0.1 Å with respect to Ru-N distances to the two outer pyridyl rings are typical features observed in the structure of other Ru(II) terpyridine complexes [103, 161-166]. The N(4)-Ru-N(5) bond angle in $[Ru(tpy)(PPP)Cl]^+$ (86.18(5)°)is 7° larger than that in $[Ru(tpy)(bpz)Cl]^+$ (78.92(6)°) (bpz=2,2'-bipyrazine) [167].

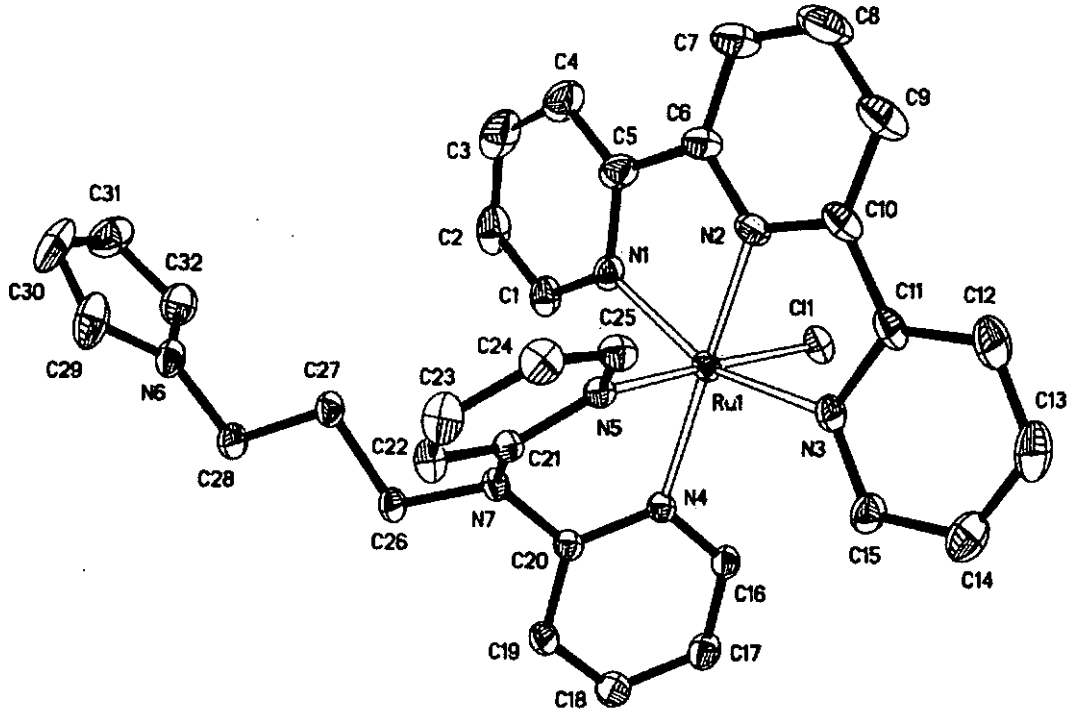

Fig. 2.2 A perspective view of $[Ru(tpy)(PPP)Cl]^+$ with atom numbering.

Table 2.2 The crystal and structure determination data of [Ru(tpy)(PPP)Cl]ClO_4•CH_3CN

	[Ru (tpy) (PPP)Cl]ClO_4•CH_3CN
Fomula	$RuC_{32}H_{29}N_7Cl$•ClO_4•CH_3CN
Formula weight	788.65
Crystal system	Triclinic
a (Å)	8.835(1), $\alpha = 78.695(3)^o$
b (Å)	13.821(5), $\beta = 81.211(2)^o$
c (Å)	15.308(3), $\gamma = 72.176(2)^o$
V ($Å^3$)	1736.5
Density (calculated) (Mg/m^3)	1.508
Absorption coefficient (mm^{-1})	0.656
Reflections collected	16442
Independent reflections	7844
Crystal size (mm)	0.18 x 0.14 x 0.12
θ range for data collection (^{o})	1.91 to 27.56
Largest diff and hole $e^-Å^{-3}$	0.87 and –0.567
Completeness to θ	97.6 %
Absorption correction	SADABS
Max. and min. transmission	0.948 and 0.932
Refinement method	Full-matrix least-squares on F^2
Temperature (K)	293(2)
R	0.0494
WR2	0.1281
F(000)	804
Goodness-of-fit on F^2	0.857

Table 2.3 Selected bond distance (Å) of [Ru (tpy)(PPP)Cl]ClO_4•CH_3CN

Ru-Cl	2.4130(5)	N(4)-C(20)	1.3429(19)
Ru-N(1)	2.0702(11)	N(7)-C(20)	1.4043(19)
Ru-N(2)	1.9586(11)	N(7)-C(21)	1.4113(16)
Ru-N(3)	2.0698(11)	N(5)-C(21)	1.3578(18)
Ru-N(4)	2.1058(10)	N(6)-C(28)	1.453(2)
Ru-N(5)	2.0730(13)	N(6)-C(29)	1.357(3)
N(6)-C(32)	1.359(2)	N(7)-C(26)	1.4927(18)

Table 2.4 Selected bond angle (°) of [Ru (tpy)(PPP)Cl]ClO_4•CH_3CN

Cl-Ru-N(1)	89.62(4)	Cl-Ru-N(2)	87.33(5)
Cl-Ru-N(3)	87.98(4)	Cl-Ru-N(4)	92.22(4)
Cl-Ru-N(5)	178.09(3)	N(1)-Ru-N(2)	79.57(5)
N(1)-Ru-N(3)	159.08(5)	N(1)-Ru-N(4)	101.73(4)
N(1)-Ru-N(5)	91.73(5)	N(2)-Ru-N(3)	79.56(5)
N(2)-Ru-N(4)	178.63(5)	N(2)-Ru-N(5)	94.25(5)
N(3)-Ru-N(4)	99.13(4)	N(3)-Ru-N(5)	91.23(5)
N(4)-Ru-N(5)	86.18(5)	Ru-N(1)-C(5)	113.79(9)
Ru-N(2)-C(6)	118.83(10)	Ru-N(2)-C(10)	118.55(10)
Ru-N(1)-C(1)	129.28(10)	Ru-N(3)-C(11)	113.01(9)
Ru-N(3)-C(15)	129.15(10)	Ru-N(4)-C(16)	119.94(10)
Ru-N(4)-C(20)	122.25(9)	Ru-N(5)-C(21)	112.82(9)
Ru-N(5)-C(25)	119.94(10)	C(20)-N(7)-C(21)	119.94(10)
N(1)-C(5)-C(6)	114.42(13)	C(5)-C(6)-N(2)	113.31(13)
N(2)-C(10)-C(11)	113.52(13)	C(10)-C(11)-N(3)	114.93(13)
C(4)-C(5)-C(6)	123.54(15)	C(5)-C(6)-C(7)	127.60(16)
C(9)-C(10)-C(11)	126.80(16)	C(10)-C(11)-C(12)	123.68(15)
C(21)-N(7)-C(26)	117.21(12)	C(20)-N(7)-C(26)	115.42(10)
C(28)-N(6)-C(32)	126.24(16)	C(28)-N(6)-C(29)	126.17(15)
C(29)-N(6)-C(32)	107.58(15)		

2.3.3 Electrochemical behaviour of the ruthenium complexes

Cyclic voltammograms of the ruthenium complexes in non-aqueous medium

The cyclic voltammogram of $[Ru(tpy)(PPP)Cl]^+$ in CH_3CN is shown in Figure 2.3. A reversible couple is observed at 0.81 V *vs.* Ag/AgCl. The stoichiometry of the redox process (n = 1.0) was established by controlled potential coulometry. A comparison of the $E_{1/2}$ value of the Ru^{III}/Ru^{II} couple with those of analogues Ru complexes for the three complexes is given in Table 2.5. The $E_{1/2}$ for the Ru^{III}/Ru^{II} couple decreases in the order $[Ru(tpy)(bpy)Cl]^+ > [Ru(tpy)(PPP)Cl]^+ \sim [Ru(tpy)(dpa)Cl]^+$. This is consistent with the sequence of π-acidity which follows the order bpy > PPP ~ dpa.

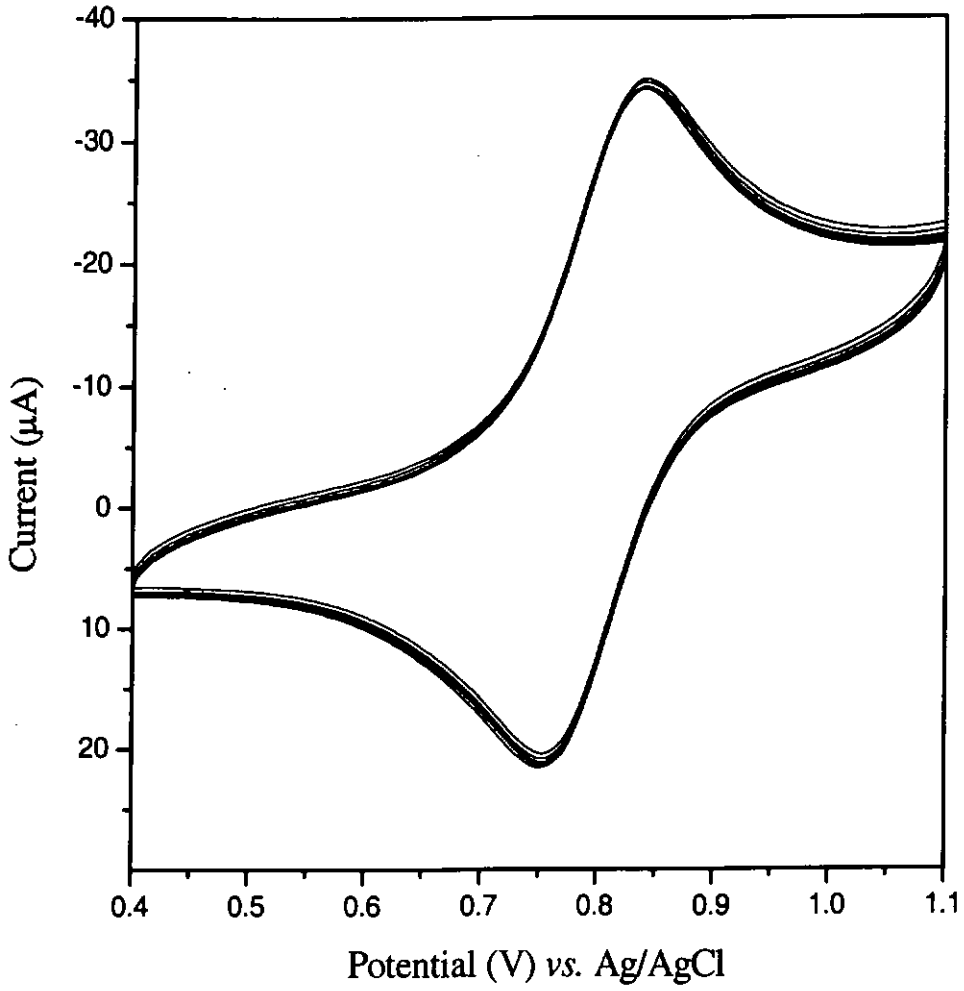

Fig. 2.3 Cyclic voltammograms of 0.5 mM $[Ru(tpy)(PPP)Cl]^+$ in 0.1 M TBAP + CH_3CN recorded below the pyrrole polymerization potential. Working electrode: 0.196 cm^2 glassy carbon. Scan rate: 100 mVs^{-1}

Table 2.5 Cyclic voltammetric data of the ruthenium complexes

Complex	$E_{1/2}$ of Ru^{III}/Ru^{II} couple (V *vs.* Ag/AgCl)	ΔE_p (mV)
$[Ru(tpy)(bpy)Cl]^+$	0.83 [168]	63
$[Ru(tpy)(PPP)Cl]^+$	0.79	57
$[Ru(tpy)(dpa)Cl]^+$	0.76	80

The ferrocenium/ferrocene couple was found to be 0.41 V vs. the Ag/AgCl

Electropolymerization of $[Ru(tpy)(PPP)Cl]^+$ and $[Ru(tpy)(PPP)(CH_3CN)]^{2+}$ in non-aqueous medium

The cyclic voltammograms of $[Ru(tpy)(PPP)Cl]^+$ and $[Ru(tpy)(PPP)(CH_3CN)]^{2+}$ were recorded in acetonitrile, dichloromethane and ethanol solution. Figure 2.4 shows the successive cyclic voltammetric scans of $[Ru(tpy)(PPP)Cl]^+$ in acetonitrile. In the first scan, a reversible couple with $E_{1/2}$ = 0.79 V is observed which corresponds to the Ru^{III}/Ru^{II} couple. Scanning the potential further towards the anodic direction leads to the appearance of an irreversible anodic peak at $E_{p,a}$ = 1.35 V which is assignable to the irreversible oxidation of the pyrrolic unit. After the first voltammetric scan, a new reversible couple starts to develop at 1.24 V upon repetitive scanning. The size of this couple is smaller than the $[Ru^{III}(tpy)(PPP)Cl]^{2+}/[Ru^{II}(tpy)(PPP)Cl]^+$ couple. Subsequent repetitive scans produce a significant increase of both couples at 0.79 V and 1.24 V. The increase in current upon repetitive scanning indicates the deposition of an electroactive film on the electrode surface, which is an evidence for film growing. This polymer film is stable and shows good adherence on the electrode surface as shown by the voltammogram of the polymer-coated electrode in pure supporting electrolyte (Figure 2.5). The electropolymerization of $[Ru^{II}(tpy)(PPP)Cl]^+$ is believed to proceed via radical-radical coupling of the pyrrole moieties accompanied by release of protons. Figure 2.6 shows the mechanism of pyrrole polymerization.

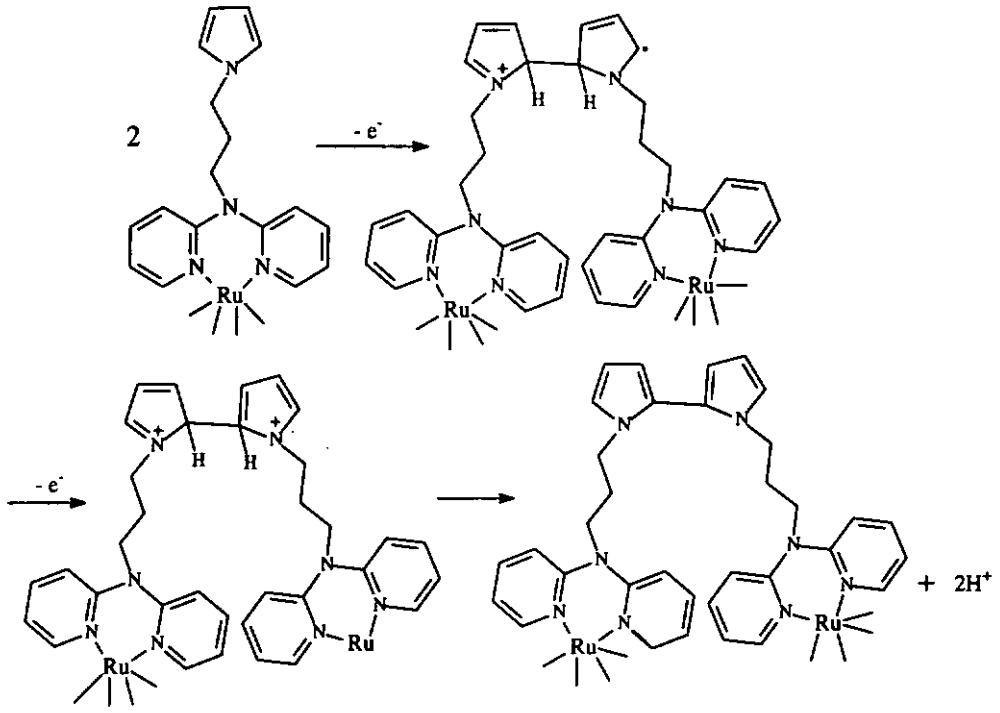

Figure 2.6 Mechanism of pyrrole polymerization.

The new couple at 1.24 V does not appear when $[Ru(tpy)(PPP)Cl]^+$ is polymerized in dichloromethane. Only one reversible couple assignable as the $[Ru^{III}(tpy)(PPP)Cl]^{2+}/[Ru^{II}(tpy)(PPP)Cl]^+$ couple at 0.8 V was observed in the cyclic voltammogram recorded in CH_2Cl_2 (Figures 2.6 and 2.7). The second couple at 1.24 V in the cyclic voltammogram recorded in CH_3CN is likely due to the substitution of chloride ligand by the solvent acetonitrile. To confirm our postulation, we have synthesized the complex $[Ru(tpy)(PPP)(CH_3CN)](ClO_4)_2$. Figures 2.8 shows the cyclic voltammograms of $[Ru(tpy)(PPP)(CH_3CN)]^{2+}$ in acetonitrile which indicate a reversible $[Ru^{III}(tpy)(PPP)(CH_3CN)]]^{3+}/[Ru^{II}(tpy)(PPP)(CH_3CN)]^{2+}$ couple at 1.24 V. This supports our argument that the second couple at in Figure 2.4 is due to the formation of $[Ru^{II}(tpy)(PPP)(CH_3CN)]^{2+}$. The appearance of this new couple is a result of the substitution of the chloride ligand by acetonitrile upon successive oxidation

and reduction, as Ru(II) complexes are known to be substitutionally labile. This agrees with the observation that no $[Ru^{III}(tpy)(PPP)(CH_3CN)]^{3+}/[Ru^{II}(tpy)(PPP)(CH_3CN)]^{2+}$ couple was observed in the first cycle in Figure 2.4 and the couple only gradually developed from the second cycle onwards. When the complex is polymerized in dichloromethane, only one reversible couple appears. This is because dichloromethane is a much weaker ligand than CH_3CN and it cannot displace the Cl^- anion in the ruthenium coordination sphere.

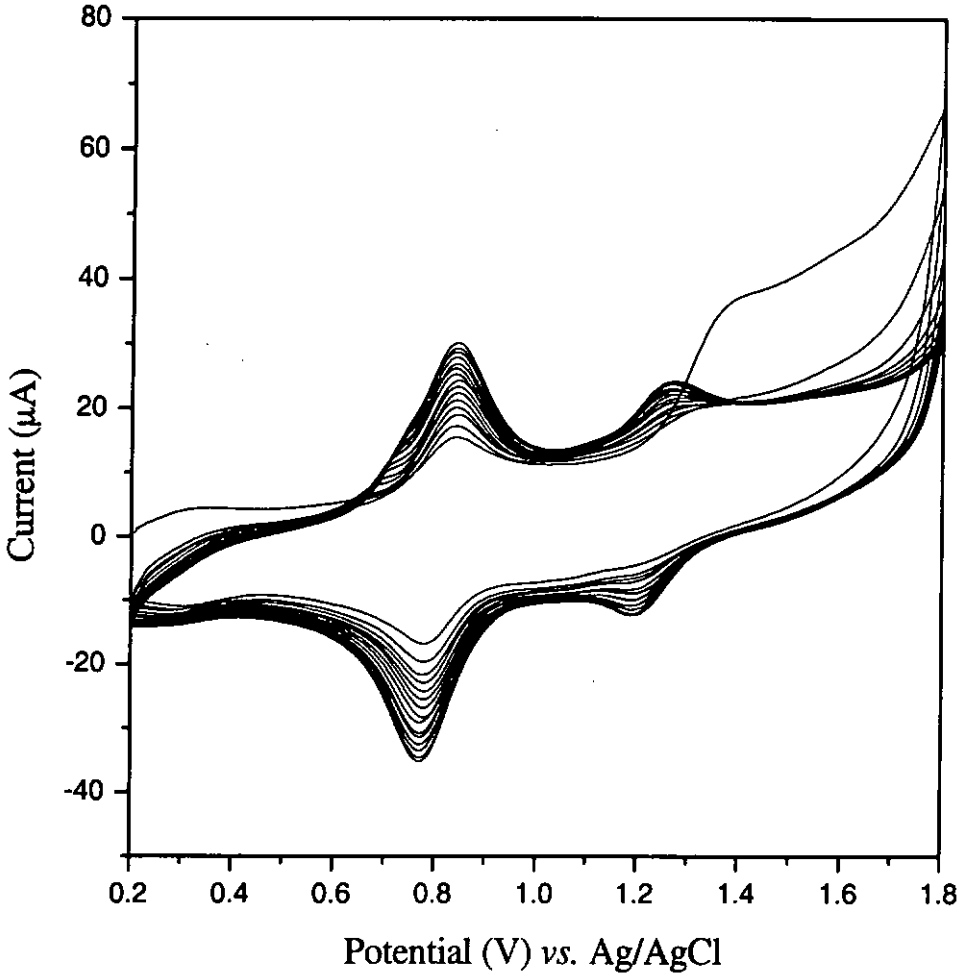

Fig 2.4 Cyclic voltammograms of 0.5 mM $[Ru(tpy)(PPP)Cl]^+$ in 0.1 M TBAP + CH_3CN. Working electrode: 0.196 cm^2 glassy carbon. Scan rate: 100 mVs^{-1}

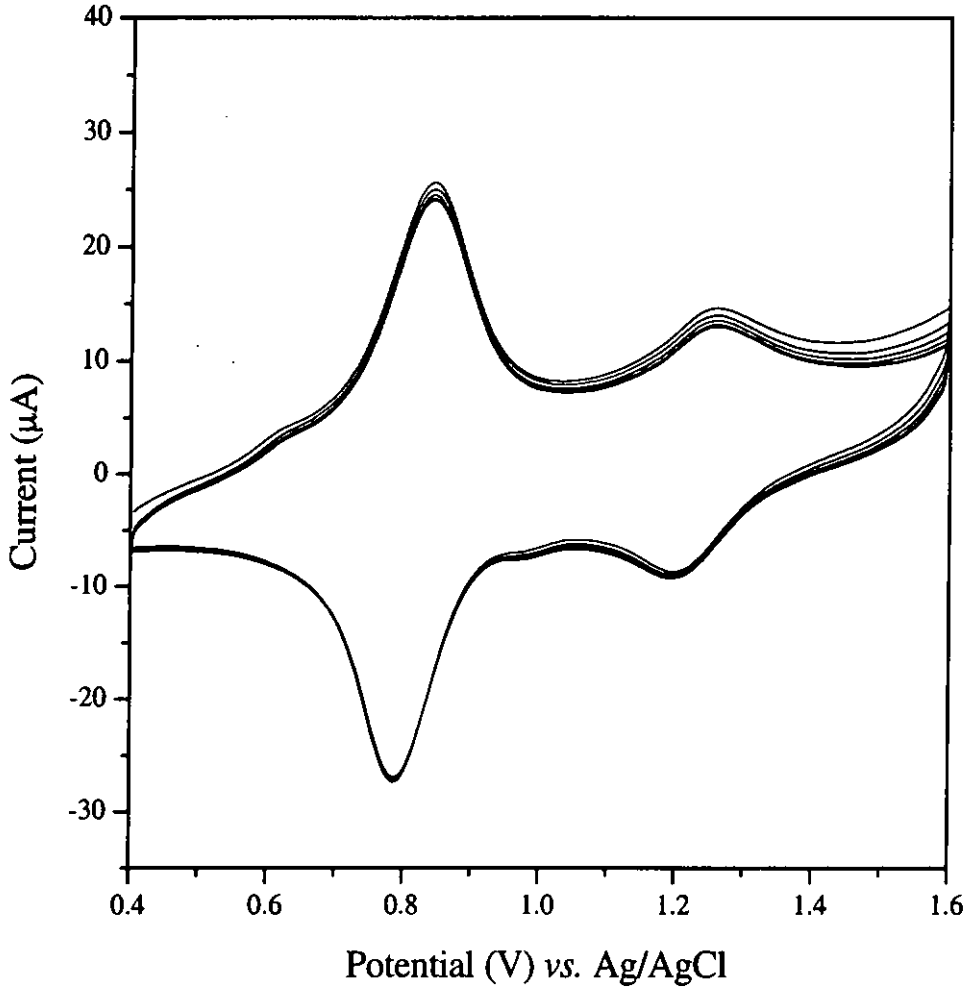

Fig 2.5 Cyclic voltammograms of poly[Ru(tpy)(PPP)Cl]$^{n+}$ in 0.1 M TBAP + CH_3CN.

Working electrode: 0.196 cm^2 glassy carbon. Scan rate: 100 mVs^{-1}

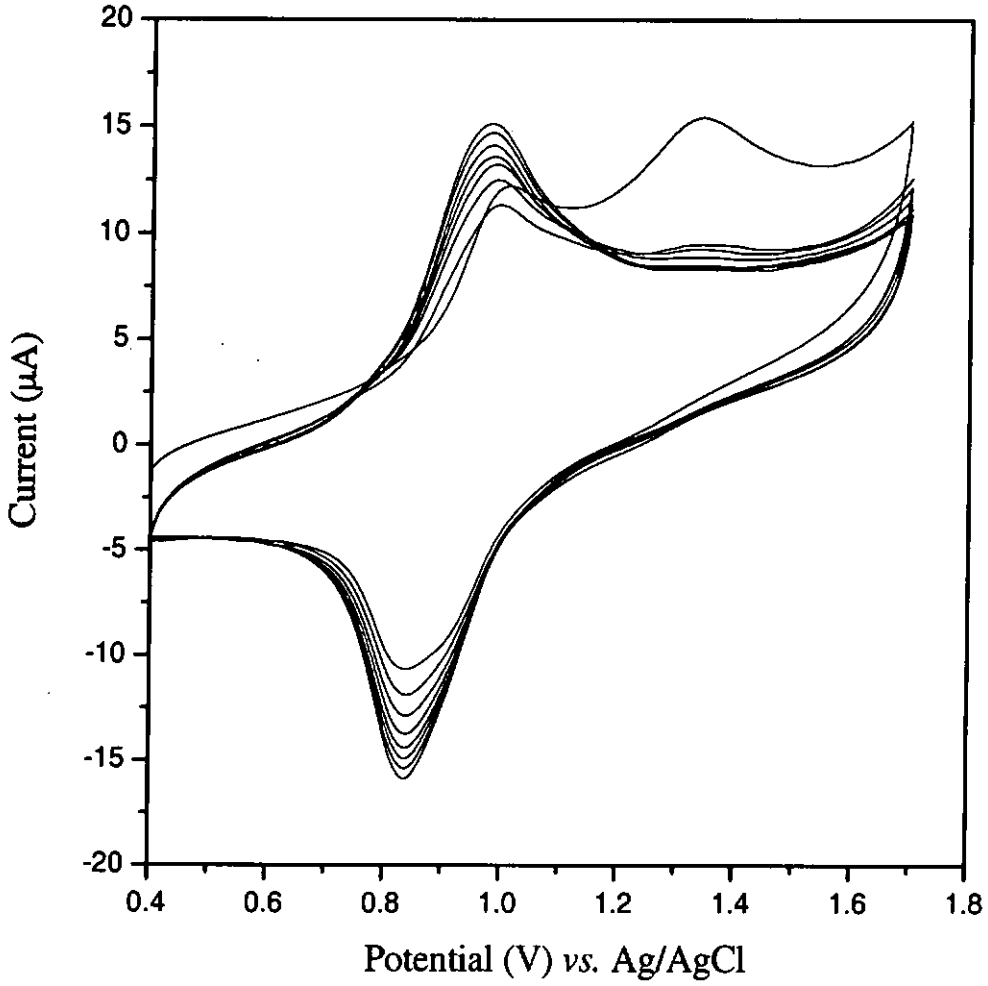

Fig 2.6 Cyclic voltammograms of 0.5 mM $[Ru(tpy)(PPP)Cl]^+$ in 0.1 M TBAP + dichloromethane. Working electrode: 0.196 cm^2 glassy carbon. Scan rate: 100 mVs^{-1}

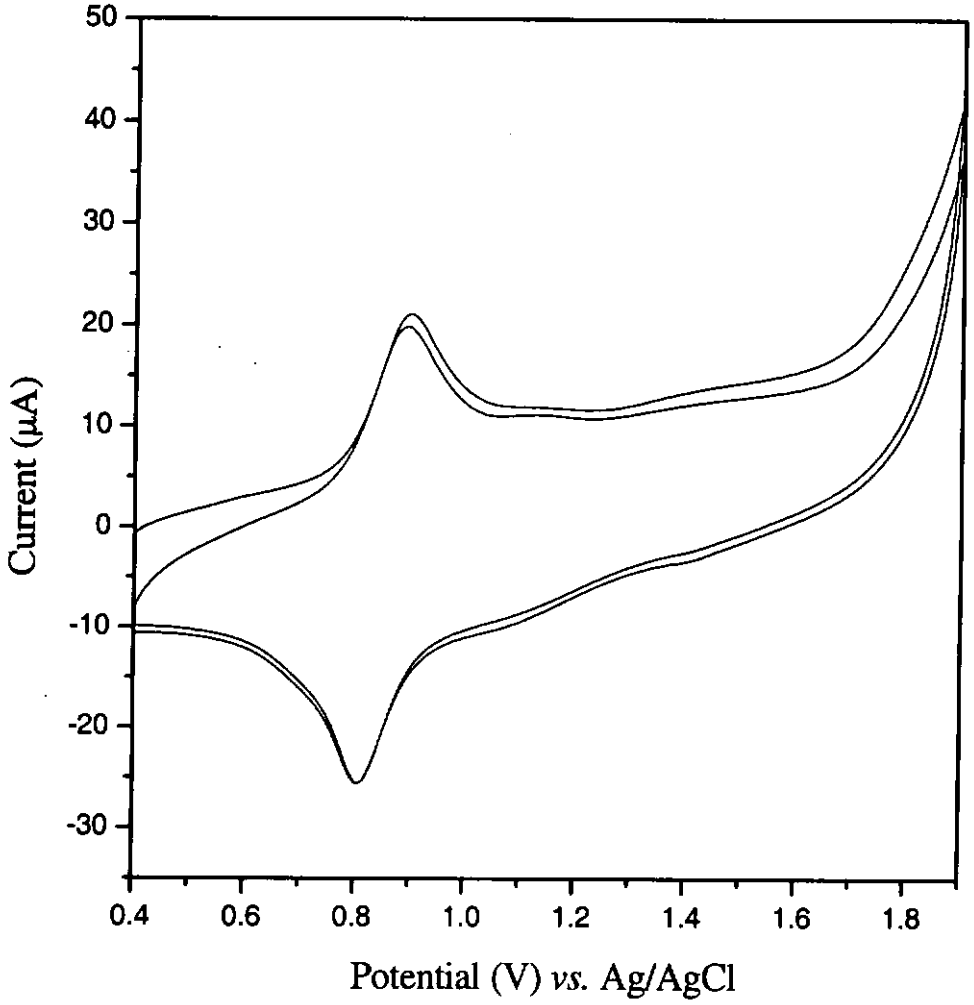

Fig 2.7 Cyclic voltammograms of poly[Ru(tpy)(PPP)Cl]$^{n+}$ in 0.1 M TBAP + dichloromethane. Working electrode: 0.196 cm^2 glassy carbon. Scan rate: 100 mVs^{-1}

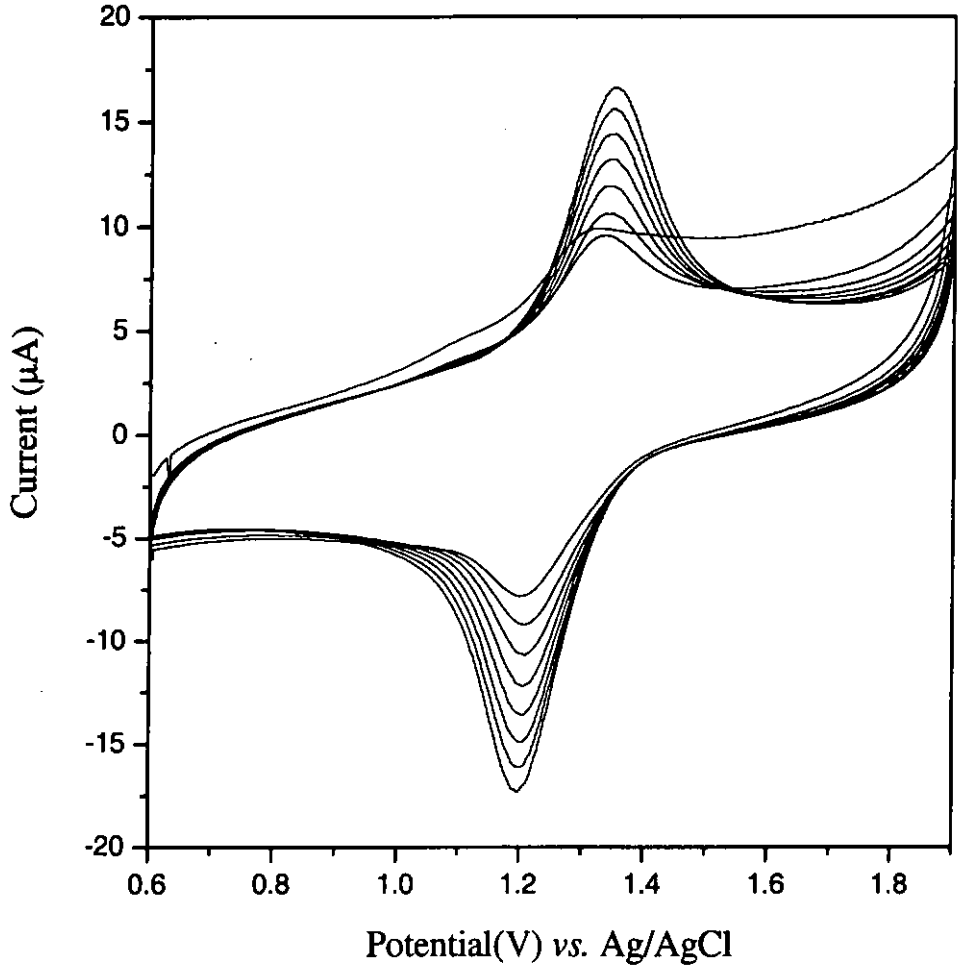

Fig 2.8 Cyclic voltammograms of 0.5 mM $[Ru(tpy)(PPP)(CH_3CN)]^{2+}$ in 0.1 M TBAP + CH_3CN. Working electrode: 0.196 cm^2 glassy carbon. Scan rate: 100 mVs^{-1}

Electrochemistry of $[Ru(tpy)(PPP)(H_2O)]^{2+}$ in Ethanol

The electrochemical behaviour of $[Ru(tpy)(PPP)(H_2O)](ClO_4)_2$ in ethanol was investigated by cyclic voltammetry. In the first scan, an irreversible anodic peak is observed at about 1.2 V corresponding to the oxidation of the pyrrolic unit. After the first scan, only one couple is observed at $E_{1/2}$ = 0.95 V which is assignable as the Ru^{III}/Ru^{II} couple (Figure 2.10). The following consecutive scans produce a significant increase of the metal-based peak indicating the formation of a polymer film. Figure 2.11 shows the cyclic voltammograms for the polymer film when transferred to a blank electrolyte solution. No waves of the polypyrrole backbone are observed since the polymer was obtained in its overoxidized form during anodic polymerization [136]. The metal-based peaks are clearly observed with the Ru^{III}/Ru^{II} couple at $E_{1/2}$ = 0.95 V. As ^1H NMR data in C_2D_5OD showed that the aqua ligand in $[Ru(tpy)(PPP)(H_2O)]^{2+}$ exchanges rapidly with the solvent molecules, the polymer obtained in ethanol is likely to be poly$[Ru(tpy)(PPP)(C_2H_5OH)]^{n+}(ClO_4)_n$.

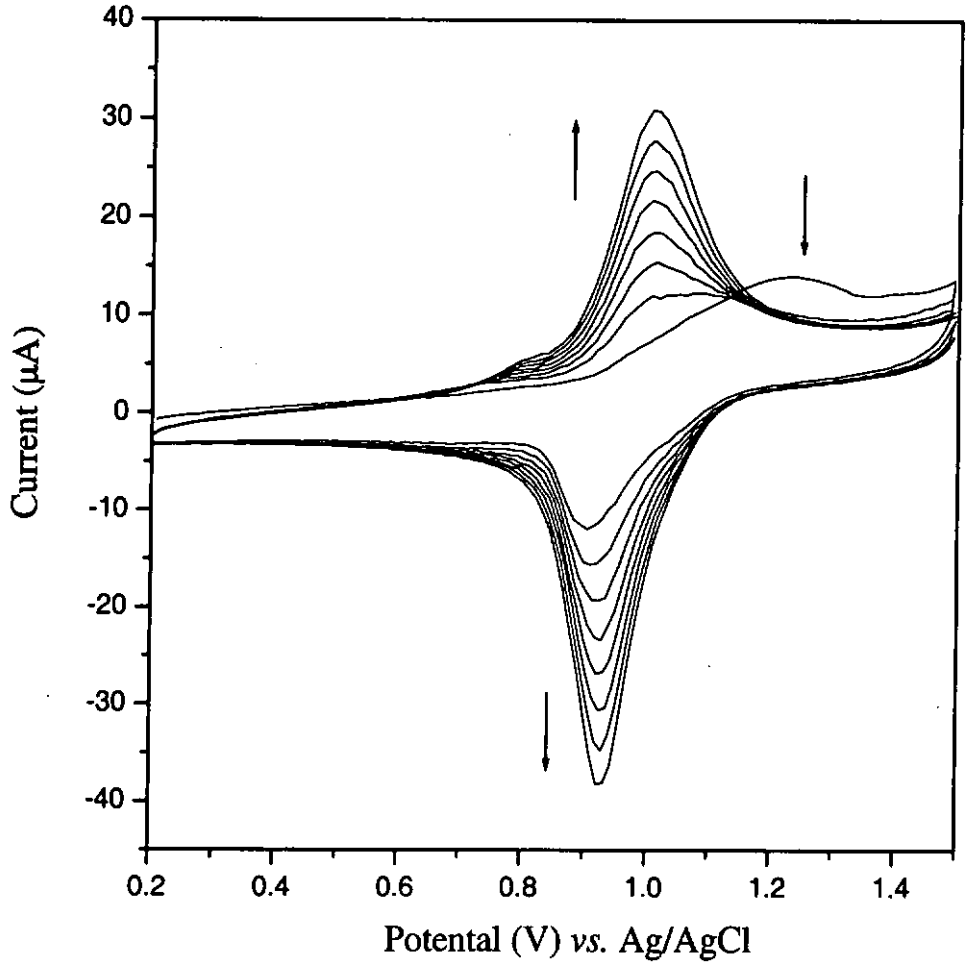

Fig 2.10 Cyclic voltammograms of 0.5 mM $[Ru(tpy)(PPP)(H_2O)]^{2+}$ in 0.1 M TBAP + EtOH. Working electrode: 0.196 cm^2 glassy carbon. Scan rate: 100 mVs^{-1}

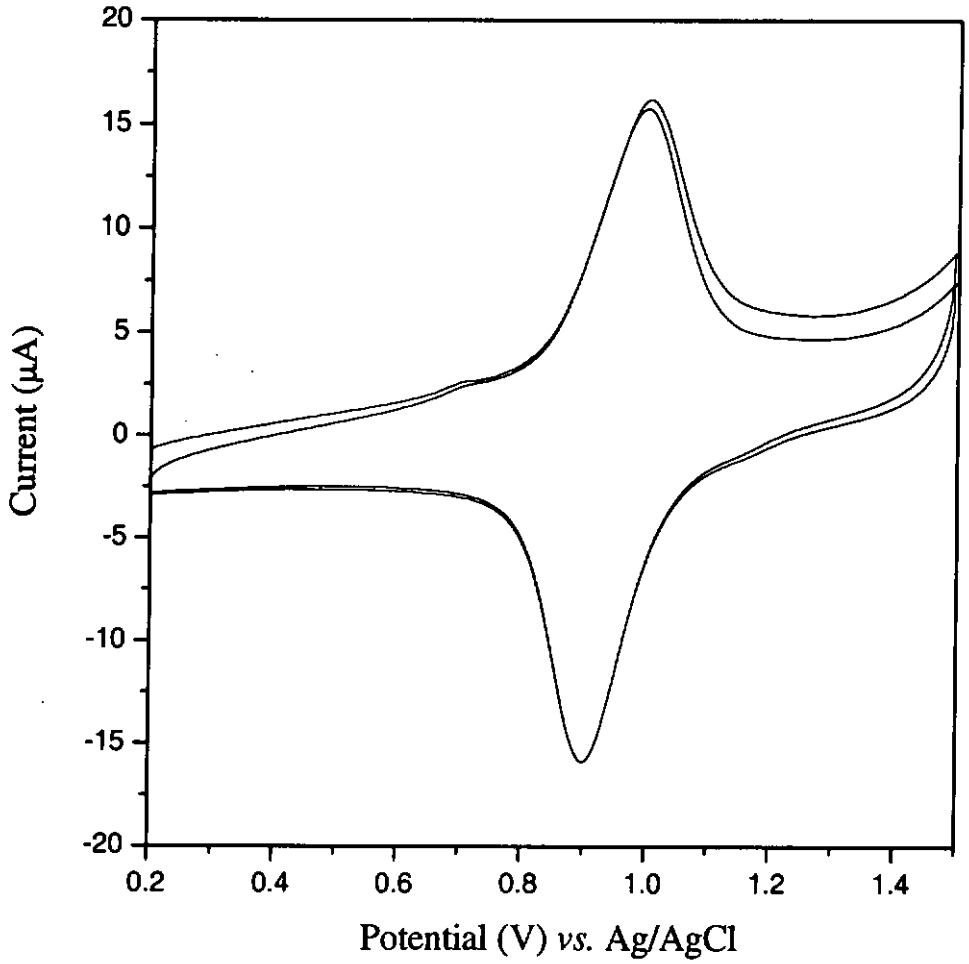

Fig.2.11 Cyclic voltammograms of poly[Ru(tpy)(PPP)(H_2O)]$^{n+}$ in 0.1 M TBAP + EtOH.

Working electrode: 0.196 cm^2 glassy carbon. Scan rate: 100 mVs^{-1}

Electropolymerization of the ruthenium complex in aqueous medium

The monomer $[Ru(tpy)(PPP)(H_2O)]^{2+}$ can be electropolymerized onto glassy carbon electrode in aqueous medium by scanning the potential repeatedly from 0 to 1.3V in 0.1 M $HClO_4$ solution (Fig. 2.12). This is the first report on the electropolymerization of a pyrrole-containing ruthenium complex in aqueous medium. The polymerization in all other reports in the literature were done in non-aqueous solvents. In the first cycle, an anodic peak with low current is observed at $E_{p,a}$ = 0.86 V corresponding to the oxidation of Ru(II) to Ru(III). A second wide peak with much higher anodic peak is also observed at $E_{p,a}$ = 0.98 V corresponding to the irreversible oxidation of the pyrrolic unit. The voltammetric reverisible couple Ru^{III}/Ru^{II} increases continuously upon repetitive scan, indicating the growth of a poly$[Ru(tpy)(PPP)(H_2O)]^{n+}$ film on the electrode surface. After the first cycle, two reversible couples are observed, one at $E_{1/2}$ = 0.8 V and the other at $E_{1/2}$ = 0.89 V. The subsequent consecutive scans produce a significant increase in size of both couples due to the formation of the polymer on the electrode surface. The couple with $E_{1/2}$ = 0.89 V corresponds to further oxidation of the metal center from Ru(III) to Ru(IV).

The cyclic voltammograms of $[Ru(tpy)(PPP)(H_2O)](ClO_4)_2$ were different in aqueous and non-aqueous medium. In aprotic medium, the oxidation of Ru(II) to Ru(III) occurs via the reaction

$$[Ru^{II}(tpy)(PPP)(R)]^{2+} \rightleftharpoons [Ru^{III}(tpy)(PPP)(R)]^{3+} + e^-$$

where R is the solvent molecule, such as CH_3CN and EtOH, replacing the aqua ligand.

In protic medium, the Ru(II) metal centre can be oxidized to Ru(III) by loss of one electron and one proton to form a Ru(III) hydroxo couple, which can then be further oxidized to give a Ru(IV) oxo species

Figure 2.13 shows the Pourbaix plot of the $E_{1/2}$ values of both couples against pH. From the Pourbaix diagram, it can be seen that at pH < 1.7, the slope for the Ru^{III}/Ru^{II} couple is zero, whereas that for the Ru^{IV}/Ru^{III} couple is 120 mV/pH.

pH < 1.7

$$[Ru^{III}(tpy)(PPP)(OH_2)]^{2+} + e^- \rightleftharpoons [Ru^{II}(tpy)(PPP)(OH_2)]^{2+}$$

$$[Ru^{IV}(tpy)(PPP)(O)]^{2+} + e^- + 2H^+ \rightleftharpoons [Ru^{III}(tpy)(PPP)(OH_2)]^{2+}$$

From pH 1.7 to 10, the slope for both the Ru^{III}/Ru^{II} and the Ru^{IV}/Ru^{III} couples in the Pourbaix diagram are equal to 60 mV/pH

1.7< pH < 10

$$[Ru^{III}(tpy)(PPP)(OH)]^{2+} + e^- + H^+ \rightleftharpoons [Ru^{II}(tpy)(PPP)(OH_2)]^{2+}$$

$$[Ru^{IV}(tpy)(PPP)(O)]^{2+} + e^- + H^+ \rightleftharpoons [Ru^{III}(tpy)(PPP)(OH)]^{2+}$$

At pH > 10, the slope for the Ru^{III}/Ru^{II} becomes zero, indicating the $E_{1/2}$ of the process becomes pH independent.

pH > 10

$$[Ru^{III}(tpy)(PPP)(OH)]^{2+} + e^- \rightleftharpoons [Ru^{II}(tpy)(PPP)(OH)]^{2+}$$

$$[Ru^{IV}(tpy)(PPP)(O)]^{2+} + e^- + H^+ \rightleftharpoons [Ru^{III}(tpy)(PPP)(OH_2)]^{2+}$$

Based on the above results, it can be estimated that the pK_a for $[Ru^{III}(tpy)(PPP)(OH_2)]^{3+}$ and $[Ru^{II}(tpy)(PPP)(OH_2)]^{2+}$ are equal to 1.7 and 10 respectively.

Figure 2.14 shows the cyclic voltammetry of the poly-$[Ru^{II}(tpy)(PPP)(H_2O)]^{n+}$ film in 0.1 M $HClO_4$ under different scan rates, and Figure 2.15 shows the relationship between the voltammetric current and the scan rate(v). The voltammetic peak current (i_p) is proportional to the square root of the scan rates$(v)^{1/2}$. This suggests a diffusion-like behaviour for the oxidation of the ruthenium complex in the polymer film. Similar observation has been reported for other metal-containing polymer films and the diffusion-like behaviour was attributed to the hopping of electrons amongst the metal centres in the polymer film.

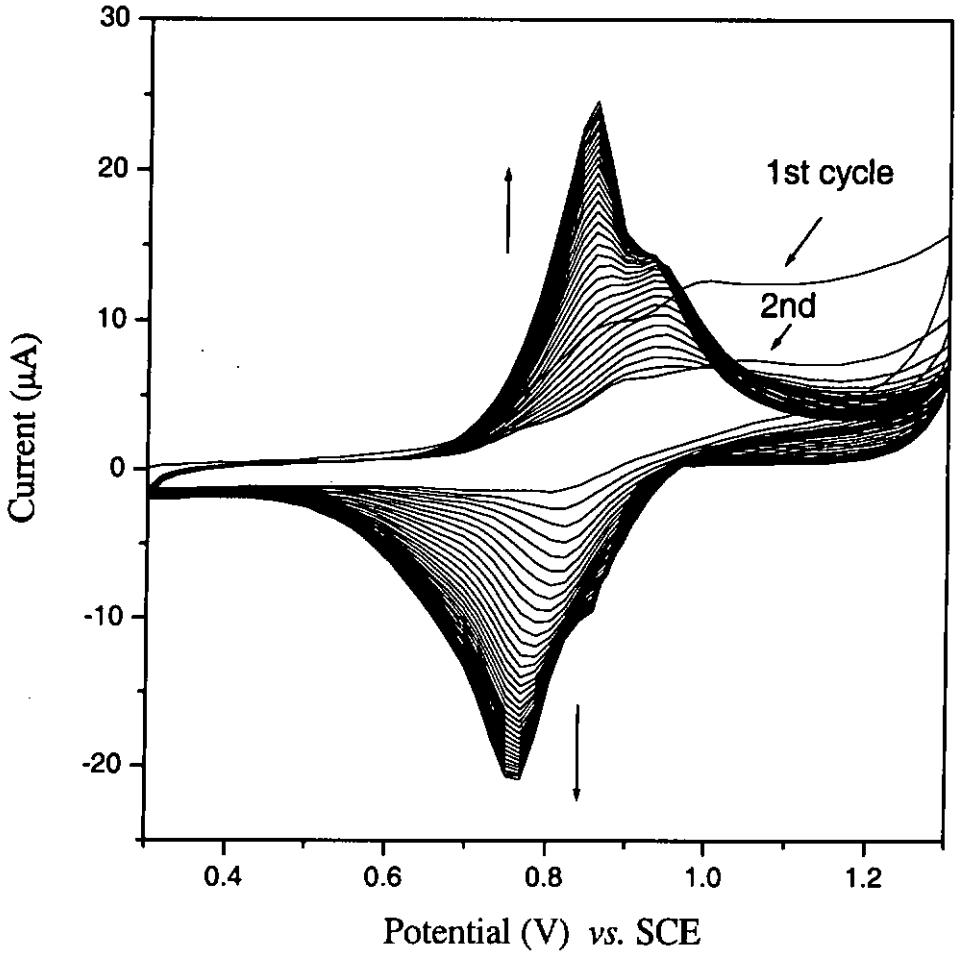

Fig 2.12 Cyclic voltammograms of 0.5 mM $[Ru(tpy)(PPP)(H_2O)]^{2+}$ in 0.1 M $HClO_4$.

Working electrode: 0.196 cm^2 glassy carbon. Scan rate: 100 mVs^{-1}

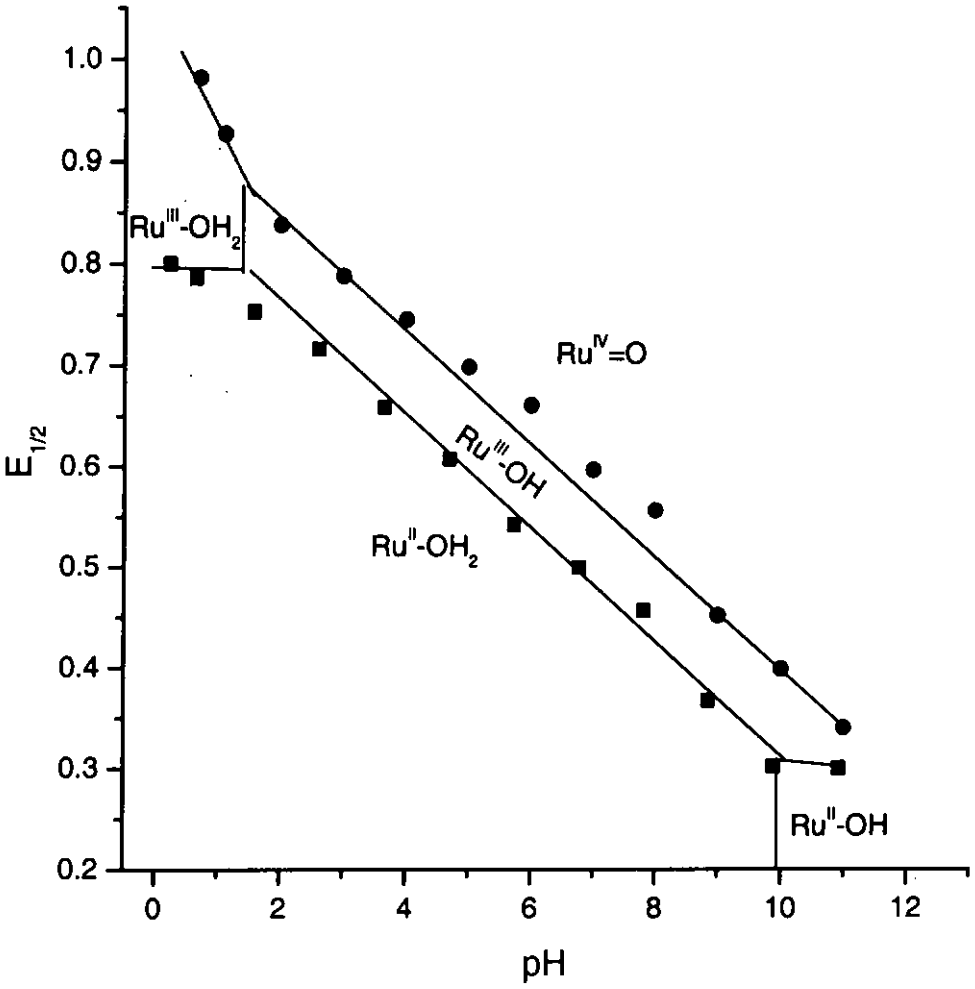

Fig 2.13 Pourbaix diagram of $E_{1/2}$ vs. pH for poly[Ru(tpy)(PPP)(H_2O)]$^{n+}$.

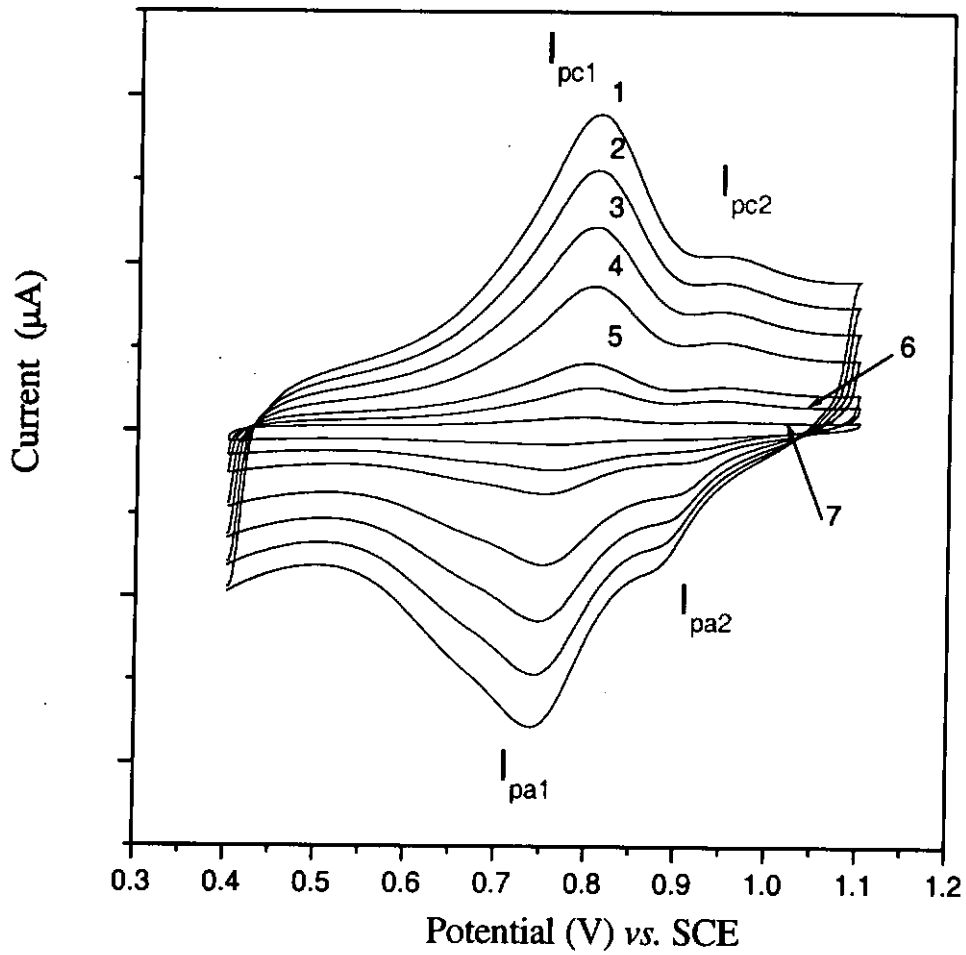

Fig 2.14 Poly[Ru^{II}(tpy)(PPP)(H_2O)]$^{2+}$ film in 0.1 M $HClO_4$ with different scan rates. (Scan rate) for curves (1~7) = 500, 400, 300, 200, 100, 50, 20 mVs^{-1} respectively.

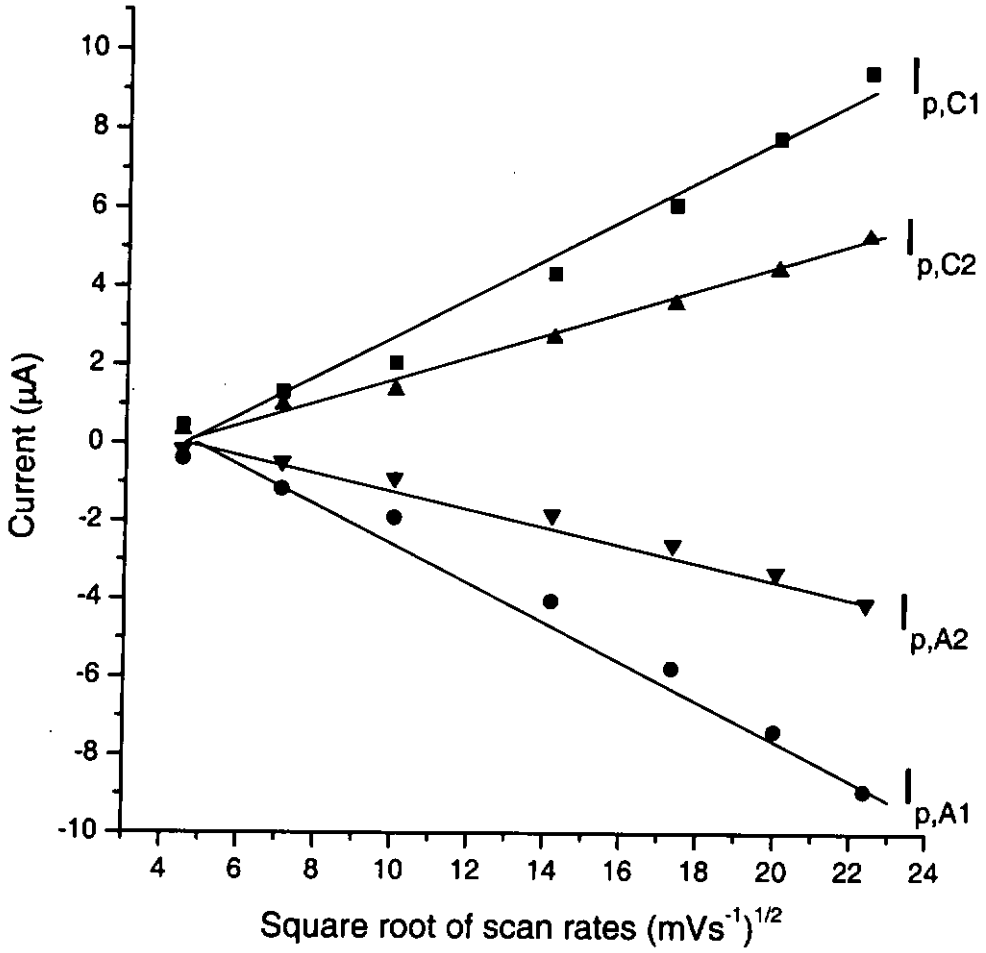

Fig 2.15 Plots of the peak current *vs.* the square root of scan rate $(v)^{1/2}$ for the poly[Ru(tpy)(PPP)(H_2O)]$^{n+}$ film.

It is noted that the size of the Ru^{IV}/Ru^{III} couple is much smaller than that of the Ru^{III}/Ru^{II}, indicating that the formation of $Ru^{IV}=O$ is kinetically slow. However, on comparing the Ru^{IV}/Ru^{III} couple in poly$[Ru(tpy)(PPP)(H_2O)]^{n+}$ with that in the monomeric couple $[Ru(tpy)(dpa)(H_2O)]^{2+}$ (see Figure 4.9 in chapter 4), it can be seen that the relative size of the Ru^{IV}/Ru^{III} couple in the polymer film in much larger than that of the free monomer in solution. This indicates that incorporation of the ruthenium aqua centres inside polymer can promote the oxidation of the complexes to $Ru^{IV}=O$. Meyer and co-workers have proposed that the formation of $Ru^{IV}=O$ occurs through a disproportionation mechanism

$$2Ru^{III}—OH \longrightarrow Ru^{II}—OH_2 + Ru^{IV}=O$$

$$Ru^{II}—OH_2 - e^- - H^+ \longrightarrow Ru^{III}—OH$$

The distance between the two Ru^{III}-OH moieties will greatly affect the above disproportionation reaction. In metal-containing polymer films, the metal centres should be close enough to one another to facilitate the interaction of Ru^{III}-OH moieties. To test this hypothesis, we have recorded the cyclic voltammograms of polymer films that were prepared in electrolytes containing different concentrations of $[Ru(tpy)(PPP)(H_2O)]^{2+}$ and free pyrrole. The resulting polymer films should contain ruthenium centres that are separated by different chain lengths of polypyrrole.

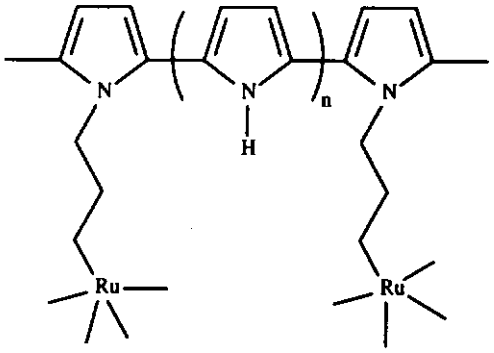

The results are shown in Fig. 2.16. It is interesting to note that the Ru^{IV}/Ru^{III} diminishes in size as the distance between the Ru centre increases. Meyer proposed the following mechanism for the formation of $Ru^{IV}=O$:

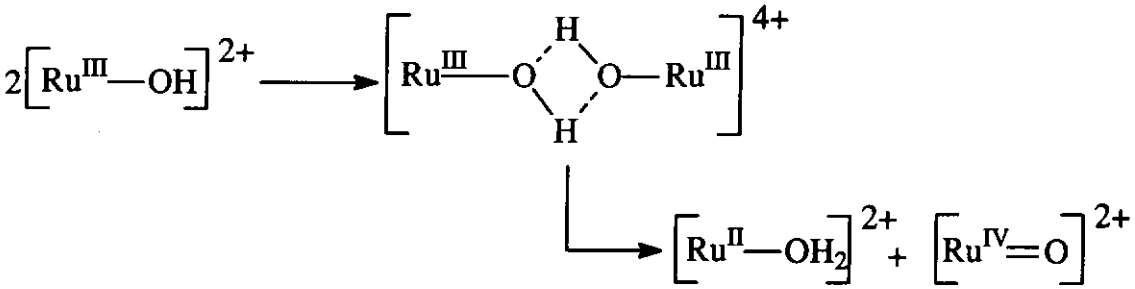

$$Ru^{II}—OH_2 - e^- - H^+ \longrightarrow Ru^{III}—OH$$

According to Meyer, the small couple that is assigned as Ru^{IV}/Ru^{III} actually results from the oxidation of the $[Ru^{II}\text{-}OH_2]^{2+}$ generated by disproportionation. We doubt why the $E_{1/2}$ for the oxidation of $[Ru^{II}\text{-}OH_2]^{2+}$ from disproportionation should occur at a different value than that of the original $[Ru^{II}\text{-}OH_2]^{2+}$. An alternative mechanism is that the formation of 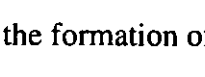 intermediate would facilitate the further oxidation the ruthenium centre through easier deprotonation.

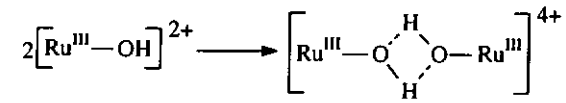

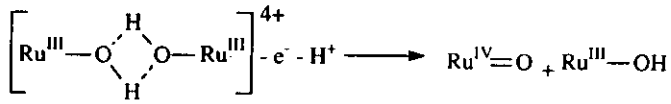

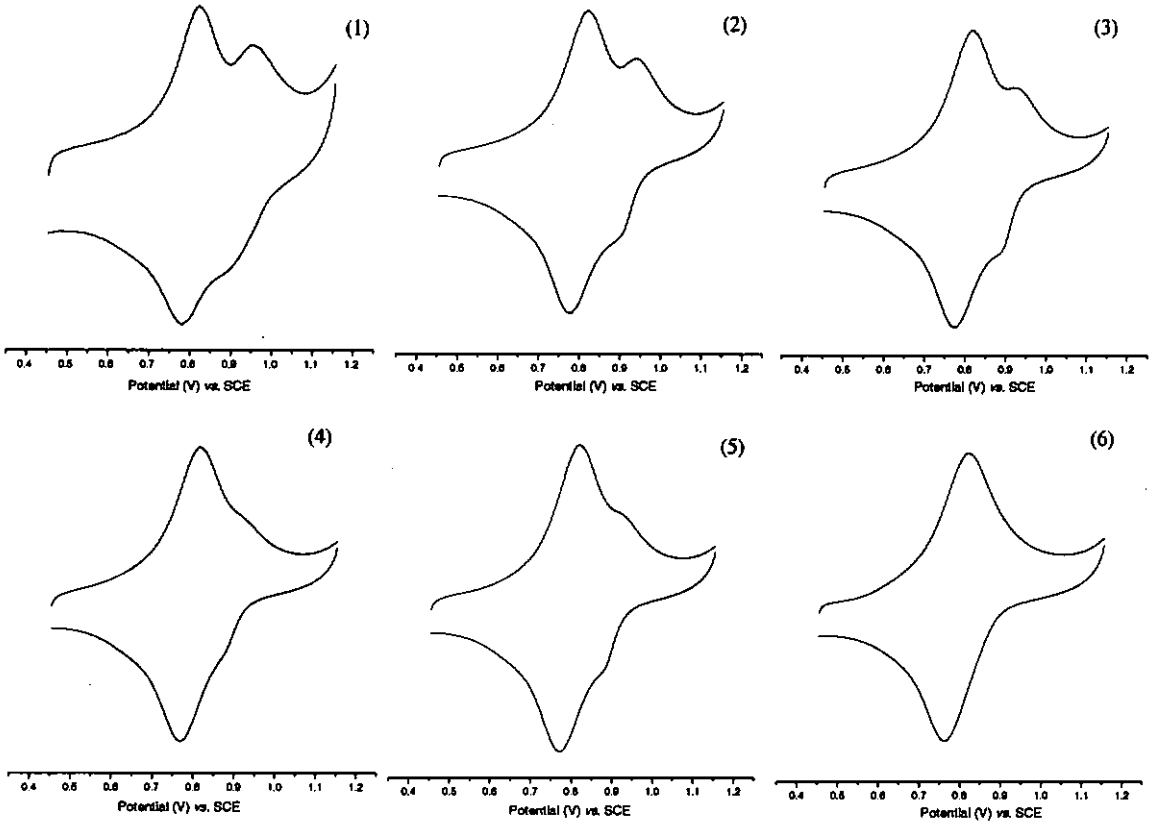

Fig 2.16 Poly[$Ru^{II}(tpy)(PPP)(H_2O)]^{n+}$ film prepared with different $[Ru^{II}(tpy)(PPP)(H_2O)]^{2+}$ and pyrrole mole ratio in 0.1 M $HClO_4$. Scan rates: 10 mVs^{-1}

Mole ratio for ruthenium complex : pyrrole (1) 75:25; (2) 50:50; (3) 44:56; (4) 40:60; (5) 36:64; (6) 30:70. The total concentration of ruthenium complex + pyrrole is 1 mM.

Electrocatalytic behaviour of poly[Ru(tpy)(PPP)(H_2O)]$^{n+}$ film toward oxidation reaction

The electrocatalytic behaviour of the poly[Ru(tpy)(PPP)(H_2O)]$^{n+}$ film towards the oxidation of benzyl alcohol was investigated. Figure 2.17 shows the cyclic voltammograms of poly[Ru(tpy)(PPP)(H_2O)]$^{n+}$ in 0.1 M $HClO_4$ in the presence of benzyl alcohol. An increase in the anodic current of the Ru^{IV}/Ru^{III} couple was observed as benzyl alcohol was added, indicating that the poly[Ru(tpy)(PPP)(H_2O)]$^{n+}$ film can catalyze the oxidation of benzyl alcohol at a reasonably fast rate.

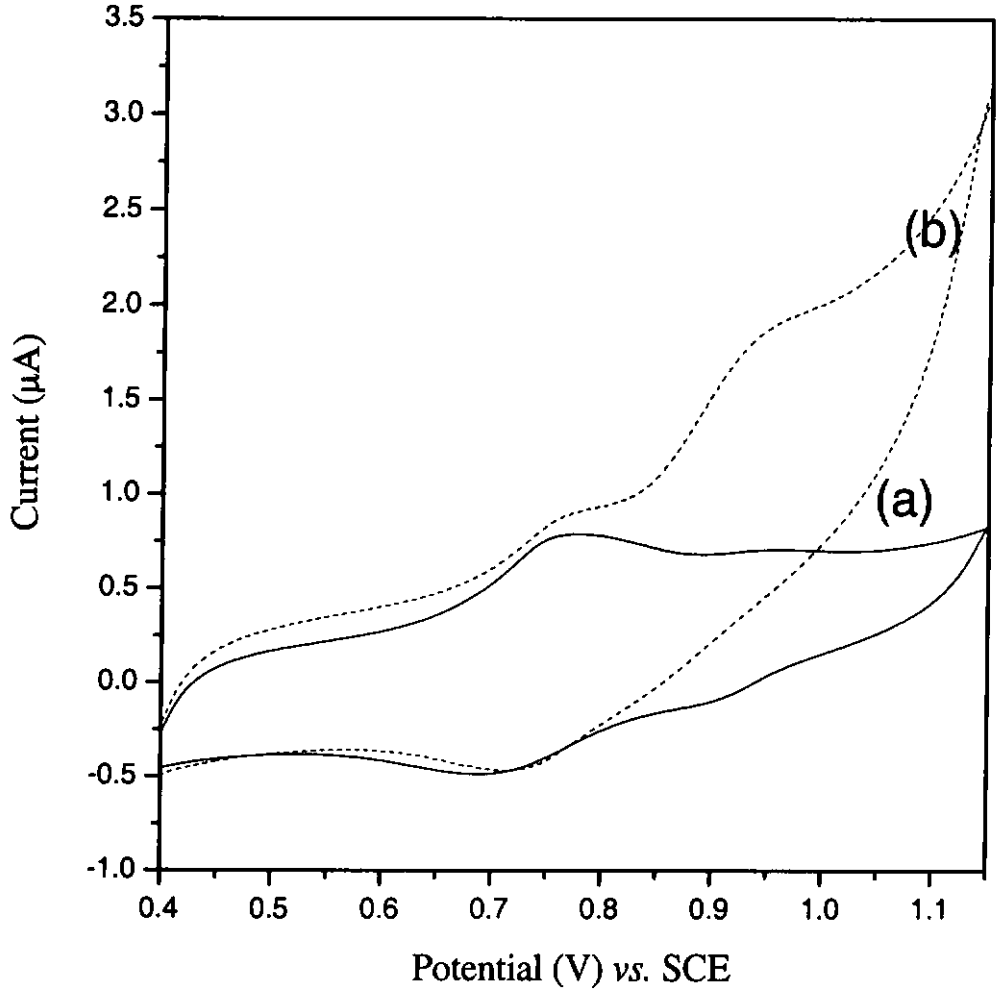

Fig 2.17 Cyclic voltammograms of poly[Ru(tpy)(PPP)(H_2O)]$^{n+}$ in (a) 0.1 M $HClO_4$. (b) Addition of 1 mM of Benzyl alcohol. Working electrode: 0.196 cm^2 glassy carbon. Scan rate: 20 mVs^{-1}

2.3.4 *In-situ* reflectance FT-IR spectroelectrochemistry

In-situ FT-IR spectroelectrochemical analysis of the polymer film gives important information on film structure and electronic properties as a function of redox potential. Figure 2.18 shows the IR reflectance spectra of poly[Ru(tpy)(PPP)$(H_2O)]^{n+}$ in 0.1 M $HClO_4$ solution recorded at different applied potentials. A new band located at 783cm^{-1} was observed to appear gradually as the potential was increased from 0.75 V to 1.0 V. This band can be assigned to the Ru^{IV}=O stretching [169].

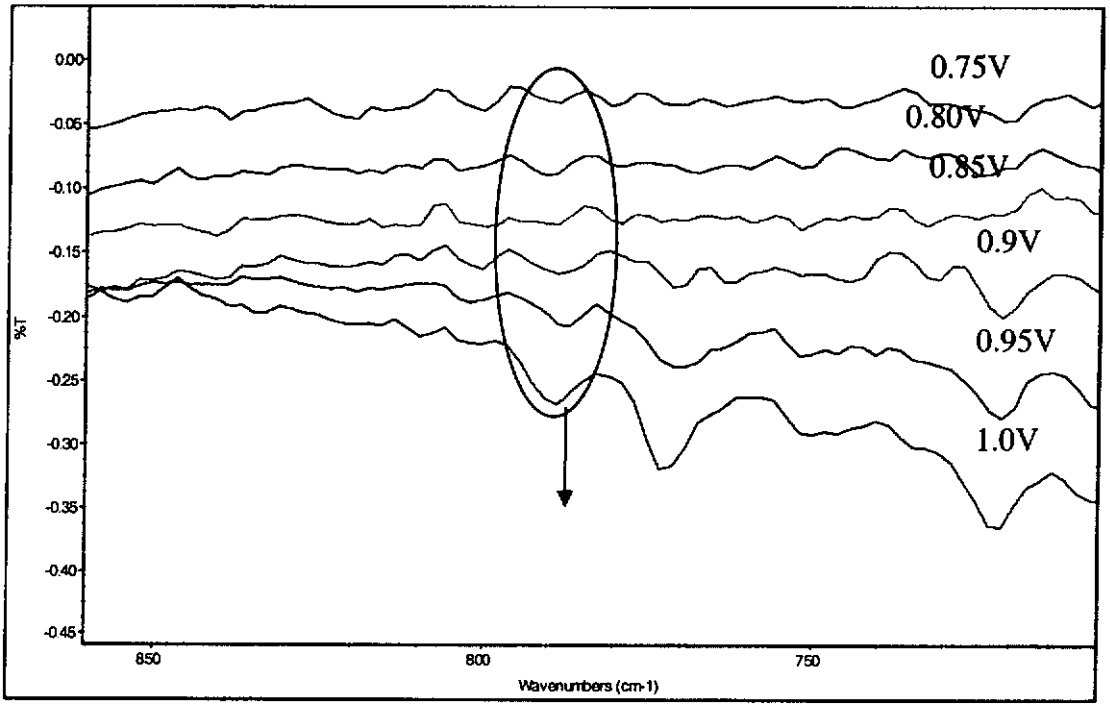

Figure 2.18 IR reflectance spectra of poly[Ru(tpy)(PPP)$(H_2O)]^{n+}$ in 0.1 M $HClO_4$ at different applied potentials.

It is interesting to note that no formation of the Ru=O stretching band can be observed in the IR spectra when the potential of the working electrode was held below 0.8 V, which is beyond the potential for the oxidation of Ru(II) to Ru(III) but below that for the oxidation of Ru(III) to Ru(IV). This observation argues against the disproportionation mechanism proposed by Meyer and co-workers. As each IR spectrum was recorded after the potential of the electrode has been held for at least 3 minutes, there should be sufficient time for the disproportionation of Ru^{III}-OH to occur as compared to that in cyclic voltammetric studies. If the Ru^{IV}/Ru^{III} couple in the cyclic voltammograms actually arises from disproportionation of Ru^{III}-OH, the Ru^{IV}=O species generated from disproportionation should be observed in the IR spectrum at potentials below 0.8 V. We therefore favour the assistance of deprotonation of Ru^{III}-OH by a nearby Ru^{III}-OH moiety in the oxidation of Ru^{III}-OH to Ru^{IV}=O rather than the oxidation of Ru^{II}-OH_2 generated from disproportionation as the electrode process for the Ru^{IV}/Ru^{III} couple.

2.3.5 Scanning electron microscopy

The morphology of poly[Ru(tpy)(PPP)Cl]$^{n+}(ClO_4)_n$ and poly[Ru(tpy)(PPP)H_2O]$^{n+}(ClO)_n$ films were studied by scanning electron microscopy. Poly[Ru(tpy)(PPP)Cl]$^{n+}(ClO_4)_n$ film and poly[Ru(tpy)(PPP)H_2O]$^{n+}(ClO_4)_n$ film were prepared from 0.5 mM monomer complex in 0.1 M TBAP + CH_3CN and 0.1 M $HClO_4$ solution respectively on glassy carbon electrodes. The poly[Ru(tpy)(PPP)Cl]$^{n+}(ClO_4)_n$ film shows a shiny violet colour, while the poly[Ru(tpy)(PPP)H_2O]$^{n+}(ClO_4)_n$ film is yellowish brown. The SEM images of the two polymers films are shown in Figure 2.19 and Figure 2.20 respectively. Both films show a surface structure with protrusions [170]. The poly[Ru(tpy)(PPP)H_2O]$^{n+}(ClO_4)_n$ film prepared in aqueous media appears to be more porous that the poly[Ru(tpy)(PPP)H_2O]$^{n+}(ClO_4)_n$ film prepared in non-aqueous media, which is consistent with those results reported for polypyrrole films [171, 172].

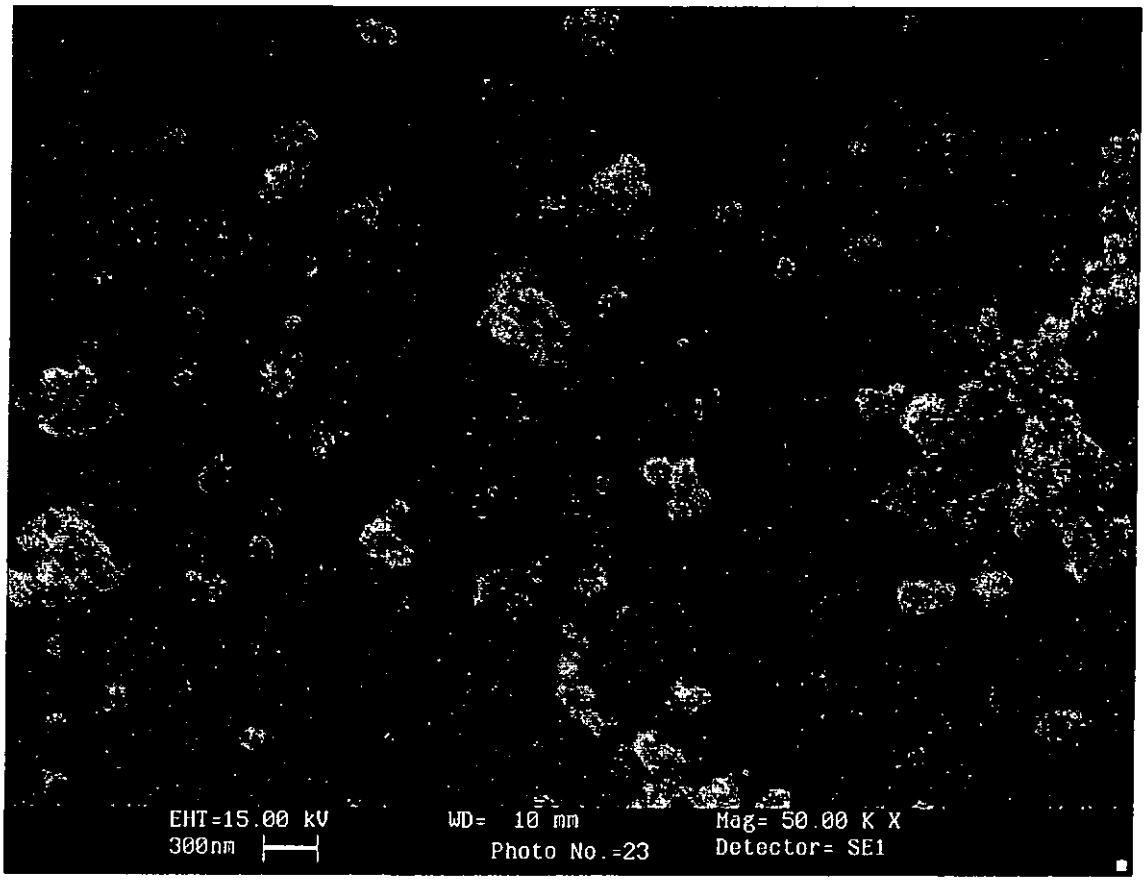

Fig 2.19 SEM image of poly[Ru(tpy)(PPP)Cl]$^{n+}$$(ClO_4)_n$ prepared from 0.5 mM complex in CH_3CN + 0.1 M TBAP solution on glassy carbon electrode.

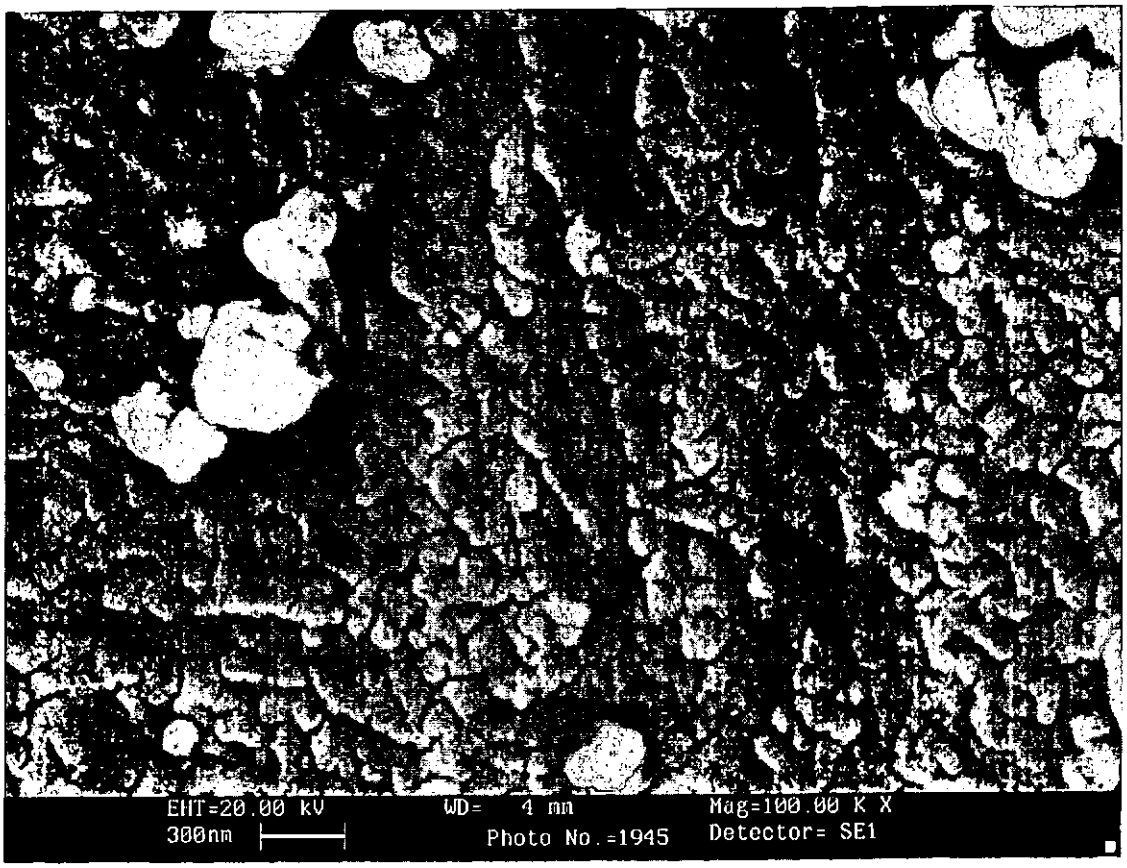

Fig 2.20 SEM image of poly[Ru(tpy)(PPP)H_2O]$^{n+}$$(ClO_4)_n$ prepared from 0.5 mM complex in 0.1 M of $HClO_4$ solution on glassy carbon electrode.

2.4 Conclusion

We have synthesized a novel ligand PPP and its ruthenium complexes. The structure of $[Ru(tpy)(PPP)(Cl)]ClO_4$ complex has been confirmed by the X-ray crystallography. The ruthenium aqua complex $[Ru(tpy)(PPP)(H_2O)]^{2+}$ can be electropolymerized onto glassy carbon electrodes via anodic oxidation of the pyrrole groups in both aqueous and non-aqueous medium. The resulting polymers are highly conductive, as shown by cyclic voltammetric studies. The formation of $Ru^{IV}=O$ in aqueous medium is promoted in the polymer as compared to that of the monomer in solution. The interaction of nearby Ru^{III}-OH moieties is proposed as the mechanism for the ease of electrochemical formation of the ruthenium oxo species in the polymer film.

Chapter 3

X-ray Structure of Ruthenium Aqua Complexes with 6,6'-Dichloro-2,2'-Bipyridine Ligand – Correlation between Structure and Electrochemistry

3.1. Introduction

Che and co-workers has prepared the Ru(IV) mono oxo complex $[Ru(tpy)(dcbpy)O]^{2+}$ [110] and Ru(VI) *cis*-dioxo *cis*-$[Ru(dcbpy)_2O_2]^{2+}$ [173] with the 6,6'-dichloro-2,2'-bipyridine ligand (dcbpy). They showed that this chloro-substituted bipyridine ligand is more resistant towards oxidative degradation and hence the ruthenium complexes are more robust catalysts in oxidation reactions. The $E_{1/2}$ of the Ru^{III}/Ru^{II} (0.55 V) and Ru^{IV}/Ru^{III} (0.74 V) couples for $[Ru(tpy)(dcbpy)(H_2O)]^{2+}$ in pH 7 are more anodic than those of $[Ru(tpy)(bpy)(H_2O)]^{2+}$ (0.49 V and 0.62 V) respectively due to the electron withdrawing effect of the chloro-substituents. It is interesting to note that the Ru^{IV}/Ru^{III} couple for $[Ru(tpy)(dcbpy)(H_2O)]^{2+}$ [110] is much more well-defined than that of $[Ru(tpy)(bpy)(H_2O)]^{2+}$ [116], indicating that the oxidation of Ru^{III}-OH to Ru^{IV}=O is more facile in $[Ru(tpy)(dcbpy)(H_2O)]^{2+}$. For *cis*-$[Ru(dcbpy)_2(H_2O)_2]^{2+}$, the Ru^{III}/Ru^{II}, Ru^{IV}/Ru^{III} and Ru^{V}/Ru^{IV}, Ru^{VI}/Ru^{V} merge to give two Ru^{IV}/Ru^{II} and Ru^{VI}/Ru^{IV} couples at 0.93 and 1.17 V respectively in 0.1 M acid, which are again much more well-defined than those of *cis*-$[Ru(bpy)_2(H_2O)_2]^{2+}$. The change in the shape of the voltammogram is unlikely due to steric effect because the cyclic voltammogram of *cis*-$[Ru(dmbpy)_2(H_2O)_2]^{2+}$ (dmbpy = 6,6'-dimethyl-2,2'-bipyridine) consists of four couples and is similar to that of *cis*-$[Ru(bpy)_2(H_2O)_2]^{2+}$ rather than *cis*-$[Ru(dcbpy)_2(H_2O)_2]^{2+}$. Moreover, previous work in our laboratory showed that replacing 2,2'-bipyridine with

4,4'-dichloro-2,2'-bipyridine, 5,5'-dichloro-2,2'-bipyridine or 5,5'-bis(trifluoromethyl)-2,2'-bipyridine only change the redox potential but not the shape of the voltammograms. These seems to be something unique in the 6,6'-dichloro-2,2'-bipyridine which would promote the oxidation of Ru-OH to Ru=O. As the X-ray crystal structure of $[Ru(tpy)(dcbpy)(H_2O)]^{2+}$ and *cis*-$[Ru(dcbpy)_2(H_2O)_2]^{2+}$ have not been reported in the literature, we therefore conducted a detailed study on the structure of these two complexes. Attempts were made to correlate the structure of these complexes with their electrochemistry.

3.2. Experimental Section

3.2.1. Synthesis

Materials

All the chemicals and solvents used in synthesis and crystallization were of analytical (A.R.) grade. Ruthenium trichloride trihydrate ($RuCl_3.xH_2O$), 2,2':6',2"-terpyridine (tpy), 2,2'-bipyridine (bpy) and silver trifluoromethanesulfonate were purchased from Aldrich Chemical Company. $[Ru(bpy)_2CO_3]$ was synthesized as described in literature [115]. All the other chemicals and regents were used as received unless otherwise noted. Elemental analyses were performed as described in chapter 2.

Synthesis of ligands

6,6'-Dichloro-2,2'-bipyridine [174]

6,6'-dichloro-2,2'-bipyridine was synthesized as reported in the literature according to the following procedure:

2,2'-Bipyridine (10g) was mixed with dimethyl sulphate (35 mL). The mixture

was heated to 100 °C for 1 hr. After cooling, anhydrous diethyl ether (100 mL) was added to the mixture with stirring. The resulting white solid was filtered and dissolved in water (250 mL). Small portions of this solution and sodium hydroxide solution (75g in 250 mL) were added alternately to an ice-cooled solution of potassium ferricyanide (60g in 200 mL), keeping the temperature of the reaction mixture below 5°C. The pH of the mixture was then adjusted to 8-9 by addition of concentrated hydrochloric acid and it was then extracted with choloroform (3x100 mL). The chloroform extracts were combined, dried with sodium sulphate and rotary evaporated to dryness. The resulting solid (2g) and phosphorus pentachloride (4.28g) were dissolved in $POCl_3$ (50 mL) and the mixture was then refluxed for 20 hrs. After removal of excess $POCl_3$ by distillation under reduced pressure, ice-cooled water was added and the solution was made alkaline with ammonia solution and then extracted with chloroform (3x100 mL). The combined chloroform extracts were dried with anhydrous sodium sulphate and then decolourized with activated charcoal. White 6,6'-dichloro-2,2'-bipyridine was isolated by evaporating the chloroform extract to dryness under reduced pressure. Yield: 7.5 g, (52%). ^{1}H-NMR ($CDCl_3$, δ ppm): 7.28 (d, 2H), 7.7 (t, 2H), 8.29 (d, 2H). ESI-MS: *m/z* 226 $(M+H)^+$

Synthesis of Ruthenium Complexes

$Ru(tpy)Cl_3$ was prepared as described in chapter 2. The literature procedures

were followed for the synthesis of the other ruthenium complexes. A summary of the synthetic procedures is given below.

[Ru(tpy)(bpy)Cl][ClO_4] [116]

A mixture of 220 mg of [Ru(tpy)Cl_3] (0.5 mmol), 0.5 g of LiCl, 78 mg of bpy (0.5 mmol) and 1.0 mL of triethylamine was gently refluxed under argon for 1.5 hrs in about 40 mL of absolute ethanol. After the mixture had been cooled to room temperature, the solution was filtered to remove any insoluble material. The filtrate was concentrated to about 3 mL, and 20 mL of saturated solution of $LiClO_4$ was added to the concentrated residue. A brown microcrystalline solid separated out upon standing which was collected by filtration, washed thoroughly with water and ether and dried in a vacuum oven. Yield: 0.27 g (85%). Elemental analysis for $C_{25}H_{19}N_5Cl_2O_4Ru$. Calcd : C, 48.01; H, 3.06; N, 11.20. Found: C, 48.1; H, 3.1; N, 11.1. ESI-MS *m/z*: 626

[Ru(tpy)(bpy)(H_2O)][CF_3SO_3]$_2$ [116]

A mixture of 0.2 g of [Ru(tpy)(bpy)Cl][ClO_4] and 0.12 g of silver trifluoromethanesulfonate was gently refluxed in the dark for 1 hr in 50 mL of water. After cooling to room temperature, the mixture was filtered to remove the precipitated AgCl. Several drops of trifluoromethanesulfonic acid were then added to the filtrate and the resulting mixture was chilled overnight in a refrigerator. The microcrystalline dark-red precipitate of [Ru(tpy)(bpy)(H_2O)][CF_3SO_3]$_2$ was collected by filtration,

washed with minimum amount of cold water and diethyl ether and air dried. Yield: 0.15 g (60%). Elemental analysis for $C_{27}H_{21}N_5F_6O_7RuS_2$. Calcd : C, 40.20; H, 2.62; N, 8.68. Found: C, 40.3; H, 2.6; N, 8.6. ESI-MS *m/z*: 246. Crystals suitable for X-ray diffraction study were obtained by first dissolving $[Ru(tpy)(bpy)(H_2O)][CF_3SO_3]_2$ in double distilled water in the presence of trifluoromethanesulfonic acid. This solution was gently heated until all the complexes had dissolved. Crystals were obtained after the solution was cooled down slowly to room temperature.

$[Ru(tpy)(dcbpy)Cl][CF_3SO_3]$ [110]

A mixture of $Ru(tpy)Cl_3$ (0.4 g) and dcbpy (0.35 g) in ethylene glycol (3 cm^3) was refluxed for 4 hrs. After cooling, ethanol (5 cm^3) was added and the mixture was filtered to remove the excess of ligand and starting metal complex. Trifluoromethanesulfonic acid (1 mL) was added dropwise to the filtrate. Upon cooling in a refrigerator the dark purple solid of $[Ru(tpy)(dcbpy)Cl][CF_3SO_3]$ was obtained. The crude product was used without further purification

$[Ru(tpy)(dcbpy)(H_2O)][CF_3SO_3]_2$[110]

The complex was synthesized by a similar procedure as described in the synthesis of $[Ru(tpy)(bpy)(H_2O)][CF_3SO_3]_2$. A mixture of 0.2 g of $[Ru(tpy)(dcbpy)Cl][CF_3SO_3]$ and 0.13 g of silver trifluoromethanesulfonate was gently refluxed in the dark for 1 h in 50 mL of water. After being cooled to room temperature, the mixture was filtered to

remove the precipitated AgCl. Several drops of trifluoromethanesulfonic acid were then added to the filtrate and the resulting mixture was chilled overnight in a refrigerator. The microcrystalline dark-red precipitate of $[Ru(tpy)(dcbpy)(H_2O)][CF_3SO_3]_2$ was collected by filtration, washed with minimum amount of cold water and diethyl ether and air dried. Yield: 0.47 g (65%). Elemental analysis for $C_{27}H_{21}N_5Cl_2O_7S_2Ru$. Calcd : C, 36.2; H, 2.3; N, 8.25. Found: C, 36.3; H, 2.35; N, 7.85. ESI-MS *m/z*: 280 Crystals suitable for X-ray diffraction study were obtained by first dissolving $[Ru(tpy)(dcbpy)(H_2O)][CF_3SO_3]_2$ in double distilled water in the presence of trifluoromethanesulfonic acid. This solution was gently heated until all the complexes had dissolved. Crystals were obtained after the solution was cooled down slowly to room temperature.

$[Ru(tpy)(dcbpy)(CH_3CN)][CF_3SO_3]_2$

A mixture of 0.3 g of $[Ru(tpy)(dcbpy)(H_2O)][CF_3SO_3]_2$ was gently refluxed for 1 hr in 50 mL of CH_3CN. After cooling, the mixture was concentrated to about 3 mL, and 20 mL of saturated $LiClO_4$ aqueous solution was added to the concentrated residue. Orange microcrystalline solid separated out upon standing which was collected by filtration, washed thoroughly with water and ether and dried in a vacuum oven. Yield: 0.23 g (75%). Elemental analysis for $C_{29}H_{20}N_6Cl_2O_6S_2Ru$. Calcd : C, 38.76; H, 2.24; N, 9.35.

Found: C, 38.7; H, 2.3; N, 9.4. ESI-MS *m/z*: 280. Crystals suitable for X-ray diffraction study were obtained by vapor diffusion of diethyl ether to an acetonitrile solution of $[Ru(tpy)(dcbpy)(CH_3CN)][CF_3SO_3]_2$.

cis-[Ru^{II}(dcbpy)$_2Cl_2$] [173]

$RuCl_3.3H_2O$ (0.5 g), dcbpy (0.9 g) and LiCl (1.25 g) were dissolved in deaerated ethylene glycerol (5 mL). The mixture was refluxed for 4 hrs under a nitrogen atmosphere. After cooling, water (10 mL) was added and the resulting purple precipitate was filtered. The product was recrystallized from chloroform/ diethyl ether. Yield: 0.72 g (60%). Elemental analysis for $C_{20}H_{12}N_4Cl_4Ru$. Calcd : C, 36.5; H, 2.4; N, 8.5. Found: C, 36.3; H, 2.2; N, 8.7.

cis-[Ru^{II}(dcbpy)$_2(H_2O)_2$][CF_3SO_3]$_2$ [173]

cis-[Ru^{II}(dcbpy)$_2Cl_2$] (0.19 g) and silver trifluoromethanesulfonate (0.18 g) were added to water (40 mL) and heated at 70°C for 10 mins. The solution was filtered hot to remove AgCl and the red filtrate was collected at about 40°C. Trifluoromethanesulfonic acid was added dropwise until the complex just precipitated. The mixture was cooled to 0°C to allow complete precipitation. Yield: 0.19 g (70%). Elemental analysis for $C_{22}H_{16}N_4Cl_4O_8S_2Ru$. Calcd : C, 29.84; H, 1.82; N, 6.33. Found: C, 29.8; H, 1.8; N, 6.3. Crystals suitable for X-ray diffraction study were obtained by

first dissolving *cis*-$[Ru(dcbpy)_2(H_2O)_2][CF_3SO_3]_2$ in double distilled water in the presence of trifluoromethanesulfonic acid. This solution was gently heated until all the complexes had dissolved. Crystals were obtained after the solution was cooled down slowly to room temperature.

3.2.2. Physical measurements

Electrochemical measurements

Glassy carbon (BAS) electrode was polished with 0.05 μm α-alumina (Buehler) on a microcloth, rinsed with double deionized water and then sonicated for 5 minutes in water before use. A platinium wire was used as the counter electrode whereas a saturated calomel electrode (SCE) was used as the reference electrode.

Cyclic voltammetry was performed under argon in a conventional two-compartment cell with a sintered glass disc separating the two compartments. A Bioanalytical Systems (BAS) model 100W electrochemical analyzer interfaced to a microcomputer was used in all electrochemical measurements. $E_{1/2}$ values are the average of cathodic and anodic potentials for the oxidative and reductive waves.

***In-situ* FTIR spectroelectrochemistry**

In our study, the IR spectra collected are presented in the form of difference spectra. A reference spectrum, S_1, was first collected at a reference potential E_1 which is usually in the electro-inactive region. The potential of the working electrode was then stepped to a potential E_2 and a second spectrum S_2 was collected at successive time intervals.

A certain number of co-added and averaged scans were taken to give the desired S/N ratio. The spectra were therefore presented as:

$$\Delta R / R = (S_2 - S_1) / S_1 \text{ versus } \nu \, (cm^{-1})$$

It follows that both positive and negative peaks can appear in the difference spectrum. A positive peak, $+\Delta R/R$ represents absorption from species that decrease in concentration in the thin layer on stepping the potential from E_1 to E_2. A negative peak, $\Delta R/R$ represents a gain in the concentration of that particular species in the thin layer.

The FTIR spectroelectrochemistry experiments were performed on a Nicolet Avatar 360 FTIR Spectrometer in the reflectance mode, equipped with a wide band mercury cadmium telluride (MCT) detector. The cell was a standard three-electrode thin layer design [175-177] with a KRS-5 (Thallium Bromide-Iodide) window, a platinum foil counter electrode, a glassy carbon working electrode (o.d. = 6mm) and a saturated calomel electrode (SCE) reference electrode. The potential of the spectroelectrochemical cell was controlled by a Princeton Applied Research model 362 potentiostat. The FTIR spectrometer was coupled with a Spectra-Tech Series 500 variable angle specular reflectance accessory, which allowed the spectral reflectance measurement to be carried out at incident angles between 30°-80°, the optimum angle fore maximum reflectance was determined before each experiment and was usually around 55°. The distance between the working electrode and the KRS-5 window can

be adjusted to accommodate a thin layer of electrolyte (ca. 1mm thick) for spectroelectrochemical measurement. All the spectra were collected at 8 cm^{-1} resolution and consisted of 100 co-added and averaged scans. The sample compartment of the FTIR spectrometer was purged by N_2 prior to the measurement to ensure complete removal of CO_2 and water vapor.

X-ray crystallographic data collection and refinement of structures

A suitable crystal of each of the complexes was mounted on a Bruker CCD area detector using MoKα radiation (λ =0.71073 Å) from generator operating at 50KV, 30 mA condition. The intensity data of $[Ru(tpy)(bpy)(H_2O)][ClO_4]_2$, $[Ru(tpy)(dcbpy)(H_2O)][CF_3SO_3]_2$, $[Ru(tpy)(dcbpy)(CH_3CN)][CF_3SO_3]_2$ and *cis*-$[Ru^{II}(dcbpy)_2(H_2O)_2][CF_3SO_3]_2$ were collected in the range of 0 to 180 degree. Frames of 1321 were taken in 4 shells. An empirical absorption correction of SADABS (Sheldrick, 1996) program based on Fourier coefficient fitting was applied. The crystal structures were determined by the direct method, yielding the positions of part of the non-hydrogen atoms, and subsequent difference Fourier syntheses were employed to locate all of the remaining non-hydrogen atoms which did not show up in the initial structure. Hydrogen atoms were located based on Difference Fourier Syntheses connecting geometrical analysis. All non-hydrogen atoms were refined anisotropically with weight function $W= 1/[\sigma^2(Fo^2)+0.1000p]^2+0.0000p$, where $p=(Fo^2+2Fc^2)/3$.

Hydrogen atoms were refined with fixed individual displacement parameters. All experiments and computations were performed on a Bruker CCD Area Detector Diffractometer and PC computer with the program of the Bruker Smart and Bruker Shelxtl packages. Further crystallographic details and selected bond distances and angles for $[Ru(tpy)(bpy)(H_2O)][ClO_4]_2$, $[Ru(tpy)(dcbpy)(H_2O)][CF_3SO_3]_2$, $[Ru(tpy)(dcbpy)(CH_3CN)][CF_3SO_3]_2$ and *cis*-$[Ru^{II}(dcbpy)_2(H_2O)_2][CF_3SO_3]_2$ can be found in the Results and Discussion section.

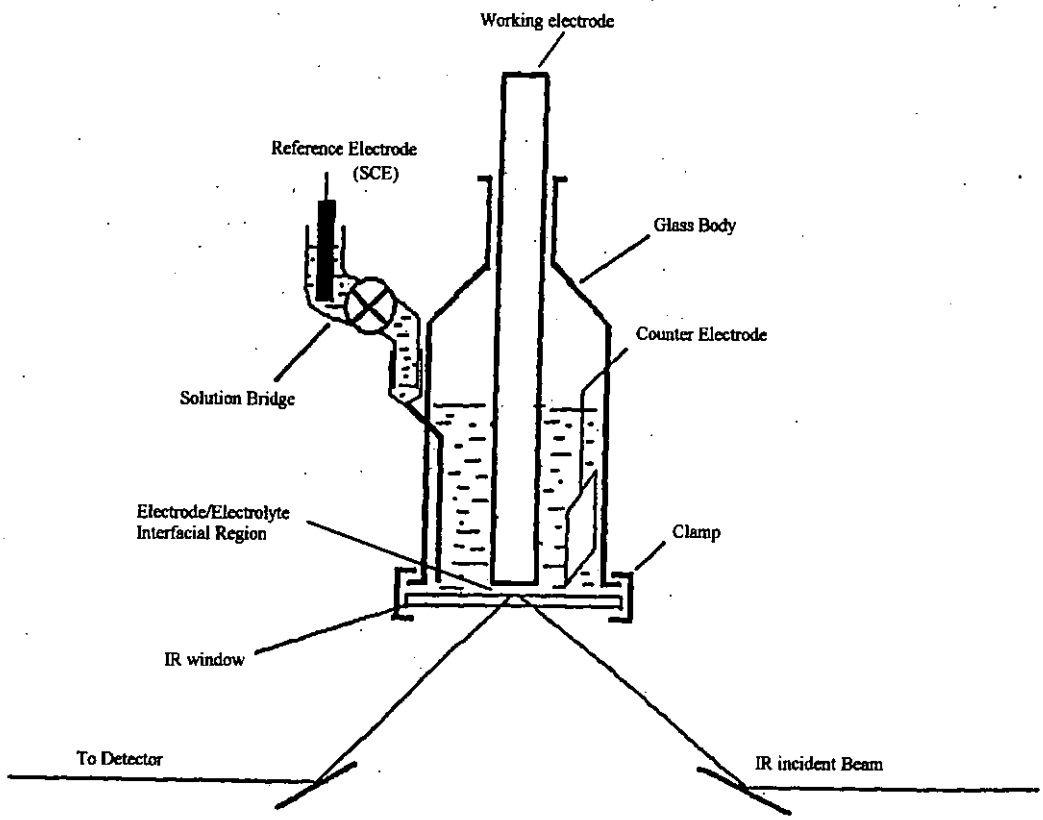

Fig 3.1 A schematic diagram showing the setup for *in-situ* FTIR spectroelectrochemistry.

3.3. Results and Discussion

3.3.1. X-ray structure of the ruthenium complexes

The ORTEP plots of the various ruthenium complexes are depicted in Figure 3.2 - 3.5, respectively. Crystallographic data are summarized in Tables 3.1 - 3.2. Selected bond distances and angles are given in Tables 3.4 - 3.10. The structural features of each individual complex are described below:

$[Ru(tpy)(dcbpy)(H_2O)](CF_3SO_3)_2$

The OPTEP plot of $[Ru(tpy)(dcbpy)(H_2O)](CF_3SO_3)_2$ with atom numbering is shown in Figure 3.2. The ruthenium ion is coordinated to 1 aqua-oxygen and 5 pyridyl nitrogens of the polypyridine ligands. The geometry about the ruthenium is regarded as a distorted octahedral structure. The ruthenium ion is positioned at the centre and displaced 0.0332 Å from plane N1-N2-N3. The Ru-N distances are normal and span a narrow range from 1.964(2) to 2.130(2) Å. The $Ru\text{-}O_{(OH_2)}$ distance between ruthenium and the aqua oxygen is 2.130(2) Å, which is similar to those in the other ruthenium aqua complexes such as $[Ru(tacn)(bpy)(OH_2)]^{2+}$ (2.168(3) Å) [178] and $[Ru(Me_3tacn)(3,3'\text{-}Me_2bpy)(OH_2)]^{2+}$ (2.176(4) Å) [111].

$[Ru(tpy)(dcbpy)(CH_3CN)](CF_3SO_3)_2$

Figure 3.3 depicts the ORTEP plot of the complex $[Ru(tpy)(dcbpy)(CH_3CN)](CF_3SO_3)_2$ with atom numbering. The ruthenium ion is ligated to 6 nitrogen atoms, 5 belong to pyridyl nitrogens and 1 belongs to acetonitrile nitrogen. The ruthenium ion is positioned at the centre and displaced 0.0694 Å from plane N1-N2-N3. The bond distances between the Ru-N are normal and span through a narrow range from 1.961(5) to 2.104(4) Å, which are similar to those in the complex $[Ru(tpy)(dcbpy)(H_2O)](CF_3SO_3)_2$.

$[Ru(tpy)(bpy)(H_2O)](CF_3SO_3)_2$

The structure of $[Ru(tpy)(bpy)(H_2O)](PF_6)_2$ has been reported in a PhD dissertation [179] but not in journal paper. As the details of the crystallography data are not available, we have re-determined the X-ray structure of $[Ru(tpy)(bpy)(H_2O)]^{2+}$. Figure 3.4 depicts the ORTEP plot of the complex $[Ru(tpy)(bpy)(H_2O)](CF_3SO_3)_2$ with atom numbering. The coordination geometry of the ruthenium centre is approximately octahedral. The three nitrogen atoms of tpy and one nitrogen atom of bpy are coordinated in the equatorial positions, while the other nitrogen of bpy and the oxygen atom of the aqua ligand are in the axial position. The Ru-N bond distances are in the range of 1.959(2) to 2.075(2) Å, while the $Ru\text{-}O_{(OH2)}$ bond length is 2.129(2) Å, which is similar to those in $[Ru(tacn)(bpy)(OH_2)]^{2+}$ (2.168(3) Å) [178] and $[Ru(Me_3tacn)(3,3'\text{-}Me_2bpy)(OH_2)]^{2+}$ (2.176(4) Å) [111].

***cis*-[Ru(dcbpy)$_2$(H$_2$O)$_2$][CF$_3$SO$_3$]$_2$**

The OPTEP plot of *cis*-[Ru(dcbpy)$_2$(H$_2$O)$_2$](CF$_3$SO$_3$)$_2$ with atom numbering is shown in Figure 3.5. The OPTEP plot shows that the two 6,6'-dichloro-2,2'-bipyridines are in a *cis*- conformation. The four Ru-N bond distances range from 2.033(2) to 2.085(2) Å, which are similar with those in $[Ru(bpy)_2(CH_3CN)_2]^{2+}$ [180] and $[Ru((CF_3)_2\text{-}bpy)_2(CH_3CN)_2]^{2+}$ [181]. The Ru-O bond distances are 2.129(2) and 2.145(2) Å, which are similar to the Ru-$O_{(OH_2)}$ bond lengths in the ruthenium *trans*-diaqua complex (2.116(2) Å) [182] and ruthenium (II) mono aqua complexes described previously.

Table 3.1 A summary of crystallographic data, intensity collection and structure refinement of the ruthenium complexes

	$[Ru(tpy)(dcbpy)(H_2O)][CF_3SO_3]_2$	$[Ru(tpy)(dcbpy)(CH_3CN)][CF_3SO_3][ClO_4]$	$[Ru(tpy)(bpy)(H_2O)][CF_3SO_3]_2$
Empirical formula	$Ru(H_2O)(C_{25}H_{17}N_5Cl_2).(CF_3SO_3)_2.H_2O$	$Ru(CH_3CN)(C_{25}H_{17}N_5Cl_2).CF_3SO_3.ClO_4$	$Ru(H_2O)(C_{25}H_{19}N_5).(CF_3SO_3)_2$
Formula weight	893.58	867.00	806.67
Temperature	294(2) K	294(2) K	301 K
Wavelength	0.71073 Å	0.71073 Å	0.71069 Å
Crystal system	Monoclinic	Monoclinic	Monoclinic
Space group	P2(1)/c	P2(1)/c	P2(1)/c
Unit cell dimensions	a = 16.549(3) Å α = 90°	a = 16.187(2) Å α = 90°	a = 17.146(7) Å α = 90°
	b = 15.935(3) Å β = 95.189(4)°	b = 15.5581(19) Å β = 98.839(3)	b = 15.760(6) Å β = 98.839(3)
	c = 12.262(2) Å γ = 90°	c = 12.9934(15) Å γ = 90°	c = 11.789(5) Å γ = 90°
Volume	3220.4(10) $Å^3$	3233.5(7) $Å^3$	3067(1) $Å^3$
Z	4	4	4
Density (calculated)	1.843 Mg /m^3	1.781 Mg /m^3	1.75 Mg /m^3
Absorption coefficient	0.876 mm^{-1}	0.875 mm^{-1}	0.74 mm^{-1}
F(000)	1784	1736	1616
Crystal size	0.48 x 0.16 x 0.08 mm^3	0.30 x 0.28 x 0.10 mm^3	0.37 x 0.17 x 0.03 mm^3
θ range for data collection	2.56 to 27.55°	2.54 to 27.52°	1.2 to 27.5°
Reflections collected	21524	21635	19171
Independent reflections	7364	7416	7080
Completeness to θ = 27.55°	99.1%	99.6%	
Absorption correction	Empirical	Multiscans	
Max. and min. transmission	0.9332 and 0.6786	0.9176 and 0.7792	
Refinement method	Full-martix least-squares on F^2	Full-martix least-squares on F^2	Full-martix least-squares on F^2
Goodness-of-fit on F2	1.018	0.991	1.11
R	0.0940	0.0596	0.032
WR2	0.1435	0.0816	0.034
Largest diff. Peak and hole	0.949 and –0.976e. $Å^{-3}$	0.817 and –0.849e. $Å^{-3}$	0.60 and –0.31e. Å

Table 3.2 A summary of crystallographic data, intensity collection and structure refinement of *cis*-$[Ru(dcbpy)_2(H_2O)_2]^{2+}$

	cis-$[Ru(dcbpy)_2(H_2O)_2][CF_3SO_3]_2$
Empirical formula	$C_{22}H_{16}Cl_4F_6N_4O_8RuS_2$
Formula weight	885.40
Temperature	301 K
Wavelength	0.71073 Å
Crystal system	triclinic
Space group	P1(#2)
Unit cell dimensions	a = 9.538(2) Å α = 80.42(1)°
	b = 12.984(3) Å β = 87.53(1)°
	c = 13.702(3) Å γ = 68.65(1)°
Volume	1558.1(6) $Å^3$
Z	2
Density (calculated)	1.887 Mg /m^3
Absorption coefficient	0.876 mm^{-1}
F(000)	876
Crystal size	0.35 x 0.18 x 0.06 mm^3
θ range for data collection	2.1.7 to 27.5°
Reflections collected	17749
Independent reflections	7084
Completeness to θ = 27.55°	99.1%
Absorption correction	Empirical
Max. and min. transmission	0.9332 and 0.6786
Refinement method	Full-martix least-squares on F^2
Goodness-of-fit on F2	1.61
R	0.030
WR2	0.045
Largest diff. Peak and hole	0.43 and –0.34e. $Å^{-3}$

Table 3.3 Selected bond length (Å) for [Ru(tpy)(dcbpy)(H_2O)](CF_3SO_3)$_2$

Ru(1)-N(1)	2.068(3)	N(1)-C(1)	1.333(4)
Ru(1)-N(2)	1.964(2)	N(1)-C(5)	1.378(4)
Ru(1)-N(3)	2.085(3)	N(2)-C(6)	1.351(4)
Ru(1)-N(4)	2.071(3)	N(2)-C(10)	1.363(4)
Ru(1)-N(5)	2.115(2)	N(3)-C(15)	1.348(4)
Ru(1)-O(1W)	2.130(2)	N(3)-C(11)	1.374(4)
Cl(1)-C(16)	1.713(4)	N(4)-C(16)	1.349(4)
Cl(2)-C(25)	1.735(4)	N(4)-C(20)	1.382(4)
O(1W)-H(1WA)	0.8771	N(5)-C(25)	1.345(4)
O(1W)-H(1WB)	0.8500	N(5)-C(21)	1.362(4)

Table 3.4 Selected bond angles (°) for $[Ru(tpy)(dcbpy)(H_2O)](CF_3SO_3)_2$

N(2)-Ru(1)-N(1)	79.80(10)	N(5)-Ru(1)-O(1W)	101.12(9)
N(2)-Ru(1)-N(4)	101.58(11)	H(1WA)-O(1W)-H(1WB)	107.7
N(1)-Ru(1)-N(4)	96.32(11)	Ru(1)-O(1W)-H(1WA)	118.8
N(2)-Ru(1)-N(3)	79.89(10)	Ru(1)-O(1W)-H(1WB)	107.3(10)
N(1)-Ru(1)-N(3)	159.66(10)	C(1)-N(1)-Ru(1)	128.6(2)
N(4)-Ru(1)-N(3)	88.81 (10)	C(5)-N(1)-Ru(1)	113.2(2)
N(2)-Ru(1)-N(5)	177.48(10)	C(6)-N(2)-Ru(1)	118.6(2)
N(1)-Ru(1)-N(5)	102.71(10)	C(10)-N(2)-Ru(1)	118.3(2)
N(4)-Ru(1)-N(5)	72.28(10)	C(15)-N(3)-Ru(1)	129.5(2)
N(3)-Ru(1)-N(5)	97.60(10)	C(11)-N(3)-Ru(1)	112.4(2)
N(2)-Ru(1)-O(1W)	78.82(9)	C(16)-N(4)-Ru(1)	130.7(2)
N(1)-Ru(1)-O(1W)	88.07(10)	C(20)-N(4)-Ru(1)	113.2(2)
N(4)-Ru(1)-O(1W)	175.59(9)	C(25)-N(5)-Ru(1)	131.2(2)
N(3)-Ru(1)-O(1W)	86.93(9)	C(21)-N(5)-Ru(1)	112.8(2)

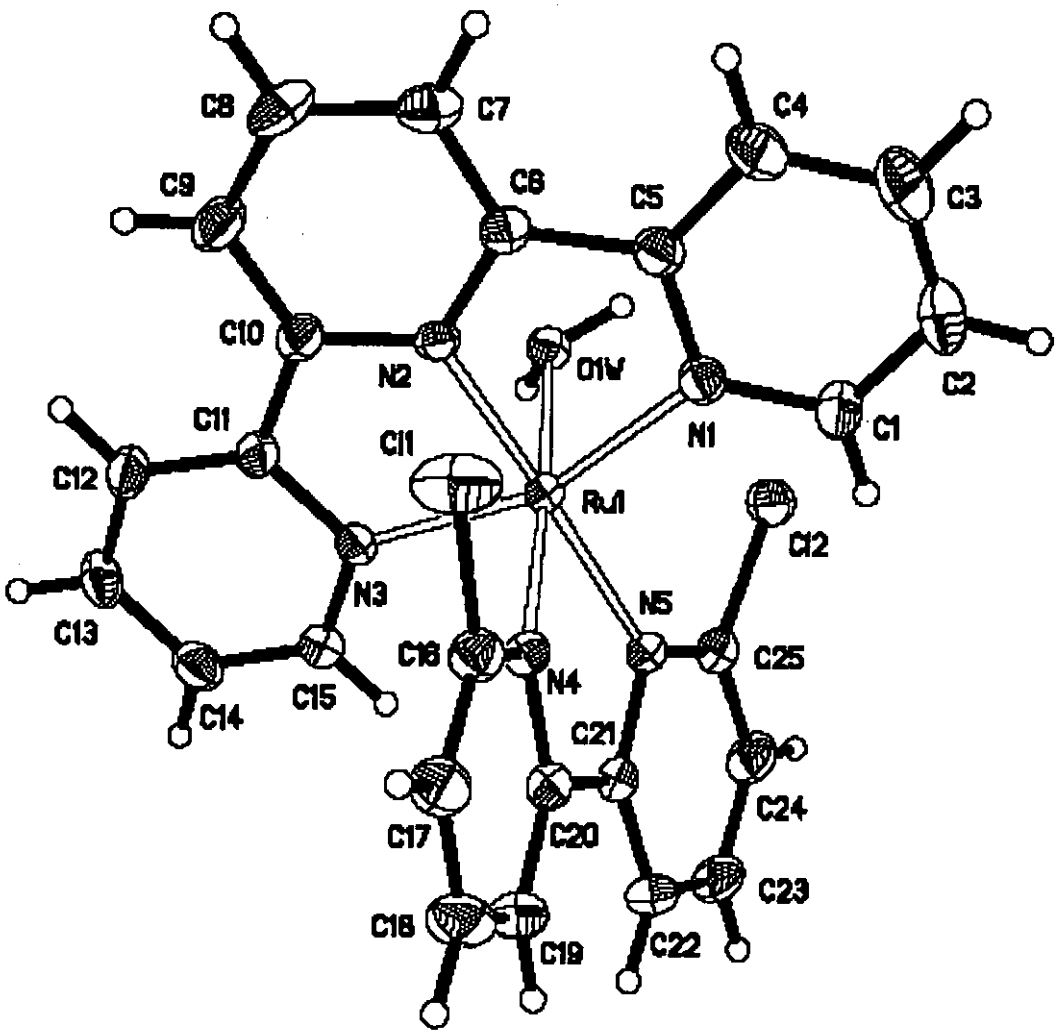

Figure 3.2 An ORTEP plot of $[Ru(tpy)(dcbpy)(H_2O)]^{2+}$ with atom numbering.

Table 3.5 Selected bond length (Å) for $[Ru(tpy)(dcbpy)(CH_3CN)](CF_3SO_3)_2(ClO_4)$

Ru(1)-N(1)	2.069(5)	N(1)-C(1)	1.334(7)
Ru(1)-N(2)	1.961(5)	N(1)-C(5)	1.401(7)
Ru(1)-N(3)	2.084(5)	N(2)-C(6)	1.364(6)
Ru(1)-N(4)	2.096(5)	N(2)-C(10)	1.349(7)
Ru(1)-N(5)	2.104(4)	N(3)-C(15)	1.343(7)
Ru(1)-N(6)	2.001(5)	N(3)-C(11)	1.367(6)
Cl(1)-C(16)	1.712(6)	N(4)-C(16)	1.350(6)
Cl(2)-C(25)	1.715(6)	N(4)-C(20)	1.378(6)
N(6)-C(26)	1.140(7)	N(5)-C(25)	1.338(6)
		N(5)-C(21)	1.377(6)

Table 3.6 Selected bond angles (°) for [Ru(tpy)(dcbpy)(CH_3CN)](CF_3SO_3).(ClO_4)

N(2)-Ru(1)-N(6)	84.74(18)	N(3)-Ru(1)-N(5)	100.39(19)
N(2)-Ru(1)-N(1)	80.1(2)	N(4)-Ru(1)-N(5)	78.39(18)
N(6)-Ru(1)-N(1)	93.21(18)	C(1)-N(1)-Ru(1)	129.4(4)
N(2)-Ru(1)-N(3)	78.8(2)	C(5)-N(1)-Ru(1)	112.9(4)
N(6)-Ru(1)-N(3)	86.47(18)	C(10)-N(2)-Ru(1)	119.4(4)
N(1)-Ru(1)-N(3)	158.8(2)	C(6)-N(2)-Ru(1)	118.4(4)
N(2)-Ru(1)-N(4)	101.02(18)	C(15)-N(3)-Ru(1)	128.1(4)
N(6)-Ru(1)-N(4)	169.90(19)	C(11)-N(3)-Ru(1)	114.2(4)
N(1)-Ru(1)-N(4)	95.94(17)	C(16)-N(4)-Ru(1)	130.9(4)
N(3)-Ru(1)-N(4)	86.53(16)	C(20)-N(4)-Ru(1)	111.9(4)
N(2)-Ru(1)-N(5)	179.0(2)	C(25)-N(5)-Ru(1)	131.3(4)
N(6)-Ru(1)-N(5)	95.72(19)	C(21)-N(5)-Ru(1)	112.4(4)
N(1)-Ru(1)-N(5)	100.71(19)	C(26)-N(6)-Ru(1)	173.6(6)

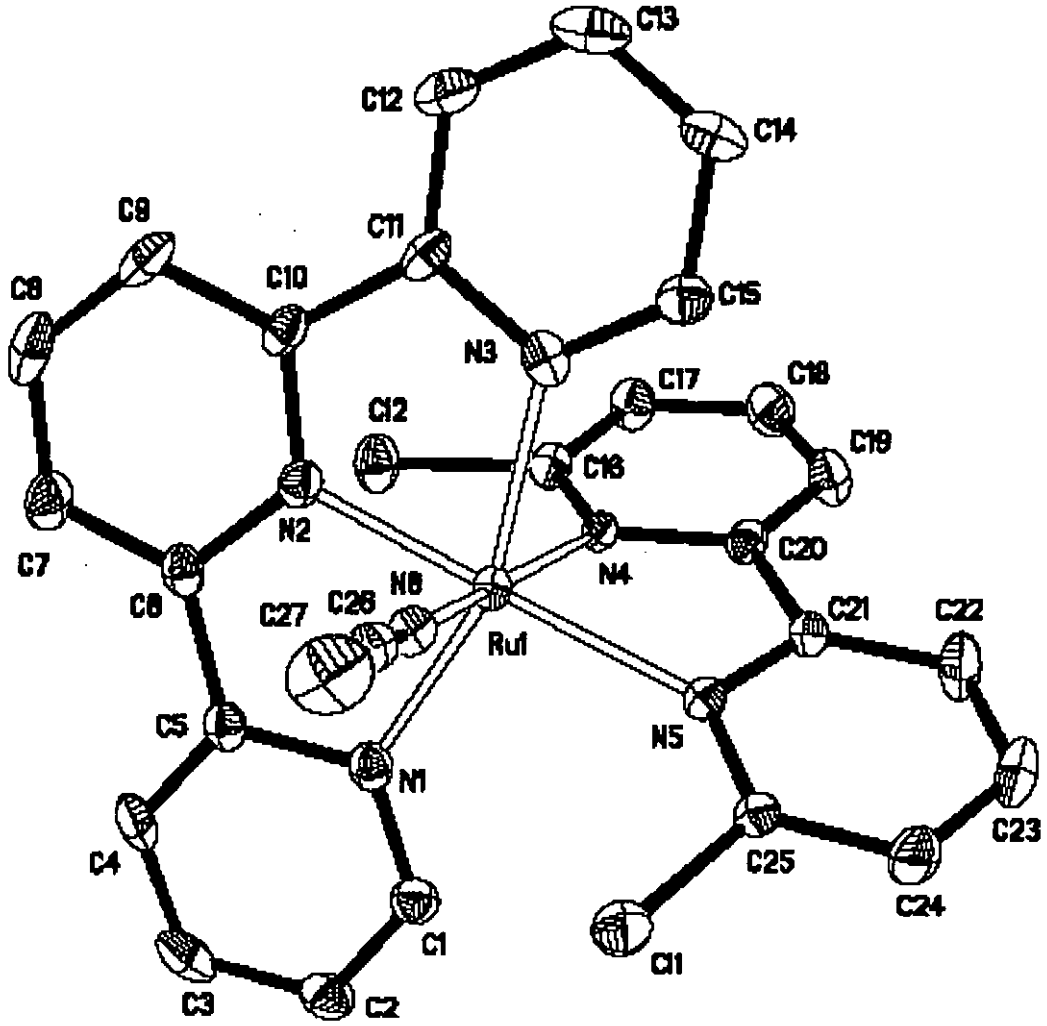

Figure 3.3 An ORTEP plot of $[Ru(tpy)(dcbpy)(CH_3CN)]^{2+}$ with atom numbering.

Table 3.7 Selected bond length (Å) for $[Ru(tpy)(bpy)(H_2O)](CF_3SO_3)_2$

Ru(1)-N(1)	2.011(2)	N(1)-C(5)	1.373(4)
Ru(1)-N(2)	2.075(2)	N(2)-C(6)	1.349(4)
Ru(1)-N(3)	2.071(2)	N(2)-C(10)	1.349(4)
Ru(1)-N(4)	1.959(2)	N(3)-C(15)	1.376(4)
Ru(1)-N(5)	2.070(2)	N(3)-C(11)	1.342(4)
Ru(1)-O(7)	2.129(2)	N(4)-C(16)	1.351(4)
O(7)-H(20)	0.92	N(4)-C(20)	1.354(3)
O(7)-H(21)	0.87	N(5)-C(25)	1.346(4)
N(1)-C(1)	1.353(3)	N(5)-C(21)	1.373(4)

Table 3.8 Selected bond angles (°) for $[Ru(tpy)(bpy)(H_2O)](CF_3SO_3)_2$

N(1)-Ru(1)-N(2)	78.76(9)	N(5)-Ru(1)-O(7)	87.47(9)
N(1)-Ru(1)-N(3)	91.39(9)	H(20)-O(7)-H(21)	117.5
N(1)-Ru(1)-N(4)	98.07(10)	Ru(1)-O(7)-H(20)	118.6
N(1)-Ru(1)-N(5)	93.09(9)	Ru(1)-O(7)-H(21)	107.3
N(2)-Ru(1)-N(3)	98.58(9)	C(1)-N(1)-Ru(1)	125.8(2)
N(2)-Ru(1)-N(4)	176.41(1)	C(5)-N(1)-Ru(1)	116.8(2)
N(2)-Ru(1)-N(5)	102.32(9)	C(6)-N(2)-Ru(1)	115.3(2)
N(3)-Ru(1)-N(4)	79.71(9)	C(10)-N(2)-Ru(1)	126.3(2)
N(3)-Ru(1)-N(5)	159.10(9)	C(11)-N(3)-Ru(1)	129.3(2)
N(4)-Ru(1)-N(5)	79.45(10)	C(15)-N(3)-Ru(1)	113.3(2)
N(1)-Ru(1)-O(7)	172.22(9)	C(16)-N(4)-Ru(1)	130.7(2)
N(2)-Ru(1)-O(7)	93.53(10)	C(20)-N(4)-Ru(1)	119.3(2)
N(3)-Ru(1)-O(7)	90.82(9)	C(21)-N(5)-Ru(1)	113.4(2)
N(4)-Ru(1)-O(7)	86.67(10)	C(25)-N(5)-Ru(1)	128.7(2)

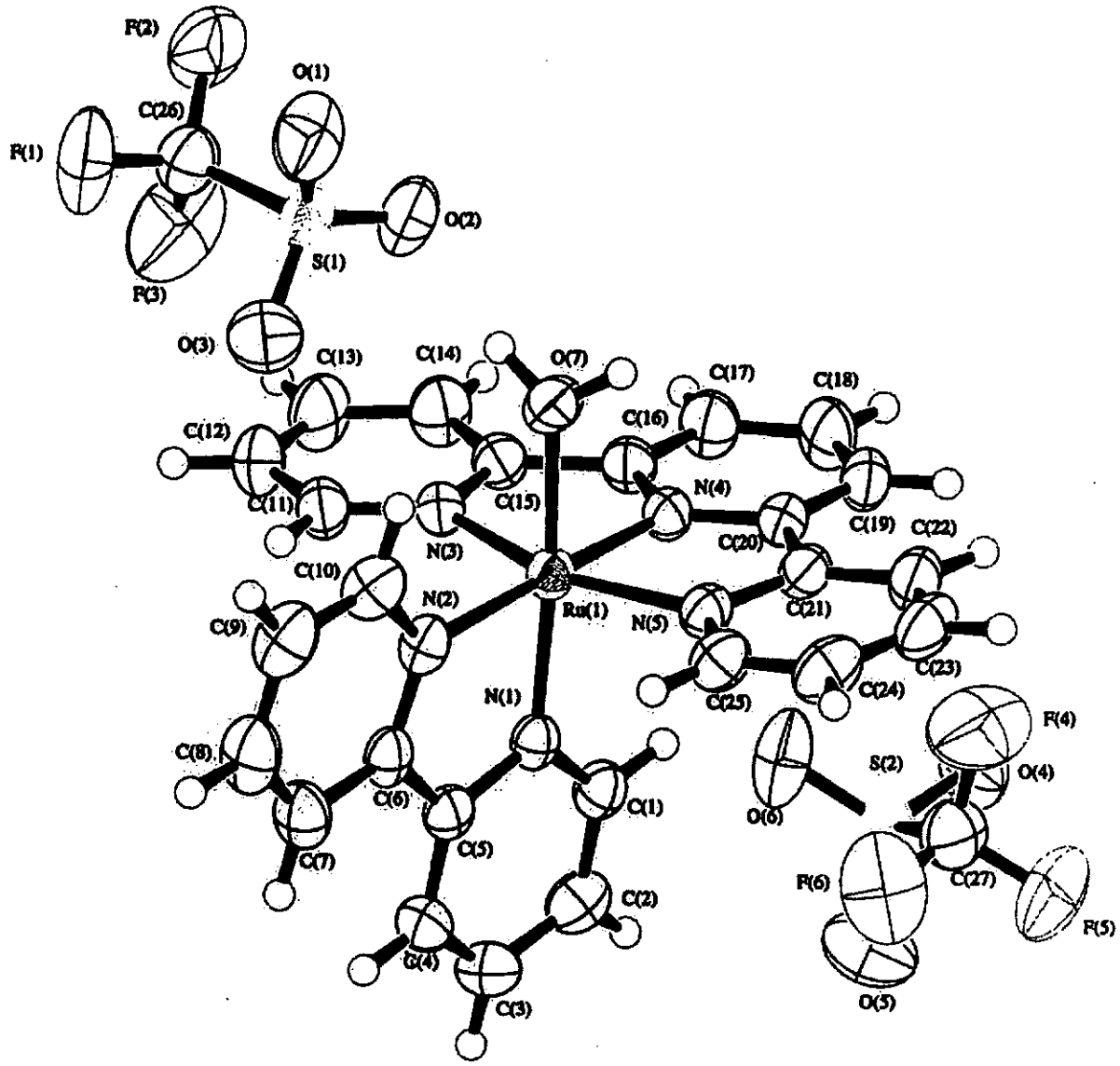

Figure 3.4 An ORTEP plot of $[Ru(tpy)(bpy)(H_2O)](CF_3SO_3)_2$ with atom numbering.

Table 3.9 Selected bond length (Å) for *cis*-$[Ru(dcbpy)_2(H_2O)_2](CF_3SO_3)_2$

Ru(1)-N(1)	2.077(2)	O(2)-H(16)	0.82
Ru(1)-N(2)	2.047(2)	N(1)-C(1)	1.333(3)
Ru(1)-N(3)	2.033(2)	N(1)-C(5)	1.370(3)
Ru(1)-N(4)	2.085(2)	N(2)-C(6)	1.377(3)
Ru(1)-O(1)	2.129(2)	N(2)-C(10)	1.338(3)
Ru(1)-O(2)	2.145(2)	N(3)-C(11)	1.350(3)
O(1)-H(13)	0.81	N(3)-C(15)	1.375(3)
O(1)-H(14)	0.84	N(4)-C(16)	1.368(3)
O(2)-H(15)	0.79	N(4)-C(20)	1.347(3)

Table 3.10 Selected bond angles (°) for *cis*-[Ru(dcbpy)$_2$(H$_2$O)$_2$](CF$_3$SO$_3$)$_2$

O(1)-Ru(1)-O(2)	83.08(7)	N(3)-Ru(1)-N(4)	79.04(8)
O(1)-Ru(1)-N(1)	82.20(7)	H(20)-O(7)-H(21)	117.5
O(1)-Ru(1)-N(2)	89.71(7)	Ru(1)-O(7)-H(20)	118.6
O(1)-Ru(1)-N(3)	170.30(7)	Ru(1)-O(7)-H(21)	107.3
O(1)-Ru(1)-N(4)	97.23(8)	C(1)-N(1)-Ru(1)	130.5(2)
O(2)-Ru(1)-N(1)	96.72(7)	C(5)-N(1)-Ru(1)	116.1(1)
O(2)-Ru(1)-N(2)	172.20(7)	C(6)-N(2)-Ru(1)	112.9(1)
O(2)-Ru(1)-N(3)	88.50(7)	C(10)-N(2)-Ru(1)	131.2(2)
O(2)-Ru(1)-N(4)	79.54(7)	C(11)-N(3)-Ru(1)	130.2(2)
N(1)-Ru(1)-N(2)	79.29(7)	C(15)-N(3)-Ru(1)	112.2(2)
N(1)-Ru(1)-N(3)	101.01(8)	C(16)-N(4)-Ru(1)	111.4(2)
N(1)-Ru(1)-N(4)	176.26(7)	C(20)-N(4)-Ru(1)	131.2(2)
N(2)-Ru(1)-N(3)	98.81(7)		
N(2)-Ru(1)-N(4)	104.42(7)		

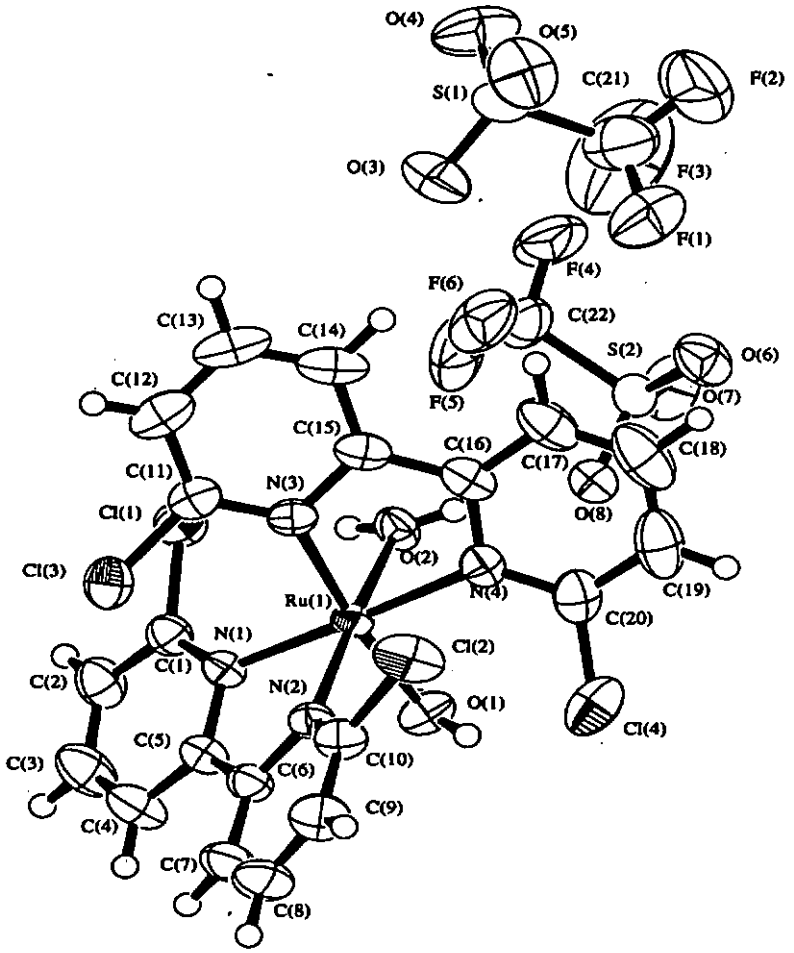

Figure 3.5 An ORTEP plot of *cis*-$[Ru(dcbpy)_2(H_2O)_2](CF_3SO_3)_2$ with atom numbering.

3.3.2. Correlation between structure and electrochemistry

Figures 3.6 and 3.7 show the cyclic voltammograms of $[Ru(tpy)(bpy)(H_2O)]^{2+}$ and $[Ru(tpy)(dcbpy)(H_2O)]^{2+}$ in 0.1 M CF_3SO_3H (pH 1.0) respectively. In both cyclic voltammograms two couples are observed: The first one (I) corresponds to the Ru^{III}/Ru^{II} couple and the second smaller one (II) is the Ru^{IV}/Ru^{III} couple. Comparison of the cyclic voltammograms of $[Ru(tpy)(dcbpy)(H_2O)]^{2+}$ with $[Ru(tpy)(bpy)(H_2O)]^{2+}$ shows that the second Ru^{IV}/Ru^{III} couple is more reversible and easier to observe in the former. This implies that the oxidation of Ru^{III}-OH to Ru^{IV}=O is more facile in $[Ru(tpy)(dcbpy)(H_2O)]^{2+}$ than $[Ru(tpy)(bpy)(H_2O)]^{2+}$. Meyer and co-workers [183, 184] proposed the oxidation of Ru^{II}-OH_2 to Ru^{IV}=O involves: (1) Oxidation of Ru^{II}-OH_2 into Ru^{III}-OH by losing one electron and one proton [couple (I), (eq 3.1)]; (2) Disproportionation of two Ru^{III}-OH into Ru-OH_2 and Ru=O (eq 3.2) and (3) Oxidation of the Ru^{II}-OH_2 generated from the disproportionational reaction (eq 3.3). It was proposed that the second couple (II) is due to the oxidation of the Ru^{II}-OH_2 species resulting from the disproportionation reaction:

$$[Ru^{II}\text{-}OH_2]^{2+} \longrightarrow [Ru^{III}\text{-}OH]^{2+} + e^- + H^+ \qquad (3.1)$$

$$2[Ru^{III}\text{-}OH]^{2+} \longrightarrow \left[Ru^{III}\text{-}O\overset{H}{\underset{H}{\cdots}}O\text{-}Ru^{III}\right]^{4+} \longrightarrow \left[Ru^{II}\text{-}OH_2\right]^{2+} + \left[Ru^{IV}=O\right]^{2+} \qquad (3.2)$$

$$[Ru^{II}\text{-}OH_2]^{2+} \longrightarrow [Ru^{III}\text{-}OH]^{2+} + e^- + H^+ \qquad (3.3)$$

The main difference between $[Ru(tpy)(dcbpy)(H_2O)]^{2+}$ and $[Ru(tpy)(bpy)(H_2O)]^{2+}$ is the chloro-substituents on the ortho-position of the bipyridine ligand. The electron-withdrawing effect of the chloro-constituents makes the ruthenium centre more electron deficient, which would affect the pK_a of the aqua and hydroxo ligands of the ruthenium complex. However, the ease of accessibility to the Ru^{IV}=O state is unlikely due to the negative inductive effect as placing the chloro or trifluoromethyl substituents in the 4,4'- and 5,5'-positions would only shift the $E_{1/2}$ of the couples towards the anodic direction but does not improve the reversibility of the Ru^{IV}/Ru^{III} couple. We suspect the chloro-substituents at the 6,6'-positions are able to form weak hydrogen bonding with the $-OH_2$ or –OH ligand on the Ru complex, which would assist the deprotonation in the proton-coupled electron transfer to the Ru=O. Formation of weak hydrogen-bond between C-Cl and H-O is known in the literature [185-187].

In literature, there are several tools to study hydrogen bondings between molecules; namely infrared (IR) spectroscopy, nuclear magnetic resonances (NMR) and X-ray crystallography [188]. NMR spectroscopy is so far the most common tool as the patterns or chemical shift of the proton signal will change in the presence of hydrogen bonding interaction. IR spectroscopy is only used for strong hydrogen bonds. Both

NMR and IR spectroscopy, however, were proved to be difficult for the ruthenium aqua complexes. The complexes $[Ru(tpy)(dcbpy)(H_2O)]^{2+}$ and $[Ru(tpy)(bpy)(H_2O)]^{2+}$ undergo fast exchange with most common solvents including acetone, methanol, ethanol acetonitrile and tetrahydrofuran (Figure A1-A3 in the Appendix). These complexes are not soluble in non-polar solvents such as dichloromethane and chloroform. Attempts have been made to record the solid state IR spectrum of these complexes using KBr-pellets, but we did not observe the IR stretching assignable to OH···Cl probably because the hydrogen bond is too weak to be observed. Due to these limitations, we used X-ray crystallography to probe the possibility of intramolecular hydrogen bondings in $[Ru(tpy)(dcbpy)(H_2O)]^{2+}$ and *cis*-$[Ru(dcbpy)_2(H_2O)_2]^{2+}$ complexes. The bond length of $Ru\text{-}O_{(OH_2)}$ in $[Ru(tpy)(dcbpy)(H_2O)]^{2+}$ and $[Ru(tpy)(bpy)(H_2O)]^{2+}$ are 2.130 Å and 2.129 Å respectively, which does not represent a significant difference between the two. However, the Ru-O bond distance in $[Ru^{II}(bpy)_2(PO^iPr\text{-}P)(OH_2)]^{2+}$ (PO^iPr-P = 2-(2-propoxy)phenyl)diphenylphosphine) which is known to contain an intramolecular hydrogen bond between the coordinated aqua ligand and the isopropyl ether oxygen [182], is 2.138 Å. The $Ru\text{-}O_{(OH_2)}$ bond length is also very similar to most ruthenium aqua complexes reported in the literature [111, 178, 182, 189-191], which ranges from 2.11 to 2.18 Å. Therefore, the Ru-O bond distance may not be a good indicator for

H-bonding. In $[Ru(tpy)(dcbpy)(H_2O)]^{2+}$, the distances between H1A, H1B and Cl are 2.7 Å and 2.8 Å respectively. These distances between the OH_2 hydrogens and Cl on bipyridine suggest the existence of "intermediate" intramolecular hydrogen bonding [185-187].

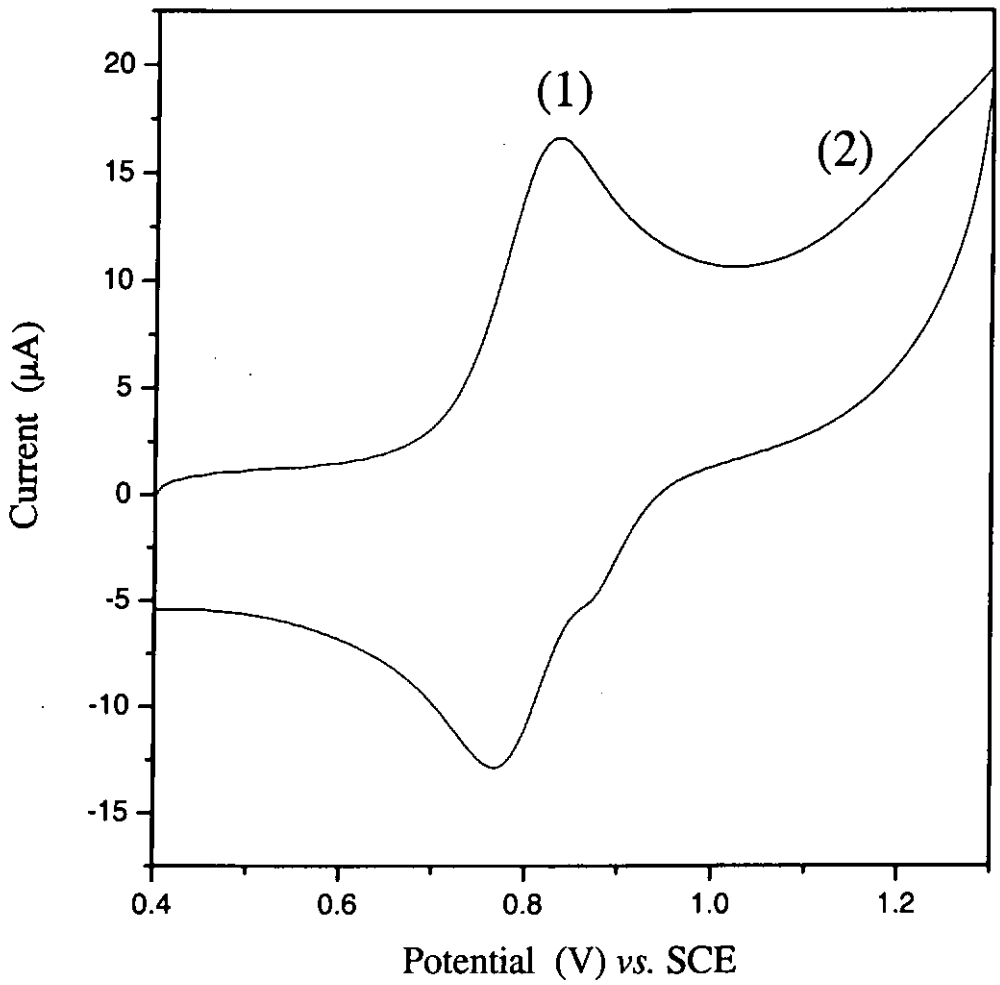

Figure 3.6 Cyclic voltammogram of 0.5mM $[Ru(tpy)(bpy)(H_2O)]^{2+}$ in 0.1 M of CF_3SO_3H solution. Working electrode: 0.196 cm^2 glassy carbon. Scan rate: 100 mVs^{-1}

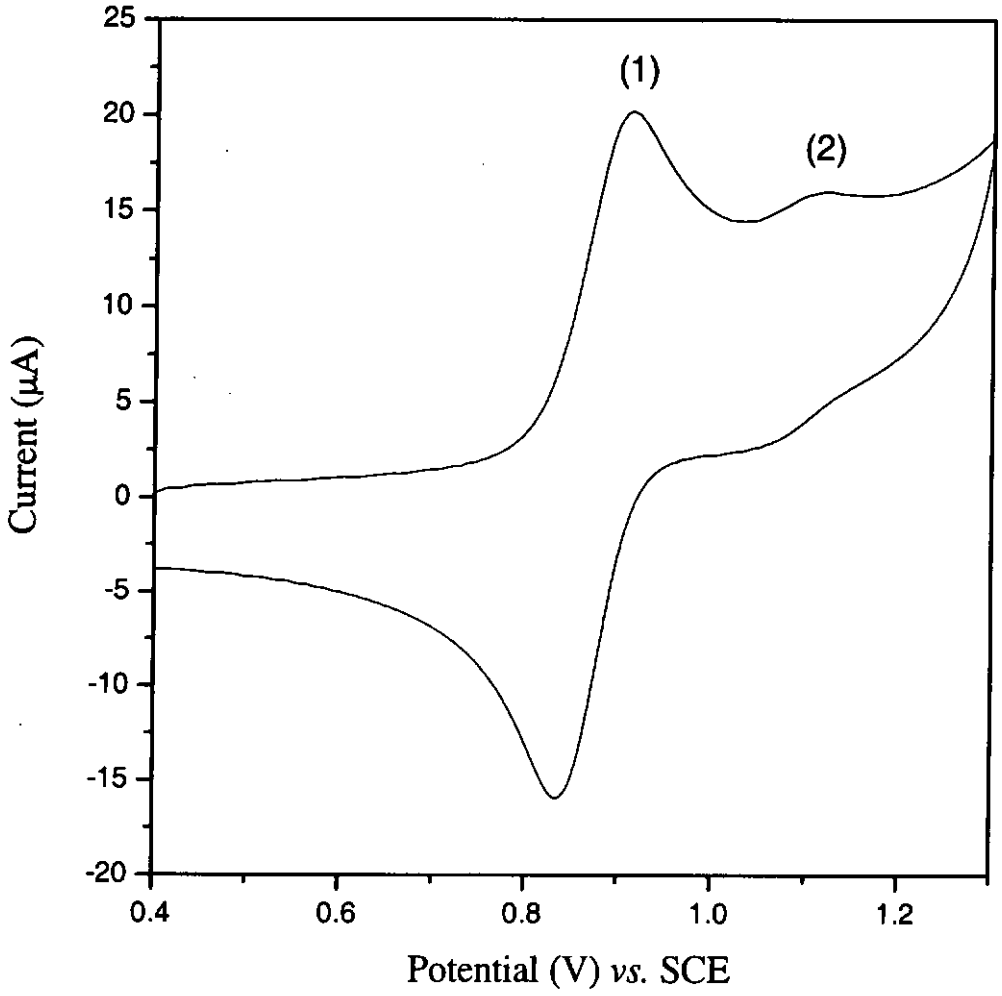

Figure 3.7 Cyclic voltammogram of 0.5mM $[Ru(tpy)(dcbpy)(H_2O)]^{2+}$ in 0.1 M of CF_3SO_3H solution. Working electrode: 0.196 cm^2 glassy carbon. Scan rate: 100 mVs^{-1}

Table 3.11 A comparison of the $O_{(OH_2)}$-Ru-$N_{(bipyridine)}$ and $N_{(CH_3CN)}$-Ru-$N_{(bipyridine)}$ angles in various ruthenium complexes.

Complex	Deviation from planarity (90°)
$[Ru(tpy)(dcbpy)(H_2O)]^{2+}$	101.1°
$[Ru(tpy)(dcbpy)(CH_3CN)]^{2+}$	95.7°
$[Ru(tpy)(bpy)(H_2O)]^{2+}$	93.5°

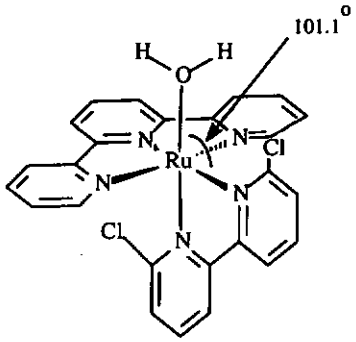

$[Ru(tpy)(dcbpy)(H_2O)]^{2+}$

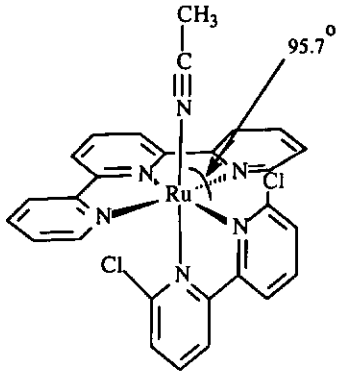

$[Ru(tpy)(dcbpy)(CH_3CN)]^{2+}$

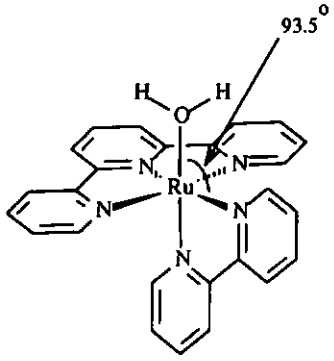

$[Ru(tpy)(bpy)(H_2O)]^{2+}$

A comparison of the $O_{(OH_2)}$-Ru-$N_{(bipyridine)}$ and $N_{(CH_3CN)}$-Ru-$N_{(bipyridine)}$ bond angles in $[Ru(tpy)(dcbpy)(H_2O)]^{2+}$, $[Ru(tpy)(bpy)(H_2O)]^{2+}$ and $[Ru(tpy)(dcbpy)(CH_3CN)]^{2+}$ yields interesting results, which are tabulated in Table 3.11. The structure of $[Ru(tpy)(dcbpy)(H_2O)]^{2+}$ and $[Ru(tpy)(dcbpy)(CH_3CN)]^{2+}$ should be similar, but the angle between the $O_{(OH_2)}$-Ru-$N_{(bipyridine)}$ and $N_{(CH_3CN)}$-Ru-$N_{(bipyridine)}$ angles are significantly different. In $[Ru(tpy)(dcbpy)(H_2O)]^{2+}$, the $O_{(OH_2)}$-Ru-$N_{(bipyridine)}$ angle is 101.1°, whereas replacing of the aqua ligand with CH_3CN decreases the angle to 95.7°. The $[Ru(tpy)(bpy)(H_2O)]^{2+}$ complex without the chloro-substituents has an

$O_{(OH_2)}$-Ru-$N_{(bipyridine)}$ angle of 93.5°, which is similar to that $[Ru(tpy)(dcbpy)(CH_3CN)]^{2+}$. Such a large difference between $[Ru(tpy)(dcbpy)(H_2O)]^{2+}$ and $[Ru(tpy)(bpy)(H_2O)]^{2+}$ cannot be attributed to random error in estimating the bond angles.

We propose that the difference in the bond angles can be accounted by the existence of intramolecular hydrogen bonding between the chloro-substituent on 6,6'-dichloro-2,2'-bipyridine and the hydrogen of the aqua ligand on the ruthenium centre in $[Ru(tpy)(dcbpy)(H_2O)]^{2+}$. The $O_{(OH_2)}$-Ru-$N_{(bipyridine)}$ angle in $[Ru(tpy)(dcbpy)(H_2O)]^{2+}$ is opened up from the ideal 90° to 101.1° in order to accommodate this intramolecular hydrogen bond, otherwise the resulting 6-membered ring (see **Scheme 3.1**) would be highly strained. The estimated distance between the hydrogen of the aqua ligand and the chloro group on 6,6'-dichloro-2,2'-bipyridine is also consistent with the existence of hydrogen bonding between them.

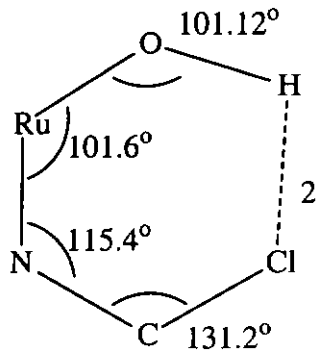

Scheme 3.1

A comparison of the cyclic voltammograms of the *cis*-diaqua complex

cis-$[Ru(dcbpy)_2(H_2O)_2]^{2+}$ with that of other diaqua ruthenium(II) polypyridyl complexes is also intriguing. The cyclic voltammogram of *cis*-$[Ru(dcbpy)_2(H_2O)_2]^{2+}$ in 0.1 M acid consists of two well-defined couples corresponding to Ru^{IV}/Ru^{II} and Ru^{VI}/Ru^{IV} respectively (Figure 3.8). The cyclic voltammogram of all the other ruthenium diaqua complexes, such as *cis*-$[Ru((bpy)_2(H_2O)_2]^{2+}$ [115], *cis*-$[Ru(dmbpy)_2(H_2O)_2]^{2+}$ [192] and *cis*-$[Ru((CF_3)_2bpy)_2(H_2O)_2]^{2+}$ [181] (dmbpy = 6,6'-dimethyl-2,2'-bipyridine, $(CF_3)_2$bpy = 5,5'-trifluoromethyl-2,2'-bipyridine) consists of 4 couples assignable as Ru^{III}/Ru^{II}, Ru^{IV}/Ru^{III}, Ru^{IV}/Ru^{V} and Rv^{VI}/Ru^{V} respectively. Only the Ru^{III}/Ru^{II} couple in these complexes is well-defined, whereas the other three couples are small and poorly shaped.

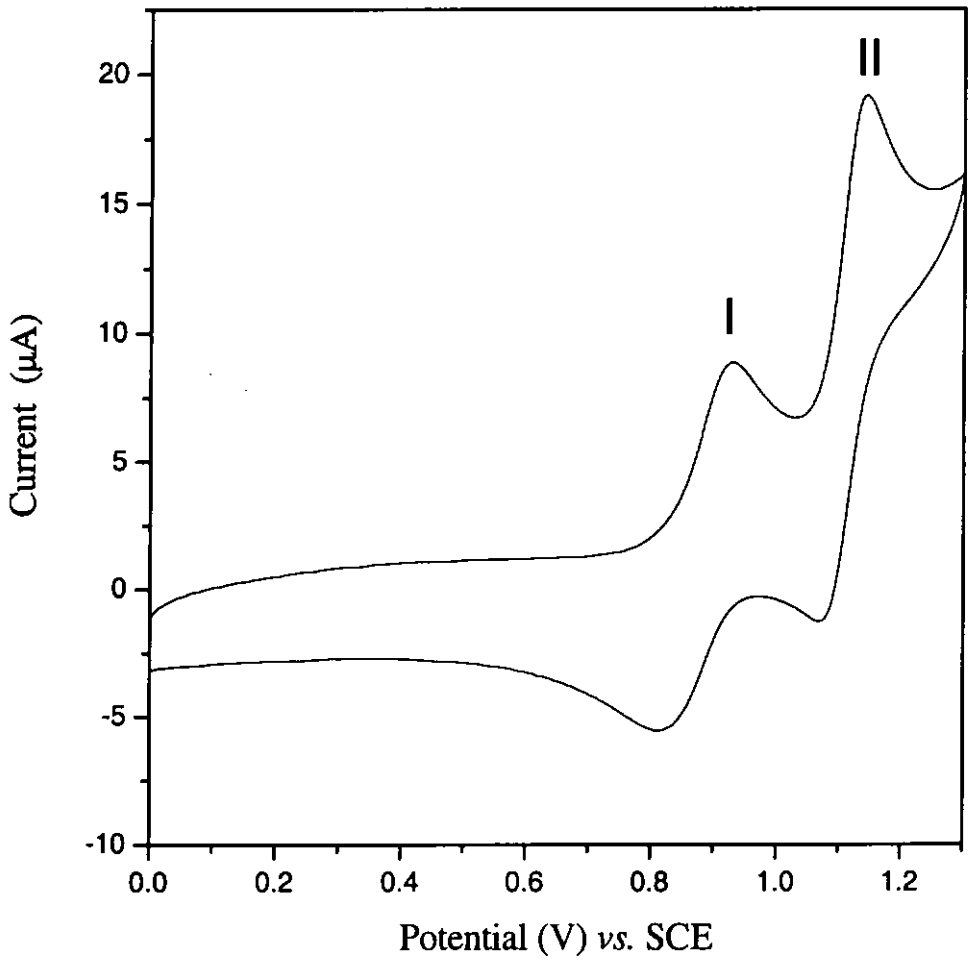

Figure 3.8 Cyclic voltammogram of 0.5mM *cis*-$[Ru(dcbpy)_2(H_2O)_2]^{2+}$ in 0.1 M CF_3SO_3H. Working electrode: 0.196 cm^2 glassy carbon. Scan rate: 100 mVs^{-1}

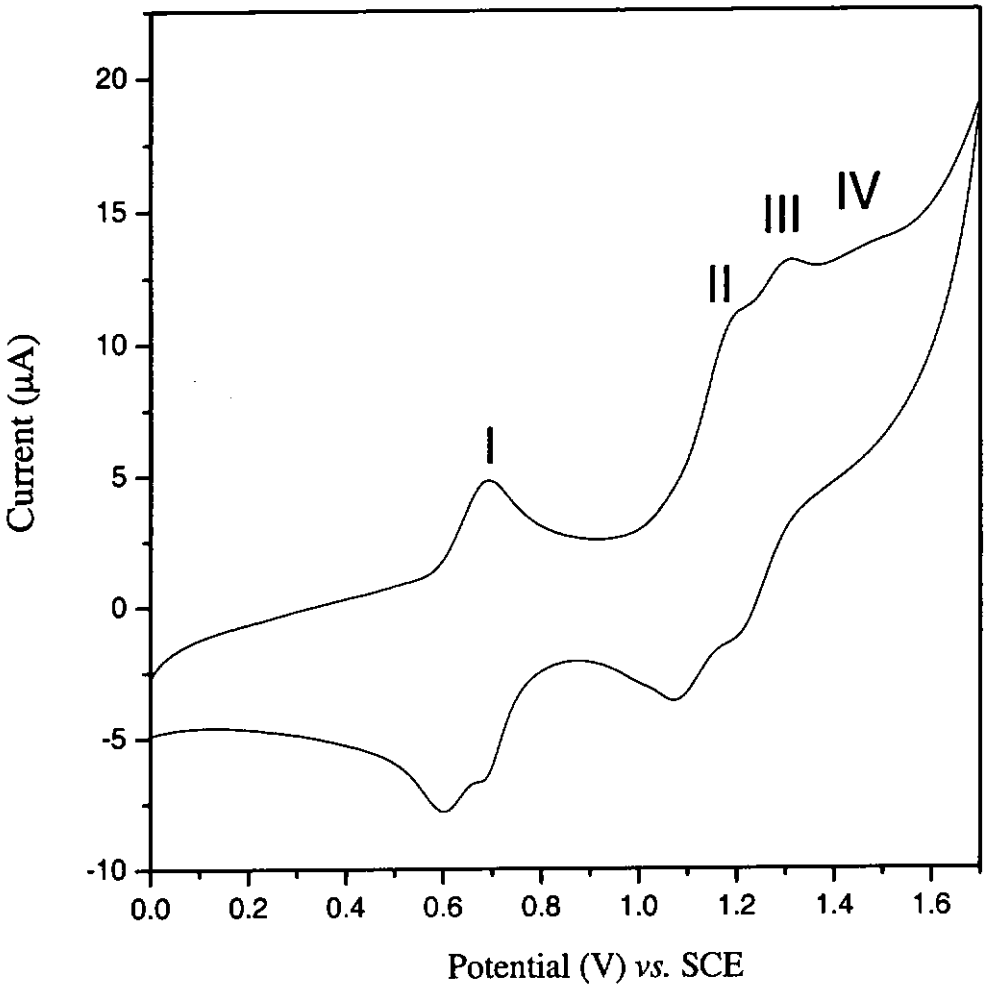

Figure 3.9 Cyclic voltammogram of 0.5mM $[Ru(bpy)_2(H_2O)_2]^{2+}$ in 0.1 M CF_3SO_3H. Working electrode: 0.196 cm^2 glassy carbon. Scan rate: 100 mVs^{-1}. The $[Ru(bpy)_2(H_2O)_2]^{2+}$ was generated from $[Ru(bpy)_2(CO_3)]$ in acid as described in [115].

A comparison of the $O_{(OH_2)}$-Ru-$N_{(bipyridine)}$ and $N_{(CH_3CN)}$-Ru-$N_{(bipyridine)}$ bond angles in *cis*-$[Ru(dcbpy)_2(H_2O)_2]^{2+}$ with those of *cis*-$[Ru((CF_3)_2bpy)_2(CH_3CN)_2]^{2+}$ [181] and *cis*-$[Ru(bpy)_2(CH_3CN)_2]^{2+}$ [180] is given in Figure 3.10

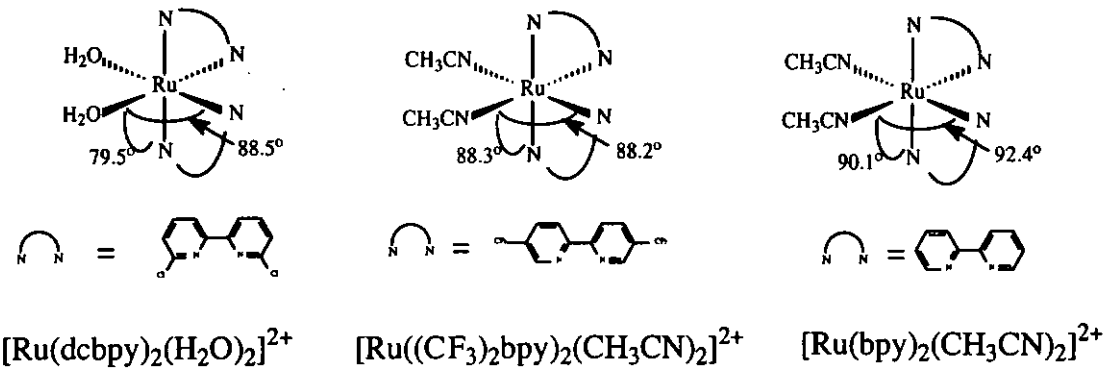

$[Ru(dcbpy)_2(H_2O)_2]^{2+}$ $[Ru((CF_3)_2bpy)_2(CH_3CN)_2]^{2+}$ $[Ru(bpy)_2(CH_3CN)_2]^{2+}$

Figure 3.10 Comparison of bond angles in three ruthenium complexes.

The O_a-Ru-N_a bond angle of 79.5° in *cis*-$[Ru(dcbpy)_2(H_2O)_2]^{2+}$ deviates greatly from the $N_{(CH_3CN)}$-Ru-$N_{(bipyridine)}$ angle of approximately 90° in the bis(acetonitrile) complexes. This observation is again consistent with the presence of intramolecular hydrogen bonding between the hydrogen atoms on the aqua ligand and the chloro-substituents on bipyridine, which pulls the aqua ligand toward the 6,6'dichloro-2,2'-bipyridine to make the O_a-Ru-N_a angle much smaller than 90° (Figure 3.11).

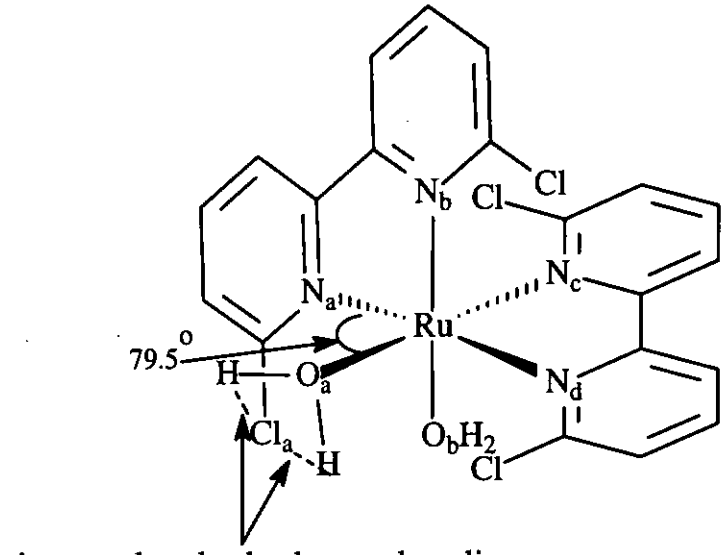

Figure 3.11 Schematic diagram of the *cis*-$[Ru(dcbpy)_2(H_2O)_2]^{2+}$ complex showing the intramolecular hydrogen bonding.

The Ru-$O_{(OH_2)}$ bond length in *cis*-$[Ru^{II}(dcbpy)_2(H_2O)_2]^{2+}$ are 2.129(2) and 2.145(2) Å respectively, which are close to those of 2.116(2) Å reported for trans-diaqua ruthenium (II) diaqua complex [190]. This Ru-$O_{(OH_2)}$ bond length is also similar to that 2.138(2) Å in the complex $[Ru^{II}(bpy)_2(PO^iPr\text{-}P)(OH_2)]^{2+}$ (PO^iPr-P = 2-(2-Propoxy)phenyl)diphenylphosphine) contains an intramolecular hydrogen bonding between the coordinated aqua ligand and the isopropyl ether oxygen [182].

This proposed hydrogen bonding should facilitate the deprotonation of the aqua

ligand in the oxidation of Ru-OH_2 to Ru=O. In *cis*-$[Ru(dcbpy)_2(H_2O)_2]^{2+}$ the extent of this assistance in deprotonation is so great that the Ru^{IV}/Ru^{III} and Ru^{VI}/Ru^{V} couples merge with that of Ru^{III}/Ru^{II} and Ru^{V}/Ru^{IV} to give two Ru^{IV}/Ru^{II} and Ru^{VI}/Ru^{IV} couples respectively.

FTIR spectroelectrochemistry

By using *in-stiu* FTIR spectroelectrochemical technique, we can monitor the formation of the ruthenium oxo species. Che and co-workers [110] have reported that $[Ru(tpy)(dcbpy)(O)]^{2+}$ exhibits an IR absorption peak at 780 cm^{-1} assignable to $\nu(Ru^{IV}=O)$. Figure 3.12 shows the IR reflectance spectra of $[Ru(tpy)(dcbpy)(H_2O)]^{2+}$ in 0.1 M CF_3SO_3H with the potential being held at 1.3 V at different time intervals. A new peak at 780 cm^{-1} slowly develops which is assigned as the $\nu(Ru=O)$ stretching. No increase in absorption at 780 cm^{-1} was observed when the potential of the working electrode was held at 0.83 V, which is below the potential required for the formation of $Ru^{IV}=O$ (Figure 3.13). The increase in absorption at 763 cm^{-1} observed in both spectra were assignable to of the C-H bending of bipyridine ligand.

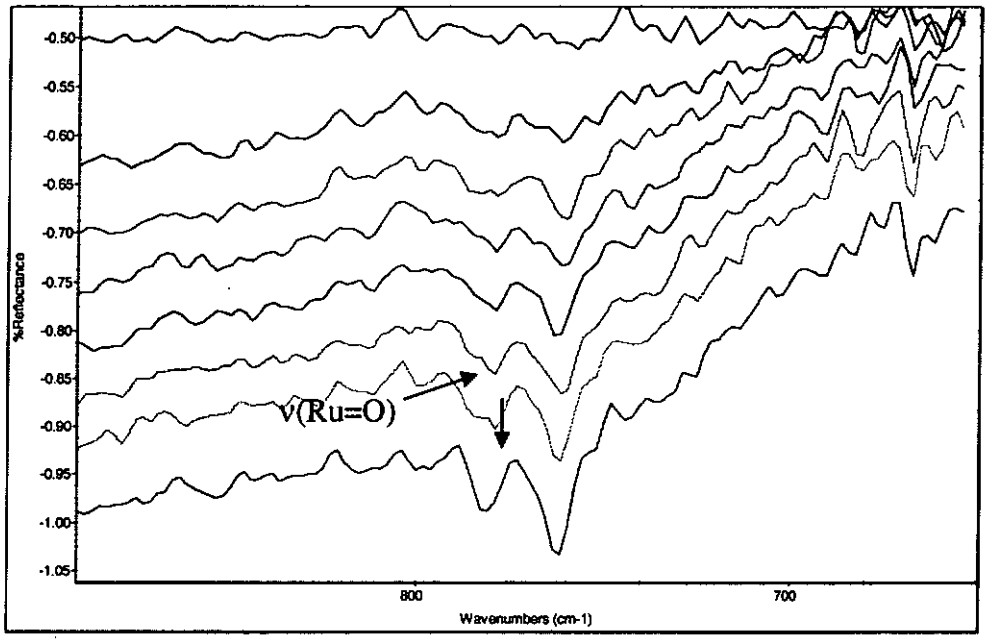

Figure 3.12 IR reflectance spectra of $[Ru(tpy)(dcbpy)(H_2O)]^{2+}$ in 0.1 M CF_3SO_3H with the potential being held at 1.3 V. The spectra were recorded at time intervals of 16 s.

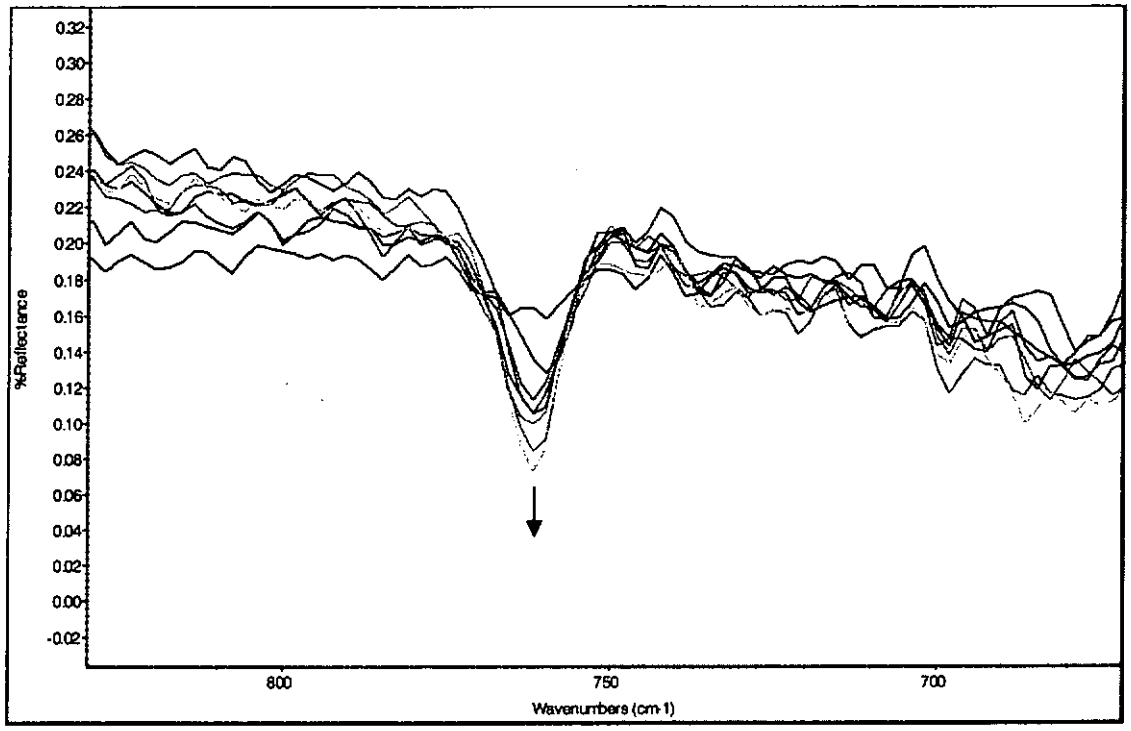

Figure 3.13 IR reflectance spectra of $[Ru(tpy)(dcbpy)(H_2O)]^{2+}$ in 0.1 M CF_3SO_3H with the potential being held at 0.83 V. The spectra were recorded at time intervals of 16 s.

3.4. Conclusion

The structure of two ruthenium aqua complexes with 6,6'-dichloro-2,2'-bipyridine ligand have been determined by X-ray crystallography. The X-ray structures suggest that intramolecular hydrogen bonding exists between the aqua hydrogen and the chloro-substituents on the ortho-position of the bipyridine ligand. This intramolecular H-bond should facilitate the deprotonation of the aqua ligand during the oxidation of $Ru\text{-}OH_2$ to Ru=O, which is consistent with the electrochemical data. The formation of Ru=O has also been demonstrated by *in-situ* FTIR spectroelectrochemistry.

Chapter 4

Synthesis and Redox Properties of Some New Binuclear Ruthenium Complexes with Specially Designed Ligands

4.1 Introduction

Binuclear ruthenium oxo complexes are of particular interest due to a number of reasons. Firstly, interaction between the two nearby ruthenium hydroxo moieties might promote the formation of ruthenium oxo species in electrochemical oxidation. Secondly, some multi-electron processes require catalysts with more than one metal centres. A typical example is the oxidation of water to dioxygen (eq 4.1):

$$2H_2O \longrightarrow O_2 + 4H^+ + 4e^- \qquad (4.1)$$

The oxidation of water to dioxygen is a four-proton four electron process. This process requires at least two metal centres in operation with each other to cleave the O-O bond. Meyer and co-workers [117, 129-131, 193-198] reported the catalytic oxidation of water to dioxygen with the binuclear Ru μ-oxo complex $[(H_2O)(bpy)_2Ru^{III}\text{-}O\text{-}Ru^{III}(bpy)_2(OH_2)]^{4+}$. The mechanism of water oxidation by the Ru μ-oxo complex has been investigated by Hurst and co-workers [199-204]. The stability of the binuclear Ru μ-oxo complex, however, is limited to 10-25 turnovers due to cleavage of the μ-oxo bond. Recently, Tanaka and co-workers [132, 133] designed a non μ-oxo ruthenium complex $[Ru^{III}(3,6\text{-}^tBu_2q)(OH)(btpyan)(HO)(3,6\text{-}^tBu_2q)Ru^{III}]^{2+}$ (btpyan = 1,8-bis(2,2':6',2"-terpyridyl)anthracene, $^tBu_2q$ = 3,6-di-tert-butyl-1,2;benzoquinone) to improve the stability of the ruthenium catalysts, but the synthesis of this complex involves complicated procedures. We have therefore

designed two new binuclear ligands N,N,N',N'-tetra(2-pyridyl) ethylenediamine (ETHPY) and 1,8-bis(2,2-dipyridylamino) anthracene (BDPAA). The binuclear ruthenium aqua complexes of these two ligands have also been prepared. The electrochemical generation of ruthenium oxo complexes from these ruthenium aqua complexes will be discussed in this chapter.

4.2 Experimental Section

4.2.1 Synthesis

Materials

All the chemicals and solvents used were of analytical (A.R.) grade. Ruthenium trichloride trihydrate ($RuCl_3.xH_2O$), 2,2':6',2"-terpyridine (tpy), silver trifluoromethanesulfonate, sodium borohydride, phthalimide, anhydrous sodium acetate, 2-bromopyridine, ethylenediamine dichloro(p-cymene)ruthenium(II) (cymene = 1-isopropyl-4-methylbenzene) and copper powder were purchased from Aldrich Co.. 1,8-Dichloroanthracene-9,10-dione was purchased from TCI Tokyo Kasei Kogyo Co. Ltd. BINAP (98%, racemic) was purchased from Strem Co. All other chemicals and reagents were used as received unless otherwise noted. $Pd_2(dba)_3$ (dba = dibenzylideneacetone) was synthesized by literature reported methods [158]. Elemental analyses were performed as previously described in chapter 2.

Synthesis of ligands

N,N,N',N'-tetra(2-pyridyl) ethylenediamine (ETHPY)

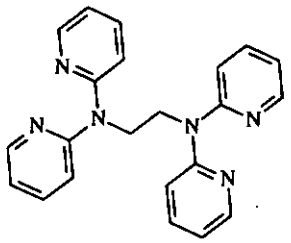

A mixture of 2-bromopyridine (10 mmol, 1.0 ml), ethylenediamine (6 mmol, 0.25 ml), $Pd_2(dba)_3$ (0.4 mmol, 16 mmol% Pd, 180 mg), BINAP (0.4 mmol, 0.25 g) and *t*-BuONa (20 mmol, 0.134 g) was stirred at room temperature under argon for 5 minutes. A solution of 2-bromopyridine in toluene (1.0 ml of 2-bromopyridine in 45 ml toluene) was added dropwisely to the above mixture at room temperature. The resulting mixture was heated at reflux under argon for 16 h. After cooling to room temperature, the mixture was washed with saturated brine (50 ml) and dry ether was added (3x 100 ml). The organic layer was dried over anhydrous sodium sulfate, and the solvents were removed under vacuum to a give dark brown oil. A 2:1 (v/v) mixture of hexane/ethyl acetate (100 mL) was added to the dark brown oil, the resulting precipitate was collected by filtration, washed with acetone (3 x 50 ml) and hexane (3 x 50 ml), and dried to give white needle-shape crystals (1.2 g, 54%). ^{1}H-NMR ($CDCl_3$, δ ppm): 4.32 (s, 4H), 6.76 (t, 4H), 7.03 (d, 4H), 7.42 (t, 4H), 8.09 (d, 4H); ESI-MS: *m/z* 379 $(M+H)^+$.

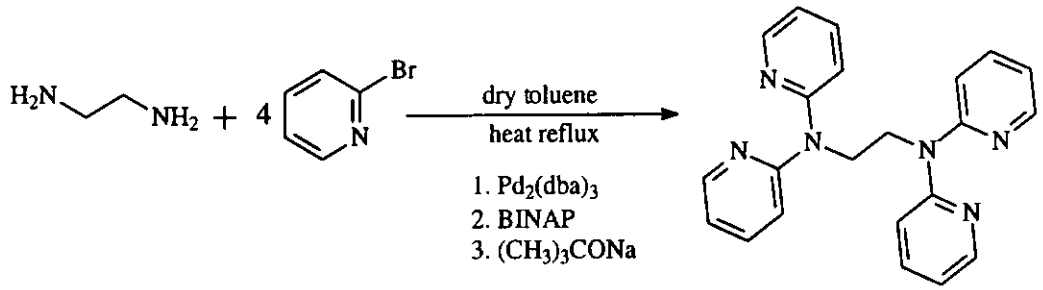

Scheme 4.1 Synthesis of N,N,N',N'-tetra(2-pyridyl) ethylenediamine (ETHPY)

1,8-Diaminoanthraquinone [205]

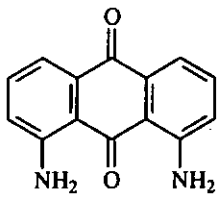

A stirred mixture of 1,8-dichloroanthracene-9,10-dione (41.6 g, 0.15 mol), phthalimide (52.7 g, 0.385 mol), anhydrous sodium acetate (29.6 g, 0.361 mol), and nitrobenzene (77 ml) was heated to 180 °C. Quinoline (25 ml) and copper powder (300 mesh, 0.72 g) were added, and the mixture was heated at 200°C for 1 h. The reaction mixture was allowed to cool and left to stand overnight. The mixture was filtered, washed with nitrobenzene (3 x 100 ml), ethanol (3 x 100 ml), hot water (2 x 100 ml), ethanol (2 x 100 ml), and ether (2 x 100 ml), and dried to give the intermediate diphthalimide intermediate as a pale-yellow/orange solid. (56.66 g, 76 %) The crude solid (56.0 g) was added to conc. H_2SO_4 (400 ml) with stirring and the mixture was heated at 95 °C for 45 minutes. The reaction mixture was cooled to 5 °C, and crushed ice (150 g) was slowly added. The mixture was poured onto ice/water (1.5 L) with stirring and the resulting precipitate was collected by filtration, washed with water until the pH became neutral, and dried in vacuo. Recrystallization from ethanol afforded

the product as red/purple needles (27 g, 98 %). ^{1}H-NMR (DMSO, δ ppm): 7.15 (dd, 2H), 7.34 (dd, 2H), 7.45 (dd, 2H), 7.86 (br s, 4H). ESI-MS: *m/z* 239 $(M+H)^+$.

1,8-Diaminoanthracene [206, 207]

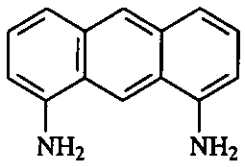

A solution of 1,8-diaminoanthraquinone (2.0 g, 8.4 mmol) in isopropanol (100 ml) was bubbled with nitrogen for 15 mins before the introduction of sodium borohydride (4.0 g, 106 mmol). The resulting suspension was heated at reflux under nitrogen atmosphere for 60 h. After cooling to room temperature, the reaction mixture was poured into ice water (250 ml). The dark precipitates were filtered off, washed thoroughly with water and then dissolved in chloroform (100 ml). The resulting solution was dried over anhydrous sodium sulfate before being concentrated on a rotary evaporator under reduced pressure. Purification was then carried out on a silica gel column using 0-3 % methanol in chloroform as the eluents to give the green product. Yield: 1.0 g (55%). ^{1}H-NMR ($CDCl_3$, δ ppm): 3.83 (br s, 4H), 6.76 (d, 2H), 7.30 (t, 2H), 7.48 (d, 2H), 8.35(s, 1H), 8.37 (s, 1H). ESI-MS: *m/z* 209 $(M+H)^+$.

1,8-Bis(2,2-dipyridylamino) anthracene (BDPAA)

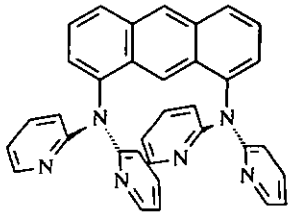

A mixture of 2-bromopyridine (10 mmol, 1.0 ml), 1,8-diaminoanthracene (6 mmol, 1.25 g), $Pd_2(dba)_3$ (0.4 mmol, 16 mmol% Pd, 180 mg), BINAP (0.4 mmol, 0.25 g) and *t*-BuONa (20 mmol, 0.134 g) was stirred at room temperature under argon for 5 minutes. A solution of 2-bromopyridine in toluene (1.0 ml of 2-bromopyridine in 45 ml toluene) was added dropwisely to the above mixture at room temperature. The resulting mixture was heated at reflux under argon for 10 h. After cooling to room temperature, the green precipitates were filtered off and washed thoroughly with acetone for several times. The solid was collected and dried in vacuo. Yield: 1.25 g (40%) ^{1}H-NMR ($CDCl_3$, δ ppm): 6.68 (d, 4H), 6.74 (t, 4H), 7.31 (d, 4H), 7.47 (d, 2H), 7.53 (t, 2H), 8.04 (d, 2H), 8.19 (s, 4H), 8.38 (s, 1H), 8.60 (s, 1H). ESI-MS: *m/z* 518 $(M+H)^+$.

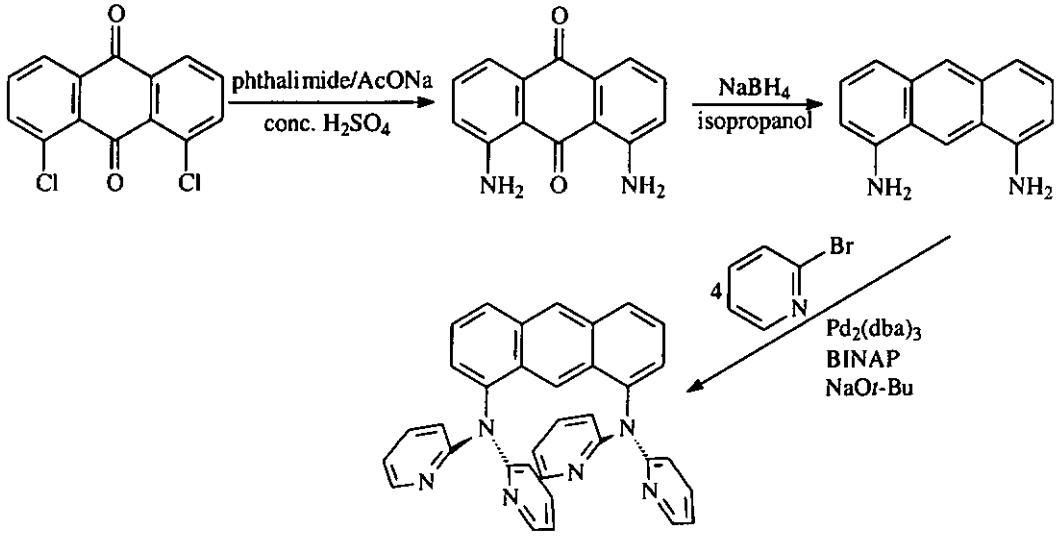

Scheme 4.2 Synthesis of 1,8-bis(2,2-dipyridylamino) anthracene (BDPAA)

Synthesis of Ruthenium Complexes

$Ru(tpy)Cl_3$ [208] and $[Ru(tpy)(dpa)Cl]ClO_4$ were prepared as described in chapter 2.

$[Ru_2(tpy)_2(ETHPY)Cl_2][ClO_4]_2$

A mixture of 440 mg of $[Ru^{III}(tpy)Cl_3]$ (1.0 mmol), 1.0 g of LiCl, 184 mg of N,N,N',N'-tetra(2-pyridyl)ethylenediamine (ETHPY) (0.5 mmol) and 2.0 ml of triethylamine was gently refluxed under argon for 1.5 h in about 40 ml of absolute ethanol. After the mixture had been cooled to room temperature, the solution was filtered to remove any insoluble material. The filtrate was concentrated to about 3 ml, and 20 ml of saturated $LiClO_4$ aqueous solution was added to the concentrated residue. Brown microcrystalline solid separated out upon standing which was collected by filtration, washed thoroughly with water and ether and dried in a vacuum oven. Yield: 0.4 g (85%). UV-Vis (CH_3CN/ λ_{max}, nm / ε, $M^{-1}cm^{-1}$): 235 (66000), 276 (72666), 318 (sh), 368 (16333), 509 (12333). Elemental analysis for $C_{52}H_{42}Cl_4N_{12}O_8Ru_2$. Calcd: C, 47.79; H, 3.24; N, 12.86. Found: C, 48.0; H, 3.20; N, 13.2.

$[Ru_2(tpy)_2(ETHPY)(H_2O)_2][ClO_4]_4$

A mixture of 0.2 g of $[Ru_2(tpy)_2(ETHPY)Cl_2][ClO_4]_2$ and 94 mg of silver trifluoromethanesulfonate was gently refluxed for 1 hr in 50 ml of water in the dark. After being cooled to room temperature, the mixture was filtered to remove the precipitated AgCl. Several drops of perchloric acid were then added to the filtrate and the resulting mixture was chilled overnight in a refrigerator. The microcrystalline dark-red precipitate of $[Ru_2(tpy)_2(ETHPY)(H_2O)_2][ClO_4]_4$ was collected by filtration, washed with minimum amount of cold water and diethyl ether and air dried. Yield: 0.14 g (60%). UV-Vis (H_2O/ λ_{max}, nm / ε, $M^{-1}cm^{-1}$): 271 (52352), 316 (52352), 370 (9706), 491 (8530). Elemental analysis for $C_{52}H_{46}Cl_4N_{12}O_{18}Ru_2$. Calcd: C, 42.46; H, 3.15; N, 11.43. Found: C, 42.6; H, 3.3; N, 11.5.

$[Ru_2(tpy)_2(ETHPY)(CH_3CN)_2][ClO_4]_4$

$[Ru_2(tpy)_2(ETHPY)(H_2O)_2][ClO_4]_4$ (0.3 g) was dissolved in 30 ml of dry CH_3CN. The mixture was gently refluxed for 30 minutes in the dark. After being cooled to room temperature, the solvents were removed under vacuum. The microcrystalline orange precipitate of $[Ru_2(tpy)_2(ETHPY)(CH_3CN)_2][ClO_4]_4$ was collected by filtration. Yield: 0.25 g (83%). UV-Vis (CH_3CN/ λ_{max}, nm / ε, $M^{-1}cm^{-1}$): 272 (65192), 308 (65385), 361 (9346), 469 (8846). Elemental analysis for $C_{56}H_{48}Cl_4N_{14}O_{16}Ru_2$ Calcd: C, 44.34; H, 3.19; N, 12.93. Found: C, 45.1; H, 4.10; N, 12.85. Crystals suitable for

X-ray diffraction study were obtained by vapor diffusion of diethyl ether to an acetonitrile solution of $[Ru_2(tpy)_2(ETHPY)(CH_3CN)_2][ClO_4]_4$

$[Ru_2(tpy)_2(BDPAA)Cl_2][ClO_4]_2$

The complex was synthesized by a similar procedure as described in the synthesis of $[Ru_2(tpy)_2(ETHPY)Cl_2][ClO_4]_2$. A mixture of 440 mg of $[Ru(tpy)Cl_3]$ (1.0 mmol), 1.0 g of LiCl, 260 mg of 1,8-bis(2,2-dipyridylamino) anthracene (BDPAA) (0.5 mmol) were refluxed under argon for 4.0 h in 30 ml of ethylene glycol. After the mixture had been cooled to room temperature, the solution was filtered to remove any insoluble material. Saturated $LiClO_4$ aqueous solution (30 ml) was added to the solution filtrate. Purple microcrystalline solid separated out upon standing which was collected by filtration, washed thoroughly with water and ether and dried in a vacuum oven. Yield: 0.39 g (54%). UV-Vis (CH_3CN/ λ_{max}, nm / ε, $M^{-1}cm^{-1}$): 276 (71166), 319 (45882), 355 (15882), 373 (17941), 394 (15588), 507 (10294). Elemental analysis for $C_{52}H_{42}Cl_4N_{12}O_8Ru_2$. Calcd: C, 47.79; H, 3.24; N, 12.86. Found: C, 48.0; H, 3.20; N, 13.2.

$[Ru_2(tpy)_2(BDPAA)(H_2O)_2][ClO_4]_4$

A mixture of 0.2 g of $[Ru_2(tpy)_2(BDPAA)Cl_2][ClO_4]_2$ and 84 mg of silver trifluoromethanesulfonate was gently refluxed for 1 h in 50 ml of water. After being

cooled to room temperature, the mixture was filtered to remove the precipitated AgCl. Several drops of perchloric acid were then added to the filtrate and the resulting mixture was chilled overnight in a refrigerator. The microcrystalline dark-red precipitate of $[Ru_2(tpy)_2(BDPAA)(H_2O)_2][ClO_4]_4$ was collected by filtration, washed with minimum amount of cold water and diethyl ether and air dried. Yield: 0.13 g (62%). UV-Vis (H_2O/ λ_{max}, nm / ε, $M^{-1}cm^{-1}$): 252 (89643), 273 (75357), 314 (48928), 356 (16535), 375 (15785), 395 (13571), 478 (8571). Elemental analysis for $C_{64}H_{50}Cl_4N_{12}O_{18}Ru_2$. Calcd: C, 47.48; H, 3.11; N, 10.38. Found: C, 48.20; H, 3.13; N, 10.40.

$[Ru_2(tpy)_2(BDPAA)(CH_3CN)_2][ClO_4]_4$

$[Ru_2(tpy)_2(BDPAA)(H_2O)_2][ClO_4]_4$ (0.3 g) was dissolved in 30 ml of dry CH_3CN. The mixture was gently refluxed for 30 minutes in the dark. After being cooled to room temperature, the solvents were removed under vacuum. The microcrystalline orange precipitate of $[Ru_2(tpy)_2(BDPAA)(CH_3CN)_2][ClO_4]_4$ was collected by filtration. Yield: 0.22 g (71 %). UV-Vis (CH_3CN/ λ_{max}, nm / ε, $M^{-1}cm^{-1}$): 256 (87857), 273 (78571), 310 (51429), 354 (15857), 395 (12857), 473 (7964). Elemental analysis for $C_{68}H_{52}Cl_2N_{14}O_{16}Ru_2$. Calcd: C, 49.05; H, 3.15; N, 11.78. Found: C, 50.10; H, 3.30; N, 11.90. Crystals suitable for X-ray diffraction study were obtained by vapor diffusion of diethyl ether to an acetonitrile solution of $[Ru_2(tpy)_2(BDPAA)(CH_3CN)_2][ClO_4]_4$

$[Ru_2(cymen)_2(BDPAA)Cl_2]Cl_2$

A mixture of 300 mg of dichloro(p-cymene)ruthenium(II) (0.5 mmol) (cymene = 1-Isopropyl-4-methylbenzene), 1.0 g of LiCl, 260 mg of BDPAA (0.5 mmol) were gently refluxed under argon for 2.0 h in about 50 ml of dry THF. After the mixture had been cooled to room temperature, the solution was filtered to remove any insoluble material. The filtrate was concentrated to about 10 ml, yellow microcrystalline solid separated out upon standing which was collected by filtration, washed thoroughly with water and ether and dried in a vacuum oven. Yield: 0.45 g (85%). UV-Vis (CH_3CN/ λ_{max}, nm / ε, $M^{-1}cm^{-1}$): 256 (60333), 304 (18000), 356 (7000), 376 (8333), 397 (7333). Elemental analysis for $C_{54}H_{52}Cl_4N_6Ru_2$. Calcd: C, 57.45; H, 4.64; N, 7.44. Found: C, 58.00; H, 4.71; N, 7.44. Crystals suitable for X-ray diffraction study were obtained by diffusing diethyl ether to CH_3CN solution of $[Ru_2(cymen)_2(BDPAA)Cl_2]Cl_2$.

$[Ru_2(cymen)_2(BDPAA)(H_2O)_2][ClO_4]_4$

A mixture of 0.2 g of $[Ru_2(cymen)_2(BDPAA)Cl_2]Cl_2$ and 100 mg of silver trifluoromethanesulfonate was gently refluxed for 1 h in 50 ml of water in the dark. After being cooled to room temperature, the mixture was filtered to remove the precipitated AgCl. Several drops of perchloric acid were then added to the filtrate and the resulting mixture was chilled overnight in a refrigerator. The microcrystalline dark-red precipitate of $[Ru_2(cymen)_2(BDPAA)(H_2O)_2][ClO_4]_4$ was collected by filtration,

washed with minimum amount of cold water and diethyl ether and air dried. Yield: 0.14 g (76%). UV-Vis (CH_3CN/ λ_{max}, nm / ε, $M^{-1}cm^{-1}$): 252 (85666), 300 (24000), 356 (9333), 374 (11000), 395 (8666). Elemental analysis for $C_{54}H_{56}Cl_4N_6O_{18}Ru_2$. Calcd: C, 45.64; H, 3.97; N, 5.91. Found: C, 45.60; H, 4.00; N, 5.92.

$[Ru(dpa)(H_2O)][ClO_4]_2$

A mixture of 0.2 g of $[Ru(dpa)Cl](ClO_4)$ and 80 mg of silver trifluoromethanesulfonate was gently refluxed for 1 h in 50 ml of water in the dark. After being cooled to room temperature, the mixture was filtered to remove the precipitated AgCl. Several drops of perchloric acid were then added to the filtrate and the resulting mixture was chilled overnight in a refrigerator. The microcrystalline dark-red precipitate of $[Ru(dpa)(H_2O)][ClO_4]_2$ was collected by filtration, washed with minimum amount of cold water and diethyl ether and air dried. Yield: 0.15 g (84%). UV-Vis (H_2O/ λ_{max}, nm / ε, $M^{-1}cm^{-1}$): 233 (24000), 272 (37353), 314 (34411), 364 (5882), 478 (5000). Elemental analysis for $C_{25}H_{22}Cl_2N_6O_9Ru$. Calcd: C, 41.56; H, 3.07; N, 11.63. Found: C, 41.80; H, 3.08; N, 11.60. Crystals suitable for X-ray diffraction study were obtained by first dissolving $[Ru(tpy)(dpa)(H_2O)][ClO_4]_2$ in double distilled water in the presence of trifluoromethanesulfonic acid. This solution was gently heated until all the complexes dissolved. Crystals were obtained after the solution had been cooled down to room temperature.

4.2.2 Physical measurements

Electrochemical and x-ray crystallpgraphic studies were performed as described in previous chapters.

4.3 Results and Discussion

4.3.1 X-ray structural determination of BDPAA and ruthenium complexes

The ORTEP plot of the binuclear ligand BDPAA and those for various ruthenium complexes are depicted in Figure 4.1 and Figures 4.2 – 4.5 respectively. The crystallographic data of DBPAA are listed in Table 4.1 and those ruthenium complexes are summarized in Table 4.4. Selected bond distances and angles are tabulated in Tables 4.2 to 4.3 and Tables 4.5 to 4.8, respectively.

BDPAA

BDPAA was recrystallized from chloroform/hexane (1/1 v/v) in the dark at room temperature to give small pale yellow crystals. The two 2,2'-dipyridylamino groups linked to the 1,8-positions of anthracene are faced towards the same direction. BDPAA has a rotation axis that includes C6 and C13, and the two 2,2'-dipyridylamino groups are crystallographically equivalent in the crystal structure. Because of the steric repulsion between the pyridyl rings attached onto N1, an angle of 122.4(3)° exists between the pyridyl rings while the angle between the pyridyl ring and anthracene is 118.6(3)°. Free rotation of the 2,2'-dipyridylamino group must be inhibited because of steric repulsion. From the crystal structure, the short distance of 4.8 Å was estimated between N1 and N4. The distance between two metals, therefore, is estimated to be in

the range 5-6 Å when BDPAA forms a binuclear complex.

$[Ru(tpy)(dpa)(H_2O)](ClO_4)_2$

The ORTEP plot of $[Ru(tpy)(dpa)(H_2O)]^{2+}$ is depicted in Figure 4.2. Crystallographic data are summarized in Table 4.4. Selected bond distances and angles are tabulated in Tables 4.5 and 4.6 respectively.

The ruthenium coordination environment is a distorted octahedron with the tpy ligand coordinated, as expected, in meridional fashion, the dpa ligand in *cis* fashion, and the aqua ligand *trans* to one of the dpa nitrogen atoms. The angle of N(1)-Ru(1)-N(3) is approximately 159° and shortening of the Ru(1)-N(2) distance to the central pyridyl of approximately 0.1 Å with respect to Ru-N distances to the two outer pyridyl rings are typical features observed in other Ru(II) tpy structures [103, 161-166]. The distance between ruthenium and the water oxygen is 2.143(2) Å, the distance for the Ru-O is similar to the other ruthenium aqua complexes such as $[Ru(tpy)(dcbpy)(H_2O)]^{2+}$, $[Ru(tpy)(bpy)(H_2O)]^{2+}$, $[Ru(tacn)(bpy)(OH_2)]^{2+}$ [178] and $[Ru(Me_3tacn)(3,3'\text{-}Me_2bpy)(OH_2)]^{2+}$ [111]. A comparison of the complex $[Ru(tpy)(dpa)(H_2O)](ClO_4)_2$ with $[Ru(tpy)(PPP)Cl]^+$ shows that the bond length of Ru-N and bond angles in both complexes are nearly the same. The N(4)-Ru-N(5) bond angle in $[Ru(tpy)(dpa)(H_2O)](ClO_4)_2$ is 88.23(11)°, which is 2° wider than that in $[Ru(tpy)(PPP)Cl]^+$ (86.18(5)°), showing that the ligand dpa is more flexible than the

PPP ligand.

$[Ru_2(tpy)_2(ETHPY)(CH_3CN)_2][ClO_4]_4$

The ORTEP plot of $[Ru_2(tpy)_2(ETHPY)(CH_3CN)_2]^{4+}$ is depicted in Figure 4.3. Crystallographic data are summarized in Table 4.4. Selected bond distances and angles are tabulated in Tables 4.7 and 4.8 respectively.

The ruthenium ligand environment is a distorted octahedron with the tpy ligand coordinated, as expected, in meridional fashion, the ETHPY ligand in *cis* fashion, and the acetonitrile ligand *trans* to one of the ETHPY nitrogen atoms. The ETHPY ligand links two ruthenium centres by an ethylene bridge, and the bond angles, bond distances are nearly identical for the two ruthenium in $[Ru_2(tpy)_2(ETHPY)(CH_3CN)_2]^{4+}$. On comparing the bond angles, bond distances of $[Ru_2(tpy)_2(ETHPY)(CH_3CN)_2]^{4+}$ with its analogue $[Ru(tpy)(dpa)(H_2O)]^{2+}$, there is no significant difference between the two ruthenium complexes.

$[Ru_2(cymen)_2(BDPAA)(Cl)_2]Cl_2$ and $[Ru_2(tpy)_2(BDPAA)(CH_3CN)_2](ClO_4)_4$

Due to the disorder of the anions presence in the crystal lattice, the bond lengths and bond angles could not be accurately determined for these two complexes. Only the ORTEP plot of the binuclear ruthenium cations were obtained which are shown in

Figure 4.4 and Figure 4.5 respectively. The X-ray structure of these two complexes suggest that the two ruthenium centres are not as close to each as originally expected. The structure of $[Ru_2(cymen)_2(BDPAA)(Cl)_2]^{2+}$ shows that with the facial cymen ligand, the two chloro ligands are facing each other in the binuclear complex. In $[Ru_2(tpy)_2(BDPAA)(CH_3CN)_2]^{4+}$, where the tridentate tpy ligand is meridonal, the two CH_3CN ligands are pointing away from one another in the complex.

Table 4.1 The crystal and structure determination data of BDPAA

	BDPAA
Empirical formula	$C_{34}H_{24}N_6$
Formula weight	516.59
Temperature	294(2) K
Wavelength	0.71073 Å
Crystal system	Monoclinic
Space group	P2(1)/n
Unit cell dimensions	a = 9.566(3) Å $\alpha = 90^\circ$
	b = 18.465(5) Å $\beta = 93.035(8)^\circ$
	c = 14.506(4) Å $\gamma = 90^\circ$
Volume	2558.7(12) $Å^3$
Z	4
Density (calculated)	1.341 Mg/m^3
Absorption coefficient	0.082 mm^{-1}
F(000)	1080
Crystal size	0.18 x 0.10 x 0.10 mm^3
θ range for data collection	2.62 to 27.57°
Reflections collected	17413
Independent reflections	5876
Completeness to $\theta = 27.57^\circ$	99.2%
Absorption correction	Empirical
Max. and min. transmission	0.9919 and 0.9854
Refinement method	Full-martix least-squares on F^2
Goodness-of-fit on F2	0.646
R	0.0496
WR2	0.0576
Largest diff. Peak and hole	0.188 and –0.209e. $Å^{-3}$

Table 4.2 Selected bond length (Å) for BDPAA

N(1)-C(15)	1.396(4)	N(4)-C(25)	1.402(4)
N(1)-C(20)	1.418(4)	N(4)-C(30)	1.411(4)
N(1)-C(1)	1.449(4)	N(4)-C(11)	1.461(4)
N(2)-C(15)	1.338(4)	N(5)-C(25)	1.329(4)
N(2)-C(19)	1.340(5)	N(5)-C(29)	1.342(5)
N(3)-C(20)	1.341(4)	N(6)-C(30)	1.322(4)
N(3)-C(24)	1.320(4)	N(6)-C(34)	1.354(4)

Table 4.3 Selected bond angles (°) for BDPAA

C(15)-N(1)-C(20)	124.1(3)	C(15)-N(1)-C(1)	118.9(3)
C(20)-N(1)-C(1)	115.0(3)	C(15)-N(2)-C(19)	115.4(4)
C(24)-N(3)-C(20)	117.4(4)	C(25)-N(4)-C(30)	122.4(3)
C(25)-N(4)-C(20)	118.4(3)	C(30)-N(4)-C(110)	118.6(3)
C(25)-N(5)-C(20)	115.8(4)	C(30)-N(6)-C(34)	117.1(3)

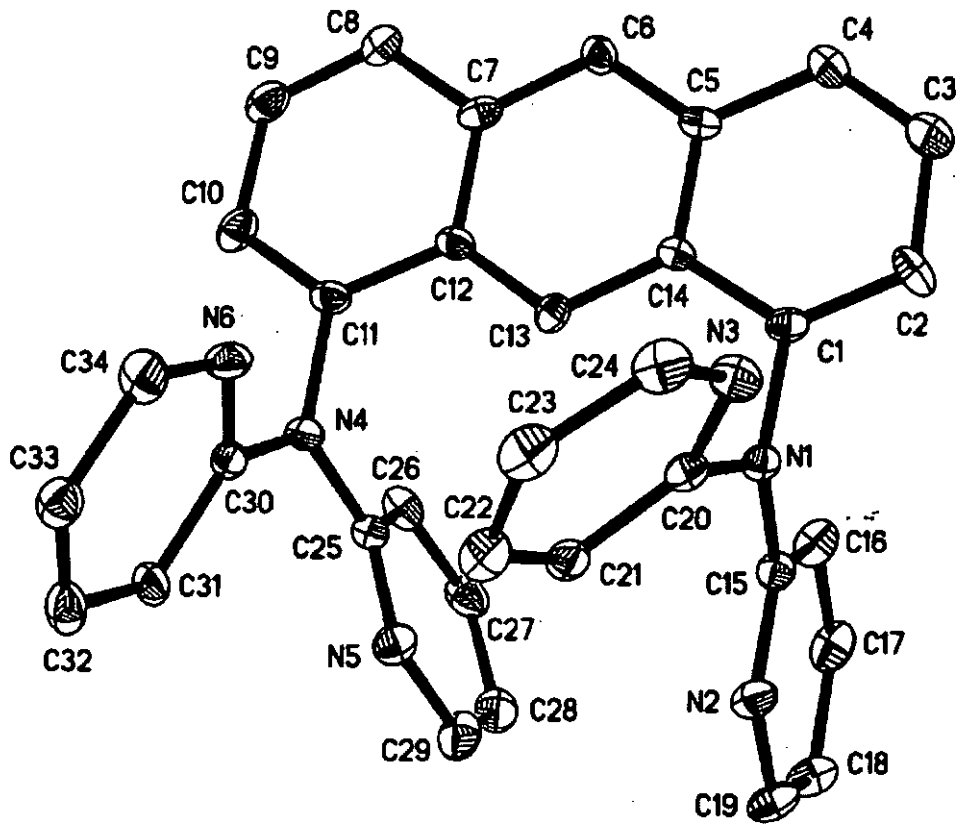

Figure 4.1 An ORTEP plot of BDPAA with atom numbering.

Table 4.4 A summary of crystallographic data, intensity collection and structure refinement of the ruthenium complexes

	$[Ru(tpy)(dpa)(H_2O)](ClO_4)_2$	$[Ru_2(tpy)_2(ETHPY)(CH_3CN)_2](ClO_4)_4.CH_3CN$
Empirical formula	$Ru(H_2O)(C_{25}H_{20}N_6).2(ClO_4).H_2O$	$Ru_2(C_{46}H_{48}N_{14}).4ClO_4.CH_3CN$
Formula weight	740.47	1558.08
Temperature	294(2) K	294(2) K
Wavelength	0.71073 Å	0.71073 Å
Crystal system	Triclinic	Triclinic
Space group	P2(1)/c	P-1
Unit cell dimensions	a = 9.8901(14) Å α = 83.639(3)°	a = 11.962(4) Å α = 83.162(7)°
	b = 10.5081(15) Å β = 75.017(3)°	b = 16.110(5) Å β = 82.520(7)°
	c = 15.438(2) Å γ = 66.842(3)°	c = 20.834(6) Å γ = 69.747(7)°
Volume	1425.0(4) $Å^3$	3722.7(19) $Å^3$
Z	2	2
Density (calculated)	1.726 Mg /m^3	1.390 Mg /m^3
Absorption coefficient	0.876 mm^{-1}	0.618 mm^{-1}
F(000)	748	1576
Crystal size	0.22 x 0.18 x 0.10 mm^3	0.30 x 0.10 x 0.10 mm^3
θ range for data collection	2.50 to 27.59°	2.51 to 27.66°
Reflections collected	9885	24396
Independent reflections	6489	16874
Completeness to θ = 27.55°	98.3%	97.0%
Absorption correction	Empirical	Multiscans
Max. and min. transmission	0.9238 and 0.8426	0.9408 and 0.8363
Refinement method	Full-martix least-squares on F^2	Full-martix least-squares on F^2
Goodness-of-fit on F2	0.996	1.001
R	0.0616	0.0976
WR2	0.1242	0.2220
Largest diff. Peak and hole	0.518 and –0.527e. $Å^{-3}$	0.976 and –0.922 e. $Å^{-3}$

Table 4.5 Selected bond length (Å) for $[Ru(tpy)(dpa)(H_2O)](ClO_4)_2.H_2O$

Ru(1)-N(1)	2.080(3)	N(3)-C(15)	1.334(5)
Ru(1)-N(2)	1.952(3)	N(3)-C(11)	1.387(5)
Ru(1)-N(3)	2.081(3)	N(4)-C(16)	1.349(4)
Ru(1)-N(4)	2.041(3)	N(4)-C(20)	1.344(4)
Ru(1)-N(5)	2.101(3)	N(5)-C(25)	1.352(5)
Ru(1)-O(1W)	2.143(2)	N(5)-C(21)	1.355(5)
N(1)-C(1)	1.333(6)	N(6)-C(20)	1.363(4)
N(1)-C(5)	1.356(5)	N(6)-C(21)	1.381(5)
N(2)-C(6)	1.358(5)	N(6)-H(6A)	0.8600
N(2)-C(10)	1.336(5)		

Table 4.6Selected bond angles (°) for $[Ru(tpy)(dpa)(H_2O)](ClO_4)_2.H_2O$

N(2)-Ru(1)-N(1)	79.25(13)	N(5)-Ru(1)-O(1W)	90.87(11)
N(2)-Ru(1)-N(4)	93.25(11)	C(1)-N(1)-Ru(1)	128.9(3)
N(1)-Ru(1)-N(4)	93.56(11)	C(5)-N(1)-Ru(1)	113.7(3)
N(2)-Ru(1)-N(3)	79.81(13)	C(6)-N(2)-Ru(1)	118.5(3)
N(1)-Ru(1)-N(3)	159.00(13)	C(10)-N(2)-Ru(1)	119.2(2)
N(4)-Ru(1)-N(3)	89.12(12)	C(15)-N(3)-Ru(1)	129.6(3)
N(2)-Ru(1)-N(5)	178.38(12)	C(11)-N(3)-Ru(1)	111.4(2)
N(1)-Ru(1)-N(5)	100.01(13)	C(16)-N(4)-Ru(1)	121.1(2)
N(4)-Ru(1)-N(5)	88.23(11)	C(20)-N(4)-Ru(1)	120.7(2)
N(3)-Ru(1)-N(5)	100.88(12)	C(25)-N(5)-Ru(1)	121.9(2)
N(2)-Ru(1)-O(1W)	87.70(11)	C(21)-N(5)-Ru(1)	120.6(3)
N(1)-Ru(1)-O(1W)	90.72(11)	C(20)-N(6)-H(6A)	115.5
N(4)-Ru(1)-O(1W)	175.72(11)	C(21)-N(6)-H(6A)	115.5
N(3)-Ru(1)-O(1W)	86.94(11)		

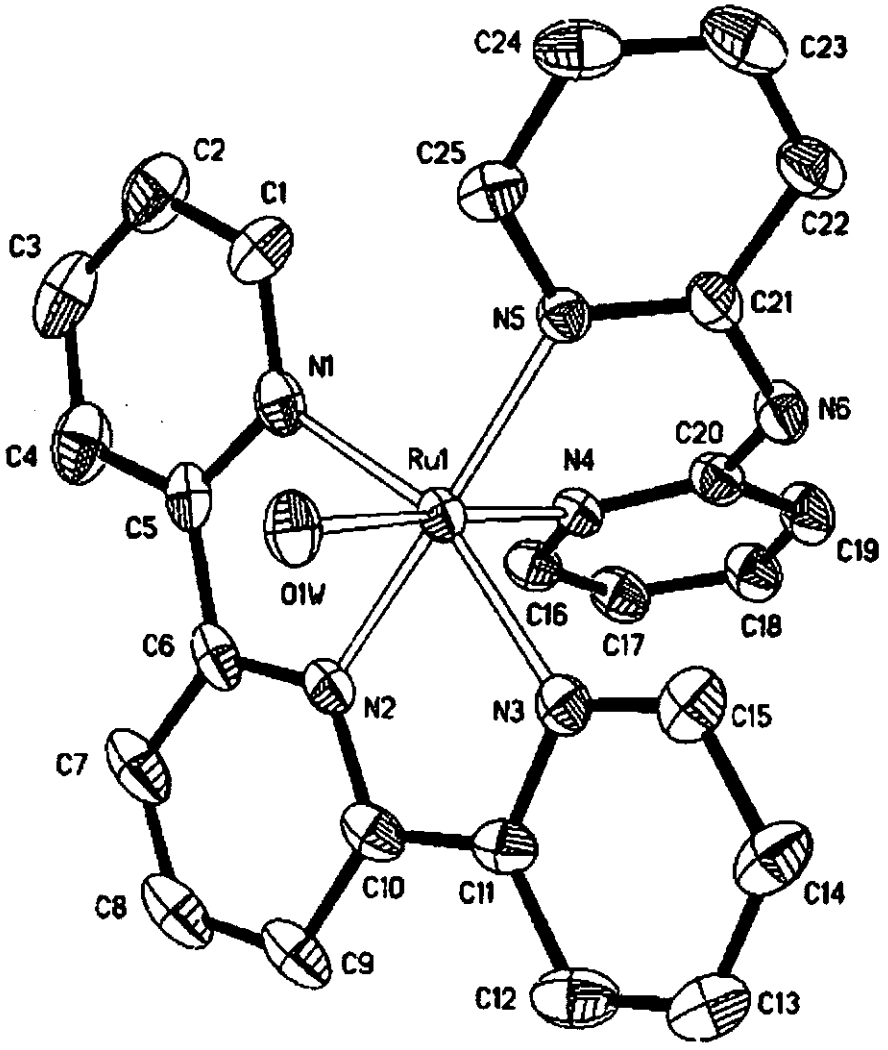

Figure 4.2 An ORTEP plot of $[Ru(tpy)(dpa)(H_2O)]^{2+}$ with atom numbering.

Table 4.7 Selected bond length (Å) for $[Ru_2(tpy)_2(ETHPY)(CH_3CN)_2][ClO_4]_4.CH_3CN$

Ru(1)-N(1)	2.038(5)	N(4)-C(17)	1.342(5)
Ru(1)-N(2)	2.071(3)	N(4)-C(13)	1.405(5)
Ru(1)-N(3)	1.975(3)	N(5)-C(18)	1.364(7)
Ru(1)-N(4)	2.034(4)	N(5)-C(22)	1.398(7)
Ru(1)-N(5)	2.158(3)	N(6)-C(23)	1.362(6)
Ru(1)-N(6)	2.046(5)	N(6)-C(27)	1.373(6)
Ru(2)-N(9)	2.110(3)	N(9)-C(30)	1.343(5)
Ru(2)-N(10)	2.042(4)	N(9)-C(34)	1.346(5)
Ru(2)-N(11)	2.041(4)	N(10)-C(39)	1.344(6)
Ru(2)-N(12)	1.956(3)	N(10)-C(35)	1.390(5)
Ru(2)-N(13)	2.043(4)	N(11)-C(40)	1.311(5)
Ru(2)-N(14)	1.961(4)	N(11)-C(44)	1.341(6)
N(1)-C(1)	1.147(7)	N(12)-C(45)	1.264(7)
N(2)-C(3)	1.289(5)	N(12)-C(49)	1.313(6)
N(2)-C(7)	1.409(5)	N(13)-C(54)	1.280(7)
N(3)-C(12)	1.342(6)	N(13)-C(50)	1.411(5)
N(3)-C(8)	1.396(6)	N(14)-C(55)	1.158(7)

Table 4.8 Selected bond angles (°) for $[Ru_2(tpy)_2(ETHPY)(CH_3CN)_2][ClO_4]_4.CH_3CN$

N(3)-Ru(1)-N(1)	92.08(15)	N(14)-Ru(2)-N(9)	91.19(14)
N(3)-Ru(1)-N(4)	78.61(13)	N(11)-Ru(2)-N(9)	100.56(14)
N(1)-Ru(1)-N(4)	85.18(16)	N(13)-Ru(2)-N(9)	98.48(14)
N(3)-Ru(1)-N(6)	92.16(16)	N(10)-Ru(2)-N(9)	85.22(13)
N(1)-Ru(1)-N(6)	175.77(13)	C(1)-N(1)-Ru(1)	177.6(4)
N(4)-Ru(1)-N(6)	95.69(16)	C(3)-N(2)-Ru(1)	131.5(3)
N(3)-Ru(1)-N(2)	80.93(14)	C(7)-N(2)-Ru(1)	112.9(3)
N(1)-Ru(1)-N(2)	90.23(16)	C(12)-N(3)-Ru(1)	119.2(3)
N(4)-Ru(1)-N(2)	158.84(13)	C(8)-N(3)-Ru(1)	117.8(3)
N(6)-Ru(1)-N(2)	90.41(16)	C(17)-N(4)-Ru(1)	129.5(3)
N(3)-Ru(1)-N(5)	177.00(17)	C(13)-N(4)-Ru(1)	113.8(3)
N(1)-Ru(1)-N(5)	89.97(16)	C(18)-N(5)-Ru(1)	120.4(3)
N(4)-Ru(1)-N(5)	99.38(14)	C(22)-N(5)-Ru(1)	116.3(3)
N(6)-Ru(1)-N(5)	85.80(16)	C(23)-N(6)-Ru(1)	122.2(3)
N(2)-Ru(1)-N(5)	101.26(14)	C(27)-N(6)-Ru(1)	122.1(3)
N(12)-Ru(2)-N(14)	92.51(15)	C(30)-N(9)-Ru(2)	120.7(2)
N(12)-Ru(2)-N(11)	81.26(15)	C(34)-N(9)-Ru(2)	120.3(3)
N(14)-Ru(2)-N(11)	86.72(17)	C(39)-N(10)-Ru(2)	122.8(3)
N(12)-Ru(2)-N(13)	80.11(15)	C(35)-N(10)-Ru(2)	123.7(3)
N(14)-Ru(2)-N(13)	87.29(17)	C(40)-N(11)-Ru(2)	132.4(3)
N(11)-Ru(2)-N(13)	160.14(13)	C(44)-N(11)-Ru(2)	112.4(3)
N(12)-Ru(2)-N(10)	91.11(14)	C(45)-N(12)-Ru(2)	120.8(3)
N(14)-Ru(2)-N(10)	176.22(13)	C(49)-N(12)-Ru(2)	118.9(3)
N(11)-Ru(2)-N(10)	92.79(16)	C(54)-N(13)-Ru(2)	129.9(3)
N(13)-Ru(2)-N(10)	94.38(15)	C(50)-N(13)-Ru(2)	110.9(3)
N(12)-Ru(2)-N(9)	175.97(14)	C(55)-N(14)-Ru(2)	174.3(4)

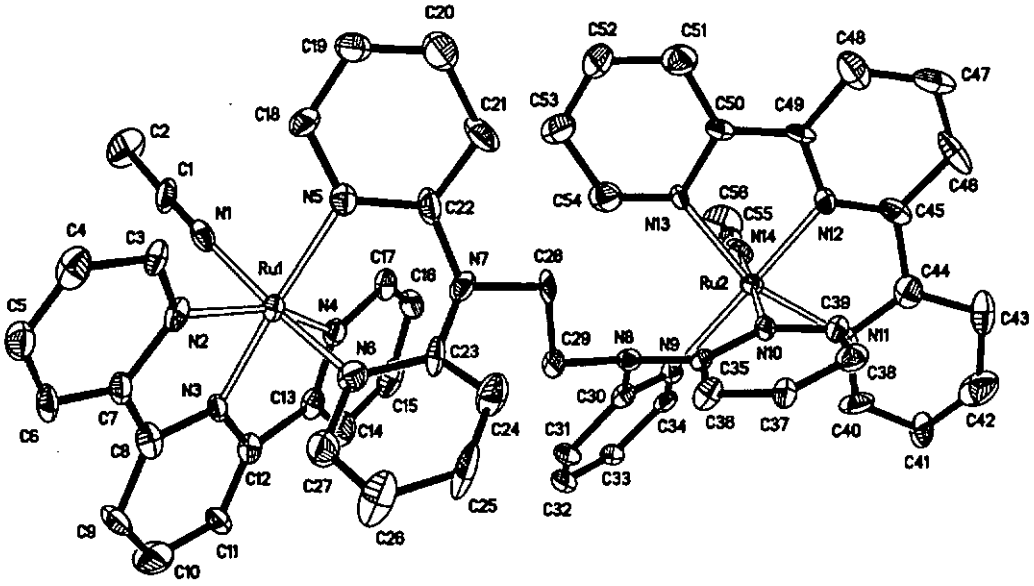

Figure 4.3 An ORTEP plot of $[Ru_2(tpy)_2(ETHPY)(CH_3CN)_2]^{4+}$ with atom numbering.

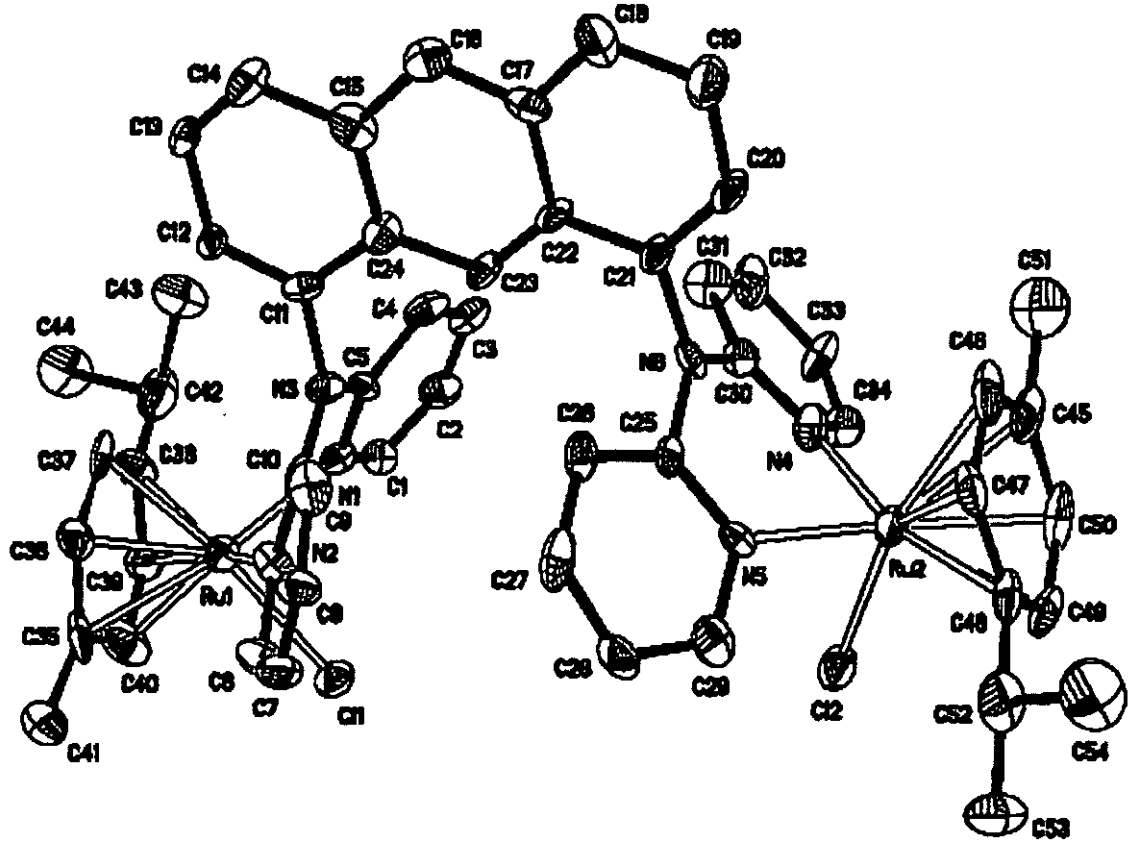

Figure 4.4 An ORTEP plot of $[Ru_2(cymen)_2(BDPAA)Cl_2]^{2+}$ with atom numbering.

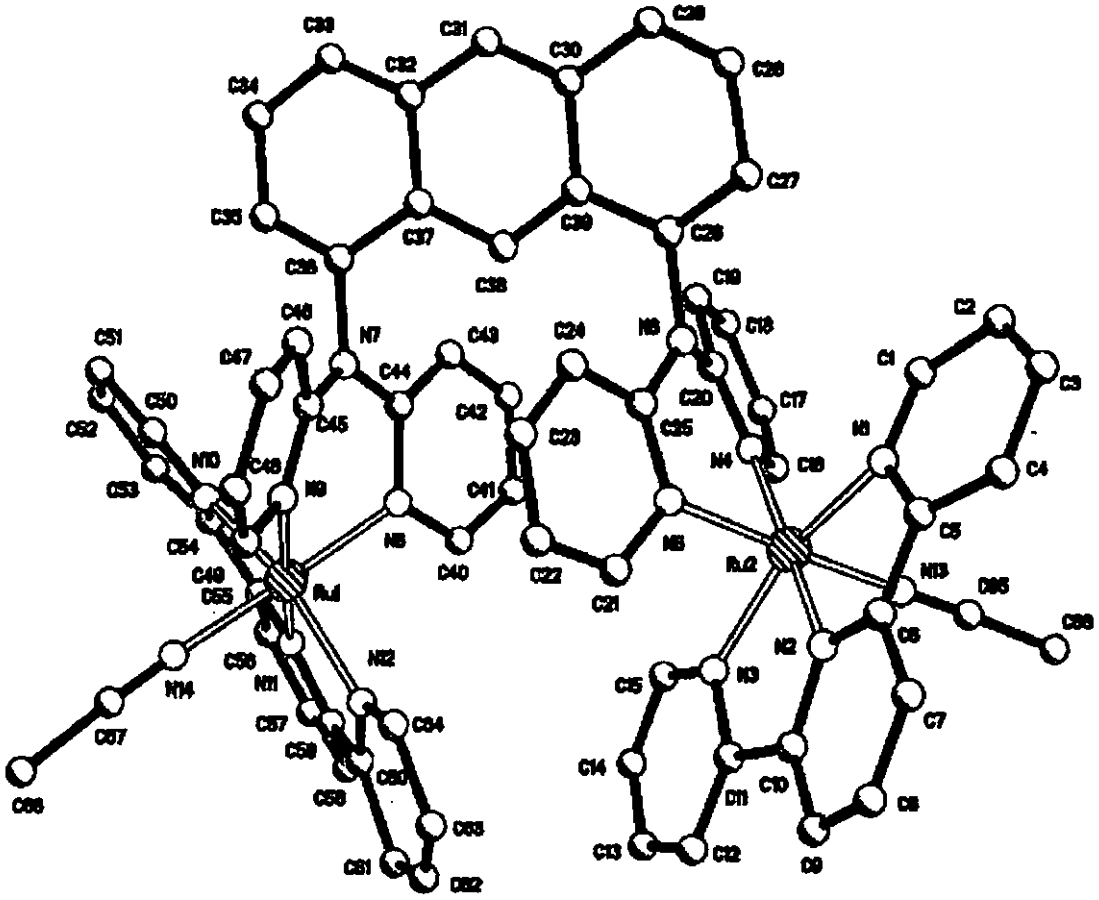

Figure 4.5 An ORTEP plot of $[Ru_2(BDPAA)(tpy)_2(CH_3CN)_2]^{4+}$ with atom numbering.

Synthesis and characterization of the binuclear ruthenium complexes

The synthesis of the binuclear ruthenium aqua complexes, as outlined in **Scheme 4.3** is similar to that of $[Ru(tpy)(dpa)(H_2O)](ClO_4)_2$. For the synthesis of the binuclear ruthenium aqua complex $[Ru_2(tpy)_2(BDPAA)(H_2O)_2][ClO_4]_4$ (**Scheme 4.4**), a higher boiling point solvent ethylene glycol has to be used. The low boiling ethanol has proved to be inefficient in the synthesis of $[Ru_2(tpy)_2(BDPAA)(Cl)_2]^{4+}$. This is probably because the two 2,2'-dipyridylamine units are closer to each other in BDPAA and the steric hindrance makes the coordination to two Ru centres more difficult. Nonetheless, this can be overcome by raising the reaction temperature with ethylene glycol.

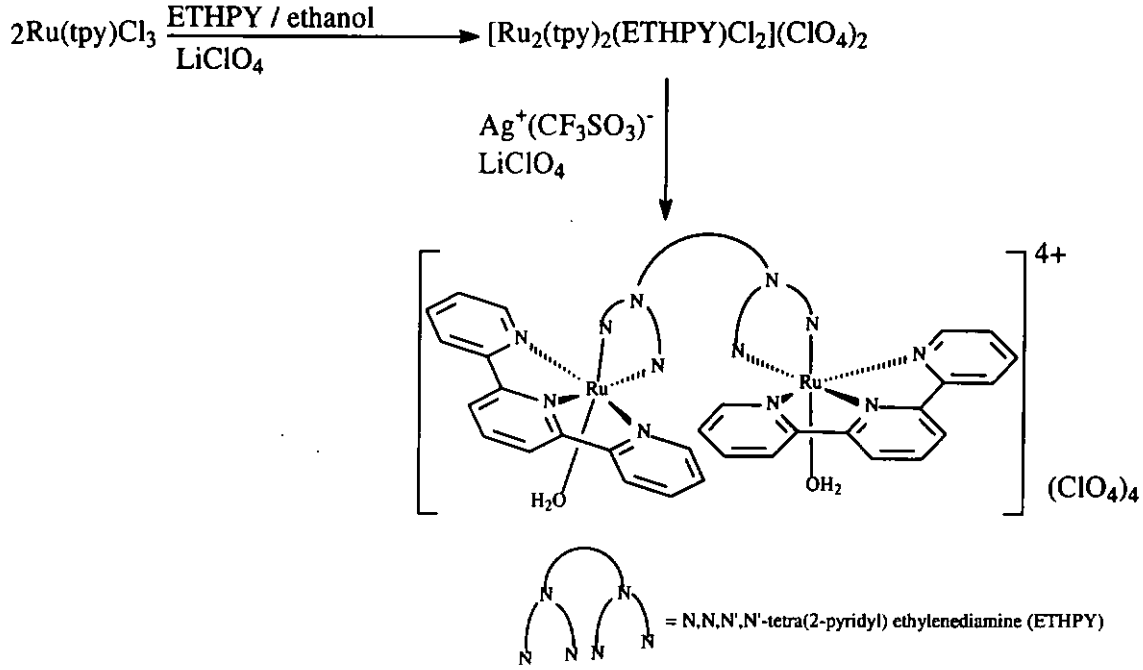

Scheme 4.3 Synthesis of the $[Ru_2(tpy)_2(ETHPY)(H_2O)_2][ClO_4]_4$

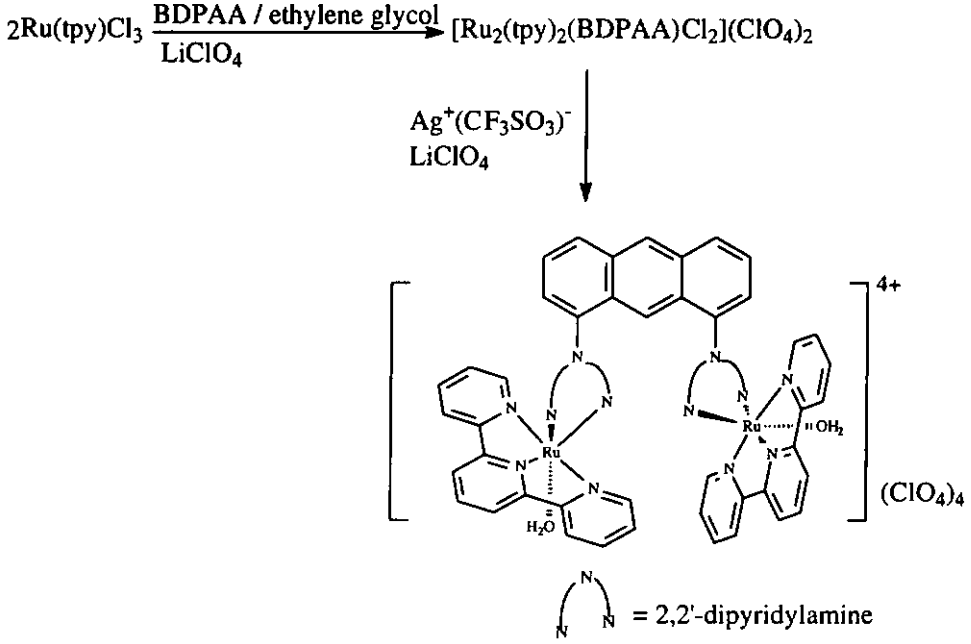

Scheme 4.4 Synthesis of the $[Ru_2(tpy)_2(BDPAA)(H_2O)_2][ClO_4]_4$

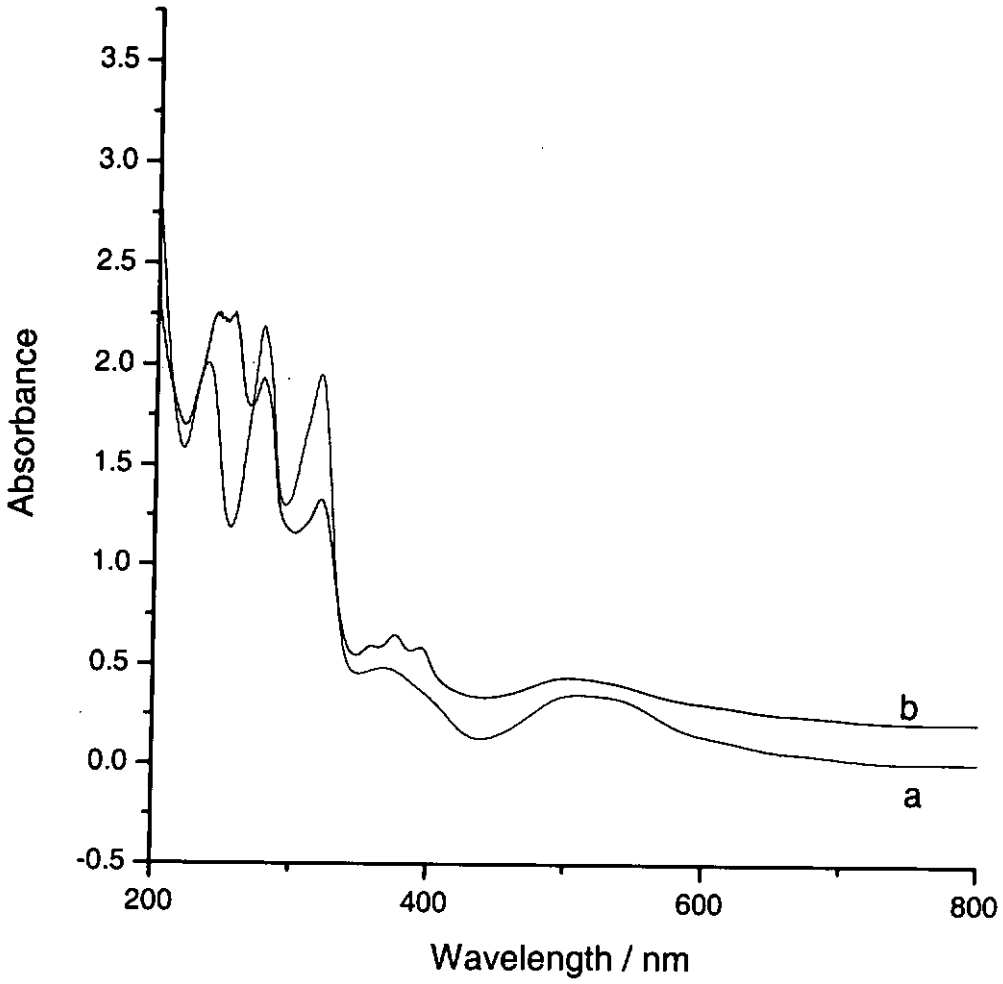

Figure 4.6 Electronic absorption spectra for (a) $[Ru_2(tpy)_2(ETHPY)Cl_2]^{2+}$ and (b) $[Ru_2(tpy)_2(BDPAA)Cl_2]^{2+}$ in acetonitrile solution at room temperature.

Table 4.9 Electronic absorption spectroscopic data for the binuclear ruthenium complexes

Complex	Wavelength (nm)	ε ($M^{-1}cm^{-1}$)	Assignment
$[Ru_2(tpy)_2(ETHPY)Cl_2]^{4+}$	236	6.6×10^4	π-π*
	276	7.2×10^4	tpy: π-π*
	318	6.3×10^4	π-π*
	509	1.2×10^4	MLCT
$[Ru_2(tpy)_2(BDPAA)Cl_2]^{4+}$	248	8.5×10^4	π-π*
	276	7.1×10^4	tpy: π-π*
	319	4.6×10^4	π-π*
	507	1.0×10^4	MLCT

Recorded at room temperature in acetonitrile solution

ETHPY=, N,N,N',N'-tetra(2-pyridyl) ethylenediamine, BDPAA = 1,8-bis(2,2-dipyridylamino) anthracene

4.3.2 Electrochemical properties of the ruthenium binuclear complexes in non-aqueous solution

The cyclic voltammograms of $[Ru_2(tpy)_2(ETHPY)Cl_2]^{2+}$ and $[Ru_2(tpy)_2(BDPAA)Cl_2]^{2+}$ in acetonitrile are shown in Figures 4.7 and 4.8 respectively. A summary of $E_{1/2}$ values for the two binuclear complexes are given in Table 4.10. Both complexes show a reversible two-electron couple which is assigned as the Ru^{III}-Ru^{III}/Ru^{II}-Ru^{II} couple. The stoichiometry of the redox process (n = 2) has been established by comparing the peak current with that of the ferrocenium/ferrocene couple under similar experimental conditions and by constant potential coulometry. A comparsion of the $E_{1/2}$ of the ruthenium binuclear complexes with $[Ru(tpy)(PPP)Cl]^+$, $[Ru(tpy)(dpa)Cl]^+$ and $[Ru(tpy)(bpy)Cl]^+$ (Table 2.5) shows that replacing PPP and dpa with ETHPY or BDPAA has almost no effect on the $E_{1/2}$ values. This is consistent with the sequence of π-acidity which follows the order of bpy > dpa ~ PPP ~ ETHPY ~ BDPAA.

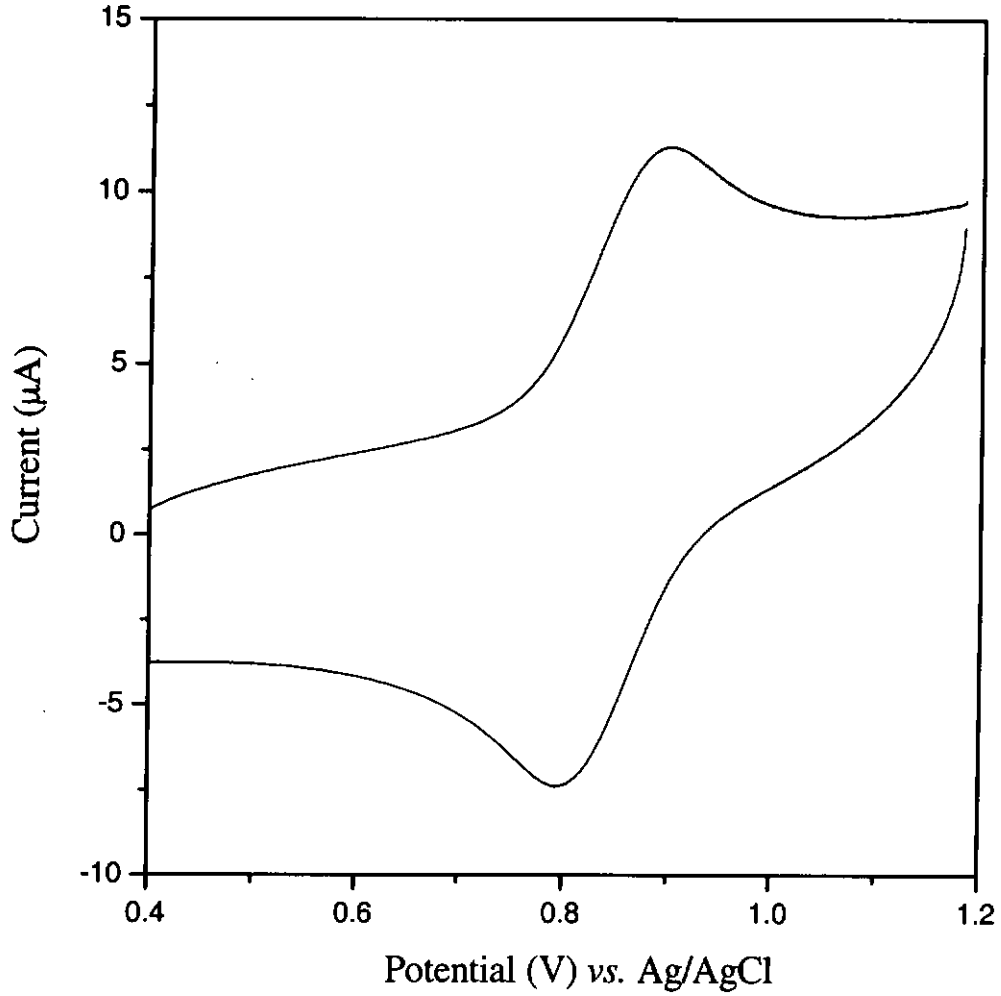

Figure 4.7 Cyclic voltammogram of 0.5 mM $[Ru_2(tpy)_2(ETHPY)Cl_2]^{2+}$ in 0.1 M TBAP + CH_3CN. Working electrode: 0.196 cm^2 glassy carbon. Scan rate: 100 mVs^{-1}

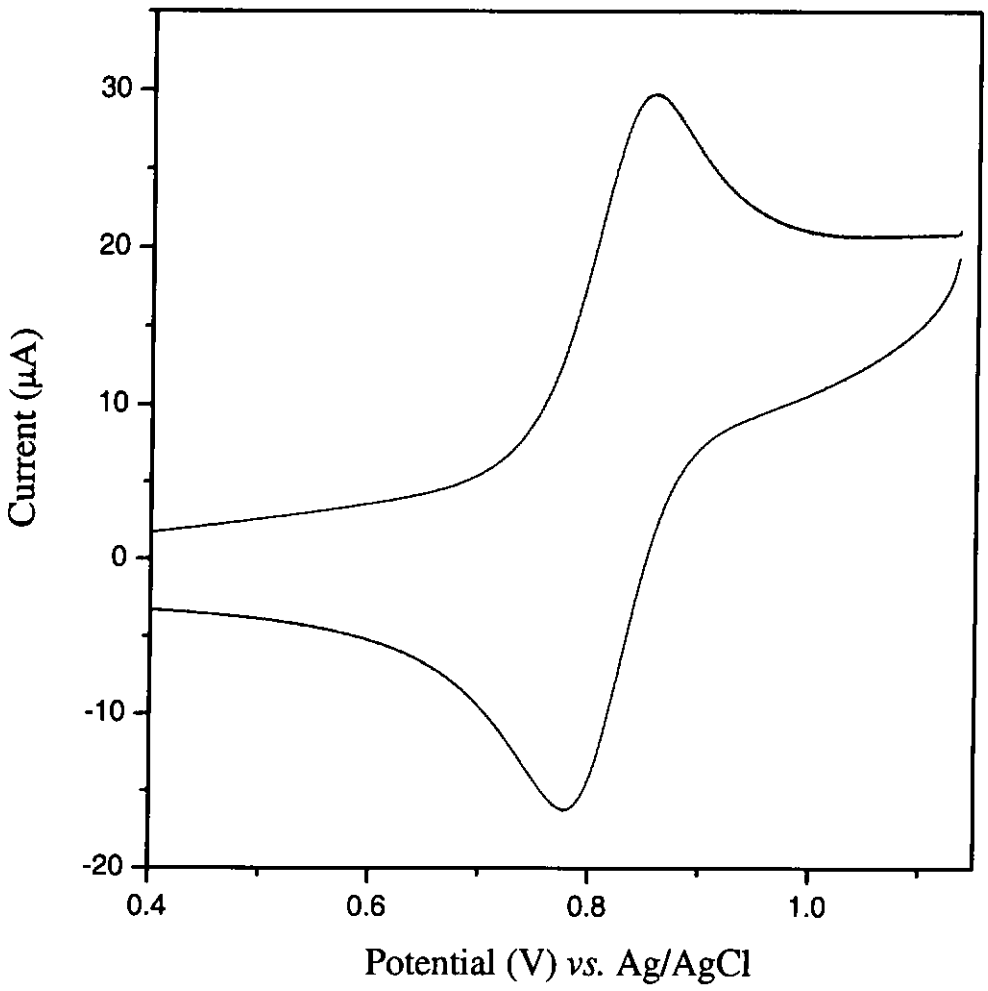

Figure 4.8 Cyclic voltammogram of 0.5 mM $[Ru_2(tpy)_2(BDPAA)Cl_2]^{2+}$ in 0.1 M TBAP + CH_3CN. Working electrode: 0.196 cm^2 glassy carbon. Scan rate: 100 mVs^{-1}

Table 4.10 Cyclic voltammetric data of the binuclear ruthenium complexes

Complex	$E_{1/2}$ of Ru^{III}-Ru^{III}/Ru^{II}-Ru^{II} couple (V *vs.* Ag/AgCl)	ΔE_p (mV)
$[Ru_2(tpy)_2(ETHPY)(Cl)_2]^{2+}$	0.81	70
$[Ru_2(tpy)_2(BDPAA)(Cl)_2]^{2+}$	0.80	87

The F_c^+/F_c couple was found to be 0.41 V vs. the Ag/AgCl

4.3.3 Electrochemical properties of the binuclear ruthenium complexes in aqueous medium

The cyclic voltammograms of $[Ru(tpy)(dpa)(H_2O)][ClO_4]_2$, $[Ru_2(tpy)_2(ETHPY)(H_2O)_2][ClO_4]_4$ and $[Ru_2(tpy)_2(BDPAA)(H_2O)_2][ClO_4]_4$ in 0.1 M acid solution and pH 7 buffer solution are shown in Figures 4.9 to 4.14 respectively. For $[Ru(tpy)(dpa)(H_2O)]^{2+}$, it shows one reversible couple (I) with $E_{1/2}$ = 0.68 V and a peak-to-peak separation ΔE_p of 86 mV. The size of this couple is similar to that of $[Fe(CN)_6]^{3-}/[Fe(CN)_6]^{4-}$ suggesting that this is a one-electron process. This couple is therefore assigned as the Ru^{III}/Ru^{II} couple. The Ru^{IV}/Ru^{III} couple (II) is only barely visible in 0.1 M $HClO_4$ (Figure 4.9).

The cyclic voltammogram of $[Ru_2(tpy)_2(ETHPY)(H_2O)_2]^{4+}$ shows two couples with $E_{1/2}$ = 0.78 V and 0.9 V respectively (Figure 4.11 and 4.12). The peak-to-peak separation ΔE_p are equal to 70 mV and 54 mV respectively for these two couples. The size of the first couple (I) at 0.78 V is roughly twice that of the $[Fe(CN)_6]^{3-}/[Fe(CN)_6]^{4-}$ couple, indicating that this is a two-electron processes. The size of the second couple (II) at 0.9 V, however, is much smaller in size than the first couple.

For complex $[Ru_2(tpy)_2(BDPAA)(H_2O)_2]^{4+}$, the cyclic voltammogram only shows one couple at 0.81 V, the size of which is about twice that of the $[Fe(CN)_6]^{3-}/[Fe(CN)_6]^{4-}$ couple, indicating that this is a two-electron process (Figure 4.13 and 4.14).

Figure 4.15 shows the RDE voltammograms of 0.5 mM $[Ru_2(tpy)_2(ETHPY)(H_2O)_2]^{4+}$ in aqueous 0.1 M CF_3SO_3H with glassy carbon as working electrode. For a diffusion-controlled electrochemical reaction, the relation between the limiting current and the rotation rate is given by the Levich equation [209]

$$i_L = 0.620nFAC_oD^{2/3}\nu^{-1/6}\omega^{1/2}$$

Where

ω =Angular velocity of the disc ($\omega=2\pi N$, N = rotation per second)
ν =Kinematic viscosity of the fluid, cm^2/s
i_L =Limiting current, mA
C_o =Concentration of reactant, mol/dm^3
n =number of electron transfer
F =Faraday constant
A =electrode surface area, cm^2
D =diffusion coefficient of the reactant, cm^2/s

A plot of i_L *vs.* $\omega^{1/2}$ will then give a straight line with a slope from which the diffusion coefficient can be calculated. The RDE voltammograms of $[Ru_2(tpy)_2(ETHPY)(H_2O)_2]^{4+}$ and $[Ru_2(tpy)_2(ETHPY)(py)_2]^{4+}$ (py = pyridine) are shown in Figure 4.15. Figure 4.16 indicated that the overall current of couples (I) and

(II) is larger than that of the two-electron process in the oxidation of $[Ru_2(tpy)_2(ETHPY)(py)_2]^{4+}$ to $[Ru_2(tpy)_2(ETHPY)(py)_2]^{6+}$ under similar experimental conditions.

The Levich plot of the $[Ru_2(tpy)_2(ETHPY)(py)_2]^{6+}/[Ru_2(tpy)_2(ETHPY)(py)_2]^{4+}$ couple is a straight line passing through the origin (Figure 4.16 b) indicating that couple is a diffusion controlled reaction from which the diffusion coefficient of $[Ru_2(tpy)_2(ETHPY)(py)_2]^{4+}$ in water was determined to be 1.74×10^{-5} cm^2s^{-1}. A comparison of the RDE voltammogram of $[Ru_2(tpy)_2(ETHPY)(H_2O)_2]^{4+}$ with that of $[Ru_2(tpy)_2(ETHPY)(py)_2]^{4+}$ indicated that the overall oxidation of $[Ru_2(tpy)_2(ETHPY)(H_2O)_2]^{4+}$ involves more than two electrons. This is consistent with the further oxidation of $[(HO\text{-}Ru^{III})(tpy)(ETHPY)(tpy)(Ru^{III}\text{-}OH)]^{4+}$ to $[(O{=}Ru^{IV})(tpy)(ETHPY)(tpy)(Ru^{IV}{=}O)]^{4+}$ as expected. The $E_{1/2}$ of the ruthenium aqua complexes vary with the pH of the solution. The Pourbaix diagrams obtained from the cyclic voltammograms recorded at different pH are discussed in the following section for the various ruthenium aqua complexes.

$[Ru(tpy)(dpa)(H_2O)]^{2+}$

As the Ru^{IV}/Ru^{III} couple of $[Ru(tpy)(dpa)(H_2O)]^{2+}$ is illy defined (Figures 4.9 and 4.10), only the $E_{1/2}$ of the Ru^{III}/Ru^{II} couple are recorded at different pH. The Pourbaix diagram is shown in Figure 4.17. From pH 1-8, the slope for the plot of $E_{1/2}$ *vs.* pH is 60 mV/pH, which is consistent with the loss of one proton and one electron in the electrode process:

$1.0 < pH < 8.0$

$$[Ru^{III}(tpy)(dpa)(OH)]^{2+} + e^- + H^+ \rightleftharpoons [Ru^{II}(tpy)(dpa)(OH_2)]^{2+}$$

At $pH > 8.0$, the $E_{1/2}$ of the Ru^{III}/Ru^{II} couple becomes pH independent

$pH > 8.0$

$$[Ru^{III}(tpy)(dpa)(OH)]^{2+} + e^- \rightleftharpoons [Ru^{II}(tpy)(dpa)(OH)]^{2+}$$

The pK_a of $[Ru(tpy)(dpa)(H_2O)]^{2+}$ is therefore estimated to be around 8.0.

$[Ru_2(tpy)_2(ETHPY)(H_2O)_2]^{4+}$

The Pourbaix diagram for $[Ru_2(tpy)_2(ETHPY)(H_2O)_2]^{4+}$ is shown in Figure 4.18.

At pH below 1.8, the slope of the $E_{1/2}$ *vs.* pH plot for the Ru^{IV}/Ru^{III} couple is linear with a slope close to –120 mV/pH unit, indicative of a four-proton two-electron transfer. In the same region, the $E_{1/2}$ of the Ru^{III}/Ru^{II} couple is independent of pH.

$pH < 1.8$

Couple I: $[Ru^{III}\text{-}OH_2)(tpy)(ETHPY)(tpy)(Ru^{III}\text{-}OH_2)]^{6+} + 2e^-$
$\rightleftharpoons [(Ru^{II}\text{-}OH_2)(tpy)(ETHPY)(tpy)(Ru^{II}\text{-}OH_2)]^{4+}$

Couple II: $[Ru^{IV}{=}O)(tpy)(ETHPY)(tpy)(Ru^{IV}{=}O)]^{4+} + 2e^- + 4H^+$
$\rightleftharpoons [(Ru^{III}\text{-}OH_2)(tpy)(ETHPY)(tpy)(Ru^{III}\text{-}OH_2)]^{6+}$

In the pH range of 1.8 – 8.0, the plot of $E_{1/2}$ *vs.* pH for both the Ru^{IV}/Ru^{III} and the Ru^{III}/Ru^{II} couples are linear with a slope close to -60 mV/pH unit, indicating that these processes are two-proton two-electron transfers.

1.8<pH<8.0

Couple I: $[Ru^{III}\text{-}OH)(tpy)(ETHPY)(tpy)(Ru^{III}\text{-}OH)]^{4+} + 2e^- + 2H^+ \rightleftharpoons [(Ru^{II}\text{-}OH_2)(tpy)(ETHPY)(tpy)(Ru^{II}\text{-}OH_2)]^{4+}$

Couple II: $[Ru^{IV}{=}O)(tpy)(ETHPY)(tpy)(Ru^{IV}{=}O)]^{4+} + 2e^- + 2H^+ \rightleftharpoons [(Ru^{III}\text{-}OH)(tpy)(ETHPY)(tpy)(Ru^{III}\text{-}OH)]^{4+}$

At pH > 8.0, the slope for the $E_{1/2}$ *vs.* pH plot for couple I is equal to -30 mV/pH unit. This is consistent with the following one-proton two-electron process:

pH > 8.0

$[Ru^{III}\text{-}OH_2)(tpy)(ETHPY)(tpy)(Ru^{III}\text{-}OH_2)]^{4+} + 2e^- + H^+ \rightleftharpoons [Ru^{II}\text{-}OH_2)(tpy)(ETHPY)(tpy)(Ru^{II}\text{-}OH)]^{4+}$

Based on the above results, it can be estimated the pK_a for $[(Ru^{III}\text{-}OH_2)_2(tpy)_2(ETHPY)]^{6+}$ and $[(Ru^{II}\text{-}OH_2)_2(tpy)_2(ETHPY)]^{4+}$ are around to 1.8 and 8.0 respectively.

Bulk electrolysis of $[Ru_2(tpy)_2(ETHPY)(H_2O)_2]^{4+}$ in 0.1 M CF_3SO_3H at 1.3 V *vs.* SCE resulted in a greenish-yellow solution. The anodic charge consumed in the electrolysis corresponds to an overall four-electron oxidation of the complex, suggesting

that the oxidized product should be $[(O=Ru^{IV})(tpy)(ETHPY)(tpy)(Ru^{IV}=O)]^{4+}$.

$[Ru_2(tpy)_2(BDPAA)(H_2O)_2]^{4+}$

The cyclic voltammogram of $[Ru_2(tpy)_2(BDPAA)(H_2O)_2]^{4+}$ only shows one two-electron couple in the pH range of 1 to 10. The Pourbaix diagram for the Ru^{III}-Ru^{III}/Ru^{II}-Ru^{II} couple is shown in Figure 4.19. The slope of the Pourbaix diagram is linear with a slope close to –60 mV/pH unit, indicative of a two-proton two electron transfer process.

$$[Ru^{III}\text{-}OH)(tpy)(BDPAA)(tpy)(Ru^{III}\text{-}OH)]^{4+} + 2e^- + 2H^+ \rightleftharpoons [(Ru^{II}\text{-}OH_2)(tpy)(BDPAA)(tpy)(Ru^{II}\text{-}OH_2)]^{4+}$$

From the above results, it appear that the formation of Ru=O is favourable in the binuclear ruthenium complex $[Ru_2(tpy)_2(ETHPY)(H_2O)_2]^{4+}$ but not in $[Ru_2(tpy)_2(BDPAA)(H_2O)_2]^{4+}$. As the X-ray structure of these complexes show that the two Ru centres are not close enough to allow direct interaction of the two Ru^{III}-OH moieties, interaction can therefore only occur through movement of the two ruthenium units. In this aspect, the ETHPY ligand should be more favourable for such interactions as it is flexible, whereas the rigidity of the BDPAA ligand should prohibit such movements. This can explain the difference in the voltammogram of these two complexes.

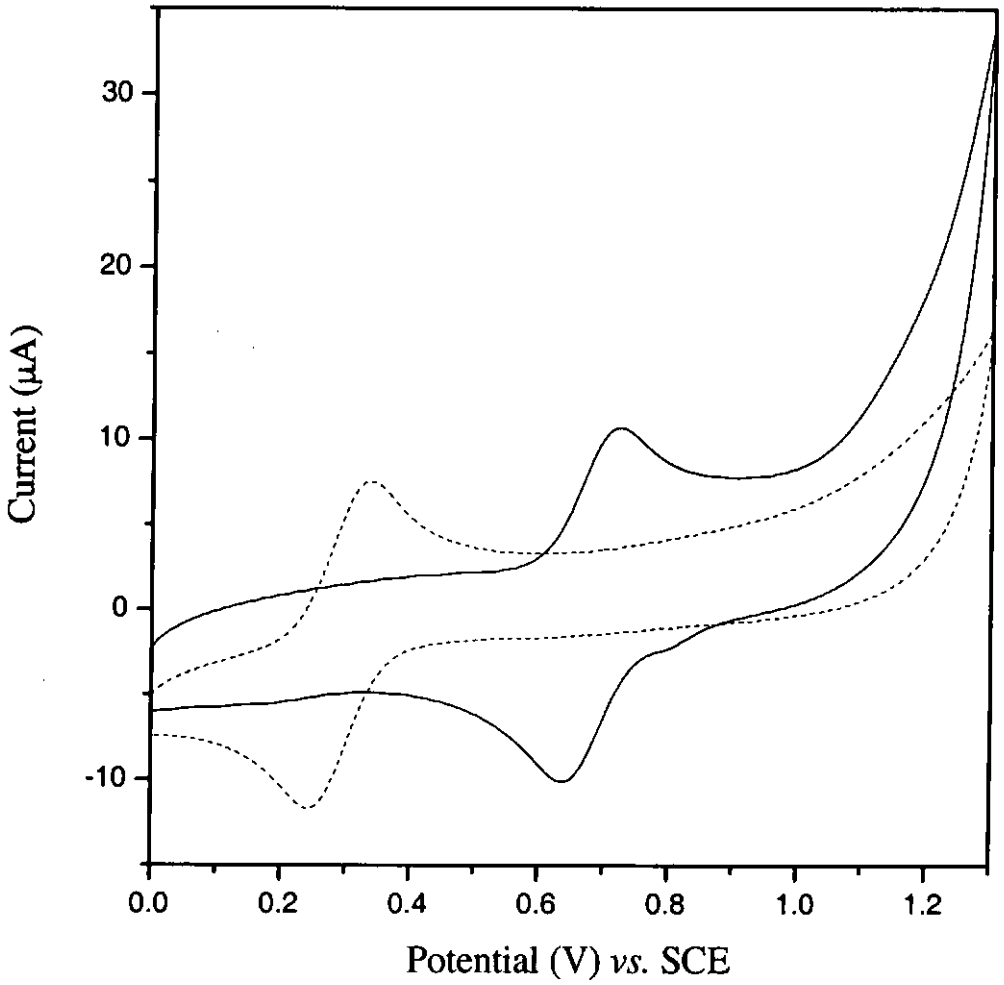

Figure 4.9 Cyclic voltammogram of 0.1mM $[Ru(tpy)(dpa)(H_2O)]^{2+}$ in 0.1 M of CF_3SO_3H solution. Working electrode: 0.196 cm^2 glassy carbon. Scan rate: 100 mVs^{-1}. (... 0.1mM $Fe(CN)_6^{4-}$ in the same electrolyte)

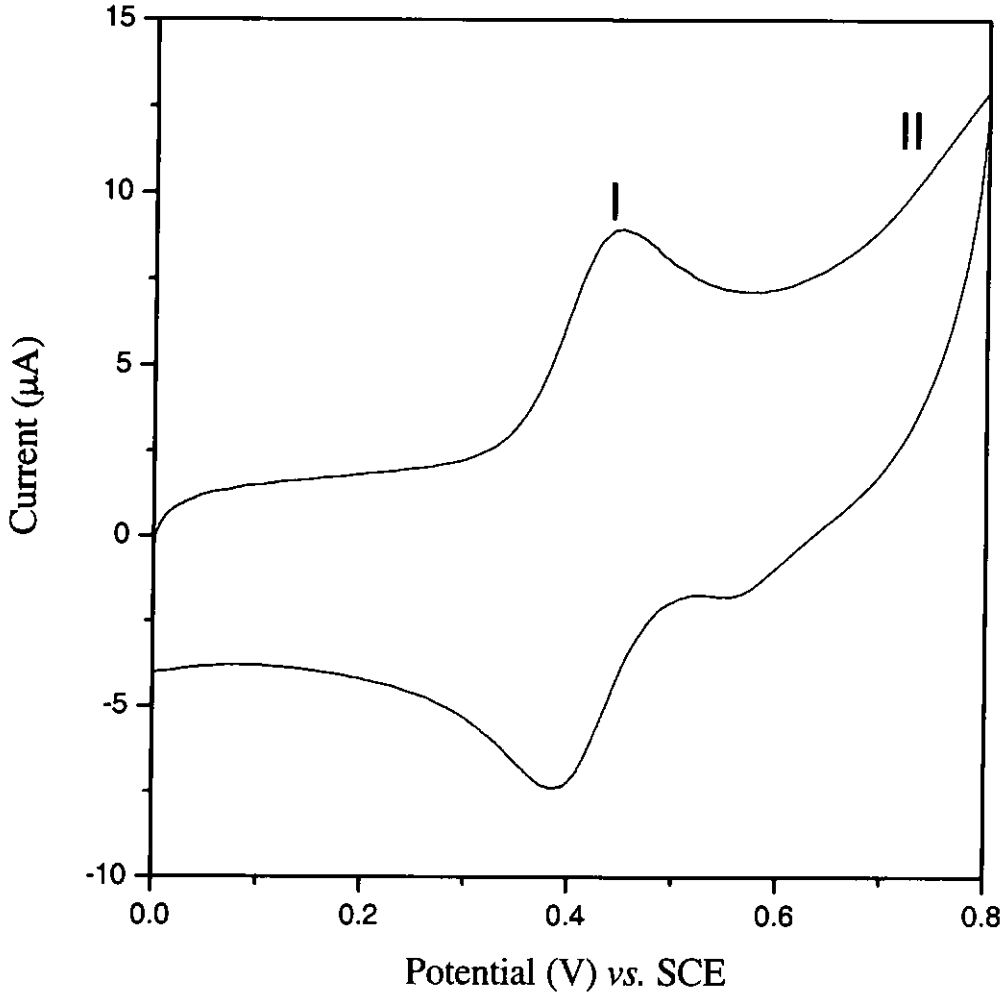

Figure 4.10 Cyclic voltammogram of 0.1mM $[Ru(tpy)(dpa)(H_2O)]^{2+}$ in pH 7 buffer. Working electrode: 0.196 cm^2 glassy carbon. Scan rate: 100 mVs^{-1}

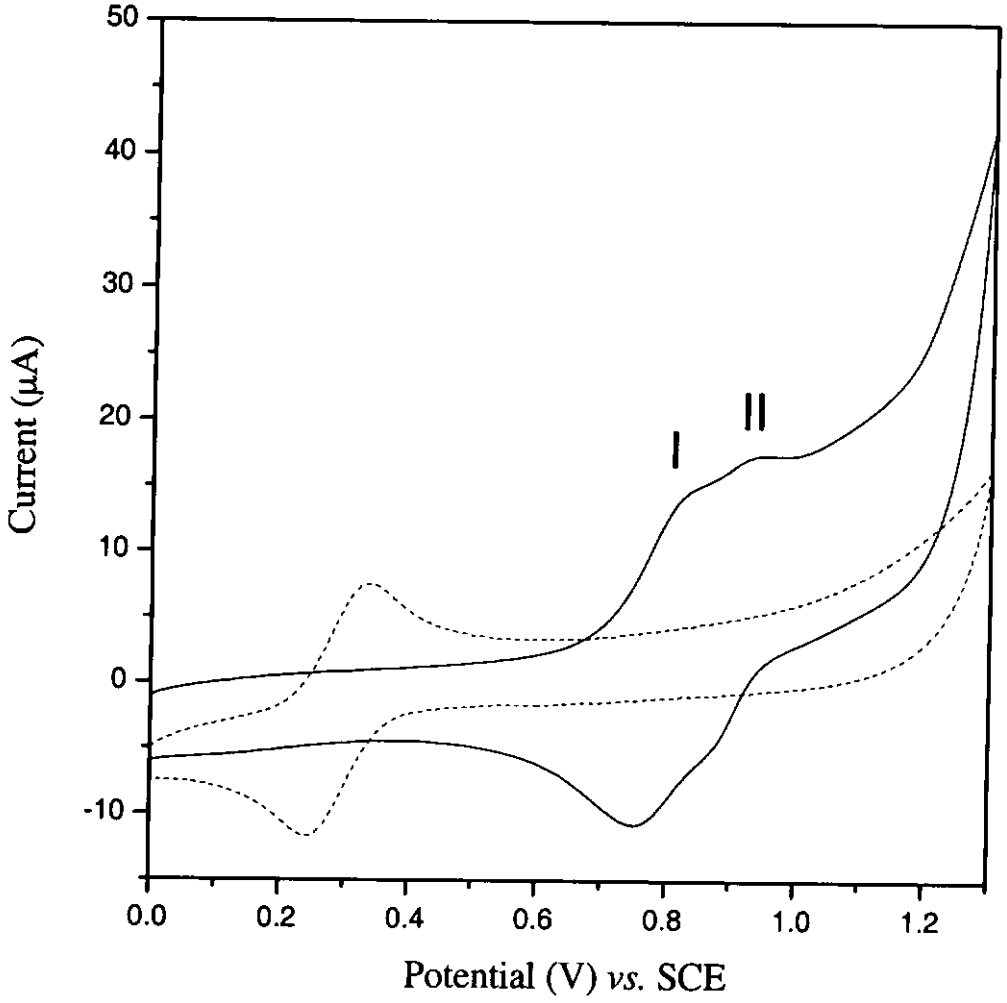

Figure 4.11 Cyclic voltammogram of 0.1mM $[Ru_2(tpy)_2(ETHPY)(H_2O)_2]^{4+}$ in 0.1 M of CF_3SO_3H solution. Working electrode: 0.196 cm^2 glassy carbon. Scan rate: 100 mVs^{-1}. (... 0.1mM $Fe(CN)_6^{4-}$ in the same electrolyte)

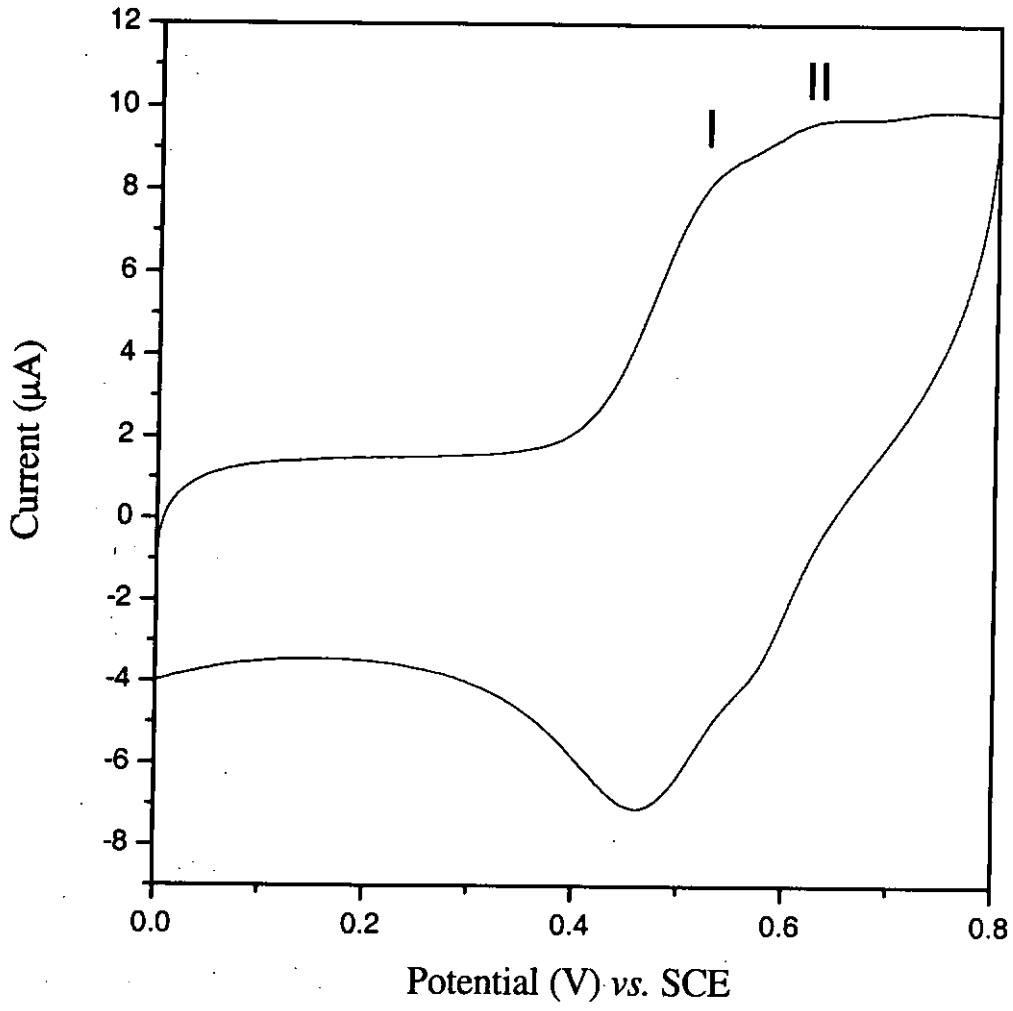

Figure 4.12 Cyclic voltammogram of 0.1mM $[Ru_2(tpy)_2(ETHPY)(H_2O)_2]^{4+}$ in pH 7 buffer solution. Working electrode: 0.196 cm^2 glassy carbon. Scan rate: 100 mVs^{-1}

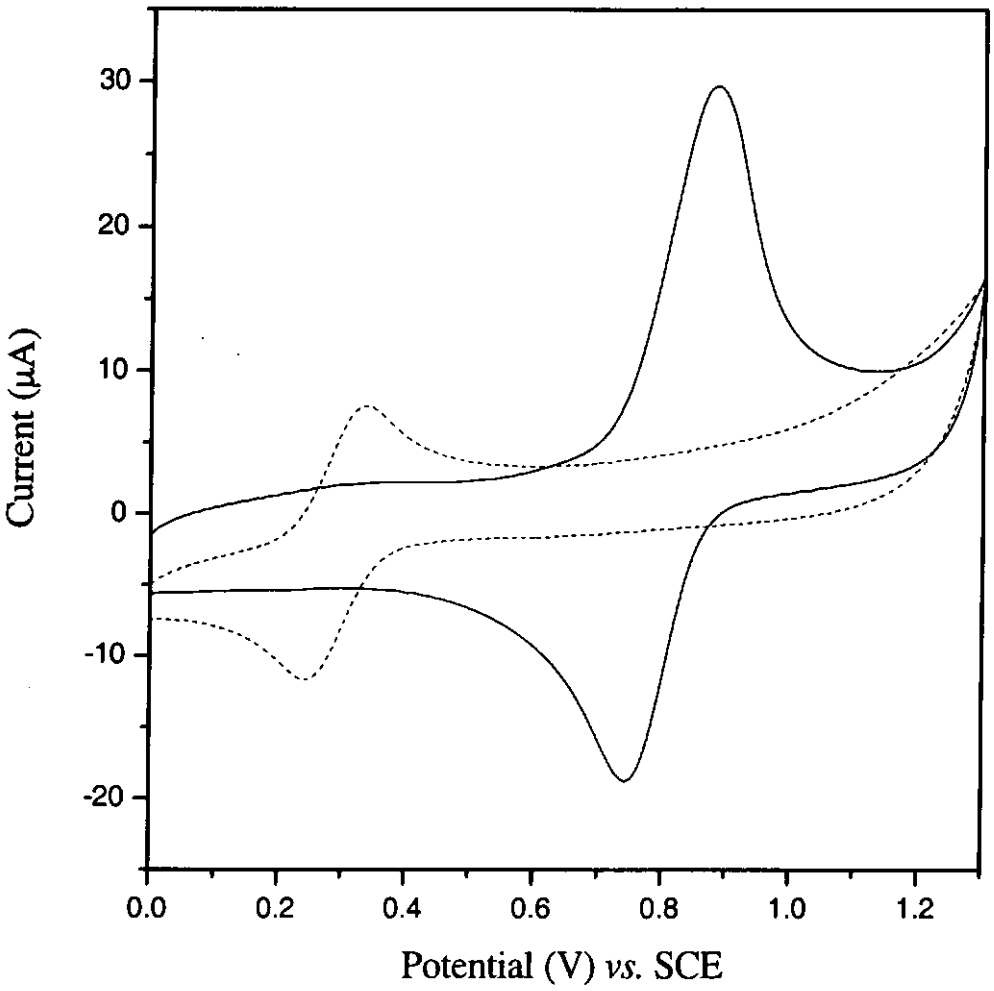

Figure 4.13 Cyclic voltammogram of 0.1mM $[Ru_2(tpy)_2(BDPAA)(H_2O)_2]^{4+}$ in 0.1 M of CF_3SO_3H solution. Working electrode: 0.196 cm^2 glassy carbon. Scan rate: 100 mVs^{-1}. (... 0.1mM $Fe(CN)_6^{4-}$ in the same electrolyte)

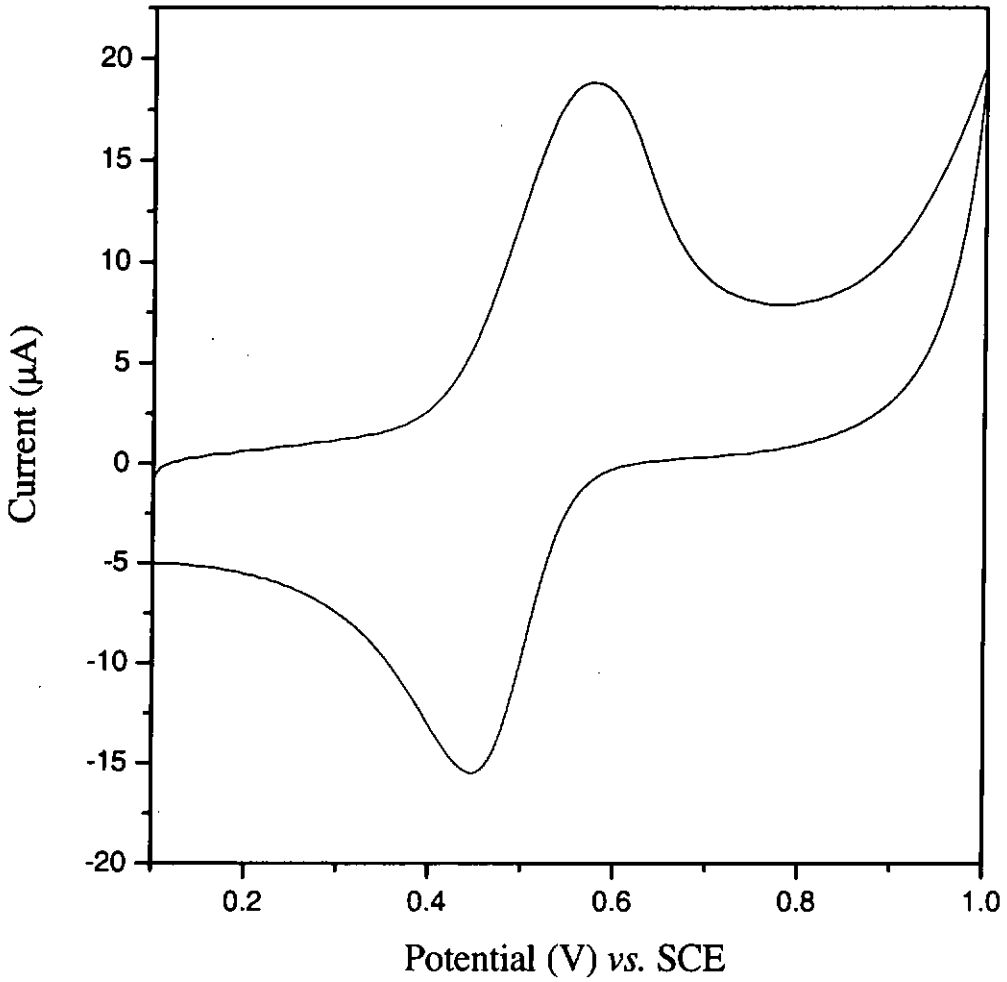

Figure 4.14 Cyclic voltammogram of 0.1mM $[Ru_2(tpy)_2(BDPAA)(H_2O)_2]^{4+}$ in pH 7 buffer solution. Working electrode: 0.196 cm^2 glassy carbon. Scan rate: 100 mVs^{-1}

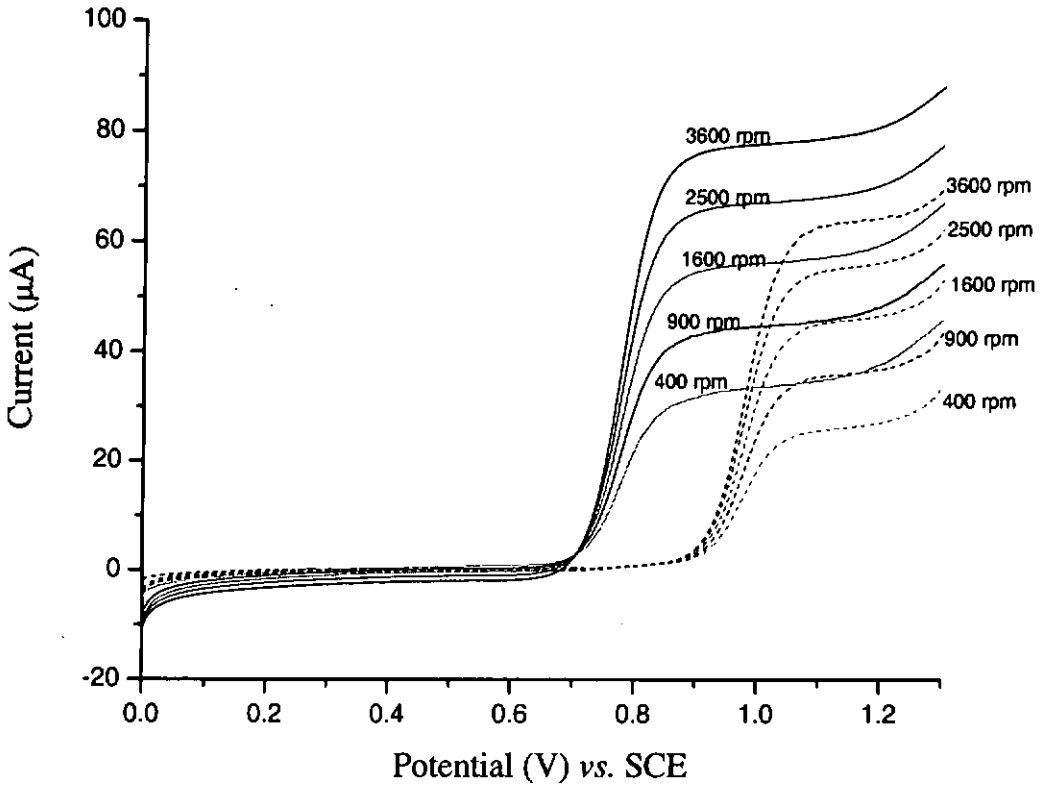

Figure 4.15 RDE voltammograms of (a) (—) 0.5 mM $[Ru_2(tpy)_2(ETHPY)(H_2O)_2]^{4+}$ and (b) (···) 0.5 mM $[Ru_2(tpy)_2(ETHPY)(py)_2]^{4+}$ in aqueous 0.1 M CF_3SO_3H. (Working electrode: 0.32 cm^2 glassy carbon. Scan rate: 5 mVs^{-1} (rpm = rotation per minute).

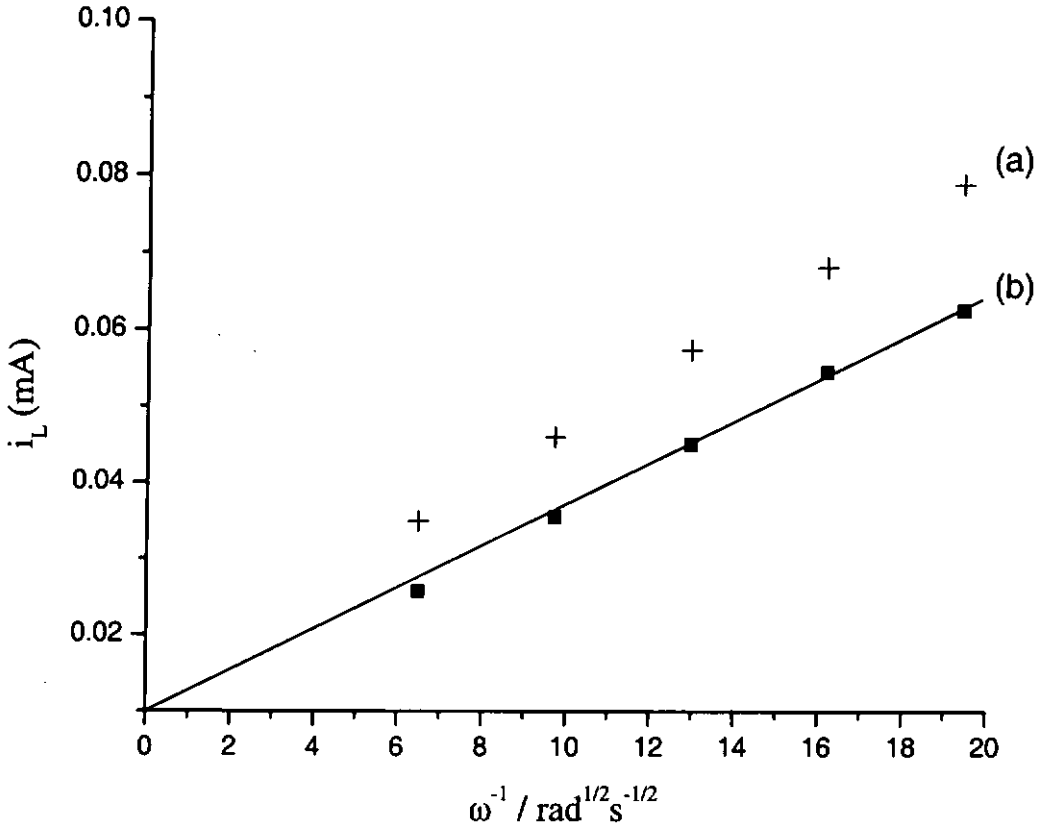

Figure 4.16 Levich plot for couple of (a) 0.5 mM $[Ru_2(tpy)_2(ETHPY)(H_2O)_2]^{4+}$ and (b) 0.5 mM $[Ru_2(tpy)_2(ETHPY)(py)_2]^{4+}$ in aqueous 0.1 M CF_3SO_3H. Working electrode: 0.32 cm^2 glassy carbon.

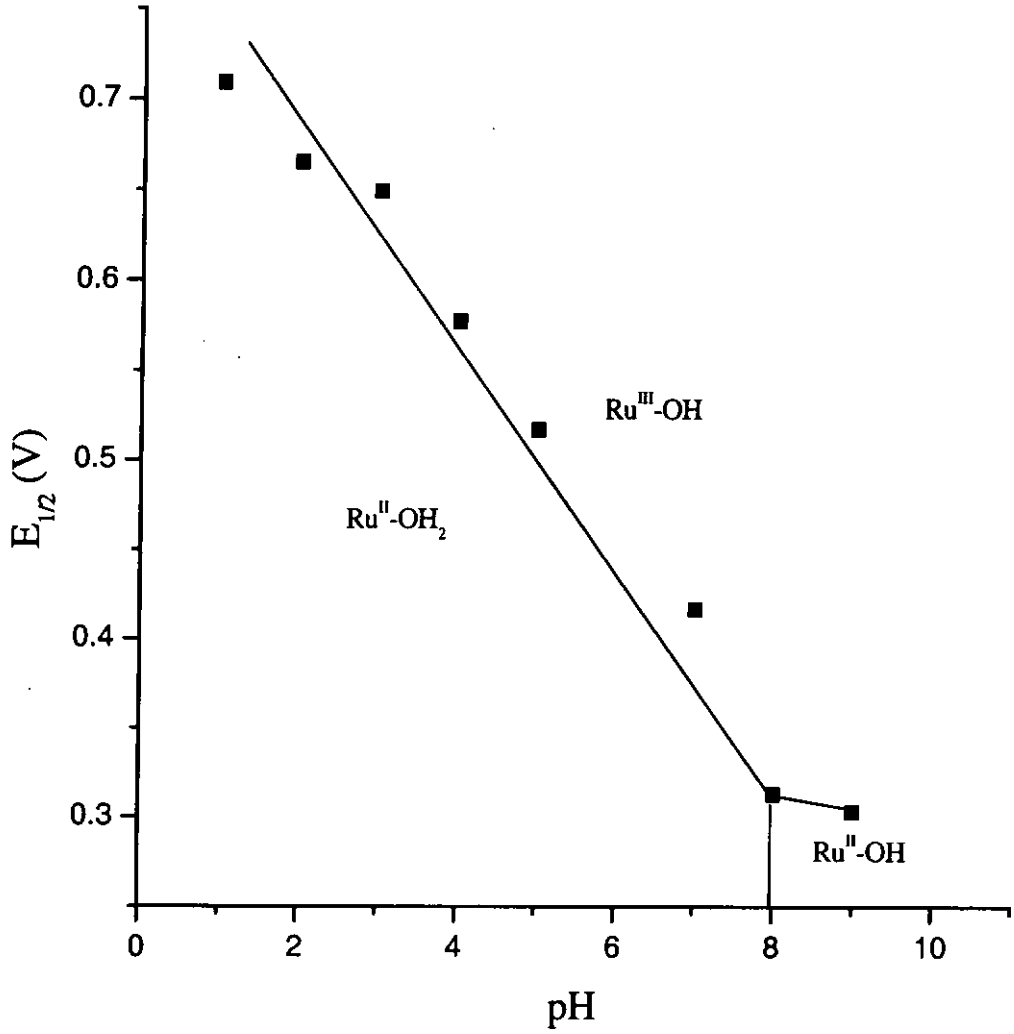

Figure 4.17 Pourbaix diagram of $E_{1/2}$ *vs.* pH for $[Ru(tpy)(dpa)(H_2O)]^{2+}$.

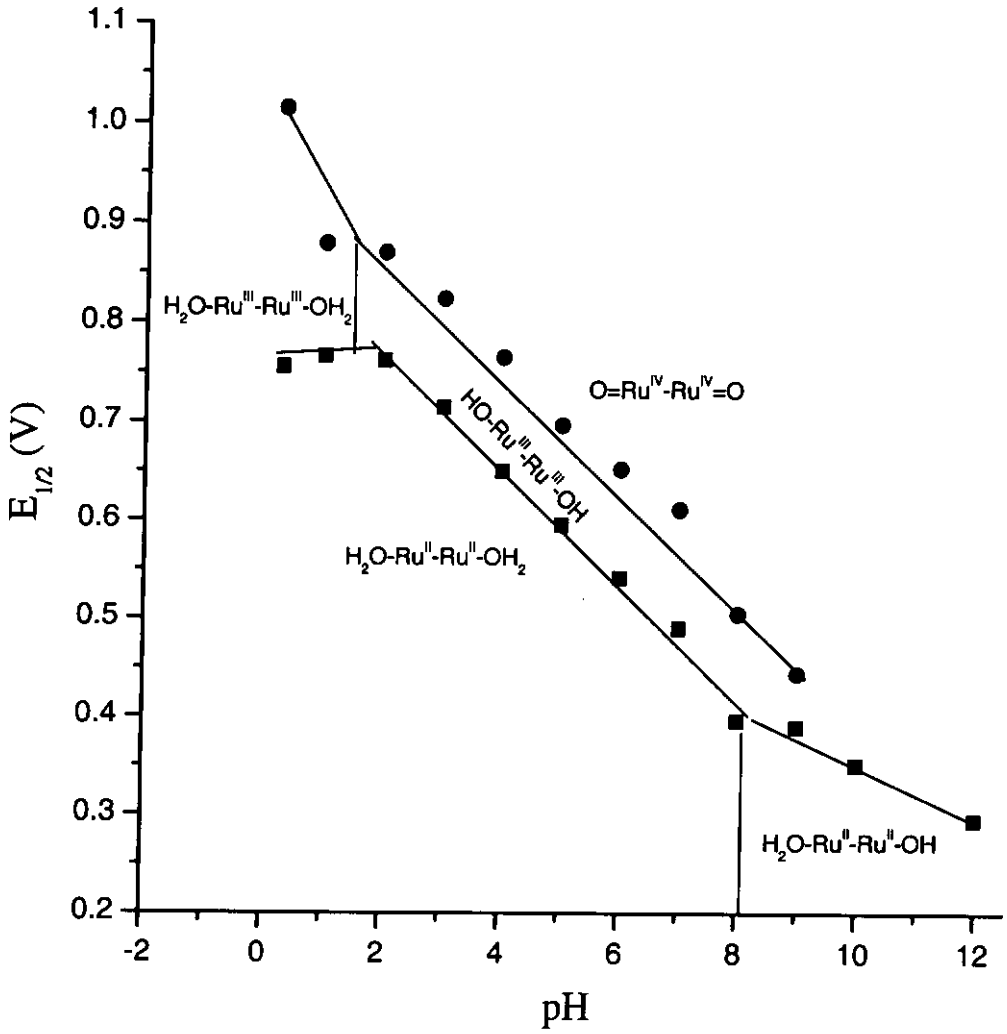

Figure 4.18 Pourbaix diagram of $E_{1/2}$ *vs.* pH for $[Ru_2(tpy)_2(ETHPY)(H_2O)_2]^{4+}$.

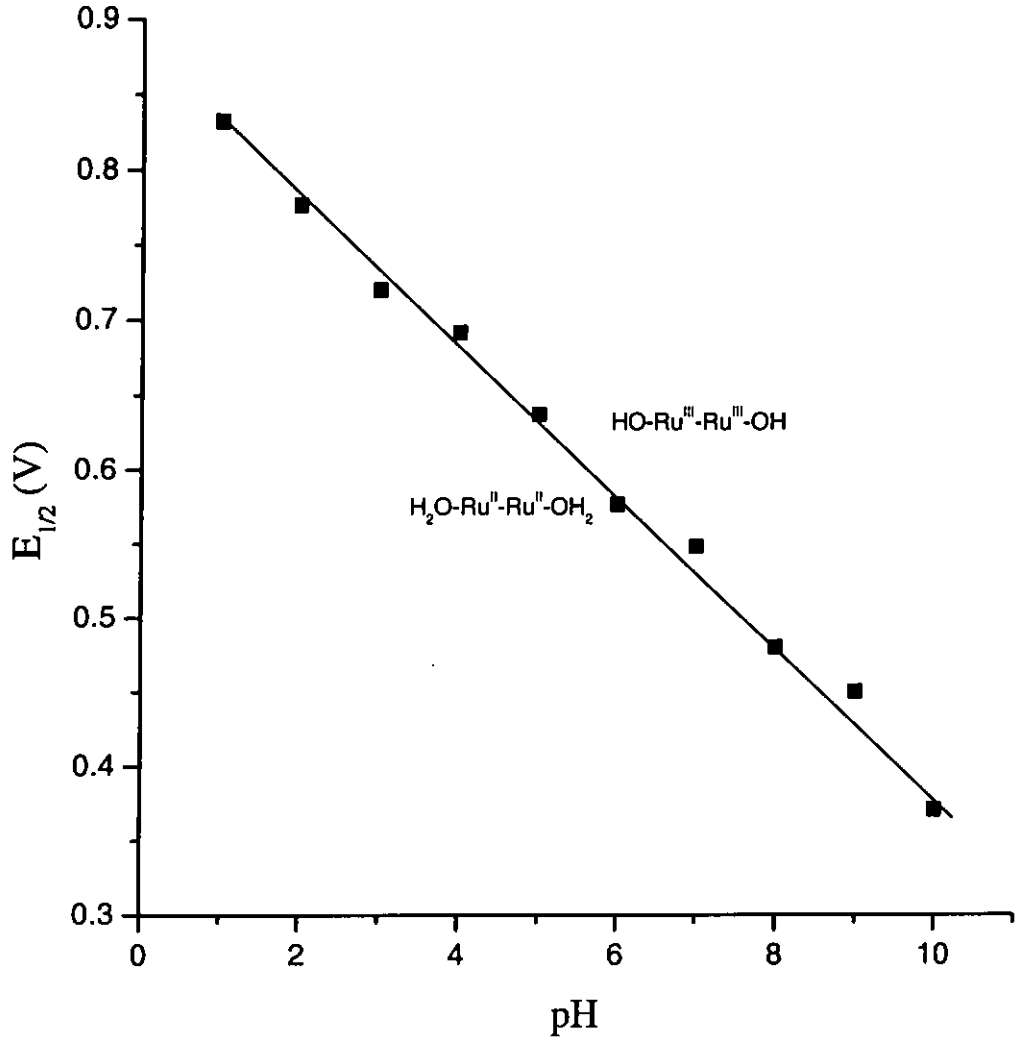

Figure 4.19 Pourbaix diagram of $E_{1/2}$ *vs.* pH for $[Ru_2(tpy)_2(BDPAA)(H_2O)_2]^{4+}$.

4.4 Conclusion

Two novel binuclear ligand ETHPY and BDPAA and their corresponding ruthenium complexes have been synthesized and characterized. The structure of the binuclear $[Ru_2(tpy)_2(ETHPY)(CH_3CN)_2](ClO_4)_4$ complex and the mononuclear analogue $[Ru(tpy)(dpa)(H_2O)](ClO_4)_2$ have been determined by X-ray crystallography. Electrochemical studies of the binulcear ruthenium aqua complexes indicated that the oxidation of $H_2O\text{-}Ru^{II}\text{-}Ru^{II}\text{-}OH_2$ to $O{=}Ru^{IV}\text{-}Ru^{IV}{=}O$ is only feasible in $[Ru_2(tpy)_2(ETHPY)(H_2O)_2]^{4+}$. As the X-ray structure suggests that the distance between two ruthenium metal centres are quite far away from each other in both $[Ru_2(tpy)_2(ETHPY)(H_2O)_2]^{4+}$ and $[Ru_2(tpy)_2(BDPAA)(H_2O)_2]^{4+}$, the flexibility of the ethylene bridge in ETHPY provides an explanation for the formation of Ru=O species through interaction of the two metal centres.

Chapter 5

Conclusions

Ruthenium oxo complexes are potential catalysts in electrochemical oxidation reactions. The slow kinetics in the electrogeneration of Ru=O species, however limit its applications. In this project, we have explored a number of ways to promote the electrochemical conversion of ruthenium aqua complexes to ruthrenium oxo species. It is found that by placing the ruthenium aqua complexes close to each other in polymer films, the oxidation to Ru=O in aqueous medium is promoted. This is attributed to the interaction between nearby Ru^{III}-OH (probably through hydrogen bonding) in the polymer film, which might assist the deprotonation of –OH in formation of Ru=O. As all previous reports on electropolymerized ruthenium-containing films were done in non-aqueous medium which inhibits the formation of ruthenium oxo species, our study on poly$[Ru(tpy)(PPP)(OH_2)]^{n+}$ is the first report on the electrogeneration of Ru=O in electropolymerized films.

The postulation that nearby functional groups capable of hydrogen bond formation with Ru-OH_2 or Ru-OH can promote the electrochemical formation of Ru=O is further supported by our study in the X-ray structure and electrochemistry of $[Ru(tpy)(dcbpy)(H_2O)]^{2+}$ and *cis*-$[Ru(dcbpy)_2(H_2O)_2]^{2+}$. The X-ray structures of these two complexes are consistent with the existence of intramolecular hydrogen bonding between the aqua hydrogen and the chloro-substituent on the ortho-position of the bipyridine ligand. The cyclic voltammograms of $[Ru(tpy)(dcbpy)(H_2O)]^{2+}$ and *cis*-$[Ru(dcbpy)_2(H_2O)_2]^{2+}$ show that the generation of Ru=O species is more facile than the analogues without chloro-substituents on the ortho-position.

Two novel binuclear ligands N,N,N'N'-tetra(2-pyridyl) ethyldiamine (ETHPY) and 1,8-bis(2,2'-dipyridylamino)anthracene (BDPAA) and their ruthenium aqua complexes were synthesized with the aim to promote the formation of Ru=O through close interaction of two nearby Ru^{III}-OH species. Electrochemical formation of Ru^{IV}=O was observed in $[Ru_2(tpy)_2(ETHPY)(H_2O)_2]^{4+}$ but not $[Ru_2(tpy)_2(BDPAA)(H_2O)_2]^{4+}$. X-ray crystal structures indicated that the two Ru centres are not close enough to each other to allow the direct interaction of Ru-OH moieties. It is possible that the flexible ethylene bridge in ETHPY still allows the two Ru centres to interact during the electrochemical oxidation, whereas the rigidity of BDPAA completely prohibits this type of interaction.

Our findings indicate that the distance between the ruthenium centres is critical in Ru=O formation. In future work, attention should be focused on shortening the distance between the two metal centres. A possible design will be through the N,N,N',N,'-tetramethyl-1,8-diaminoanthracence ligand.

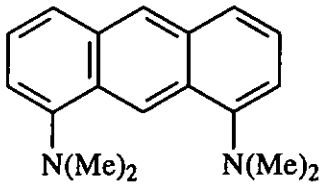

Figure 5.1 Structure of ligand N,N,N',N,'-tetramethyl-1,8-diaminoanthracence

It will be interesting to synthesize the binuclear ruthenium complex with the ligand N,N,N',N,'-tetramethyl-1,8-diaminoanthracence as shown in Figure 5.1. The estimated distance between the two ruthenium centres is about 4.2 Å, which should be sufficiently close for two Ru^{III}-OH moieties to interact. Investigation of this kind of binuclear complexes will shed light on the mechanism of formation of Ru=O species..

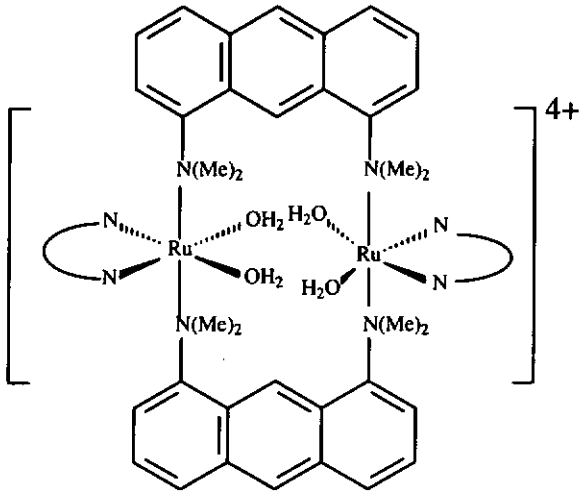

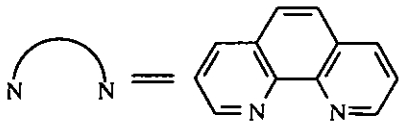

1,10-phenanthroline

References

1. http://www.ch.ic.ac.uk/kucernak/Research/electrocatalysis.html.

2. Seto, K., Iannelli, A., Love, B. and Lipkowski, J. The Influence of Surface Crystallography on the Rate of Hydrogen Evolution at Pt Electrodes. *Journal of Electroanalytical Chemistry*, 1987, **226**, 351-360.

3. Barber, J., Morin, S. and Conway, B. E. Specificity of the kinetics of H-2, evolution to the structure of single-crystal Pt surfaces, and the relation between opd and upd H. *Journal of Electroanalytical Chemistry*, 1998, **446**, 125-138.

4. Markovic, N. M., Grgur, B. N. and Ross, P. N. Temperature-dependent hydrogen electrochemistry on platinum low-index single-crystal surfaces in acid solutions. *Journal of Physical Chemistry B*, 1997, **101**, 5405-5413.

5. Markovic, N. M., Sarraf, S. T., Gasteiger, H. A. and Ross, P. N. Hydrogen electrochemistry on platinum low-index single-crystal surfaces in alkaline solution. *Journal of the Chemical Society-Faraday Transactions*, 1996, **92**, 3719-3725.

6. Gomez, R., Fernandezvega, A., Feliu, J. M. and Aldaz, A. Hydrogen Evolution on Pt Single-Crystal Surfaces - Effects of Irreversibly Adsorbed Bismuth and Antimony on Hydrogen Adsorption and Evolution on Pt(100). *Journal of Physical Chemistry*, 1993, **97**, 4769-4776.

7. Kita, H., Ye, S. and Gao, Y. Mass-Transfer Effect in Hydrogen Evolution Reaction on Pt Single-Crystal Electrodes in Acid-Solution. *Journal of Electroanalytical Chemistry*, 1992, **334**, 351-357.

8. Protopopoff, E. and Marcus, P. Effects of Chemisorbed Sulfur on the Hydrogen Adsorption and Evolution on Metal Single-Crystal Surfaces. *Journal De Chimie Physique Et De Physico-Chimie Biologique*, 1991, **88**, 1423-1452.

9. Lipkowski, J. and Ross, P. N. *Electrocatalysis*. New York: Wiley-VCH, 1998.

10. Markovic, N. M., Gasteiger, H. A., Grgur, B. N. and Ross, P. N. Oxygen reduction reaction on Pt(111): effects of bromide. *Journal of Electroanalytical Chemistry*, 1999, **467**, 157-163.

11. Grgur, B. N., Markovic, N. M. and Ross, P. N. Temperature dependent oxygen electrochemistry on platinum low index single crystal surfaces in acid solutions. *Canadian Journal of Chemistry-Revue Canadienne De Chimie*, 1997, **75**, 1465-1471.

12. Markovic, N., Gasteiger, H. and Ross, P. N. Kinetics of oxygen reduction on Pt(hkl) electrodes: Implications for the crystallite size effect with supported Pt electrocatalysts. *Journal of the Electrochemical Society*, 1997, **144**, 1591-1597.

13. Markovic, N. M., Gasteiger, H. A. and Ross, P. N. Oxygen Reduction on Platinum Low-Index Single-Crystal Surfaces in Sulfuric-Acid-Solution - Rotating Ring-Pt(hkl) Disk Studies. *Journal of Physical Chemistry*, 1995, **99**, 3411-3415.

14. Markovic, N. M., Adzic, R. R., Cahan, B. D. and Yeager, E. B. Structural Effects in Electrocatalysis - Oxygen Reduction on Platinum Low-Index Single-Crystal Surfaces in Perchloric-Acid Solutions. *Journal of Electroanalytical Chemistry*,

1994, **377**, 249-259.

15. Kita, H., Gao, Y. and Ohnishi, K. Effects of Adsorbed Bisulfate Ion, Adsorbed Hydrogen and Surface-Structure on the Oxygen Reduction at Platinum Single-Crystal Electrodes. *Chemistry Letters*, 1994, 73-76.

16. Elkadiri, F., Faure, R. and Durand, R. Electrochemical Reduction of Molecular-Oxygen on Platinum Single-Crystals. *Journal of Electroanalytical Chemistry*, 1991, **301**, 177-188.

17. Kondrikov, N. B., Ilin, I. E., Kiselev, E. Y., Postnova, I. V., Berdyugina, V. P., Solomin, P. V., Shchitovskaya, E. V., Shalaginov, V. V. and Belinskii, D. G. Electrocatalysis, Selectivity, and Acceleration of Anodic Electrosynthetic Processes. *Russian Electrochemistry*, 1993, **29**, 688-696.

18. Cornell, A., Hakansson, B. and Lindbergh, G. Ruthenium based DSA((R)) in chlorate electrolysis - critical anode potential and reaction kinetics. *Electrochimica Acta*, 2003, **48**, 473-481.

19. Ezerskis, Z. and Jusys, Z. Oxidation of chlorophenols on Pt electrode in alkaline solution studied by cyclic voltammetry, galvanostatic electrolysis, and gas chromatography-mass spectrometry. *Pure and Applied Chemistry*, 2001, **73**, 1929-1940.

20. Lassali, T. A. F., Boodts, J. F. C. and Trasatti, S. Electrocatalytic Activity of the Ternary Oxide Ru0.3ptxti(0.7-X)O2 for Chlorine Evolution. *Electrochimica Acta*, 1994, **39**, 1545-1549.

21. Beden, B., Bilmes, S., Lamy, C. and Leger, J. M. Electrosorption of Carbon-Monoxide on Platinum Single-Crystals in Perchloric-Acid Medium. *Journal of Electroanalytical Chemistry*, 1983, **149**, 295-302.

22. Markovic, N. M., Lucas, C. A., Grgur, B. N. and Ross, P. N. Surface electrochemistry of CO and H-2/CO mixtures at Pt(100) interface: Electrode kinetics and interfacial structures. *Journal of Physical Chemistry B*, 1999, **103**, 9616-9623.

23. Lucas, C. A., Markovic, N. M. and Ross, P. N. The adsorption and oxidation of carbon monoxide at the Pt(111)/electrolyte interface: atomic structure and surface relaxation. *Surface Science*, 1999, **425**, L381-L386.

24. Gomez, R., Feliu, J. M., Aldaz, A. and Weaver, M. J. Validity of double-layer charge-corrected voltammetry for assaying carbon monoxide coverages on ordered transition metals: comparisons with adlayer structures in electrochemical and ultrahigh vacuum environments. *Surface Science*, 1998, **410**, 48-61.

25. Couto, A., Perez, M. C., Rincon, A. and Gutierrez, C. Necessity of CO-free Pt sites for the electrooxidation at low potentials of dissolved CO on polycrystalline Pt. *Journal of Physical Chemistry*, 1996, **100**, 19538-19544.

26. Hayden, B. E., Murray, A. J., Parsons, R. and Pegg, D. J. UHV and electrochemical transfer studies on Pt(110)-(1 x 2): The influence of bismuth on hydrogen and oxygen adsorption, and the electro-oxidation of carbon monoxide.

Journal of Electroanalytical Chemistry, 1996, **409**, 51-63.

27. Kita, H., Naohara, H., Nakato, T., Taguchi, S. and Aramata, A. Effects of Adsorbed Co on Hydrogen Ionization and Co Oxidation Reactions at Pt Single-Crystal Electrodes in Acidic Solution. *Journal of Electroanalytical Chemistry*, 1995, **386**, 197-206.

28. Wieckowski, A., Rubel, M. and Gutierrez, C. Reactive Sites in Bulk Carbon-Monoxide Electrooxidation on Oxide-Free Platinum(111). *Journal of Electroanalytical Chemistry*, 1995, **382**, 97-101.

29. Villegas, I. and Weaver, M. J. Carbon-Monoxide Adlayer Structures on Platinum(111) Electrodes - a Synergy between in-Situ Scanning-Tunneling-Microscopy and Infrared-Spectroscopy. *Journal of Chemical Physics*, 1994, **101**, 1648-1660.

30. Kita, H., Narumi, H., Ye, S. and Naohara, H. Analysis of Irreversible Oxidation Wave of Adsorbed Co at Pt(111), Pt(100) and Pt(110) Electrodes. *Journal of Applied Electrochemistry*, 1993, **23**, 589-596.

31. Weaver, M. J., Chang, S. C., Leung, L. W. H., Jiang, X., Rubel, M., Szklarczyk, M., Zurawski, D. and Wieckowski, A. Evaluation of Absolute Saturation Coverages of Carbon-Monoxide on Ordered Low-Index Platinum and Rhodium Electrodes. *Journal of Electroanalytical Chemistry*, 1992, **327**, 247-260.

32. Orts, J. M., Fernandezvega, A., Feliu, J. M., Aldaz, A. and Clavilier, J. Electrochemical-Behavior of Co Layers Formed by Solution Dosing at Open

Circuit on Pt(111) - Voltammetric Determination of Co Coverages at Full Hydrogen Adsorption Blocking in Various Acid-Media. *Journal of Electroanalytical Chemistry*, 1992, **327**, 261-278.

33. Kinomoto, Y., Watanabe, S., Takahashi, M. and Ito, M. Infrared-Spectra of Co Adsorbed on Pt(100), Pt(111), and Pt(110) Electrode Surfaces. *Surface Science*, 1991, **242**, 538-543.

34. Feliu, J. M., Orts, J. M., Fernandezvega, A., Aldaz, A. and Clavilier, J. Electrochemical Studies in Sulfuric-Acid-Solutions of Absorbed Co on Pt (111) Electrodes. *Journal of Electroanalytical Chemistry*, 1990, **296**, 191-201.

35. Zurawski, D., Wasberg, M. and Wieckowski, A. Low-Energy Electron-Diffraction and Voltammetry of Carbon-Monoxide Electrosorbed on Pt(111). *Journal of Physical Chemistry*, 1990, **94**, 2076-2082.

36. Leung, L. W. H., Wieckowski, A. and Weaver, M. J. Insitu Infrared-Spectroscopy of Well-Defined Single-Crystal Electrodes - Adsorption and Electrooxidation of CO on Pt(111). *Journal of Physical Chemistry*, 1988, **92**, 6985-6990.

37. Sun, S. G., Clavilier, J. and Bewick, A. The Mechanism of Electrocatalytic Oxidation of Formic-Acid on Pt (100) and Pt (111) in Sulfuric-Acid Solution - an Emirs Study. *Journal of Electroanalytical Chemistry*, 1988, **240**, 147-159.

38. Kitamura, F., Takeda, M., Takahashi, M. and Ito, M. Co Adsorption on Pt(111) and Pt(100) Single-Crystal Surfaces in Aqueous-Solutions Studied by Infrared

Reflection Absorption-Spectroscopy. *Chemical Physics Letters*, 1987, **142**, 318-322.

39. Greef, R. and Southampton Electrochemistry Group. *Instrumental Methods in Electrochemistry*. Chichester: Ellis Horwood, 1985.

40. Fleischm, M., Korinek, K. and Pletcher, D. Oxidation of Organic Compounds at a Nickel Anode in Alkaline Solution. *Journal of Electroanalytical Chemistry*, 1971, **31**, 39-49.

41. Marioli, J. M., Luo, P. F. and Kuwana, T. Nickel-Chromium Alloy Electrode as a Carbohydrate Detector for Liquid-Chromatography. *Analytica Chimica Acta*, 1993, **282**, 571-580.

42. Casella, I. G., Deimoni, F. and Cataldi, T. R. I. Study of a Nickel-Catalyzed Glassy-Carbon Electrode for Detection of Carbohydrates in Liquid-Chromatography and Flow-Injection Analysis. *Analytica Chimica Acta*, 1991, **248**, 117-125.

43. Luo, P. F., Zhang, F. Z. and Baldwin, R. P. Comparison of Metallic Electrodes for Constant-Potential Amperometric Detection of Carbohydrates, Amino-Acids and Related-Compounds in Flow Systems. *Analytica Chimica Acta*, 1991, **244**, 169-178.

44. Casella, I. G., Desimoni, E. and Salvi, A. M. Chemically Modified Electrode for the Detection of Carbohydrates. *Analytica Chimica Acta*, 1991, **243**, 61-63.

45. Hui, B. S. and Huber, C. O. Amperometric Detection of Amines and

Amino-Acids in Flow-Injection Systems with a Nickel-Oxide Electrode. *Analytica Chimica Acta*, 1982, **134**, 211-218.

46. Robertson, P. M. On the Oxidation of Alcohols and Amines at Nickel-Oxide Electrodes - Mechanistic Aspects. *Journal of Electroanalytical Chemistry*, 1980, **111**, 97-104.

47. Taraszewska, J. and Roslonek, G. Electrocatalytic Oxidation of Methanol on a Glassy-Carbon Electrode Modified by Nickel-Hydroxide Formed by Ex-Situ Chemical Precipitation. *Journal of Electroanalytical Chemistry*, 1994, **364**, 209-213.

48. Losada, J., del Peso, I. and Beyer, L. Redox and electrocatalytic properties of electrodes modified by films of polypyrrole nickel(II) Schiff-base complexes. *Journal of Electroanalytical Chemistry*, 1998, **447**, 147-154.

49. Dawson, J. H. and Sono, M. Cytochrome.P-450 and Chloroperoxidase - Thiolate-Ligated Heme Enzymes - Spectroscopic Determination of Their Active-Site Structures and Mechanistic Implications of Thiolate Ligation. *Chemical Reviews*, 1987, **87**, 1255-1276.

50. Groves, J. T. Key Elements of the Chemistry of Cytochrome-P-450 - the Oxygen Rebound Mechanism. *Journal of Chemical Education*, 1985, **62**, 928-931.

51. Guengerich, F. P. and Macdonald, T. L. Chemical Mechanisms of Catalysis by Cytochromes-P-450 - a Unified View. *Accounts of Chemical Research*, 1984, **17**, 9-16.

52. Ostovic, D. and Bruice, T. C. Mechanism of Alkene Epoxidation by Iron, Chromium, and Manganese Higher Valent Oxo-Metalloporphyrins. *Accounts of Chemical Research*, 1992, **25**, 314-320.

53. Ortiz de Montellano, P. R. *Cytochrome P450 : structure, mechanism, and biochemistry*. New York: Plenum Press, 1995.

54. Kadish, K. M., Smith, K. M. and Guilard, R., Biochemistry and binding: activation of small molecules, 17-40, in *The porphyrin handbook*. San Diego: Academic Press, 2000.

55. Schroder, D. and Schwarz, H. C-H and C-C Bond Activation by Bare Transition-Metal Oxide Cations in the Gas-Phase. *Angewandte Chemie-International Edition in English*, 1995, **34**, 1973-1995.

56. Meunier, B. *Biomimetic oxidations catalyzed by transition metal complexes*. London: Imperial College Press, 2000.

57. Balasubramanian, P. N., Smith, J. R. L., Davies, M. J., Kaaret, T. W. and Bruice, T. C. Dynamics of Reaction of [Meso-Tetrakis(2,6-Dimethyl-3-Sulfonatophenyl)Porphinato]-Iron(III) Hydrate with Tert-Butyl Hydroperoxide in Aqueous-Solution .2. Establishment of a Mechanism That Involves Homolytic O-O Bond Breaking and One-Electron Oxidation of the Iron(III) Porphyrin. *Journal of the American Chemical Society*, 1989, **111**, 1477-1483.

58. Balahura, R. J., Sorokin, A., Bernadou, J. and Meunier, B. Origin of the oxygen

atom in C-H bond oxidations catalyzed by a water-soluble metalloporphyrin. *Inorganic Chemistry*, 1997, **36**, 3488-3492.

59. Groves, J. T. and Quinn, R. Models of Oxidized Heme-Proteins - Preparation and Characterization of a Trans-Dioxoruthenium(VI) Porphyrin Complex. *Inorganic Chemistry*, 1984, **23**, 3844-3846.

60. Collman, J. P., Kodadek, T., Raybuck, S. A., Brauman, J. I. and Papazian, L. M. Mechanism of Oxygen Atom Transfer from High Valent Iron Porphyrins to Olefins - Implications to the Biological Epoxidation of Olefins by Cytochrome-P-450. *Journal of the American Chemical Society*, 1985, **107**, 4343-4345.

61. Meunier, B. Metalloporphyrins as Versatile Catalysts for Oxidation Reactions and Oxidative DNA Cleavage. *Chemical Reviews*, 1992, **92**, 1411-1456.

62. Yu, C. J., Chong, Y. C., Kayyem, J. F. and Gozin, M. Soluble ferrocene conjugates for incorporation into self-assembled monolayers. *Journal of Organic Chemistry*, 1999, **64**, 2070-2079.

63. Collman, J. P., Lee, V. J., Kellenyuen, C. J., Zhang, X. M., Ibers, J. A. and Brauman, J. I. Threitol-Strapped Manganese Porphyrins as Enantioselective Epoxidation Catalysts of Unfunctionalized Olefins. *Journal of the American Chemical Society*, 1995, **117**, 692-703.

64. Collman, J. P., Lee, V. J., Zhang, X. M., Ibers, J. A. and Brauman, J. I. Enantioselective Epoxidation of Unfunctionalized Olefins Catalyzed by

Threitol-Strapped Manganese Porphyrins. *Journal of the American Chemical Society*, 1993, **115**, 3834-3835.

65. Schaus, S. E., Larrow, J. F. and Jacobsen, E. N. Practical synthesis of enantiopure cyclic 1,2-amino alcohols via catalytic asymmetric ring opening of meso epoxides. *Journal of Organic Chemistry*, 1997, **62**, 4197-4199.

66. Larrow, J. F., Jacobsen, E. N., Gao, Y., Hong, Y. P., Nie, X. Y. and Zepp, C. M. A Practical Method for the Large-Scale Preparation of [N,N'-Bis(3,5-Di-Tert-Butylsalicylidene)1,2-Cyclohexanediaminato(2-)]Mangan ese(III) Chloride, a Highly Enantioselective Epoxidation Catalyst. *Journal of Organic Chemistry*, 1994, **59**, 1939-1942.

67. Wei, Z., Loebach, J. L., Wilson, S. R. and Jacobsen, E. N. Enantioselective Epoxidation of Unfunctionalized Olefins Catalyzed by (Salen)Manganese Complexes. *Journal of the American Chemical Society*, 1990, **112**, 2801-2803.

68. Hong, F., Look, G. C., Wei, Z., Jacobsen, E. N. and Wong, C. H. Mechanistic Study of a Synthetically Useful Monooxygenase Model Using the Hypersensitive Probe Trans-2-Phenyl-1-Vinylcyclopropane. *Journal of Organic Chemistry*, 1991, **56**, 6497-6500.

69. Palucki, M., Finney, N. S., Pospisil, P. J., Guler, M. L., Ishida, T. and Jacobsen, E. N. The mechanistic basis for electronic effects on enantioselectivity in the (salen)Mn(III)-catalyzed epoxidation reaction. *Journal of the American Chemical Society*, 1998, **120**, 948-954.

70. Eggleston, D. S., Goldsby, K. A., Hodgson, D. J. and Meyer, T. J. Structural Variations Induced by Changes in Oxidation-State and Their Role in Electron-Transfer - Crystal and Molecular-Structures of Cis-$Ru(bpy)_2Cl_2$.$3.5H_2O$ and Cis- $Ru(bpy)_2Cl_2$ Cl.$2H_2O$. *Inorganic Chemistry*, 1985, **24**, 4573-4580.

71. Moyer, B. A. and Meyer, T. J. Oxobis(2,2'-bipyridine)pyridineruthenium(IV) Ion, $(bpy)_2(py)Ru{=}O^{2+}$. *Journal of the American Chemical Society*, 1978, **100**, 3601-3603.

72. Moyer, B. A. and Meyer, T. J. Properties of the Oxo-Aquo System "$(bpy)_2(py)RuO^{2+}$- $(bpy)_2(py)Ru(OH_2)_2^{+}$. *Inorganic Chemistry*, 1981, **20**, 436-444.

73. Binstead, R. A., Moyer, B. A., Samuels, G. J. and Meyer, T. J. Proton-Coupled Electron-Transfer between $Ru(bpy)_2(py)OH_2^{2+}$ and Ru(bpy)2(py)O $^{2+}$ - a Solvent Isotope Effect (kH_2O-kD_2O) of 16.1. *Journal of the American Chemical Society*, 1981, **103**, 2897-2899.

74. Meyer, T. J. and Huynh, M. H. V. The Remarkable Reactivity of high Oxidation State Ruthenium and Osmium Polypyridyl Complexes. *Inorganic Chemistry*, 2003, **42**, 8140-8160.

75. Binstead, R. A., McGuire, M. E., Dovletoglou, A., Seok, W. K., Roecker, L. E. and Meyer, T. J. Oxidation of Hydroquinones by $(bpy)_2(py)Ru^{IV}(O)^{2+}$ and $(bpy)_2(py)Ru^{III}(OH)^{2+}$ - Proton-Coupled Electron-Transfer. *Journal of the*

American Chemical Society, 1992, **114**, 173-186.

76. Rong, C. Y. and Anson, F. C. Simplified Preparations and Electrochemical-Behavior of 2 Chromium-Substituted Heteropolytungstate Anions. *Inorganic Chemistry*, 1994, **33**, 1064-1070.

77. Creager, S. E. and Murray, R. W. Electrochemical Studies of Oxo(Meso-Tetraphenylporphinato)Chromium(IV) - Direct Evidence for Epoxidation of Olefins by an Electrochemically Generated Formal Chromium(V) State. *Inorganic Chemistry*, 1985, **24**, 3824-3828.

78. Jeon, S. and Bruice, T. C. Electrochemical Potentials and Associated Pka Values for the Various Oxidation-States of a Water-Soluble, Non Mu-Oxo Dimer Forming Chromium Tetraphenylporphyrin in Aqueous-Solution. *Inorganic Chemistry*, 1991, **30**, 4311-4315.

79. He, G. X., Arasasingham, R. D., Zhang, G. H. and Bruice, T. C. The Rate-Limiting Step in the One-Electron Oxidation of an Alkene by Oxo Meso-Tetrakis(2,6-Dibromophenyl)Porphinato -Chromium(V) Is the Formation of a Charge-Transfer Complex. *Journal of the American Chemical Society*, 1991, **113**, 9828-9833.

80. Farrell, R. P., Judd, R. J., Lay, P. A., Dixon, N. E., Baker, R. S. U. and Bonin, A. M. Chromium(V)-Induced Cleavage of DNA - Are Chromium(V) Complexes the Active Carcinogens in Chromium(VI)-Induced Cancers. *Chemical Research in Toxicology*, 1989, **2**, 227-229.

81. Rossi, S. C. and Wetterhahn, K. E. Chromium(V) Is Produced Upon Reduction of Chromate by Mitochondrial Electron-Transport Chain Complexes. *Carcinogenesis*, 1989, **10**, 913-920.

82. Creager, S. E., Raybuck, S. A. and Murray, R. W. An Efficient Electrocatalytic Model Cytochrome-P-450 Epoxidation Cycle. *Journal of the American Chemical Society*, 1986, **108**, 4225-4227.

83. Nishihara, H., Pressprich, K., Murray, R. W. and Collman, J. P. Electrochemical Olefin Epoxidation with Manganese Meso-Tetraphenylporphyrin Catalyst and Hydrogen-Peroxide Generation at Polymer-Coated Electrodes. *Inorganic Chemistry*, 1990, **29**, 1000-1006.

84. Horwitz, C. P., Creager, S. E. and Murray, R. W. Electrocatalytic Olefin Epoxidation Using Manganese Schiff-Base Complexes and Dioxygen. *Inorganic Chemistry*, 1990, **29**, 1006-1011.

85. Moutet, J. C. and Ourari, A. Electrocatalytic epoxidation and oxidation with dioxygen using manganese(III) Schiff-base complexes. *Electrochimica Acta*, 1997, **42**, 2525-2531.

86. Bedioui, F., Devynck, J. and Biedcharreton, C. Immobilization of Metalloporphyrins in Electropolymerized Films - Design and Applications. *Accounts of Chemical Research*, 1995, **28**, 30-36.

87. Gutierrezgranados, S., Bedioui, F. and Devynck, J. Electroanalytical Study of the Activation of Dioxygen in Acetonitrile Solution by Manganese Porphyrin Films

Deposited onto Carbon Electrodes. *Electrochimica Acta*, 1993, **38**, 1747-1751.

88. Guo, P. and Wong, K. Y. Enantioselective electrocatalytic epoxidation of olefins by chiral manganese Schiff-base complexes. *Electrochemistry Communications*, 1999, **1**, 559-563.

89. Tanaka, H., Kuroboshi, M., Takeda, H., Kanda, H. and Torii, S. Electrochemical asymmetric epoxidation of olefins by using an optically active Mn-salen complex. *Journal of Electroanalytical Chemistry*, 2001, **507**, 75-81.

90. Limburg, J., Vrettos, J. S., Chen, H. Y., de Paula, J. C., Crabtree, R. H. and Brudvig, G. W. Characterization of the O_2 evolving reaction catalyzed by $[(terpy)(H_2O)Mn^{III}\text{-}O_2\text{-}Mn^{IV}(OH_2)(terpy)](NO_3)$ (terpy=2,2 ': 6,2 "-terpyridine). *Journal of the American Chemical Society*, 2001, **123**, 423-430.

91. Ruttinger, W. and Dismukes, G. C. Synthetic water-oxidation catalysts for artificial photosynthetic water oxidation. *Chemical Reviews*, 1997, **97**, 1-24.

92. Shimazaki, Y., Nagano, T., Takesue, H., Ye, B.-H., Tani, F. and Naruta, Y. Characterization of a Dinuclear $Mn^{V}O$ Complex and Its Efficient Evolution of O_2 in the Presence of Water. *Angewandte Chemie-International Edition in English*, 2003, **43**, 98-100.

93. Chiu, K. W., Wong, W. W., Wilkinson, G., Galas, A. M. R. and Hursthouse, M. B. Reaction of Phenylimidotrichlorobis(Triphenyl-Phosphine)Rhenium(V) - Reaction with Trimethyl-Phosphine and Reduction of Trimethylphosphine Complex to Phenylamido Complexes of Rhenium(I, III) - the X-Ray

Crystal-Structures of Phenylamido-(Dinitrogen) Tetrakis(Trimethylphosphine)-Rhenium(I) and Phenylamido(Buta-1,3-Diene)-Tetrakis-(Trimethylphosphine)Rhenium(I)). *Polyhedron*, 1982, **1**, 37-44.

94. Middleton, A. R., Masters, A. F. and Wilkinson, G. Schiff-Base Complexes of Rhenium(IV) and Rhenium(V). *Journal of the Chemical Society-Dalton Transactions*, 1979, 542-546.

95. Winkler, J. R. and Gray, H. B. Electronic Absorption and Emission-Spectra of Dioxorhenium(V) Complexes - Characterization of the Luminescent 3eg State. *Inorganic Chemistry*, 1985, **24**, 346-355.

96. Pipes, D. W. and Meyer, T. J. Electrochemistry of Trans-Dioxo Complexes of Rhenium(V) in Water. *Inorganic Chemistry*, 1986, **25**, 3256-3262.

97. Pipes, D. W. and Meyer, T. J. Redox Properties of Polypyridyl Aqua Complexes of Osmium. *Inorganic Chemistry*, 1986, **25**, 4042-4050.

98. Che, C. M., Cheng, W. K. and Yam, V. W. W. Syntheses, Spectroscopy, and Electrochemistry of High-Valent Osmium-(V) and Osmium(VI) Oxo Complexes of Macrocyclic Tertiary Amine Ligands. *Journal of the Chemical Society-Dalton Transactions*, 1990, 3095-3100.

99. Barf, G. A. and Sheldon, R. A. Ruthenium-Catalyzed Epoxidations - Mechanistic and Synthetic Aspects. *Journal of Molecular Catalysis a-Chemical*, 1995, **102**, 23-39.

100. Binstead, R. A., Stultz, L. K. and Meyer, T. J. Proton-Coupled Electron-Transfer

in Acetonitrile Solution - Irreversible Disproportionation of $[Ru^{III}(bpy)_2(py)(OH)]^{2+}$. *Inorganic Chemistry*, 1995, **34**, 546-551.

101. Stultz, L. K., Binstead, R. A., Reynolds, M. S. and Meyer, T. J. Epoxidation of Olefins by $[Ru^{IV}(bpy)_2(py)(O)]^{2+}$ in Acetonitrile Solution - a Global Kinetic-Analysis of the Epoxidation of Trans-Stilbene. *Journal of the American Chemical Society*, 1995, **117**, 2520-2532.

102. Stultz, L. K., Huynh, M. H. V., Binstead, R. A., Curry, M. and Meyer, T. J. Allylic oxidation of cyclohexene and indene by cis-$[Ru^{IV}(bpy)_2(py)(O)]^{2+}$. *Journal of the American Chemical Society*, 2000, **122**, 5984-5996.

103. Grover, N., Gupta, N., Singh, P. and Thorp, H. H. Studies of Electrocatalytic DNA Cleavage by Oxoruthenium(IV) - X-Ray Crystal-Structure of $Ru(tpy)(tmen)OH_2$ $(ClO_4)_2$ (tmen = N,N,N',N'-tetramethylethylenediamine, tpy = 2,2',2"- terpyridine). *Inorganic Chemistry*, 1992, **31**, 2014-2020.

104. Farrer, B. T., Pickett, J. S. and Thorp, H. H. Hydride transfer in oxidation of nucleic acid sugars: Electronic effects of 2 '-substituents on activation of the 1 '-C-H bond by oxoruthenium(IV). *Journal of the American Chemical Society*, 2000, **122**, 549-553.

105. Welch, T. W., Ciftan, S. A., White, P. S. and Thorp, H. H. Electron-rich oxoruthenium(IV) cleavage agents: A zero-order rate law for DNA catalysis. *Inorganic Chemistry*, 1997, **36**, 4812-4821.

106. Cheng, C. C., Goll, J. G., Neyhart, G. A., Welch, T. W., Singh, P. and Thorp, H. H.

Relative Rates and Potentials of Competing Redox Processes During DNA Cleavage - Oxidation Mechanisms and Sequence-Specific Catalysis of the Self-Inactivation of Oxometal Oxidants by DNA. *Journal of the American Chemical Society*, 1995, **117**, 2970-2980.

107. Neyhart, G. A., Cheng, C. C. and Thorp, H. H. Kinetics and Mechanism of the Oxidation of Sugars and Nucleotides by Oxoruthenium(IV) - Model Studies for Predicting Cleavage Patterns in Polymeric DNA and RNA. *Journal of the American Chemical Society*, 1995, **117**, 1463-1471.

108. Welch, T. W., Neyhart, G. A., Goll, J. G., Ciftan, S. A. and Thorp, H. H. Thymidine-Specific Depyrimidination of DNA by Oxopolypyridylruthenium(IV) Complexes. *Journal of the American Chemical Society*, 1993, **115**, 9311-9312.

109. Gupta, N., Grover, N., Neyhart, G. A., Singh, P. and Thorp, H. H. Synthesis and Properties of New DNA Cleavage Agents Based on Oxoruthenium(IV). *Inorganic Chemistry*, 1993, **32**, 310-316.

110. Che, C. M., Ho, C. and Lau, T. C. Tuning the Reactivities of Ruthenium-Oxo Complexes with Robust Ligands - a Ruthenium(IV)-Oxo Complex of 6,6'-Dichloro-2,2'- Bipyridine as an Active Oxidant for Stoichiometric and Catalytic Organic Oxidation. *Journal of the Chemical Society-Dalton Transactions*, 1991, 1901-1907.

111. Cheng, W. C., Yu, W. Y., Cheung, K. K. and Che, C. M. Syntheses of Novel Monomeric 1,4,7-Trimethyl-1,4,7-Triazacyclononane Ruthenium Complexes -

Reactivities and Structure of Sterically Encumbered Cationic Monoaquaruthenium(II) and Monooxoruthenium(IV) Complexes. *Journal of the Chemical Society-Dalton Transactions*, 1994, 57-62.

112. Llobet, A., Doppelt, P. and Meyer, T. J. Redox Properties of Aqua Complexes of Ruthenium(II) Containing the Tridentate Ligands 2,2'-6',2"-terpyridine and Tris(1-pyrazolyl)methane. *Inorganic Chemistry*, 1988, **27**, 514-520.

113. Kubow, S. A., Marmion, M. E. and Takeuchi, K. J. Synthesis and Characterization of Oxoruthenium(Iv) Complexes That Utilize a 2,2'-Biquinoline Ligand. *Inorganic Chemistry*, 1988, **27**, 2761-2767.

114. Szczepura, L. F., Maricich, S. M., See, R. F., Churchill, M. R. and Takeuchi, K. J. Synthesis, Characterization, and Reactivity of an Oxoruthenium(IV) Complex Containing a bis(oxazoline) Ligand. Crystal Structure of [Ru((S)-bpop)(Cl)(trpy)](BF_4). *Inorganic Chemistry*, 1995, **34**, 4198-4205.

115. Dobson, J. C. and Meyer, T. J. Redox Properties and Ligand Loss Chemistry in Aqua Hydroxo Oxo Complexes Derived from Cis- $(bpy)_2Ru^{II}(OH_2)_2^{2+}$ and Trans- $(bpy)_2Ru^{II}(OH_2)_2^{2+}$. *Inorganic Chemistry*, 1988, **27**, 3283-3291.

116. Takeuchi, K. J., Thompson, M. S., Pipes, D. W. and Meyer, T. J. Redox and Spectral Properties of Monooxo Polypyridyl Complexes of Ruthenium and Osmium in Aqueous-Media. *Inorganic Chemistry*, 1984, **23**, 1845-1851.

117. Guadalupe, A. R., Chen, X. H., Sullivan, B. P. and Meyer, T. J. Oxo Complexes, Ph Effects, and Catalysis in Films Formed by Electropolymerization. *Inorganic*

Chemistry, 1993, **32**, 5502-5512.

118. Thompson, M. S., Degiovani, W. F., Moyer, B. A. and Meyer, T. J. Novel Electrocatalytic Procedure for the Oxidation of Alcohols, Aldehydes, Cyclic-Ketones, and C-H Bonds Adjacent to Olefinic or Aromatic-Groups. *Journal of Organic Chemistry*, 1984, **49**, 4972-4977.

119. Meyer, T. J. Redox Pathways - Applications in Catalysis. *Journal of the Electrochemical Society*, 1984, **131**, C221-C228.

120. Ho, C., Che, C. M. and Lau, T. C. A Ruthenium(IV) Oxo Complex That Contains a Tertiary Diamine Ligand. *Journal of the Chemical Society-Dalton Transactions*, 1990, 967-970.

121. Che, C. M., Ho, C. and Lau, T. C. Mechanism of C-H Bond Oxidation by a Monooxoruthenium(V) Complex. *Journal of the Chemical Society-Dalton Transactions*, 1991, 1259-1263.

122. Marmion, M. E. and Takeuchi, K. J. Ruthenium(IV)-Oxo Complexes - the Novel Utilization of Tertiary Pnictogen Ligands. *Journal of the American Chemical Society*, 1988, **110**, 1472-1480.

123. Cabaniss, G. E., Diamantis, A. A., Murphy, W. R., Linton, R. W. and Meyer, T. J. Electrocatalysis of Proton-Coupled Electron-Transfer Reactions at Glassy-Carbon Electrodes. *Journal of the American Chemical Society*, 1985, **107**, 1845-1853.

124. Wong, K. Y. and Anson, F. C. Attempts to Accelerate the Rates of Oxidation of

Ruthenium and Osmium Tetramethylcyclam Complexes at Graphite and Glassy-Carbon Electrodes and within Nafion Coatings. *Journal of Electroanalytical Chemistry*, 1987, **237**, 69-79.

125. Che, C. M., Wong, K. Y. and Anson, F. C. Effects of Electrode Surface Pretreatments on the Electrochemistry of a Macrocyclic Dioxoruthenium(VI) Complex. *Journal of Electroanalytical Chemistry*, 1987, **226**, 211-226.

126. Lee, W. O., Che, C. M. and Wong, K. Y. Electronic and Kinetic Isotope Effects on the Electrooxidation of Benzyl Alcohols by a Monoxo Ruthenium(V) Complex of Tetramethylcyclam. *Journal of Molecular Catalysis*, 1994, **89**, 57-62.

127. Che, C. M., Wong, K. Y. and Poon, C. K. Stabilization of Transition-Metal Complexes in High Oxidation-States by Macrocyclic Tertiary-Amines - Electrochemical Generation and Spectroscopic Properties of Novel Dihalogeno and Pseudohalogeno Tetraamine Complexes of Ruthenium(Iv). *Inorganic Chemistry*, 1986, **25**, 1809-1813.

128. Poon, C. K., Lau, T. C. and Che, C. M. Structural and Mechanistic Studies of Coordination-Compounds .36. Electronic-Spectra and Photochemistry of Some Trans-(Tetraamine)Ruthenium(III) Complexes. *Inorganic Chemistry*, 1983, **22**, 3893-3898.

129. Vining, W. J. and Meyer, T. J. Redox Properties of the Water Oxidation Catalyst $(bpy)_2(H_2O)RuORu(H_2O)(bpy)_2^{4+}$ in Thin Polymeric Films - Electrocatalytic

Oxidation of Cl^- to Cl_2. *Inorganic Chemistry*, 1986, **25**, 2023-2033.

130. Geselowitz, D. and Meyer, T. J. Water Oxidation by $(bpy)_2(O)Ru^{V}ORu^{V}(O)(bpy)_2^{4+}$ - an Oxygen- Labeling Study. *Inorganic Chemistry*, 1990, **29**, 3894-3896.

131. Binstead, R. A., Chronister, C. W., Ni, J. F., Hartshorn, C. M. and Meyer, T. J. Mechanism of water oxidation by the μ-oxo dimer $[(bpy)_2(H_2O)(Ru^{III}\text{-}O\text{-}Ru^{III}(OH_2)(bpy)_2]^{4+}$. *Journal of the American Chemical Society*, 2000, **122**, 8464-8473.

132. Wada, T., Tsuge, K. and Tanaka, K. Electrochemical oxidation of water to dioxygen catalyzed by the oxidized form of the bis(ruthenium-hydroxo) complex in H_2O. *Angewandte Chemie-International Edition*, 2000, **39**, 1479.

133. Wada, T., Tsuge, K. and Tanaka, K. Syntheses and redox properties of bis(hydroxoruthenium) complexes with quinone and bipyridine ligands. Water-oxidation catalysis. *Inorganic Chemistry*, 2001, **40**, 329-337.

134. Cosnier, S., Deronzier, A. and Moutet, J. C. Oxidative Electropolymerization of Polypyridinyl Complexes of Ruthenium(II)-Containing Pyrrole Groups. *Journal of Electroanalytical Chemistry*, 1985, **193**, 193-204.

135. Degiovani, W. F. and Deronzier, A. Electrochemical Preparation and Behavior of Poly(Pyrrole- $Ru(trpy)(bpy)(OH_2)^{2+}$) (trpy = 2,2'/6',2"-terpyridine) (bpy = 2,2'-bipyridine) Films - Application to the Electrocatalytic Oxidation of Alcohols. *Journal of Electroanalytical Chemistry*, 1992, **337**, 285-298.

136. Deronzier, A. and Moutet, J. C. Polypyrrole films containing metal complexes: Syntheses and applications. *Coordination Chemistry Reviews*, 1996, **147**, 339-371.

137. CollombDunandSauthier, M. N., Deronzier, A., LeBozec, H. and Navarro, M. Electrochemistry of cis-diaquo ruthenium(II) complexes with substituted 2,2'-bipyridine ligands in a non-coordinating solvent. Application to the elaboration of corresponding functionalized polypyrrole films. *Journal of Electroanalytical Chemistry*, 1996, **410**, 21-29.

138. Romero, I., Rodriguez, M., Llobet, A., Collomb-Dunand-Sauthier, M. N., Deronzier, A., Parella, T. and Stoeckli-Evans, H. Synthesis, structure and redox properties of a new ruthenium(II) complex containing the flexible tridentate ligand N,N-bis(2-pyridylmethyl)ethylamine, *cis-fac*-$Ru(bpea)_2^{2+}$, and its homologue attached covalently to a polypyrrole film. *Journal of the Chemical Society-Dalton Transactions*, 2000, **11**, 1689-1694.

139. Navarro, M., Collomb, M. N. and Deronzier, A. Electrochemical preparation and properties of poly-cis- $\{Ru^{III}(L)_2(OH_2)\}_2O^{4+}$ (L = pyrrole-substituted-2,2 '-bipyridine) modified electrodes. Their electroinduced transformations into poly-cis-$[Ru^{II}(L)_2(H_2O)_2]^{2+}$ and poly-cis-$[Ru^{II}(L)_2(CH_3CN)_2]^{2+}$ films. *Journal of Electroanalytical Chemistry*, 2002, **520**, 150-156.

140. Rodriguez, M., Romero, I., Sens, C., Llobet, A. and Deronzier, A. Redox and catalytic properties of new polypyrrole modified electrodes functionalized by

[Ru(bpea)(bpy)H_2O]$^{2+}$ complexes; bpea=N,N '-bis(2-pyridylmethyl)ethylamine, bpy=2,2 '-bipyridine. *Electrochimica Acta*, 2003, **48**, 1047-1054.

141. Cosnier, S., Deronzier, A. and Llobet. Triruthenium cluster-polypyrrole films: a remarkably stable immobilized relay at largely positive potentials: its appliction to the electrocatalytic oxidation of benzoyl alcohol. *Journal of Electroanalytical Chemistry*, 1990, **280**, 213-219.

142. Takada, K., Storrier, G. D., Pariente, F. and Abruna, H. D. EQCM studies of the redox process during and after electropolymerization of films of transition-metal complexes of vinylterpyridine. *Journal of Physical Chemistry B*, 1998, **102**, 1387-1396.

143. Bakir, M., Sullivan, B. P., MacKay, S. G., Linton, R. W. and Meyer, T. J. Coordination chemistry in thin polymeric films of poly[Fe(vbpy)$_2$(CN)$_2$], poly-vbpy. Binding and reduction of [Rh(COD)Cl] and $PdCl_2$. *Chemistry of Materials*, 1986, **8**, 2461-2467.

144. Sende, J. A. R., Arana, C. R., Hernandez, L., Potts, K. T., Keshevarz-k, M. and Abruna, H. D. Electrocatalysis of CO_2 reduction in aqueous media at modified electrodes: modified electropolymerized films of vinylpyridine complexes of transition metals. *Inorganic Chemistry*, 1995, **34**, 3339-3348.

145. Arana, C., Keshavarz, M., Potts, K. T. and Abruna, H. D. Electrocatalytic reduction of CO_2 and O_2 with electropolymerized films of vinyl-terpyridine complexes of Fe, Ni and Co. *Inorganica Chimica Acta*, 1994, **225**, 285-295.

146. Cabrera, C. R. and Abruna, H. D. Electrocatalysis of CO_2 reduction at surface modified metallic and semiconducting electrodes. *Journal of Electroanalytical Chemistry*, 1986, **209**, 101-107.

147. O'Toole, T. R., Sullivan, B. P., Bruce, M. R. M., Margerum, L. D., Murray, R. W. and Meyer, T. J. Electrocatalytic reduction of CO_2 by a complex of rhenium in their polymeric films. *Journal of Electroanalytical Chemistry*, 1989, **259**, 217-239.

148. Ochmanska, J. and Pickup, P. G. Conducting Polypyrrole Films Containing [Ru(2,2'-Bipyridine)2(3-(Pyrrol-1-ylmethyl)pyridine)Cl]+ - Electrochemistry, Spectroelectrochemistry, Electronic Conductivity, and Ionic-Conductivity. *Journal of Electroanalytical Chemistry*, 1989, **271**, 83-105.

149. Cosnier, S., Deronizer, A. and Moutet, J.-M. Electrochemcial coating of a platinum electrode by a poly(pyrrole)film containing the *fac*-[Re(2,2'-bipyridine)$(CO)_3$Cl] application to electrocatalytic reduction of CO_2. *Journal of Electroanalytical Chemistry*, 1986, **207**, 315-321.

150. Cosnier, S., Deronizer, A. and Moutet, J.-M. Electrocatalytic reduction of CO_2 on electrodes modified by *fac*-Re(2,2'-bipyridine)$(CO)_3$Cl complexes bonded to polypyrrole films. *Journal of Molecular Catalysis*, 1988, **45**, 381-391.

151. Cosnier, S., Deronizer, A. and Moutet, J.-M. Substitution effects on the electrochemical behaviour of the (2,2'-bipyridine)tricarbonylrhenium(I) complex in solution or in polymeric form and their relation to the catalytic reduction of

carbon dioxide. *New Journal of Chemistry*, 1990, **14**, 831-839.

152. Cosnier, S., Deronzier, A. and Moutet, J.-C. Oxidative electropolymerization of polypyridyl complexes of ruthenium(II)-containing pyrrole groups. *Journal of Electroanalytical Chemistry*, 1985, **193**, 193-204.

153. De Giovani, W. F. and Deronzier, A. Electrochemical preparation and behaviour of poly{pyrrole-$[Ru(trpy)(bpy)(H_2O)]^{2+}$} (trpy = 2,2':6',2"-terpyridine, bpy = 2,2'-bipyridine). *Journal of Electroanalytical Chemistry*, 1992, **337**, 285-298.

154. De Giovani, W. F. and Deronzier, A. Films of poly[pyrrole-$[Ru^{II}(bpy)_2(Cl_2]$; their transformations into films containing *cis*- and *trans*-$[Ru^{II}(bpy)_2(H_2O)_2]^{2+}$, -$[Ru^{II}(bpy)_2(CH_3CN)_2]^{2+}$ and $[\{Ru^{III}(bpy)_2(H_2O)_2\}O]^{4+}$ complexes, application to electrocatalysis (bpy = 2,2'-bipyridine). *Chemical Communications*, 1992, 1461-1462.

155. Deronizer, A., Devaux, R., Limsion, D. and Latour, J.-M. Poly(pyrrole-metallo-tetraphenylporphyrin) modified electrode, part 2. *Journal of Electroanalytical Chemistry*, 1992, **324**, 325-337.

156. Collombdunandsauthier, M. N. and Deronzier, A. Electrodes Modified by Polymeric Films Containing Oxo Manganese Clusters. *Journal of Electroanalytical Chemistry*, 1995, **391**, 211-214.

157. Ho, C., Raistrick, I. D. and Huggins, R. A. Application of ac techniques to the study of lithium diffusion in tungsten trioxide thin films. *Journal of Electrochemical Society*, 1980, **127**, 343-350.

158. Ukai, T., Kawazura, H., Ishii, Y., Bonnet, J. J. and Ibers, J. A. Chemistry of Dibenzylideneacetone-Palladium(0) Complexes .1. Novel Tris(Dibenzylideneacetone)Dipalladium(Solvent) Complexes and Their Reactions with Quinones. *Journal of Organometallic Chemistry*, 1974, **65**, 253-266.

159. Foulds, N. C. and Lowe, C. R. Immobilization of Glucose-Oxidase in Ferrocene-Modified Pyrrole Polymers. *Analytical Chemistry*, 1988, **60**, 2473-2478.

160. Bartlett, P. N., Chung, L. Y. and Moore, P. Conducting Polymer-Films - Attachment of Pyrrole Groups to Open-Chain Nitrogen-Containing Ligands and Related Species. *Electrochimica Acta*, 1990, **35**, 1273-1278.

161. Spek, A. L., Gerli, A. and Reedijk, J. (2,2'-biquinoline-κ-2N,N')Chloro-(2,2',6':2"-terpyridine-κ-3n,N',N")-Ruthenium(II) Hexafluorophosphate, $RuCl(C_{18}H_{12}N_2)(C_{15}H_{11}N_3)$ PF_6. *Acta Crystallographica Section C-Crystal Structure Communications*, 1994, **50**, 394-397.

162. Adcock, P. A., Keene, F. R., Smythe, R. S. and Snow, M. R. Oxidation of Isopropylamine and Related Amines Coordinated to Ruthenium - Formation of Monodentate Imine and Alkylideneamido Complexes of Ruthenium. *Inorganic Chemistry*, 1984, **23**, 2336-2343.

163. Hecker, C. R., Fanwick, P. E. and McMillin, D. R. Evidence for Dissociative

Photosubstitution Reactions of $Ru(trpy)(bpy)(NCCH_3)^{2+}$ - Crystal and Molecular-Structure of $Ru(trpy)(bpy)(py)$ $(PF_6)_2.(CH_3)_2CO$. *Inorganic Chemistry*, 1991, **30**, 659-666.

164. Leising, R. A., Kubow, S. A., Churchill, M. R., Buttrey, L. A., Ziller, J. W. and Takeuchi, K. J. Synthesis, Characterization, and X-Ray Crystal-Structure of $Ru(NO_2)(PMe_3)_2(trpy)$ (ClO_4). *Inorganic Chemistry*, 1990, **29**, 1306-1312.

165. Thummel, R. P. and Jahng, Y. Polyaza Cavity-Shaped Molecules .9. Ruthenium(II) Complexes of Annelated Derivatives of 2,2'-6,2"-Terpyridine and Related Systems - Synthesis, Properties, and Structure. *Inorganic Chemistry*, 1986, **25**, 2527-2534.

166. Gupta, N., Grover, N., Neyhart, G. A., Liang, W. G., Singh, P. and Thorp, H. H. $RuO(dppz)(tpy)^{2+}$ - a DNA Cleavage Agent with High DNA Affinity. *Angewandte Chemie-International Edition in English*, 1992, **31**, 1048-1050.

167. Gerli, A., Reedijk, J., Lakin, M. T. and Spek, A. L. Redox Properties and Electrocatalytic Activity of the Oxo Aqua System $Ru(terpy)(bpz)(O)^{2+}/Ru(terpy)(bpz)(H_2O)^{2+}$ - X-ray Crystal Structure of $Ru(terpy)(bpz)Cl$ PF_6 MeCN (terpy=2,2',2"-terpyridine, bpz=2,2'-bipyrazine). *Inorganic Chemistry*, 1995, **34**, 1836-1843.

168. Roecker, L., Kutner, W., Gilbert, J. A., Simmons, M., Murray, R. W. and Meyer, T. J. Instability of the Oxidation Catalysts $[(bpy)_2(py)Ru(O)]^{2+}$ and $[(trpy)(phen)Ru(O)]^{2+}$ in Basic Solution. *Inorganic Chemistry*, 1985, **24**,

3784-3791.

169. Griffith, W. P. Tmc Literature Highlights .22. Organic Oxidations by Osmium and Ruthenium Oxo Complexes. *Transition Metal Chemistry*, 1990, **15**, 251-256.

170. Vork, F. T. A., Schuermans, B. C. A. M. and Barendrecht, E. Influence of Inserted Anions on the Properties of Polypyrrole. *Electrochimica Acta*, 1990, **35**, 567-575.

171. Chen, W. C. and Wen, T. C. Electrochemical and capacitive properties of polyaniline-implanted porous carbon electrode for supercapacitors. *Journal of Power Sources*, 2003, **117**, 273-282.

172. Ko, J. M., Rhee, H. W., Park, S. M. and Kim, C. Y. Morphology and Electrochemical Properties of Polypyrrole Films Prepared in Aqueous and Nonaqueous Solvents. *Journal of the Electrochemical Society*, 1990, **137**, 905-909.

173. Wong, K. Y., Lee, W. O., Che, C. M. and Anson, F. C. Synthesis and Electrocatalytic Properties of a Cis-Diaquo- Ruthenium(II) Complex with 6,6'-dichloro-2,2'-bipyridine. *Journal of Electroanalytical Chemistry*, 1991, **319**, 207-216.

174. Ogawa, S. and Shiraishi, S. A Tautomerizable Macrocyclic Compound Containing 2 Aza-Bridged 2,2'-bipyridine Moieties. *Journal of the Chemical Society-Perkin Transactions 1*, 1980, 2527-2530.

175. Ishida, H., Tanaka, K. and Tanaka, T. Electrochemical CO_2 Reduction Catalyzed by $Ru(bpy)_2(CO)_2^{2+}$ and $Ru(bpy)_2(CO)Cl^+$ - the Effect of pH on the Formation of CO and HCOO. *Organometallics*, 1987, **6**, 181-186.

176. Sun, S. G., Yang, D. F. and Tian, Z. W. *In-situ* FTIR Studies on the Adsorption and Oxidation of Normal- Propanol and Isopropanol at a Platinum-Electrode in Sulfuric- Acid-Solutions. *Journal of Electroanalytical Chemistry*, 1990, **289**, 177-187.

177. Sun, S. G. and Chen, A. C. *In-situ* FTIR Features During Oxygen-Adsorption and Carbon- Monoxide Oxidation at a Platinum-Electrode in Dilute Alkaline Solutions. *Journal of Electroanalytical Chemistry*, 1992, **323**, 319-328.

178. Cheng, W. C., Yu, W. Y., Zhu, J., Cheung, K. K., Peng, S. M., Poon, C. K. and Che, C. M. Chiral ruthenium(IV)-oxo complexes. Structure, reactivities of $[Ru(terpy)(N\cap N)O]^{2+}$ ($N\cap N$ = N,N,N',N'-teramethyl-1,2-diaminocycloxhexane) and $[Ru(Me_3tacn)(cbpy)O]^{2+}$ (cbpy=(-)-3,3'-[(4S-trans)-1,3-dioxolane -4,5-dimethyl]-2,2'-bipyridine). *Inorganica Chimica Acta*, 1996, **242**, 105-113.

179. Thompson, M. S., Ph.D Thesis, University of North Carolina (1981).

180. Heeg, M. J., Kroener, R. and Deutsch, E. Structure of cis-bis(acetonitrile)bis(2,2'-bipyridine)Ruthenium(II) Hexafluorophosphate, $[Ru(C_2H_3N)_2(C_{10}H_8N_2)_2](PF_6)_2$. *Acta Crystallographica Section C-Crystal Structure Communications*, 1985, **41**, 684-686.

181. Lau, S. H., Ph.D Thesis, The Hong Kong Polytechnic University (2001).

182. Rogers, C. W., Zhang, Y., Patrick, B. O., Jones, W. E. and Wolf, M. O. Photophysical effect of the coordination of water by ruthenium(II) bipyridyl complexes containing hemilabile phosphine-ether ligands. *Inorganic Chemistry*, 2002, **41**, 1162-1169.

183. Trammell, S. A., Wimbish, J. C., Odobel, F., Gallagher, L. A., Narula, P. M. and Meyer, T. J. Mechanisms of surface electron transfer. Proton-coupled electron transfer. *Journal of the American Chemical Society*, 1998, **120**, 13248-13249.

184. Gallagher, L. A. and Meyer, T. J. Surface control of oxidation by an adsorbed Ru-IV-oxo complex. *Journal of the American Chemical Society*, 2001, **123**, 5308-5312.

185. Doppiu, A., Cinellu, M. A., Minghetti, G., Stoccoro, S., Zucca, A., Manassero, M. and Sansoni, M. Neutral and cationic methyl complexes of platinum(II) with 6-substituted 2,2 '-bipyridines: Synthesis, characterisation and reactivity with carbon monoxide - Molecular structures of PtCl(methyl)(6-ethyl-2,2 '-bipyridine) and of Pt(methyl)(acetonitrile)(6-ethyl-2,2 '-bipyridine) BF_4. *European Journal of Inorganic Chemistry*, 2000, 2555-2563.

186. Aullon, G., Bellamy, D., Brammer, L., Bruton, E. A. and Orpen, A. G. Metal-bound chlorine often accepts hydrogen bonds. *Chemical Communications*, 1998, 653-654.

187. Stalhandske, C. M. V., Persson, I., Sandstrom, M. and Alberg, M. Crystal structure of bis(N,N-dimethylthioformamide)mercury(II) iodide, bromide, and

chloride and solvation of the neutral mercury(II) halide complexes in N,N-dimethylthioformamide, a resonance-induced hydrogen-bonding solvent and ligand. *Inorganic Chemistry*, 1997, **36**, 4945-4953.

188. Kui, S. C. F., Zhu, N. Y. and Chan, M. C. W. Observation of intramolecular C-H .....F-C contacts in non-metallocene polyolefin catalysts: Model for weak attractive interactions between polymer chain and noninnocent ligand. *Angewandte Chemie-International Edition*, 2003, **42**, 1628-1632.

189. Reddy, K. B., Cho, M. O. P., Wishart, J. F., Emge, T. J. and Isied, S. S. cis-bis(bipyridine)ruthenium imidazole derivatives: A spectroscopic, kinetic, and structural study. *Inorganic Chemistry*, 1996, **35**, 7241-7245.

190. Weathers, N. R., Sadoski, R. C., Durham, B. and Cordes, A. W. trans-diaquabis(2,2'-bipyridine-N,N')-ruthenium(II) bis(hexafluorophosphate). *Acta Crystallographica Section C-Crystal Structure Communications*, 1997, **53**, 1047-1049.

191. Durham, B., Wilson, S. R., Hodgson, D. J. and Meyer, T. J. Cis-Trans Photoisomerization in $Ru(bpy)_2(OH_2)_2^{2+}$ - Crystal-Structure of *trans*-$[Ru(bpy)_2(OH_2)(OH)](ClO_4)_2$. *Journal of the American Chemical Society*, 1980, **102**, 600-607.

192. Collin, J. P. and Sauvage, J. P. Synthesis and Study of Mononuclear Ruthenium(Ii) Complexes of Sterically Hindering Diimine Chelates - Implications for the Catalytic-Oxidation of Water to Molecular-Oxygen.

Inorganic Chemistry, 1986, **25**, 135-141.

193. Bartolotti, L. J., Pedersen, L. G. and Meyer, T. J. Quantum mechanical study of the oxidation pathway of the oxygen-evolving catalyst, $[(bpy)_2(H_2O)Ru^{III}\text{-}O\text{-}Ru^{III}(H_2O)(bpy)_2]^{4+}$. *International Journal of Quantum Chemistry*, 2001, **83**, 143-149.

194. Hartshorn, C. M., Daire, N., Tondreau, V., Loeb, B., Meyer, T. J. and White, P. S. Synthesis and characterization of dinuclear ruthenium complexes with tetra-2-pyridylpyrazine as a bridge. *Inorganic Chemistry*, 1999, **38**, 3200-3206.

195. Lebeau, E. L., Adeyemi, S. A. and Meyer, T. J. Water oxidation by $[(tpy)(H_2O)_2(Ru^{III}\text{-}O\text{-}Ru^{III})(H_2O)_2(tpy)]^{4+}$. *Inorganic Chemistry*, 1998, **37**, 6476-6484.

196. Chronister, C. W., Binstead, R. A., Ni, J. F. and Meyer, T. J. Mechanism of water oxidation catalyzed by the μ-oxo dimer $[(bpy)_2(OH_2)Ru^{III}\text{-}O\text{-}Ru^{III}(OH_2)(bpy)_2]^{4+}$. *Inorganic Chemistry*, 1997, **36**, 3814-3815.

197. Schoonover, J. R., Ni, J. F., Roecker, L., Whiter, P. S. and Meyer, T. J. Structural and resonance Raman studies of an oxygen-evolving catalyst. Crystal structure of $(bpy)_2(H_2O)Ru^{III}\text{-}O\text{-}Ru^{IV}(OH)(bpy)_2\ (ClO_4)_4$. *Inorganic Chemistry*, 1996, **35**, 5885-5892.

198. Gilbert, J. A., Eggleston, D. S., Murphy, W. R., Geselowitz, D. A., Gersten, S. W., Hodgson, D. J. and Meyer, T. J. Structure and Redox Properties of the Water-Oxidation Catalyst $(bpy)_2(OH_2)RuORu(OH_2)(bpy)_2\ ^{4+}$. *Journal of the*

American Chemical Society, 1985, **107**, 3855-3864.

199. Rotzinger, F. P., Munavalli, S., Comte, P., Hurst, J. K., Gratzel, M., Pern, F. J. and Frank, A. J. A Molecular Water-Oxidation Catalyst Derived from Ruthenium Diaqua Bis(2,2'-bipyridyl-5,5'-dicarboxylic Acid). *Journal of the American Chemical Society*, 1987, **109**, 6619-6626.

200. Hurst, J. K., Zhou, J. Z. and Lei, Y. B. Pathways for Water Oxidation Catalyzed by the $(bpy)_2Ru(OH_2)_2^{4+}$ Ion. *Inorganic Chemistry*, 1992, **31**, 1010-1017.

201. Lei, Y. B. and Hurst, J. K. Dynamical Investigations of the Catalytic Mechanisms of Water Oxidation by the $(bpy)_2Ru(OH_2)_2O^{4+}$ Ion. *Inorganica Chimica Acta*, 1994, **226**, 179-185.

202. Lei, Y. B. and Hurst, J. K. Structural Investigations of the Catalytic Mechanisms of Water Oxidation by the $(bpy)_2Ru(OH_2)(O^{2-})^{4+}$ Ion. *Inorganic Chemistry*, 1994, **33**, 4460-4467.

203. Yamada, H. and Hurst, J. K. Resonance Raman, optical spectroscopic, and EPR characterization of the higher oxidation states of the water oxidation catalyst, cis,cis- $(bpy)_2Ru(OH_2)_2O^{4+}$. *Journal of the American Chemical Society*, 2000, **122**, 5303-5311.

204. Yamada, H., Koike, T. and Hurst, J. K. Water exchange rates in the diruthenium μ-oxo ion *cis,cis-* $(bpy)_2Ru(OH_2)_2O^{4+}$. *Journal of the American Chemical Society*, 2001, **123**, 12775-12780.

205. Perry, P. J., Reszka, A. P., Wood, A. A., Read, M. A., Gowan, S. M., Dosanjh, H.

S., Trent, J. O., Jenkins, T. C., Kelland, L. R. and Neidle, S. Human telomerase inhibition by regioisomeric disubstituted amidoanthracene-9,10-diones. *Journal of Medicinal Chemistry*, 1998, **41**, 4873-4884.

206. Sessler, J. L., Mody, T. D., Ford, D. A. and Lynch, V. A Nonaromatic Expanded Porphyrin Derived from Anthracene - a Macrocycle Which Unexpectedly Binds Anions. *Angewandte Chemie-International Edition in English*, 1992, **31**, 452-455.

207. Gosztola, D., Wang, B. and Wasielewski, M. R. Factoring through-space and through-bond contributions to rates of photoinduced electron transfer in donor-spacer-acceptor molecules. *Journal of Photochemistry and Photobiology a-Chemistry*, 1996, **102**, 71-80.

208. Sullivan, B. P., Calvert, J. M. and Meyer, T. J. Cis-Trans Isomerism in (trpy)(PPh_3)$RuCl_2$ - Comparisons between the Chemical and Physical-Properties of a Cis-Trans Isomeric Pair. *Inorganic Chemistry*, 1980, **19**, 1404-1407.

209. Wang, J. *Electroanalytical Techniques in Clinical Chemistry and Laboratory Medicine*. New York: VCH, 1988.

Appendix

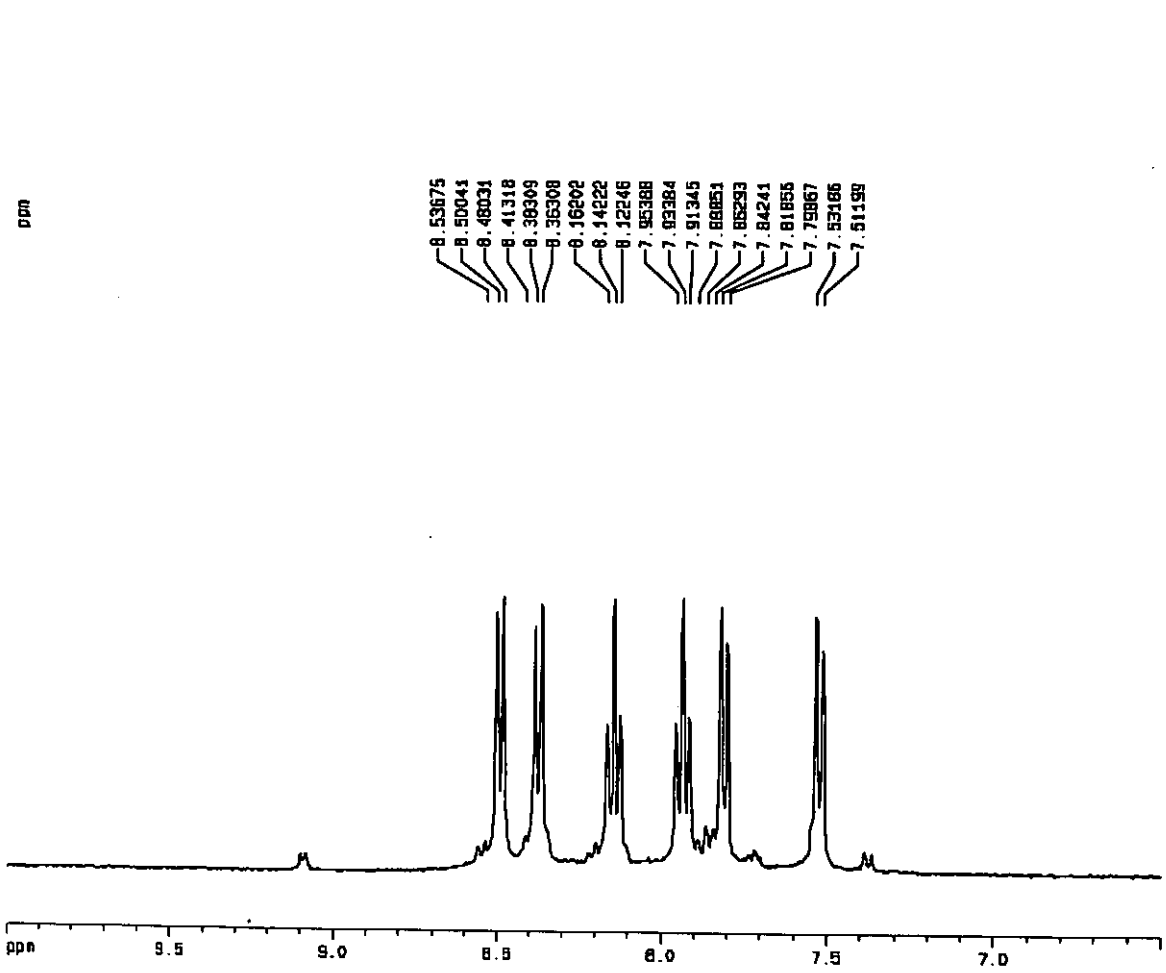

Figure A1 NMR spectrum of *cis*-$[Ru^{II}(dcbpy)_2(H_2O)_2]^{2+}$ in D_2O.

Current data parameters
NAME ysn
EXPNO 1
PROCNO 1

F2 - Acquisition Parameters
Date_ 20020823
Time 15.34
INSTRUM dpx400
PROBHD 5 mm QNP 1H
PULPROG zg30
TD 32768
SOLVENT D2O
NS 64
DS 0
SWH 16025.641 Hz
FIDRES 0.489064 Hz
AQ 1.0224118 sec
RG 812.7
DW 31.200 usec
DE 4.60 usec
TE 300.0 K
D1 1.00000000 sec

---------- CHANNEL f1 ----------
NUC1 1H
P1 9.50 usec
PL1 -6.00 dB
SFO1 400.1278883 MHz

F2 - Processing parameters
SI 16384
SF 400.1300000 MHz
WDW EM
SSB 0
LB 0.30 Hz
GB 0
PC 1.00

1D NMR plot parameters
CX 20.00 cm
F1P 10.000 ppm
F1 4001.20 Hz
F2P 6.500 ppm
F2 2600.84 Hz
PPMCM 0.17500 ppm/cm
HZCM 70.02274 Hz/cm

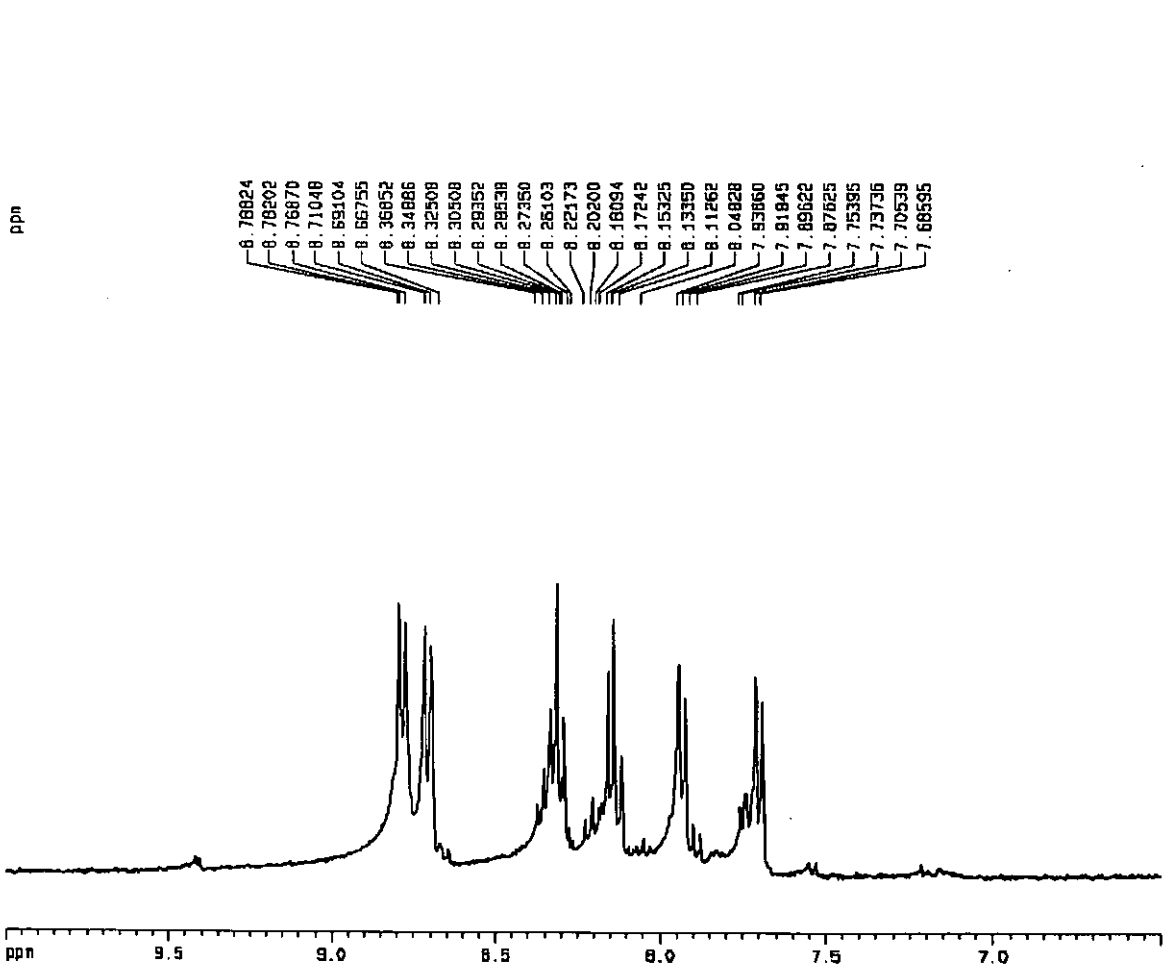


```
Current Data Parameters
NAME        Ru(dcbpy)l 2H2
EXPNO                    3
PROCNO                   1

F2 - Acquisition Parameters
Date_             20030721
Time                 14.19
INSTRUM              dpx400
PROBHD     5 mm QNP  1H
PULPROG              zg30
TD                   32768
SOLVENT              Aceton
NS                       16
DS                        0
SWH              16025.641 Hz
FIDRES            0.489064 Hz
AQ                1.0224416 sec
RG                    574.7
DW                   31.200 usec
DE                    4.60 usec
TE                   300.0 K
D1                1.00000000 sec

---------- CHANNEL f1 ----------
NUC1                     1H
P1                    9.50 usec
PL1                  -6.00 dB
SFO1             400.1276889 MHz

F2 - Processing parameters
SI                       16384
SF               400.1300150 MHz
WDW                      EM
SSB                       0
LB                    0.30 Hz
GB                        0
PC                    1.00

1D NMR plot parameters
CX                   20.00 cm
F1P                 10.000 ppm
F1                 4001.20 Hz
F2P                  0.500 ppm
F2                 200.84 Hz
PPMCM             0.17800 ppm/cm
HZCM             70.02275 Hz/cm
```

Figure A2 NMR spectrum of *cis*-$[Ru^{II}(dcbpy)_2(H_2O)_2]^{2+}$ in D_6-Acetone.

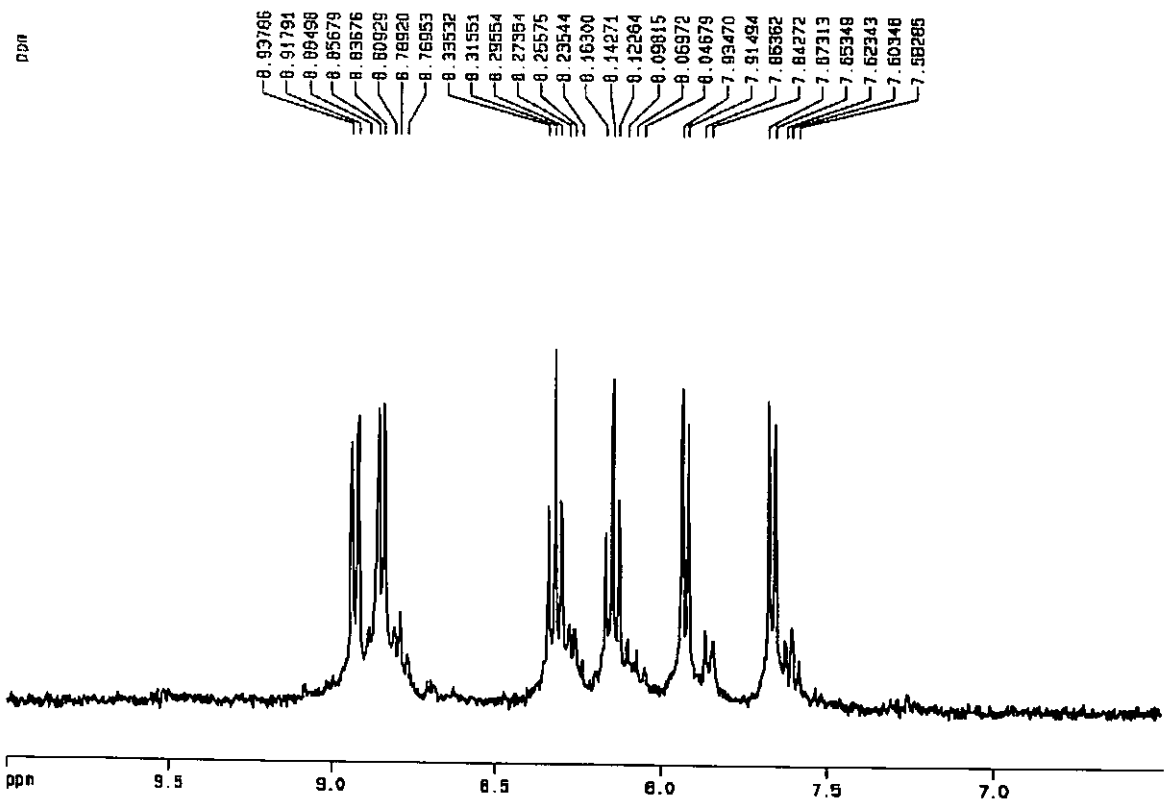

Figure A3 NMR spectrum of *cis*-$[Ru^{II}(dcbpy)_2(H_2O)_2]^{2+}$ in D_8-THF.

```
Current Data Parameters
NAME                  ruclbpyw
EXPNO                        1
PROCNO                       1

F2 - Acquisition Parameters
Date_              20031118
Time                    16.10
INSTRUM                 dpx400
PROBHD     5 mm QNP  1H
PULPROG                 zg30
TD                      32768
SOLVENT                   THF
NS                         16
DS                          0
SWH                16025.641 Hz
FIDRES              0.489084 Hz
AQ                  1.0224118 sec
RG                        362
DW                     31.200 usec
DE                      4.50 usec
TE                     200.0 K
D1                 1.00000000 sec

========== CHANNEL f1 ==========
NUC1                      1H
P1                      9.50 usec
PL1                    -6.00 dB
SFO1               400.1378989 MHz

F2 - Processing parameters
SI                        16384
SF                 400.1282822 MHz
WDW                        EM
SSB                         0
LB                       0.30 Hz
GB                          0
PC                       1.00

1D NMR plot parameters
CX                      20.00 cm
F1P                    10.000 ppm
F1                    4001.28 Hz
F2P                    0.000 ppm
F2                    2500.84 Hz
PPMCM                 0.17500 ppm/cm
HZCM                 70.02281 Hz/cm
```